Characterisation and Design of Ultrasound Contrast Agent Particles

by

Eleanor Phoebe Jane Stride

A dissertation submitted for
the degree of Doctor of Philosophy
at the
University of London

Department of Mechanical Engineering
University College London
Torrington Place
London WC1E 7JE

ProQuest LLC
789 East Eisenhower Parkway
P.O. Box 1346
Ann Arbor, MI 48106-1346

Abstract

Ultrasound contrast agents, consisting of gas bubbles coated with a surfactant or polymer shell, offer benefits in a range of diagnostic and therapeutic applications. However, their behaviour both *in vitro* and *in vivo* is by no means fully understood and there remains considerable scope for increasing their effectiveness. The aim of the work described in this thesis is to improve the characterisation of existing contrast agents and to determine how future agents might be designed in order to optimise their performance.

Previous theoretical and experimental work relating to both contrast agents and free gas bubbles will be reviewed. This will be followed by an assessment of the validity of the assumptions underlying existing models for contrast agents. In particular, examination will be made of: the modelling of the material coating the contrast agent particles (CAPs), the influence of blood cells upon CAP dynamics and multiple scattering of ultrasound in CAP suspensions. The results from a combination of computer simulations and experimental testing will be used to derive a new, generalised model for CAP behaviour.

The model will be used to carry out a sensitivity analysis in order to identify the most significant factors controlling CAP behaviour. Based on these findings, a number of new designs will be developed, with the aim of enhancing CAP detectability at low insonation pressures. The designs will be evaluated in terms of their performance, based on the results of experiments using scale models. Finally, an assessment of the areas for future work will be made.

Contents

2 Review

List of symbols

A	area
$A_{1\,or\,2}$	interfacial area for inner or outer shell surface
A_d	diffraction correction factor
$A_{i\,or\,j}$	signal amplitude for first or second echo
a	attenuation coefficient
b_p	specific heat capacity at constant pressure
B	universal gas constant
c	sound velocity
c_G	sound velocity in the filling gas
c_L	sound velocity in the surrounding liquid
c_{Lo}	sound velocity in the surrounding liquid for constant density
c_S	sound velocity in the encapsulating shell
C_i	initial gas concentration
C_s	saturation gas concentration
d_s	shell thickness
D_G	gas thermal diffusivity
d	transmission distance
$\mathbf{E}$	elastic modulus
E	energy
f	scattering function
f_{Sv}	shell viscosity factor
f_{Ss}	shell stiffness factor
f_{Lv}	liquid viscosity factor
f_{Ls}	liquid stiffness factor
f_σ	surface forces factor
f_{brad}	re-radiation damping factor
f_{bth}	thermal damping factor
F	scattering function for second order scattering
G_S	shell shear modulus
H	enthalpy
h	size distribution function

I_i	incident intensity
$\mathbf{I}$	identity matrix
K_{eff}	acoustic wave number in the effective medium
k_L	acoustic wave number in the surrounding fluid
K_G	thermal conductivity of the filling gas
K_L	thermal conductivity of the surrounding fluid
K_S	thermal conductivity of the encapsulating shell
M	number of iterations
M_G	gas molecular weight
$\mathbf{M}_{1,2}$	time derivatives of the strain tensor
n	scatterer concentration
N	number of iterations
p_{inc}	incident pressure
p_A	insonation pressure amplitude
p	pressure
p_o	hydrostatic pressure
p_L	pressure in the surrounding liquid
p_∞	pressure at large distances from the point of interest
p_v	vapour pressure
p_σ	Laplace pressure
p_s	radiated pressure
P	power
P_{dis}	dissipated power
P_{vis}	power dissipated through viscous friction
P_{scat}	power dissipated through acoustic re-radiaiton
Q	compressibility factor
R_o	initial radius of the cavity/bubble
R	instantaneous radius of the cavity/bubble
$\dot{R}$	radial velocity of the cavity/bubble wall
$\ddot{R}$	radial acceleration of the cavity/bubble wall
R_{o1}	initial CAP inner radius prior to insonation.
R_{o2}	initial CAP outer radius prior to insonation.
R_{1e}	inner CAP radius in the absence of surface tension
r	radial coordinate
s_{ext}	extinction cross section

S_f	shell viscosity parameter
S_p	shell elasticity parameter
S	Fresnel parameter
$\mathbf{T}$	stress tensor with components T_{rr}, $T_{\theta\theta}$, $T_{\phi\phi}$ *etc.*
T_{eff}	effective stress
T	absolute temperature
t_p	pulse length
t	time
t'	retarded time
u	radial velocity
V	volume
Vs	shell volume parameter
V_B	cell layer volume parameter
x	non-dimensionalisation factor
X	simplification factor
y	distance along the axis of the ultrasound beam
X	spherical harmonic
Z	acoustic impedance
z	non-dimensional shell parameter
α	non-dimensional shell parameter
β	volume fraction of bubbles/CAPs
γ	ratio of specific heats for the filling gas
δ	sound diffusivity
δ_{rad}	approximate acoustic radiation damping factor
δ_{th}	approximate thermal damping factor
δ_d	viscous damping factor
ε_{rr}	radial component of the strain tensor
η_L	thermal diffusivity of the surrounding liquid
ϑ	phase angle
θ	spherical coordinate
κ	polytropic index for the filling gas
λ_G	characteristic wavelength for pressure variations in the gas
λ_l	fluid viscoelasticity parameter

λ_2	fluid viscoelasticity parameter
λ_S	Lamé parameter for the shell material and
μ_L	viscosity of the surrounding fluid
μ_S	shell viscosity
$\xi_{1 \text{ or } 2}$	resistance to compression of the inner and outer surfaces respectively
ρ_{eff}	density of the effective medium
ρ_S	density of the shell material
ρ_L	density of the surrounding liquid
ρ_{Lo}	initial density of the surrounding liquid
ρ_G	density of the gas
ρ_{Gp}	density of the gas for a gas/liquid interface of zero curvature
σ	surface tension at the bubble wall
σ_1	surface tension at the inner surface of the shell
σ_2	surface tension at the outer surface of the shell
$\tau_{1,2}$	time variables of integration,
τ	non-dimensionalised time $\tau = \sqrt{\left(\frac{2\kappa C_s}{\rho_G R_o^2}\right)} t$
Φ	velocity potential
ϕ	spherical coordinate
χ_s	membrane elasticity parameter
$\psi_{1,2}$	experimentally determined material function
ω	insonation frequency
ω_o	undamped natural frequency

List of figures

Figure 5.6: Acceleration factor plot for a 3.635 μm radius Albunex® CAP insonated at 3 MHz and 100 kPa.

Figure 5.7: Acceleration factor plot for a 3.635 μm radius albumin shelled CAP having a 5 nm thick shell, insonated at 3 MHz and 50 kPa.

Figure 5.8: Acceleration factor plot for a 3.635 μm radius albumin shelled CAP having a 50 nm thick shell, insonated at 3 MHz and 50 kPa.

Figure 5.9: Acceleration factor plot for a 3.635 μm radius albumin shelled CAP having a 5 nm thick shell, insonated at 1 MHz and 50 kPa.

Figure 5.10: Acceleration factor plot for a 3.635 μm radius CAP having a shear modulus of 10 MPa, shear viscosity of 1.77 Pas and a shell thickness of 15 nm, insonated at 3 MHz and 50 kPa.

Figure 5.11 Acceleration factor plot for a 3.635 μm radius CAP having a shear modulus of 88.8 MPa, shear viscosity of 1.0 Pas and a shell thickness of 15 nm, insonated at 3 MHz and 50 kPa.

Figure 5.12: Acceleration factor plot for a 3.635 μm radius CAP having a shear modulus of 200 MPa, shear viscosity of 1.77 Pas and a shell thickness of 15 nm, insonated at 3 MHz and 50 kPa.

Figure 5.13: Acceleration factor plot for a 3.635 μm radius CAP having a shear modulus of 88.8 MPa, shear viscosity of 3.0 Pas and a shell thickness of 15 nm, insonated at 3 MHz and 50 kPa.

Figure 5.14: Acceleration factor plot for a 3.635 μm radius CAP having a shear modulus of 88.8 MPa, shear viscosity of 1.77 Pas, density of 2000 kgm^{-3} and a shell thickness of 15 nm, insonated at 3 MHz and 50 kPa.

Figure 5.28: Schematic illustration of how the structure of a CAP could be modified to enhance non-linear behaviour at low insonation pressures.

Figure 5.29: Schematic illustration of an alternative CAP design.

Figure 5.30: Schematic illustration of another alternative CAP design.

Figure 5.31: Schematic of the experimental apparatus.

Figure 5.32: Illustrating the analysis of the photographic results.

Figures in appendices

Figure Aiv.1: Variation in attenuation coefficient for Albunex® CAPs with insonation pressure at 3 MHz and 106 CAPs/ml (no multiple scattering effects were included).

Figure Bi.1: Demonstrating the influence of thermal damping upon the amplitude of oscillation of a resonant Albunex®CAP insonified at 3 MHz and 0.1 MPa (i) with no correction for thermal damping (ii) including an approximate thermal damping factor (iii) full solution of equations Bi.8 and Bi.11.

Figure Bi.2: Demonstrating the influence of thermal damping upon the amplitude of oscillation of a resonant Albunex®CAP insonified at 3 MHz and 1 MPa (i) with no correction for thermal damping (ii) including an approximate thermal damping factor (iii) full solution of equations Bi.8 and Bi.11.

Figure Biii.1: Response of an Albunex® CAP to pulsed and continuous insonation at 2.25 MHz and 0.1MPa.

Figure Biii.2:Variation in radial displacement with time for CAPs insonated at 2.25 MHz and 0.3 MPa.

Figure Ci.1: Geometry of the experimental system.

Figure Cii.1: Average frequency spectra for transmission through water.

Figure Cii.2: Transducer beam profile in water at (i) 2 cm and (ii) 3 cm from the transducer face.

Figure Cii.3: Variation in hydrophone sensitivity with frequency.

Figure Cii.4: Insonating pulse in (i) Time domain and (ii) Frequency domain for different transmission distances.

Figure Bv.1: Demonstrating the variation in phase velocity in CAP suspensions with frequency for different CAP sizes and concentrations.

Figure Dii.1: Radial amplitude of oscillation for an Albunex® CAP with and without an inner viscous layer.

Figure Diii.1: Model used to calculate the temperature rise generated within a CAP population.

Figure Diii.2: Model used to calculate the temperature rise generated by CAP oscillation over a series of pulses.

Figure Diii.3: Change in temperature in the water surrounding a CAP insonified by a single pulse of 3 MHz, 0.1 MPa due to acoustic radiation.

Figure Diii.4: Change in temperature in the water surrounding a CAP insonified by a single pulse of 3 MHz, 0.1 MPa due to viscous dissipation.

Figure Diii.5: Change in temperature in the water surrounding a free bubble insonified by a single pulse of 3 MHz, 0.2 MPa due to viscous dissipation.

Figure Diii.6: Change in temperature in the water surrounding a CAP insonified by a single pulse of 3 MHz, 0.2 MPa due to viscous dissipation.

Figure Diii.7a: Temperature rise in water surrounding an Albunex® CAP insonified by 5 pulses of 3 MHz, 0.1 MPa at a pulse repetition frequency of 30 kHz.

Figure Diii.7b: Temperature rise in water surrounding an Optison® CAP insonified by 5 pulses of 3 MHz, 0.1 MPa at a pulse repetition frequency of 10 kHz.

Figure Diii.8: Temperature rise in fluid surrounding a population of 10 Albunex® CAPs insonified by a single pulse of 3 MHz, 0.1 MPa.

Figure Diii.9: Variation in radial displacement of a CAP insonified by a single pulse of 3 MHz, 0.1 MPa at 293 K (dashed) and 373 K (solid).

List of tables

Tables in appendices

List of publications

Refereed Journal papers[1]

Stride, E. & Saffari, N. (2003) On the destruction of microbubble ultrasound contrast agents. Ultrasound in Medicine & Biology 29: 563-573.

Stride, E. & Saffari, N. (2003) Microbubble ultrasound contrast agent: a review. Journal of Engineering in Medicine. Proceedings of the Institute of Mechanical Engineers: Part H. 217: 429-447.

Stride, E. & Saffari, N. (2004) The potential for thermal damage posed by microbubble ultrasound contrast agents. Ultrasonics 42: 907-913.

Stride, E. & Saffari, N. (2004) The behaviour of microbubble ultrasound contrast agent particles in whole blood. Ultrasound in Medicine & Biology 30: 144-158.

Stride, E. & Saffari, N. (2005) Investigating the significance of multiple scattering in ultrasound contrast agent particle populations. IEEE Transactions in Ultrasonics, Ferroelectrics & Frequency Control (in press).

Books

Stride E. Characterisation and Design of Microbubble-based Contrast Agents Suitable for Diagnostic Imaging. In: Contrast Media in Ultrasonography: Basic Principles and Clinical Applications. Ed. E. Quaia. Berlin: Springer-Verlag, 2005.

[1] Reprints of the papers have been included in Appendix E.

Acknowledgements

First and foremost I would like to thank my supervisor Dr. Nader Saffari for his constant support and friendship, particularly in the darkest phase of 2003. I would also like to thank Dr. Tony Harker for his many helpful comments and for casting an expert eye over the development of the new models. A huge debt of thanks is owed to Prof. Peter Dawson who initiated the project and who has provided invaluable assistance and advice over the course of the work. On the experimental side, I would like to thank Nick Hutchinson for his infinite patience in battling with the particle sizer; Drs. Paul Beard and Ben Cox for the loan of the hydrophone; Julia Markusen for her help with the centrifuge and Kevin Lee for the use of the vacuum equipment. I am immensely grateful to the UCL Graduate School for the award of a graduate studentship. Finally, in spite of his rechristening me "Hermione," I would like to thank Dr. Alistair Greig for maintaining my sanity via the 100 club; and Matt for 007 in every sense.

This thesis is dedicated to the memory of my Mother

April Mavis Penelope Stride

1941-2003

quos amor verus tenuit, tenebit

1

Introduction

1.1 Overview

Ultrasound represents the safest, fastest and least expensive method of scanning for many types of medical diagnosis. Compared with techniques such as magnetic resonance imaging, however, image quality is often inferior, and methods for improving image contrast are therefore highly desirable. Gas microbubbles, coated with a surfactant or polymer shell, have become well established over the past 20-30 years as the most effective type of contrast agent available for ultrasound radiography. They have been successfully employed with a wide range of imaging techniques, and more recently, their potential use in therapeutic applications such as targeted drug delivery has also become an active area of research.

However, existing theoretical descriptions of contrast agent particles (CAPs) are inadequate in several respects and, despite considerable investigation, CAP behaviour is by no means fully understood. There is consequently substantial scope for improving the effectiveness of contrast agents and, notwithstanding a lack of definite evidence for harmful effects, there inevitably remain some concerns as to their safety. The aim of the work described in this thesis is to address the deficiencies in contrast agent characterisation and develop designs for new agents. In this chapter the principles and applications of contrast agents are summarised and the specific objectives of the work defined.

1.2 Background

1.2.1 History

The development of microbubble ultrasound contrast agents came about as the result of an accidental discovery by Dr. Claude Joyner in the late 1960's (Feigenbaum *et al* 1970). An M-mode echocardiogram was being performed at the same time as a study of cardiac output was being made, using injections of indocyanine green dye into the patient's left ventricle. After each injection of dye, a temporary increase in the ultrasound signal from the ventricle was observed. Initially it was thought that the contrast enhancement was due to the nature of the dye. It was found subsequently, however, that the same effect could be observed with a range of other fluids, including saline. It was suggested by Gramiak and Shah (1968) that the effect was, in fact, due to the presence of air microbubbles forming at the catheter tip. The validity of this theory was confirmed by demonstrating that no contrast enhancement was observed when the ambient pressure was increased in order to suppress bubble formation (Kremkau *et al* 1970).

1.2.2 Physics

The effectiveness of gas microbubbles for ultrasound contrast enhancement *in vivo* is due to the fact that they have a very high compressibility compared with that of their surroundings. This gives rise, firstly, to a large difference in acoustic impedance between the CAPs and the liquid in which they are suspended and secondly, causes the CAPs to undergo volumetric oscillations of finite amplitude when exposed to an ultrasound field. Consequently, the CAPs both reflect and absorb and re-radiate sound energy to a much greater extent than liquid-filled particles of similar size, such as red blood cells. There is, moreover, a fortuitous coincidence between the size of CAP able to pass through human capillaries (< 8 μm) and that which is resonant at the frequencies typically used for ultrasound imaging (1-10 MHz). Thus, the amplitude of CAP oscillations and hence the contrast enhancing effect, is maximised under diagnostic conditions.

There is a further feature of CAP behaviour which is perhaps even more important in terms of image enhancement and that is the fact that CAP oscillations are non-linear. If the CAPs are excited at sufficient amplitude, the re-radiated signal will contain distinct harmonics of the insonation frequency. This enables the signal to be

distinguished from that produced by the surrounding tissue, which will contain a much smaller proportion of harmonics. A clearer image of the CAPs' location may thus be obtained. In addition, if the amplitude of excitation is increased further, the CAPs may be rapidly destroyed. This results not only in a strongly non-linear signal being produced during the destruction process itself, but also in a distinct change in the nature of the signal before and after destruction has taken place. Again these properties may be exploited for imaging, as will be discussed below.

1.2.3 Types of contrast agent

Following Joyner's discovery, it was proposed that an ultrasound contrast agent could be developed for clinical use. However, whilst the microbubbles formed during the injection of dye or saline were clearly effective for contrast enhancement, they dissolved very rapidly owing to the high surface tension forces at the gas/air interface. As a result, the contrast effect was both short-lived and difficult to reproduce. Moreover, the bubbles were too large to cross the lung capillary bed and could not be used for imaging the left side of the heart or the arterial circulation. Further research showed that the stability of the microbubbles could be improved considerably by mixing the suspension with a small amount of the patient's blood. This was found to be due to the formation of a coating of serum albumin on the surface of the bubbles, which counteracted the effects of surface tension (Feinstein 1984). The discovery led to the development of one of the first commercial contrast agents, Albunex® (Amersham Health PLC, Amersham, UK).

Albunex® CAPs were produced by insonifying a solution of serum albumin prior to injection. This made their administration somewhat inconvenient, and whilst their stability was far better than that of free air bubbles, the albumin coating was too thin to prevent the outwards diffusion of air entirely. Consequently, the time over which image enhancement could be obtained was still relatively short. New products have since been developed in order to overcome these difficulties. For example, Optison® CAPs (Amersham Health PLC, Amersham, UK) are also encapsulated with albumin, but contain perfluoropropane, whose relative molecular mass (188) is approximately six times that of air (29). The CAPs are consequently much more stable in terms of their rate of dissolution. They are, in addition, pre-formed during manufacture and may be directly injected from the vial in which they are supplied.

The presence of the albumin coating inevitably reduces the amplitude of CAP oscillation compared with that of a free bubble. Hence the degree of contrast enhancement that can be achieved at a given insonation pressure is also reduced. Alternative coating materials have therefore been investigated to determine whether a more favorable compromise between contrast enhancement and stability may be obtained. For example, Sonavist® (Schering AG, Berlin, Germany), consists of air microbubbles enclosed by a biodegradable polymer (cyanoacrylate), whilst Sonovue® (Bracco International B.V. The Netherlands) and EchoGen® (Sonus Pharmaceuticals Inc. Bothell, USA) are stabilised by biological membranes and surfactant layers respectively. These coatings are more flexible than albumin or polymer shells and restrain CAP oscillations to a lesser extent. Data for a range of ultrasound contrast agents are shown in table 1.1.

Manufacturer	**Name**	**Stabilising coating**	**Filling gas**
ImaRx Pharmaceutical Corp.	Aerosomes™	phospholipid	perfluoropropane
Schering AG.	Imavist™	surfactant	perfluorohexane & air
Bracco International B.V.	Sonovue™	phospholipid	sulphur hexafluoride
Cav-Con Inc.	Filmix™	phospholipid	air
Dupont	Definity™	phospholipid	perfluoropropane
Amersham health PLC.	Optison®	crosslinked human serum albumin	perfluoropropane
Amersham health PLC.	Albunex®	sonicated human serum albumin	air
Amersham health PLC.	Sonazoid™	lipid	perfluorocarbon
Point Biomedical Corp.	Bisphere™	polymer bilayer	air
Quadrant Healthcare PLC.	Quantison™	spray dried serum albumin	air
Schering AG.	Echovist®	none	air
Schering AG.	Levovist®	phospholipid	air
Schering AG.	Sonavist™	polymer	air
Sonus Pharmaceuticals Inc.	Echogen®	surfactant	dodecafluoropentane

Table 1.1: Examples of commercial contrast agents.

Alternative means of producing CAPs have also been developed. For example, EchoGen® CAPs are formed after injection by the vaporisation of perfluoropentane, whose boiling point coincides with normal body temperature (37°C). Echovist® and its successor Levovist® (Schering AG, Berlin, Germany) are formed when an injected suspension of galactose microcrystals dissolves in the blood, releasing air microbubbles from defects on the crystal surfaces. In the case of Levovist®, stability is provided by the presence of a layer of palmitic acid on the bubble surface which reduces surface tension and inhibits gas diffusion.

The most recent developments in CAP design have been concerned mainly with their therapeutic applications such as thrombolysis and targeted drug delivery (c.f. section 1.2.5). Protein ligands, which bind to receptors on particular types of cell, may be attached to the surfaces of the CAPs to encourage them to accumulate in specific areas. This enables treatment to be targeted, for example, to the site of a thrombus or a tumour. Hence the risk of harmful side effects may be reduced. A number of commercial products are being developed on this basis, including Aerosomes® (ImaRx Pharmaceutical Corp. Tucson, USA) and Filmix® (Cav-Con Inc. Farmington, USA). CAPs are also being developed which incorporate therapeutic compounds, either dissolved in the shell material or in an inner oil layer (figure 1.1). For example, Bisphere™ (Point Biomedical Corp. San Carlos, USA) CAPs consist of an inner shell of a biodegradable polymer, with a biocompatible outer coating. The polymer shell provides physical rigidity and may be filled with gas and/or therapeutic compounds, whilst the outer coating provides a "scaffold" for targeting species.

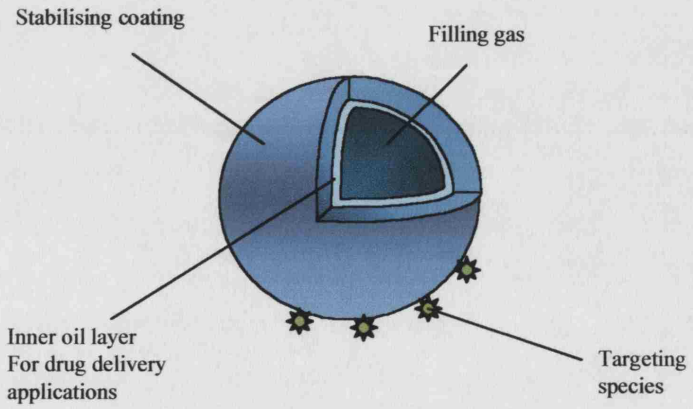

Figure 1.1: Schematic of a contrast agent particle (CAP).

1.2.4 Diagnostic applications

Since their discovery, ultrasound contrast agents have found application in a wide range of imaging techniques, including several developed specifically for their use. They were employed initially with conventional (B-mode) imaging methods to provide enhancement of the backscattered signal and hence in the definition of features such as the endocardium in echocardiography (Gramiak *et al* 1969). Subsequently, they were used to improve the sensitivity of Doppler measurements by increasing the amplitude of the signal from blood vessels (Bleeker *et al* 1990).

It was found, however, that greater benefits could be derived by exploiting the non-linear behaviour of CAPs and this led to the development of harmonic imaging (Schrope *et al* 1992). As described above, if a CAP is excited with sufficient amplitude, the frequency spectrum of its radiated signal will contain both the excitation frequency and its harmonics. The ultrasound system can be tuned to receive at a particular harmonic and to use this information for creating the scan image. Since the harmonic components will be due predominantly to the CAPs rather than the surrounding tissue, the signal:noise ratio can be greatly increased. The second harmonic is the most commonly used frequency component but the possibility of using of higher harmonics, subharmonics and ultraharmonics of the insonation frequency is currently under research (Shi & Forsberg 2000).

Harmonic imaging has two main disadvantages. Firstly, image resolution is limited because the bandwidth of the transmitting transducer must be kept narrow in order to avoid overlap between the fundamental and second harmonic in the received signal. Secondly, whilst it is true that the harmonic content of the received signal will be due mainly to the CAPs, the contribution from the surrounding tissue will not be entirely negligible at the pressures required to excite significant non-linear CAP behaviour. Alternative imaging strategies have been devised to overcome these drawbacks. For example, in "pulse inversion imaging" (Hope Simpson *et al* 1999) an initial imaging wave is transmitted into the subject, followed, after a suitable delay, by an inverted copy of itself. If the two waves are scattered linearly, the sum of the resulting echoes will be zero. If, however, they encounter non-linear scatterers such as CAPs, there will be a residual signal after summation, which will be proportional to the degree of non-linearity (figure 1.2). Superior image resolution may be attained because in this case the signal bandwidth does not need to be limited.

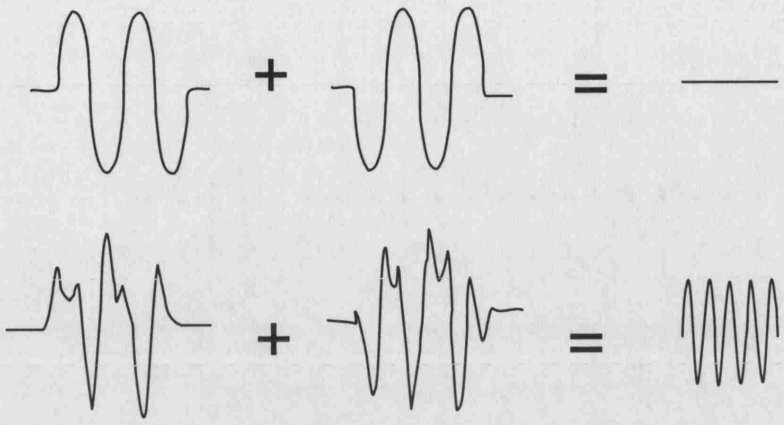

Figure 1.2: Illustration of the principle of pulse inversion imaging

Loss-of-correlation imaging (variously called "transient scattering," "power enhanced scattering" and "stimulated acoustic emission") utilises the large change in the signal produced by CAP destruction. This registers as a strong transient signal in Doppler imaging mode and enables the sensitivity to small features such as metastases to be greatly increased (Harvey *et al* 2002). New imaging techniques continue to be devised as scanning technology improves. This section is only intended to provide a brief overview.

1.2.5 Therapeutic applications

Ultrasound contrast agents are currently under investigation for use in a number of therapeutic applications. As mentioned above, CAPs may be employed as vehicles for drug delivery or gene therapy which may be targeted to specific areas of the body. Their passage through the body can be traced using low intensity ultrasound and the treatment released by increasing the intensity at the appropriate location. The destruction of the CAPs may also enhance the uptake of the drugs by temporarily increasing the membrane permeability of the nearby cells (sonoporation) (Bao *et al* 1997). The precise mechanism responsible for this phenomenon is currently unclear, but it is thought to be related to the collapse of the free gas bubbles that are released when the CAPs are destroyed. This process may result in the formation of high velocity microjets of liquid capable of puncturing the cell membranes. There may also be a strong heating effect which increases cell permeability (Stride & Saffari 2003). Similar processes are likely to be responsible for the fact CAPs have been

found to enhance the effectiveness of thrombolytic procedures and therapeutic techniques such as HIFU (high intensity focused ultrasound) (Poliachik *et al* 1999). Recently it has been suggested that CAPs may also be used to inhibit the development of blood vessel networks supplying cancerous tumours (angiogenesis) (Forsberg *et al* 2004) and this is a growing area of research.

1.2.6 Contrast agent safety

The safety of contrast agents is a somewhat controversial topic and a detailed discussion would be outside the scope of this thesis. Potentially, there are a number of mechanisms which could lead to damaging effects *in vivo*. The most obvious concern is the risk of inertial cavitation and the associated phenomena, including the formation of microjets, heating of the surroundings and the synthesis of harmful chemicals in the CAP interior at high insonation pressures (Mornstein 1997). Even at lower insonation pressures, a CAP oscillating within the confines of a narrow blood vessel could damage the surrounding tissue. In a larger vessel the stresses produced as a result of streaming in the fluid around the CAP could be sufficient to disrupt the membranes of nearby cells (Wu 2002). Allied to this is the fact that an ultrasound beam may cause CAPs to accelerate rapidly towards nearby cells and damage them directly (Nyborg 2001). It is also true that any body introduced into the blood stream presents a risk of embolism.

As regards the evidence for unwanted bio-effects, clearly the effectiveness of CAPs for enhancing procedures such as thrombolysis and HIFU demonstrates their potential for causing damage at high insonation pressures. In addition, the presence of CAPs in a suspension of blood cells *in vitro* has been shown to increase the degree of ultrasound induced hemolysis (Dalecki *et al* 1997). However, this has only been observed at much higher CAPs concentrations than would be used *in vivo*. The evidence for damage under diagnostic conditions is scarce. Queries have nevertheless been raised over the validity of existing guidelines for contrast agent use (Khismatullin 2001; Stride & Saffari 2003) and Postema *et al* (2004) have reported observations of microjet formation from phospholipid-coated CAPs under conditions which would be permitted for diagnostic scanning. Further work is needed in order to resolve this matter. It has been assumed for the purposes of this thesis that the minimum concentrations and insonation pressures should be used to produce the desired contrast enhancement or therapeutic effect.

1.3 Aims and objectives

1.3.1 Statement of problem

It is clear from the above that ultrasound contrast agents offer considerable benefits in both diagnostic and therapeutic applications. There are, however, a number of reasons why existing agents are unsatisfactory. First of all, their behaviour cannot be reliably predicted at present. This is due both to a lack of accurate modelling, as will be shown in the next chapter, and to variability in the responses of individual CAPs within a population (Postema *et al* 2003). Secondly, in order to achieve maximum contrast enhancement, it is necessary to use relatively high insonation pressures in order to excite non-linear behaviour. This limits the maximum signal to noise ratio which can be obtained, since at high pressures the surrounding tissue will also scatter non-linearly. It also limits the imaging time and/or increases the size of the dose required since the higher the pressure the larger the proportion of CAPs that will be destroyed during the scan. This is particularly undesirable in therapeutic applications where CAP destruction could lead to drugs being released in the wrong location. Moreover, as noted above, high pressures are more likely to present a risk to patient safety.

The third disadvantage of contrast agents relates to their effect upon the viability of ultrasound as a scanning method. One of the main attractions of using ultrasound for diagnostic scanning is that it is non-invasive. Administering contrast agents increases the time and skill requirements and hence the overall cost associated with performing a scan. Clearly the fact that contrast agents have to be administered cannot be overcome. However, administration procedures can be simplified in order to lessen this problem and there are applications in which the benefits of using contrast agents outweigh the costs. These include certain types of Doppler imaging and new applications such as elastography for which techniques such as MRI (magnetic resonance imaging) or CT (computed tomography) do not offer a viable alternative (Lewin 2004). Moreover, many of the therapeutic applications discussed above involve procedures which are necessarily invasive; for example, drug delivery and thrombolysis. It is important therefore to have an agent whose behaviour is fully characterised and which presents a minimal risk to patient safety. This thesis is concerned with the design of such an agent.

1.3.2 Objectives

The overall aim of the work is to improve the characterisation of ultrasound contrast agent particles in order to facilitate their design.

The specific objectives are as follows:

- To review the existing theoretical and experimental work on contrast agents and identify areas requiring further research.
- To examine the assumptions underlying the existing models and assess their validity for particular conditions.
- To derive a new generalised model for CAP behaviour.
- To define the requirements for contrast agents for different applications and formulate designs for new types of CAP.
- To construct and test scale models of the new CAPs in order to evaluate the designs.
- To define areas suitable for future development.

1.3.3 Outline

Previous work on contrast agents will be reviewed in Chapter 2. In Chapter 3, the assumptions upon which existing models rely will be examined theoretically and a generalised model derived for a specified range of conditions. In Chapter 4, the experimental work carried out in order to validate the new model will be described, whilst in Chapter 5 the requirements for different CAP applications will be considered and a sensitivity analysis performed using the new model in order to determine the most important variables determining CAP behaviour. The findings will be used in the development of designs for new types of CAPs whose acoustic response may be tailored to suit a particular application. The designs will then be evaluated, based on the results of experiments performed using scale models, and their manufacturing requirements discussed. The conclusions from the work will be presented in Chapter 6 followed by a discussion of the areas for future work.

1.4 Summary

The benefits of coated microbubble contrast agents for ultrasound image enhancement have been clearly demonstrated since the development of the first commercial agents in the 1970s. There is also a growing interest in their use in therapeutic applications such as targeted drug delivery and thrombolysis. However, there remains a high degree of uncertainty regarding contrast agent behaviour and there is consequently considerable scope for improving their effectiveness. The aim of the work described in this thesis is to review the existing work on contrast agents, to derive a new model for CAP behaviour and to use the model to investigate how CAP design may be improved. In this chapter a brief introduction to the history, function and applications of contrast agents has been given and the objectives of the work defined.

2

Review

2.1 Overview

The behaviour of contrast agent particles (CAPs) in an ultrasound field has been the subject of investigation for the past three decades. The majority of the work has been based upon earlier studies of free gas bubbles, for which there is a relatively extensive literature. The aim of this chapter is to review the existing theoretical and experimental work pertaining to the characterization and design of CAPs and to identify areas requiring further research. In particular, the following topics will be addressed: modelling of individual CAPs; experimental determination of CAP properties; the influence of the surrounding fluid upon CAP behaviour; the influence of the insonating field; the response of a CAP population; CAP destruction and, finally, recent developments in CAP design. The findings from this review will form the basis of the new work described in the subsequent chapters.

2.2 Theoretical treatments

2.2.1 CAP characterisation

2.2.1.1 Models for a single free spherical bubble

The origins of the existing models for CAPs may be traced back to the equation of motion derived by Besant (1859), for the collapse of a spherical cavity.

$$R\ddot{R}+\frac{3}{2}\dot{R}^2=\frac{p_L-p_\infty}{\rho_L} \tag{2.1}$$

In this equation, R is the instantaneous cavity radius whilst $\dot{R}$ and $\ddot{R}$ denote the velocity and acceleration of the cavity wall respectively. ρ_L is the density of the liquid surrounding the cavity, p_L is the pressure in the liquid at the cavity wall and p_∞ is the pressure at a large distance from the cavity.

The problem was reconsidered by Lamb (1879) and later by Lord Rayleigh (1917) in his analysis of a collapsing cavity. Equation 2.1 was subsequently reformulated for a vapour-filled bubble by Plesset (1949) and for a gas bubble by Noltingk and Neppiras (1950, 1951). Finally, an additional term was included to account for viscous dissipation in the surrounding fluid. According to Young (1989) this was originally given by Taylor in 1943, although it is generally attributed to Poritsky (1952). The result was the so-called Rayleigh-Plesset or Rayleigh-Plesset-Noltingk-Neppiras-Poritsky (RPNNP) equation (Lauterborn 1976).

$$R\ddot{R}+\frac{3}{2}\dot{R}^2=\frac{1}{\rho_L}\left(\left(p_o+\frac{2\sigma}{R}-p_v\right)\left(\frac{R_o}{R}\right)^{3\kappa}+p_v-\frac{2\sigma}{R}-\frac{4\mu_L\dot{R}}{R}-p_\infty(t)\right) \tag{2.2}$$

In this case, σ is the surface tension at the bubble wall, p_v is the vapour pressure inside the bubble, R_o is the initial bubble radius, κ is the polytropic index for the gas and μ_L is the viscosity of the surrounding fluid. The other symbols are as defined above.

The derivation of equation 2.2 ignores the compressibility of the surrounding fluid and its influence upon bubble dynamics. This may become significant, however, for situations in which the velocity of the bubble wall is comparable with the acoustic velocity in the surrounding fluid. Herring (1941) and Trilling (1952) rederived

equation 2.1 to take into account the energy stored in the liquid during bubble oscillation and the damping effect produced by the re-radiation of sound waves.

$$\left(1-\frac{2\dot{R}}{c_L}\right)R\ddot{R}+\frac{3}{2}\left(1-\frac{4\dot{R}}{3c_L}\right)\dot{R}^2=\frac{1}{\rho_L}\left(p_L+\frac{R}{c_L}\left(1-\frac{\dot{R}}{c_L}\right)\frac{dp_L}{dt}-p_\infty(t)\right) \qquad (2.3)$$

This treatment assumed that the sound velocity in the surrounding liquid, c_L, was constant, and was therefore limited in terms of the maximum amplitude of oscillation for which it was valid. Gilmore (1952) improved upon this assumption by employing the Kirkwood-Bethe hypothesis (1942). This states that the wave velocity will be equal to the sum of the velocity of the fluid and the local velocity of sound at the bubble wall. The resulting equation may be expressed as

$$\left(1-\frac{\dot{R}}{c_L(t)}\right)R\ddot{R}+\frac{3}{2}\left(1-\frac{\dot{R}}{3c_L(t)}\right)\dot{R}^2=\left(1-\frac{\dot{R}}{c_L(t)}\right)H+\frac{R}{c_L(t)}\left(1-\frac{\dot{R}}{c_L(t)}\right)\frac{dH}{dt} \qquad (2.4)$$

where H is the difference in liquid enthalpy between the bubble wall and infinity and $c_L(t)$ is the velocity of sound in the liquid at the bubble wall. Both H and $c_L(t)$ are functions of time.

For smaller amplitudes of oscillation an approximate damping factor may be used to take account of the acoustic re-radiation. This was defined by Devin (1959) as

$$\delta_{rad}\approx k_L R_o=\frac{\omega R_o}{c_L} \qquad (2.5)$$

where ω is the insonation frequency and k_L is the corresponding wave number.

Similarly, for the damping effect due to conduction from the filling gas to the surrounding liquid a further term may be defined as

$$\delta_{th}\approx\frac{2(\gamma-1)}{15\gamma}\left(\frac{\omega R_o}{2D_G}\right)^2 \text{ for } \left(\frac{\omega R_o}{2D_G}\right)^2\le 1 \qquad (2.6)$$

where γ is the ratio of specific heats for the gas and D_G is its thermal diffusivity (Neppiras 1980). Both δ_{rad} and δ_{th} may be included inside the bracket on the right hand side of equation 2.2, multiplied by a factor of $4\pi R_o^2\omega\rho_L\dot{R}$.

In 1980, Keller and Miksis published a more complete treatment of large amplitude bubble oscillations, which included surface tension and liquid viscosity; both of which were neglected in equations 2.3 and 2.4. This was subsequently refined by Prosperetti (1988), by removing the assumption of ideal gas behaviour and coupling the equation of motion for the bubble to the equations of mass and energy conservation. These treatments will be considered in more detail below.

2.2.1.2 Models for single coated bubbles

Equations 2.2 and 2.3 provide the foundations for existing CAP models. As explained in the previous chapter, however, the majority of CAPs are coated with a surfactant or polymer shell in order to improve their stability. Models for bubbles coated with organic films were derived by Fox and Herzfeld (1954), Avetisyan (1977) and Glazman (1983) in order to examine the influence of such films upon the behaviour of bubbles in the ocean. In each case, an additional term was included on the right hand side of equation 2.2 to account for the elastic effect of the coating.

$$R\ddot{R}+\frac{3}{2}\dot{R}^2=\frac{1}{\rho_L}\left(\left(p_o+\frac{2\sigma}{R}-p_v\right)\left(\frac{R_o}{R}\right)^{3\kappa}+p_v-\frac{2}{R}\left[\sigma+\chi_s\left(\frac{R_o}{R}\right)^2\right]-\frac{4\mu_L\dot{R}}{R}-p_\infty(t)\right) \quad (2.7)$$

The methods used to derive the elasticity parameter χ_s and corresponding function vary considerably, but, as will be shown in the next chapter, the results are mathematically equivalent.

2.1.1.3 Models for CAPs

The first model developed specifically for contrast agents was published by de Jong *et al* in 1992 (de Jong *et al* 1992; 1994). Their approach was similar to that of Fox and Herzfeld, but in this case the CAP coating was modelled as a viscoelastic solid shell rather than a purely elastic outer layer.

$$R\ddot{R}+\frac{3}{2}\dot{R}^2=\frac{1}{\rho_L}\left(\begin{array}{l}p_o\left(\frac{R_o}{R}\right)^{3\kappa}+p_v-\frac{2\sigma}{R}-2S_p\left(\frac{1}{R_o}-\frac{1}{R}\right)-\frac{S_f\dot{R}}{4\pi R^2}\\-\frac{4\mu_L\dot{R}}{R}-\omega\rho_L R\dot{R}(\delta_{rad}+\delta_{th})-p_\infty(t)\end{array}\right) \quad (2.8)$$

The two parameters S_f and S_p relate to the viscous and elastic response of the shell respectively. δ_{rad} and δ_{th} are the approximate acoustic re-radiation and thermal damping factors defined above.

A more mathematically rigorous[1] derivation of equation 2.6 was carried out by Church (1995) for a CAP coated with a shell of finite thickness, $d_s = R_2 - R_1$, using the constitutive equations for a linear viscoelastic solid.

$$\begin{aligned} &R_1\ddot{R}_1\left(1+\left(\frac{\rho_L-\rho_s}{\rho_s}\right)\frac{R_1}{R_2}\right)+\dot{R}_1^2\left(\frac{3}{2}+\left(\frac{\rho_L-\rho_s}{\rho_s}\right)\left(\frac{4R_2^3-R_1^3}{2R_2^3}\right)\frac{R_1}{R_2}\right) \\ &=\frac{1}{\rho_s}\left(p_o\left(\frac{R_{o1}}{R_1}\right)^{3\kappa}-p_\infty(t)-\frac{2\sigma_1}{R_1}-\frac{2\sigma_2}{R_2}-4\frac{\dot{R}_1}{R_1}\left(\frac{V_s\mu_s-R_1^3\mu_L}{R_2^3}\right)-\frac{4V_sG_s}{R_2^3}\left(1-\frac{R_{1e}}{R_1}\right)\right) \end{aligned} \tag{2.9}$$

R_{o1} is the inner radius of the CAP prior to insonation whilst R_{1e} is the inner radius which would be measured in the absence of surface tension and is given by

$$R_{1e}=R_{o1}\left(1+\frac{R_{o2}^3}{4V_sG_s}\left(\frac{2\sigma_1}{R_1}-\frac{2\sigma_2}{R_2}\right)\right) \tag{2.10}$$

where $V_s=R_2^3-R_1^3$, σ_1 and σ_2 represent the surface tension at the inner and outer surfaces of the shell respectively, ρ_s is the density of the shell material, G_s is its shear modulus and μ_s its viscosity.

Thermal and acoustic re-radiation damping were neglected in equation 2.9, although Church did suggest that additional terms could be added to the right hand side of equation 2.9 to correct for these effects. Morgan *et al* (1999) used a modified version of the Herring-Trilling equation 2.3 to enable a more accurate investigation of re-radiation damping.

$$\begin{aligned} &\rho_L\left(R\ddot{R}+\frac{3}{2}\dot{R}^2\right)=\left(p_o+\frac{2\sigma}{R}+\frac{2\chi_s}{R_o}\right)\left(1-\frac{3\kappa\dot{R}}{c_L}\right)\left(\frac{R_o}{R}\right)^{3\kappa}-\frac{4\mu_L\dot{R}}{R} \\ &-\frac{2\sigma}{R}\left(1-\frac{\dot{R}}{c_L}\right)-\frac{2\chi_s}{R}\left(1-\frac{3\dot{R}}{c_L}\right)\left(\frac{R_o}{R}\right)^2-\frac{12\mu_sd_s\dot{R}}{R(R-d_s)}-p_\infty(t) \end{aligned} \tag{2.11}$$

[1] Notwithstanding the additional rigor with which it was derived, it has been shown by Hoff (1996) that equation 2.9 may be reduced to equation 2.8 in the limit of an infinitely thin shell.

2.1.1.4 Solutions

Equations 2.7-2.11 and their free bubble counterparts are all non-linear, and solutions must therefore be obtained either by using analytical approximations for small amplitude oscillations, or by using numerical methods. Linear solutions are of limited use since, as explained in Chapter 1, it is the non-linear response which is of interest for the majority of CAP applications. Analytical solutions for CAP oscillations generating second harmonics have been derived by de Jong *et al* (1994) and Church (1995) but are not suitable for large amplitude behaviour or for modelling CAP destruction.

Numerical methods provide a more complete description of CAP behaviour (Frinking 1998) but are more susceptible to instability and errors, owing to the finite number of decimal places to which calculations may be carried out. Their usefulness is therefore restricted to certain regimes. Both types of solution have been applied to the equations for free bubbles and CAPs, and investigation has also been made of the chaotic behaviour of free bubbles (Lauterborn and Parlitz 1987). To date, chaotic behaviour has not been observed for CAPs and, according to Morgan *et al* (1999), is unlikely under typical diagnostic conditions. This may not be the case in therapeutic applications however, where much higher pressures are used. Both analytical and numerical methods will be employed in this thesis, as appropriate to the amplitudes of oscillation being considered.

2.1.1.5 Models for non-spherical bubbles

Equations 2.1-2.11, and the majority of the analysis which will be considered in this thesis, refer to a spherical cavity or bubble. However, bubbles may oscillate non-spherically under certain conditions, for example in the vicinity of a boundary, as will be discussed in the next section. This review would therefore be incomplete without some reference to the work which has been carried out in this area. Analysis of the non-spherical oscillations of liquid drops was made by Lord Rayleigh in 1879 (Rayleigh 1879). The work was again extended by Lamb (1924) to predict the different modes in which a gas bubble would oscillate in the linear regime. More recently, a second order analysis of bubble modes and the corresponding acoustic emissions was published by Longuet-Higgins (1989a; 1989b) for an incompressible and inviscid liquid.

As yet no such treatment has been carried out for CAPs. Marmottant & Hilgenfeldt (2003) modelled the asymmetric oscillations of a free bubble close to a cell in their investigation of sonoporation. However, their analysis did not include the encapsulating shell. The stiffening effect of the shell and the small size of CAPs relative to the wavelength of the insonating field would be expected to make them more resistant to distortion than free bubbles. Countering this, however, is the fact that any inhomogeneities in the shell, such as variations in thickness, could encourage asymmetric behaviour.

In terms of the effect upon the radiated signal, the significance of non-spherical oscillations is likely to be relatively small for the majority of CAP applications. Linear analyses by Stokes (1868) and Neppiras (1980) indicate that it is the radiation due to the spherically symmetric ("breathing") mode of oscillation which predominates over that due to higher order modes (Appendix A.i). Longuet-Higgins (1989a) showed that radiation from higher-order modes may propagate to a greater degree than indicated by linear analysis, but his analysis did not take into account any form of damping. This area will be discussed further in Chapter 6.

2.2.2 Modelling the surrounding fluid

Equation 2.9 relates to a CAP suspended in an infinite, homogeneous and Newtonian liquid in which T_{rr}, the radial component of the shear stress tensor **T**, is proportional to the rate of shear, i.e.

$$T_{rr} = 2\mu_L \frac{\partial u}{\partial r} \qquad (2.12)$$

where r is the radial distance from the CAP centre and u is radial velocity.

However, this is not an accurate representation of conditions *in vivo*, where CAPs are confined within blood vessels and surrounded by a high volume fraction (40%) of blood cells (Guyton and Hall 1990). The behaviour of a free bubble in linear and non-linear viscoelastic liquids has been investigated by Allen and Roy (2000a; 2000b) using the linear Jeffreys and upper convective Maxwell equations respectively.

In spherical polar coordinates, r, ϕ, θ, these may be expressed as

$$T_{rr} + \lambda_1 \frac{\partial T_{rr}}{\partial r} = -2\mu_{Lo}\left(\frac{\partial u}{\partial r} + \lambda_1 \frac{\partial T_{rr}}{\partial r}\right) \tag{2.13}$$

$$T_{rr} + \lambda_1\left(\frac{\partial T_{rr}}{\partial r} + \frac{R^2\dot{R}}{r^2}\frac{\partial T_{rr}}{\partial r} + \frac{4R^2\dot{R}}{r^3}T_{rr}\right) = \frac{4\mu_L R^2\dot{R}}{r^3} \tag{2.14a}$$

$$T_{\theta\theta} + \lambda_1\left(\frac{\partial T_{\theta\theta}}{\partial r} + \frac{R^2\dot{R}}{r^2}\frac{\partial T_{\theta\theta}}{\partial r} - \frac{2R^2\dot{R}}{r^3}T_{\theta\theta}\right) = \frac{-2\mu_L R^2\dot{R}}{r^3} \tag{2.14b}$$

Similar studies have been carried out by Khismatullin & Nadim (2002) and Machado & Valente (2003) for a CAP with a linear viscoelastic shell, using the 4-constant Oldroyd equation. The results of these investigations indicate that the nature of the surrounding tissue may, in theory, have a significant effect upon CAP behaviour. However, none of the above authors consider the properties of specific tissues or the conditions encountered by CAPs *in vivo*. Dayton *et al* (2001) modelled a CAP oscillating inside a cell in order to examine the effects of phagocytosis[2] upon contrast enhancement. However, the cell was treated simply as an increase in the viscosity of the surrounding fluid, μ_L, in equation 2.11 and the interface between the cell and the surrounding liquid was neglected.

The influence of nearby boundaries upon the behaviour of free bubbles has been investigated fairly extensively (Lauterborn and Bolle 1975, Crum 1979, Blake *et al* 1986, Vogel *et al* 1989). These treatments include the formation of microjets, which occurs during involution of the bubble, as mentioned in Chapter 1. More recent investigations in this area have built on these earlier studies (e.g. Sato *et al* 1994; Akhatov *et al* 1997) and examined their significance in bio-medical applications such as ultrasound examinations of the lungs (Krasovitski and Kimmel 2001), sonoporation (Marmottant and Hilgenfeldt 2003; Gracewski *et al* 2004) and lithotripsy (Brujan 2004). Investigation has also been made of the effects of free bubble oscillation upon the wall of a capillary (Sassaroli and Hynynen 2004). To date however, there have been no theoretical treatments of coated microbubbles in enclosed surroundings.

[2] envelopment by certain types of white blood cells (phagocytes).

2.2.3 Modelling the sound field

2.2.3.1 The incident field

The nature of the incident field has a strong influence upon the behaviour of CAPs and free bubbles, owing to their compressibility and the fact that they resonate at a specific frequency. Analytical treatments have tended to model the incident field as an infinite, plane, continuous, sinusoidal wave for the sake of mathematical simplicity (e.g. Church 1995; Hoff *et al* 2000). The majority of medical applications and experimental studies, however, involve pulsed insonation. This is relatively simple to model if equation 2.9 is solved numerically, since $p_\infty(t)$ may be replaced by an arbitrary waveform in the time domain. For example, Postema *et al* (2003) used pulse waveforms recorded from their experimental equipment. In considering the response of a single CAP, the assumption of an infinite plane wave is normally valid, owing to the small size of the CAP (3×10^{-3} mm) relative to the wavelength of sound in blood at diagnostic frequencies (0.3 mm @ 5 MHz) and the width of the ultrasound beam ($\approx$ 1-50 mm, depending upon the type of focusing[3]).

A number of investigations have been made to determine whether image quality may be improved by modifying the incident spectrum to optimise CAP response and several reviews of these techniques have been made, e.g., Frinking *et al* (2000). One of the most common methods is to use a combination of two frequencies (ω_1 and ω_2) in order to generate an enhanced response at the difference frequency ($\omega_1 - \omega_2$). Various different versions of this technique have been developed (Wyzalkowski *et al* 2003) and the use of coded excitation ("chirps") has also been examined (Borsboom *et al* 2003). Each of these studies was performed using numerical methods by including the appropriate function $p_\infty(t)$ in equation 2.9 or 2.10. The effects of transmission through the surrounding tissue were neglected (c.f. section 2.2.3.3).

[3] The effect of beam focusing upon the behaviour of a single CAP is negligible because the size of the focal region is large compared with the diameter of the CAP. It is relevant to the behaviour of a CAP population, however, and this will be discussed in chapter 3.

2.2.3.2 The radiated field

The radiation from a single bubble or CAP may be modelled in a number of different ways. The simplest approach has been to neglect the passive[4] component of the scattered field and to treat the bubble/CAP as a rigid, spherical, pulsating source whose internal pressure does not vary during oscillation (de Jong *et al* 1994; Church 1995; Hoff *et al* 2000). The pressure radiated by such a source may be expressed as (Leighton 1994)

$$p_s = \frac{\rho_L R_o^2 \dot{R} \omega}{r} e^{i\left(\frac{\pi}{2} - k_L r\right)} \tag{2.15}$$

$\dot{R}$ may be substituted directly from the solution to, e.g., equation 2.9. Alternatively, it may be found analytically using $R_1 = R_{o1}(1 + x(t))$, $\dot{R}_1 = R_{o1}\dot{x}(t)$, $\ddot{R}_1 = R_{o1}\ddot{x}(t)$.

Substituting these expressions into equation 2.2 and retaining only terms linear in x, yields the equation

$$\ddot{x} + \delta_d \dot{x} + \omega_o^2 x = -\frac{p_A \sin(\omega t)}{\rho_s R_{o1}^2 \alpha} \tag{2.16}$$

where, following Church's notation

$$\omega_o^2 = \left[3\kappa p_o - \frac{2\sigma_1}{R_{o1}} - \frac{2\sigma_2 R_{o1}^3}{R_{o2}^4} + \frac{4V_s G_s}{R_{o2}^3}\left(1 + z\left(1 + \frac{3R_{o1}^3}{R_{o2}^3}\right)\right)\right]\left(R_{o1}^2 \rho_s \alpha\right)^{-1} \tag{2.17}$$

$$\alpha = \left[1 + \left(\frac{\rho_L - \rho_s}{\rho_s}\right)\frac{R_{o1}}{R_{o2}}\right] \tag{2.18}$$

$$\delta_d = 4\left(\frac{\mu_s V_s + \mu_L R_{o1}^3}{R_{o2}^3 R_{o1}^2 \rho_s \alpha}\right) + \delta_{rad} + \delta_{th} \tag{2.19}$$

$$z = \left[\frac{2\sigma_1}{R_{o1}} + \frac{2\sigma_2}{R_{o2}}\right]\frac{R_{o2}^3}{4V_s G_s}. \tag{2.20}$$

[4] i.e. that due simply to the presence of the bubble/CAP regardless of whether or not it is pulsating. This has been shown to be negligible for free bubbles and for CAPs with thin, flexible shells (Hilgenfeldt *et al* 1998).

Thus

$$p_s = \left(\frac{\rho_L R_{o1}}{\rho_S \alpha \left(\left(\frac{\omega_o^2}{\omega^2} - 1 \right)^2 + \frac{\delta_d^2}{\omega^2} \right)} \right) \frac{p_A i \sin(\omega t + \vartheta)}{r} e^{-ik_L r} = f \frac{p_{inc}(t)}{r} e^{-ik_L r} \quad (2.21)$$

where f is defined as the scattering function for the CAP or bubble[5].

This treatment neglects the work done on the gas inside the bubble or CAP during compression and is therefore valid only for very small amplitudes of oscillation. An improved estimate may be obtained by applying the analysis of Vokurka (Leighton 1994) to a CAP to yield

$$p_s(r) = \rho_L \left(\frac{R_2}{r} \left(R_2 \ddot{R}_2 + 2\dot{R}_2^2 \right) - \frac{\dot{R}_2^2 R_2^4}{2r^4} \right) - p_\infty \quad (2.22)$$

The derivation of this equation is shown in Appendix A.ii.

An alternative approach has been to treat the CAPs as elastic spherical shells and obtain the scattered acoustic field from a modal series solution of the linear wave equation. As shown by Hilgenfeldt *et al* (1998), the results are equivalent to those obtained from equation 2.22 in the linear limit (i.e. at very low insonation pressures). This method was applied by Ye (1996) to thin-shelled CAPs and more recently by Allen *et al* (2001) to CAPs with shells of varying thickness. It was suggested by the latter that Lamb waves excited on the CAP shell might produce extra, potentially useful, resonances responses and that CAPs might be manufactured with specific shell thicknesses to make them radiate at particular frequencies. This suggestion, however, does not take into account the fact that the higher mode responses may not propagate significantly into the surrounding fluid.

[5] Equations 2.17-2.22 refer to a CAP but equivalent expressions for a free bubble may be obtained by assuming $R_1=R_2=R$, $r_s=r_L$ and $G_s = \mu_s = 0$.

2.2.3.3 Additional effects

In the investigations discussed above, the incident and radiated fields have been considered in the immediate vicinity of the bubble or CAP. There are, however, a number of additional factors to consider in relating these fields to the signal which is transmitted initially and that which is actually detected by the receiving transducer. First of all, the transducers themselves have a finite diameter and bandwidth which defines the shape of the incident field and the sensitivity with which the radiated field can be detected. For the reasons given above, this is not usually taken into account in modelling a single CAP. However, simulations based on beam profiles recorded from medical scanners have been carried out by Chin and Burns (2000) to investigate the response from a CAP population.

Both the incident and radiated sound fields are also modified as a result of being propagated through the surrounding tissue. They may be reflected, refracted or diffracted at boundaries between different types of tissue, for example, between fat and muscle. However, these effects are likely to be relatively small compared with the signal produced by the CAPs, owing to the large difference in impedance contrast between tissue:tissue and tissue:gas interfaces. A more significant effect is likely to be non-linear propagation. The medium through which a sound wave is travelling is alternately compressed and expanded. Since the velocity of a given wavefront depends upon the local density of the medium, there is consequently a difference in the velocity at which compressions and rarefactions travel. The shape of the wave thus becomes increasingly distorted the further it travels through the medium (figure 2.1) and this distortion corresponds to an increase in the harmonic content of the frequency spectrum. Hence the sound field incident upon a CAP may differ considerably from that initially emitted by the transducer.

This phenomenon has been studied in a wide range of fluids, including different types of tissue (Duck 1990). One of the most common means of modelling non-linear propagation is to use the Khokhlov–Zabolotskaya–Kuznetsov (KZK) equation (Zabolotskaya and Khokhlov 1969).

This may be expressed as

$$\frac{\partial^2 p}{\partial y \partial t'} = \frac{c_{Lo}}{2}\nabla_{\perp}^2 p + \frac{\delta}{2c_{Lo}^2}\frac{\partial^3 p}{\partial t'^3} + \frac{\beta}{2\rho_{Lo}c_{Lo}^3}\frac{\partial^2 p^2}{\partial t'^2} \qquad (2.23)$$

where y is distance in the direction of the beam, β is the nonlinearity coefficient for the medium, δ is the sound diffusivity and t' is the retarded time $t - \frac{y}{c_{Lo}}$.

Kvikliene *et al* (2004) examined the effects of pulse distortion upon the response of a single CAP for insonation frequencies between 1-10 MHz, using equation 2.23 for propagation lengths of 50 mm in water and blood. Their results showed that the amplitude of the second harmonic in the received signal was underestimated when non-linear propagation was ignored. However, the discrepancy was only observable for CAPs having diameters greater than 2.5 μm and insonation pressures larger than 0.4 MPa. Moreover, the effect upon the frequency spectrum was small compared with the harmonic contribution from the CAPs. The effects of propagation through a volume of CAPs will be discussed in the next section.

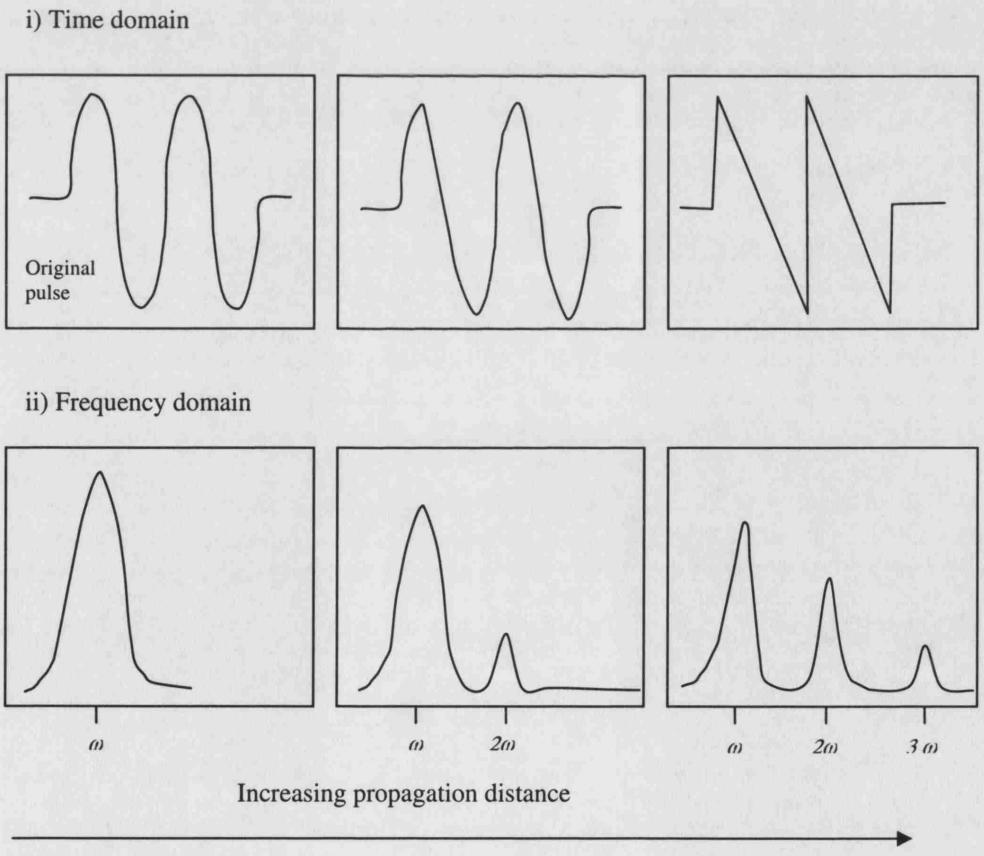

Figure 2.1: Illustrating the distortion of an ultrasound pulse due to non-linear propagation.

2.2.4 Modelling CAP populations

The models considered so far have been concerned with the behaviour of a single, bubble or CAP (equations 2.1-2.11). In practice, however, CAPs are administered in the form of high concentration suspensions (10^8 - 10^9 CAPs/ml) (Amersham Health PLC, 2003). Clearly these suspensions will be diluted after injection, but even if it is assumed that the CAPs will be uniformly distributed throughout the circulation, their concentration[6] will be of the order of 10^5 CAPs/ml. CAP behaviour may therefore be influenced not only by the surroundings *in vivo,* but also by interactions with other CAPs.

The simplest treatments for populations of free bubbles determine the overall acoustic properties for the suspension by summing the contributions of individual bubbles weighted according to the size distribution. For example Medwin (1977) gives the attenuation coefficient for a bubbly liquid as

$$a = 10\log_{10} e \int_0^\infty s_{ext} n(R) dR \tag{2.24}$$

where $n(R)\,dR$ is the number of bubbles of radius R per unit volume and s_{ext} is the extinction cross section for an individual bubble. This is defined as the ratio of the dissipated power P_{dis} to the intensity of the incident wave I_i

$$s_{ext} = \frac{\langle P_{dis} \rangle_t}{\langle I_i \rangle_t} \tag{2.25}$$

where subscripted brackets, $\langle\ \rangle_t$, indicates temporal averaging.

A similar approach has been adopted in the majority of CAP studies (e.g. de Jong 1994; Church 1995; Marsh *et al* 1997; Hoff *et al* 2000; Gorce and Schneider 2000). The extinction cross section s_{ext} may be obtained analytically using the linearization procedure described earlier to give

$$s_{ext} = \frac{4\pi R_o^2 \delta_d c_L \rho_L}{\left(\left(\omega_o^2 - \omega^2\right)^2 + \omega^2 \delta_d^2\right) \alpha \rho_s} \tag{2.26}$$

Alternatively, the average intensity and power dissipated over the course of a single pulse may be calculated via numerical integration (e.g. Hilgenfeldt *et al* 2000).

[6] assuming an average adult human blood volume of 5 litres (Guyton and Hall 1990) and and injected volume of 1 ml (Amersham Health PLC, 2003).

The use of equation 2.24, however, ignores the fact that the sound field incident on a particular bubble will consist not only of the insonating signal, but also of contributions from the radiated fields of neighbouring bubbles (figure 2.2). The resulting multiple scattering problem was addressed by Foldy (1945) who defined an effective wave number K_{eff} for a random distribution of scatterers, such as a suspension of bubbles. This may be expressed as

$$K_{eff}^2 = k_L^2 + 4\pi nf \qquad (2.27)$$

where $k_L = \omega/c_L$ is the wave number of the suspending fluid with no scatterers present, n is the scatterer concentration and f is the scattering function for an individual scatterer, obtained as shown in the previous section (equation 2.21).

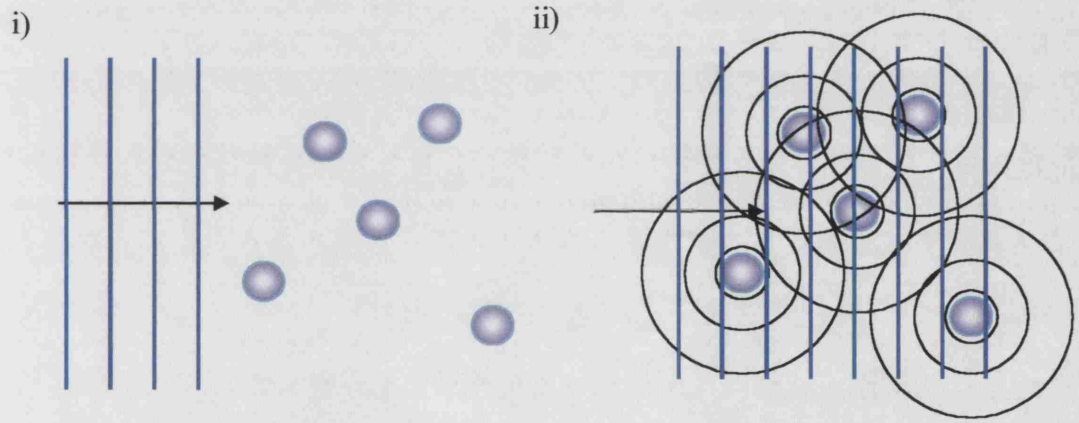

Figure 2.2: Schematic illustration of multiple scattering in CAP populations.

In deriving equation 2.27 it was assumed that the mean field incident upon any one scatterer is large compared with the field scattered by its close neighbours and that each scatterer rescatters the field just once. The validity of Foldy's model is therefore restricted to relatively low concentration suspensions. A more recent model for multiple scattering, which takes account of additional scattering events from each scatterer and is therefore valid for higher concentrations, was derived by Henyey (1999) and states that:

$$K_{eff}^2 = k_L^2 + 4\pi nF \qquad \text{where} \qquad F = \left(\frac{1}{f} k_L - K_{eff} \right)^{-1} \qquad (2.28)$$

The validity of equation 2.28 is restricted to the regime $n|f|^3<<1$ as contributions of this order and beyond are not considered. An alternative approach has been to consider the individual bubbles in a population and determine the total sound field at each point in space and time (e.g. Ye *et al* 2000). This enables higher concentrations to be modelled, but is only suitable for relatively small numbers of CAPs owing to the high computational requirements.

Equations 2.27 and 2.28 and treatments of higher order multiple scattering such as those due to Waterman and Truell (1961) and Lloyd and Berry (1967), are valid for linear oscillations and therefore have limited application to bubbles or CAPs. In 1968, Van Wijngaarden presented a heuristic treatment of the non-linear multiple scattering problem for free bubbles (Van Wijngaarden 1968). A more mathematically rigorous derivation of his results was provided by Caflisch *et al* (1985) and was subsequently modified by Commander & Prosperetti (1989) to include a more realistic treatment of the filling gas. A number of other models (e.g. Omta 1987, D'Agostino and Brennen 1988) have also been presented, but these do not differ fundamentally from the Van Wijngaarden/Caflisch treatment. The derivation of this model will be described fully in Chapter 3.

The problem of non-linear multiple scattering in CAP populations has received relatively little attention. The simulations by Chin and Burns (2000) did not consider multiple scattering between CAPs and neglected the presence of an encapsulating shell around each CAP. Church (1995) cited some approximate equations for determining the phase velocity and attenuation of ultrasound in a CAP suspension, based on Commander and Prosperetti's linear analysis. These were only valid for relatively low concentrations, however, at frequencies far below those corresponding to CAP resonance. They were consequently of little use in determining the significance of multiple scattering under diagnostic conditions. A new model for non-linear multiple scattering has recently been developed by the author (Stride and Saffari 2005) which is suitable for CAP concentrations up to 10^6 CAPs/ml. This will be described in Chapter 3.

There is a further, important, aspect of modelling a CAP population, which has been identified, although not addressed, by several authors (e.g. Chin and Burns 2000; Shi and Forsberg 2000). This involves the changes in the population and hence in the

acoustic response, which take place with time once the CAPs have been injected into the body. These changes may be due to a number of processes, including mechanical damage in the heart, phagocytosis and the effects of pressure fluctuations and variations in blood gas content. Mechanisms of CAP destruction are discussed further in the next section. Clustering between CAPs may also take place as a result of "secondary radiation" or "Bjerknes" forces which arise from the pressure gradient set up around each CAP due to energy dissipation during insonation (Leighton 1994). As shown in Appendix A.iii however, these forces are unlikely to be significant under diagnostic conditions.

2.2.5 Modelling CAP destruction

There are a number of different mechanisms by which both free bubbles and CAPs may be destroyed. In the absence of any external influences, such as an ultrasound field, a bubble or CAP will eventually dissolve as a result of surface tension, which gives rise to a positive pressure p_σ (the Laplace pressure) at the CAP surface

$$p_\sigma = \frac{2\sigma}{R} \tag{2.29}$$

The dissolution time may be determined for a free bubble from the equation given by Epstein and Plesset (1950)

$$\frac{dR}{d\tau} = -\frac{3R_o((1-C_i/C_s)R+\delta R_o)}{3R+2\delta R_o}\left(\frac{\tau R_o}{R}+2\sqrt{\left(\frac{C_s}{2\pi\rho_G}\right)}\right) \tag{2.30}$$

Where C_i is the initial gas concentration in the surrounding fluid, C_s is the saturation gas concentration, M_G is the molecular weight of the gas, B is the gas constant, T is absolute temperature and ρ_{Gp} is the density of the gas for a gas/liquid interface of zero curvature. τ is non-dimensionalised time

$$\tau = \sqrt{\left(\frac{2\kappa C_s}{\rho_G R_o^2}\right)}t \qquad \text{and} \qquad \delta = \frac{2M_G\sigma}{BT\rho_{Gp}R_o}.$$

In the case of a CAP, the dissolution process is inhibited significantly by the presence of the encapsulating shell. However, whilst the effect of a surfactant layer upon surface tension has been studied extensively (c.f. e.g. Israelachvili 2003) there

has been no theoretical analysis of CAP dissolution in which the shell has been taken into account. In the case of a free bubble, the imposition of a sound field may accelerate dissolution or, under certain conditions, it may in fact promote bubble growth. The latter process of "rectified diffusion" takes place because the surface area of the bubble is smaller during compression than during expansion. The degree to which gas diffuses into the bubble may therefore exceed that to which it diffuses outwards into the liquid. There is also a "shell effect" due to the fact that the local concentration of gas in the surrounding fluid is higher during bubble expansion than during compression. This again encourages inwards diffusion (Leighton 1995).

Whether or not a bubble undergoes rectified diffusion depends up on its initial size, the insonation frequency and pressure and the solubility and content of the gas in the surrounding fluid. Several thresholds for rectified diffusion have been defined for free bubbles (e.g. Crum 1984; Church 1988) but once again there have been no treatments which include an encapsulating shell, although this will clearly have a significant effect. Based on the existing thresholds, only air-filled[7] CAPs would be expected to exhibit rectified diffusion and only then if insonation were continuous and the influence of the shell were negligible.

At higher insonation pressures, CAPs and bubbles may also undergo much more rapid destruction processes. The disintegration of free bubbles undergoing "inertial" or "transient" collapse has been treated extensively in the numerous studies of acoustic cavitation (c.f. e.g. Neppiras 1980). As a result, the conditions for the onset of inertial collapse and fragmentation have been well established, in the form of threshold bubble sizes and acoustic pressures (Flynn 1964; Apfel and Holland 1991). The few theoretical treatments of CAP destruction have been based upon these conditions (Chomas *et al* 2001) and have neglected the effect of the encapsulating shell. Similarly, studies of loss-of-correlation imaging (e.g. Frinking *et al* 1999) have concentrated on the behaviour of the free gas bubbles released after shell rupture, rather than the destruction process itself, although, as will be shown in Chapter 3, a preliminary investigation of the influence of the shell has been made by the author (Stride and Saffari 2003).

[7] the concentration in the blood of other filling gases such as perfluorocarbons would be too low for significant inwards diffusion to occur.

2.3 Experimental investigations

2.3.1 Characterisation

Equations 2.8 and 2.9 were initially used to model Albunex®, which was the most widely available commercial agent during the early 1990s. Subsequently, however, equations 2.8-2.11 have been applied to a variety of polymer and surfactant-shelled CAPs (Hoff *et al* 2000; Gorce and Schneider 2000; Postema *et al* 2003). According to Hoff *et al*, their results for suspensions of polymer encapsulated CAPs showed good agreement between the measured and expected attenuation for "low" incident pressure amplitudes and concentrations, although these quantities were not specified. Morgan *et al* (1999) similarly reported good agreement between their model results and optical measurements of individual CAP oscillations using "streak" imaging.

In contrast, de Jong *et al* (1994) found that there were considerable discrepancies between their experimental and theoretical scattering and attenuation coefficients for Albunex® at higher acoustic pressures. These were attributed to a number of factors including: invalidity of the assumptions made regarding the CAP size distribution; uncertainty regarding the nature of the incident field; inadequacy of analytical methods for describing harmonic response; and pressure dependency of model parameters. Frinking *et al* (1997; 1999) also showed that the RPNNP model could not accurately predict scattering above a certain level of incident pressure (≈200 kPa) and Shi & Forsberg (2000) found that none of the existing models were capable of predicting effects such as the sub-harmonic and ultra-harmonic generation which they observed at high acoustic pressures.

Forsberg *et al* (1999) reported discrepancies between their model predictions and *in vivo* measurements of contrast enhancement for CAPs with a range of different surfactant coatings and filling gases. It was suggested that these were due to their neglect of multiple scattering and uncertainty in the shell parameters which could have been affected by chemical interactions after injection. Marsh *et al* (1999) also found that there was considerable variation in the value of the shell parameters (G_s and μ_s) derived from scattering and attenuation measurements for Albunex® suspensions with different concentrations (table 2.1). Moreover, their results were in poor agreement with those obtained by de Jong *et al* (1994) for the same agent, using similar methods (table 2.1).

Investigator	Concentration	Pulse centre frequency	Peak pressure	Shell shear modulus	Shell viscosity
	(10^6CAPs/ml)	(MHz)	(MPa)	(dyn/cm)	(dyn s/cm)
de Jong *et al* (1994)	0.02-2	5.0	not given	8000	0.004
Marsh *et al* (1999)	0.059-1.9	5.0	0.24	4200 (±1000)	0.0054 (±0.0015)

Table 2.1: Variation in the shell parameters derived for Albunex®.

The evidence for multiple scattering effects is discussed below, but there are indications that this may not be the sole explanation of the above discrepancies. Despite reporting good agreement between their theoretical and experimental results, Hoff *et al* (2000) found that the variation in the shell parameters derived for different runs of the same experiment was large compared with the uncertainty in their measurements. This indicates that there may be considerable variability between individual CAPs, for example, in shell thickness and/or material properties. This conclusion is reinforced by optical observations made by Postema *et al* (2003) of phospholipid CAPs oscillating in an ultrasound field, which demonstrated a wide variation in the response of ostensibly identical CAPs.

To date there have been no independent measurements of CAP shell properties. Extensive measurements of the rheological properties of organic films have been made using a variety of methods (c.f. Israelachvili 2003). More recent techniques include surface wave measurements (Sonin *et al* 1993), atomic force microscopy (Dufrene *et al* 1998) and optical tweezers (e.g. Helfer *et al* 2001). Similarly, the mechanical properties of red blood cell membranes have been determined using micropipette aspiration (Evans 1973; Evans *et al* 1976). The latter method was adopted by Kim *et al* (2003) to measure the properties of phospholipid membranes but it was not possible to derive a constitutive equation from the results obtained. Gorce and Schneider (2000) attempted to address the problem of variation in shell thickness by comparing their experimental results with simulations from two different models. In the first model, the shells were considered to have constant thickness. In the second, thickness was taken to be a certain fraction of the CAP radius. Unfortunately the error in the results was too great to enable a reliable conclusion to be drawn.

A further problem with the use of broadband acoustic measurements to derive CAP properties was identified by Sboros *et al* (2002) and independently by Chen *et al* (2002). These investigators found that the scattering and attenuation coefficients for suspensions of Quantison™, Definity® and Optison® were sensitive to changes in the insonation pressure. This may be explained in terms of the increase in the non-linear character of CAP response with increasing amplitudes of excitation (Appendix A.iv). Consequently, the scattering and attenuation coefficients must be treated as functions of both the incident frequency and pressure.

2.3.2 Influence of the surrounding fluid

The majority of the experiments conducted on ultrasound contrast agents have been performed in distilled water, isoton® or saline (e.g. de Jong *et al* 1994; Moran *et al* 1998). Experiments involving CAPs suspended in blood have been carried out, but with the aim of examining the effect upon cell integrity, rather than upon CAP response (Miller *et al* 1995; Dalecki *et al* 1997; Khanna al 2003; Chelly *et al* 2002). Dayton *et al* (2000) accompanied their theoretical investigation with optical and acoustic observations of phagocytosed CAPs. They found that phagocytosis reduced the amplitude of CAP oscillation in accordance with their predictions. However, with the exception of recent work by the author (Stride and Saffari 2004b, c.f. Chapter 3), there have been no specific investigations of the effects of changing the surrounding fluid upon CAP behaviour.

There have been fairly extensive experimental investigations of the influence of a nearby boundary upon the behaviour of a free bubble. The first experimental evidence for bubble involution leading to the formation of a jet was obtained by Naudé and Ellis (1961). Subsequently, Lauterborn and Bolle (1975) also photographed the collapse of laser-generated bubbles oscillating close to a solid surface and found that their results compared favourably with the predictions of Plesset and Chapman (1971). Similar studies have been conducted, e.g. by Crum, as described in Prosperetti (1984), and have been comprehensively reviewed by Leighton (1994). There has been relatively little experimental investigation, however, of the behaviour of CAPs near boundaries.

Zhong *et al* (2001) performed experiments to assess how the presence of a vessel wall, simulated by silicone and cellulose tubes, affected the oscillation and inertial collapse of a CAP induced by lithotripter shock waves. However, they used a free bubble rather than a CAP and the insonation pressures and pulse repetition frequencies were far higher than would be used diagnostically. Recent experimental evidence (Postema *et al* 2004) indicates that phospholipid-coated microbubbles will exhibit some of the phenomena which have been observed with free bubbles, including the formation of microjets. However, further work is needed to improve the definition of the conditions under which these observations were made, since the sound field was not fully characterised and the results were somewhat surprising given that the nominal insonation pressures were very low.

2.3.3 The sound field

There have been many experimental investigations demonstrating the effectiveness of the insonation schemes used with contrast agents, such as pulse inversion (Hope Simpson *et al* 1999) and dual frequency techniques (Bouakaz *et al* 2002). These illustrate the sensitivity of CAPs both to the frequency spectrum of the incident field and to the insonation pressure, in terms of the degree of non-linearity in the response and whether or not the CAPs are destroyed. There have been far fewer investigations of the nature of the incident and radiated sound fields themselves however.

Kvikilene *et al* (2004) made measurements of the distortion of an ultrasonic pulse for different insonation pressures in water. They then used the resulting waveforms to investigate the effect of non-linear propagation upon CAP response theoretically. Similarly, there have been numerous studies of non-linear propagation in a wide range of fluids for medical imaging (Humphrey 2000; Duck 2002). To date, however, there have been no attempts to examine the effects of non-linear propagation, or any other type of distortion, upon CAP response experimentally. Moreover, the characterisation of the sound fields used for *in vitro* experiments tends to be based on single hydrophone measurements of the pressure at the focus of the transducer, rather than measurements of the whole beam profile. *In vivo* characterisation depends upon the accuracy of the parameters defined by the scanner and is even less certain.

Measurements of the field radiated by a CAP have been made mainly from whole populations in order to derive scattering cross sections (e.g. de Jong *et al* 1992; Gorce and Schneider 2000; Forsberg *et al* 1999; Hoff *et al* 2000). Measurements of the backscatter from individual CAPs have been made by Sboros *et al* (2003) and used to investigate the pressure dependence of CAP response for Quantison® and Definity®. However, the measurements were based on the intensity of the image produced by a medical scanner rather than recorded waveforms or frequency spectra. Kamiyama *et al* (1999) recorded the echoes from Levovist® suspensions whose concentrations were sufficiently low to enable single CAP responses to be identified. Similarly, Dayton *et al* (1999) and Chomas *et al* (2001) recorded responses from single Albunex®, Optison® and phospholipid-coated CAPs. The main interest of these investigations, however, was CAP destruction and the results were not compared with theoretical simulations.

2.3.4 Population response

2.3.4.1 Secondary radiation forces

In 1975 Crum obtained photographic evidence of free bubble clustering as a result of secondary radiation forces and carried out measurements of the relative speeds of approach (Crum 1975). Similar investigations of the secondary radiation forces between CAPs were made by Dayton *et al* (1997; 1999). These confirmed the occurrence of clustering and there was found to be good agreement between the predicted and measured speeds of approach of neighbouring CAPs. The clusters were found to be resistant to separation during insonation, even at low pressures, but dispersed as soon as transmission was stopped. Thus the effects of secondary radiation forces were only found to be significant at high pulse repetition frequencies (>10 kHz). Under these conditions however, the CAPs were found to have increased resistance to destruction. The exposure geometry was such that shielding of the centre of the cluster by the outer CAPs could not explain the effect. There was also found to be a change in acoustic response, as discussed below, indicating that the dynamic response of each CAP was affected by the presence of its neighbours.

2.3.4.2 Multiple scattering

Numerous experimental studies of free bubble arrays have been made, demonstrating a wide variety of collective bubble behaviour. These have been comprehensively reviewed in the articles by Commander and Prosperetti (1989), Chahine (1993) and Leighton (1995). However, the conditions under which the majority of these studies were carried out differ considerably from those relevant to ultrasound contrast agents. The discussion will therefore be restricted to CAPs and the most recent studies of free bubbles under relevant conditions.

Marsh *et al* (1997) performed attenuation and phase velocity measurements in suspensions of Albunex® and found that the peak attenuation was underestimated by equation 2.24 for suspensions with concentrations greater than 10^6 particles/ml by up to 10 dB. Similarly, Soetanto & Chan (2000) found that the discrepancy between their experimental results and model predictions became increasingly pronounced the higher the concentration used. As mentioned above, Dayton *et al* (1999) observed a distinct variation in the acoustic response of a CAP cluster compared with that of a low concentration suspension. This took the form of a reduction in the harmonic content of the scattered signal. A similar effect was reported by Moran *et al* (2002) who observed a reduction in the backscattered power with increasing concentration from suspensions of four different contrast agents (Optison®, Definity®, Sonazoid® and Sonovue®) with concentrations greater than 10^6 CAPs/ml. Further effects relating to CAP populations and the influence of CAP interactions upon destruction processes will be discussed in the next section.

2.3.5 CAP destruction

2.3.5.1 Static diffusion

As might be expected, the stability of CAPs in the absence of an ultrasound field has been shown to depend upon both the nature of the filling gas and the encapsulating shell. CAPs containing high molecular weight gases and having phospholipid coatings have been found to be more stable than those containing air or having polymer or albumin shells. These, in turn, have been shown to be more stable than those with other surfactant coatings such as Levovist® (Dayton *et al* 1999; Sboros *et al* 2000). Podell *et al* (1999) conducted extensive tests of the stability of Optison® and concluded that, in the absence of ultrasound, the gas content of the surrounding

fluid was also a significant factor in CAP destruction. Gas deficiency in the surrounding fluid was found to produce an irreversible outward diffusion of the filling gas, causing the CAPs to shrink down to an undetectable size in a relatively short time. In contrast, chemical dissolution of the shell in a variety of solutions (acid, alkaline, reducing etc.) was found to be relatively negligible.

2.3.5.2 Acoustically driven diffusion

Podell *et al* (1999) also found that the rate of CAP dissolution was increased, both by reducing the concentration of the CAP suspension and by the imposition of an external pressure. This indicated that the process would also be accelerated by the presence of an ultrasound field and this was indeed found to be the case for Levovist® (Sboros *et al* 2000), Optison® and MP1950 (Dayton *et al* 1999)[8]. Conversely, Sboros *et al* (2000) found that Quantison™, DMP115 and Myomap™ were stable over long periods of insonation[9] under the same conditions, even when the oxygen concentration of the surrounding fluid was varied.

Chomas *et al* (2001) investigated the change in radius of Optison® and MP1950 CAPs at 2.25 MHz and 0.24 MPa. They also found that dissolution was enhanced by ultrasound excitation, but observed that the Optison® CAPs appeared to be disrupted by the first pulse of ultrasound and then shrank continuously, whilst the phospholipid-coated CAPs shrank in finite steps corresponding to the periods of insonation. It should be noted that these studies did not take into account the differences in shell properties or size distributions and the resulting differences in resonance frequency. To date, rectified diffusion has not been observed experimentally for CAPs.

2.3.5.3 Fragmentation

At higher insonation pressures (>1 MPa) both Dayton *et al* (1999) and Chomas *et al* (2001) observed that Albunex®, Optison® and MP1950 CAPs fragmented into arrays of smaller bubbles. Qualitatively, this behaviour is similar to that exhibited by free bubbles and there is some controversy as to whether CAP fragmentation and inertial cavitation are in fact the same process. Shi *et al* (2000) found that the acoustic response of Sonazoid® differed from that expected for inertial cavitation,

[8] The insonation conditions were 3 MHz, 0.27 MPa and 2.25 MHz, 0.1 MPa respectively.
[9] up to several days.

being more prolonged and lacking the characteristic pressure "spikes." Uhlendorf (2000) and Chen *et al* (2000) also found that the thresholds for CAP rupture and inertial cavitation thresholds were different, the latter being considerably higher. However, Church & Carstensen (2001) reinterpreted Shi *et al*'s results and suggested that the disparity between the acoustic signals corresponding to high pressure CAP destruction and inertial cavitation, was in fact due to the signal processing employed by Shi *et al*, rather than any physical difference in these processes.

The matter has yet to be resolved, but regardless of whether or not Sonazoid® CAPs undergo inertial cavitation, it is unlikely that the findings for one type of agent can be applied to all others. It is clear from the results discussed above that the nature of the encapsulating shell is an important factor in determining CAP stability in the absence of ultrasound or at low insonation pressures. It is also clear that it has a strong influence upon CAP behaviour. For example, Dayton *et al* observed that albumin-shelled CAPs do not pulsate spherically even at relatively low insonation pressures. Rather, they were seen to buckle during the initial compression, after which a part of the shell underwent low amplitude expansion and contraction.

It would also seem logical to assume that the shell must play some role in CAP destruction. Fragmentation of a solid or semi-solid object must necessarily involve fracture of the material from which it is made. CAP destruction must therefore be affected by the mechanical properties of the shell and is thus distinct from a true cavitation collapse. Again the results of Dayton *et al* support this conclusion. At moderate insonation pressures (0.4 MPa) Optison® CAPs were seen to develop defects resulting in the release of a free gas bubble. Takeuchi *et al* (1997), Kudo *et al* (2000) and Postema *et al* (2004) reported similar observations of "sonic-cracking" for both albumin and polymer-coated CAPs. These observations support the hypothesis of Frinking and de Jong (1997) that the non-linear signal, used for imaging at high insonation pressures, is due to the release of a free bubble. This was also the conclusion drawn by Moran *et al* (2000). Clearly once shell rupture has taken place, the resulting free bubble could undergo genuine inertial cavitation, stable or unstable, depending on its size.

Shell rupture has not been observed for phospholipid-coated CAPs and their behaviour would appear to be more closely related to that of free bubbles. At lower insonation pressures for example, MP1950 CAPs were seen to remain spherical during oscillation (Chomas *et al* 2001) rather than buckling. The amplitudes of oscillation, however, were found to be smaller than would be predicted for a free bubble, indicating that the coating does influence CAP behaviour to some extent. Chomas *et al* also found that there was very poor agreement between their experimental results and theoretical stability criteria for the fragmentation of free bubbles.

2.3.5.4 Shielding

Klibanov *et al* (1998) found, by direct observation, that the destruction of insonified Albunex® CAPs tethered to a polystyrene plate occurred by a process of gradual deflation. The rate of deflation increased with: i) reducing CAP concentration, ii) the presence of a flow, iii) increasing acoustic pressure and iv) increasing pulse length and repetition rate. Two explanations were proposed for the "self protection" effect observed with high CAP concentrations. The first was that a layer of gas saturated fluid would be built up around a high concentration CAP cluster which would discourage further diffusion.

This was in agreement with the finding that the protective effect was less evident in the presence of a flow, which would have prevented the formation of a saturated layer. It did not concur, however, with the fact that only the edges of each cluster were affected, since the CAPs were not so closely spaced that the flow could not penetrate between them. The preferred explanation was that the response of the CAPs was modified by the influence of the radiated fields from its neighbours and that this slowed down the diffusion process. This would concur with the observations of multiple scattering discussed earlier and the fact that Dayton *et al* (1999) observed that clustering due to secondary radiation forces limited CAP destruction. This may also explain the large differences in the degree of CAP destruction reported by Frinking *et al* (1999) and Chomas *et al* (1% as opposed to 70%) under similar insonation conditions but for very different CAP concentrations.

2.3.6 Contrast agent design

The use of high molecular weight gases such as sulphur hexafluoride in order to improve the stability of contrast agents has already been discussed in Chapter 1. Similarly, the development of new agents having composite shells, to enable them to be used for both diagnostic and therapeutic applications, has also been examined. There are several other areas of development. For example, the possibility of producing nanobubble CAPs is being explored (Oeffinger and Wheatley 2004) with a view to extending the range of ultrasound imaging to the smallest capillaries. There is also growing interest in the creation of new agents designed specifically for imaging at high frequencies (>30 MHz) to improve image resolution for, e.g., detection of arterial plaque (Moran *et al* 2003). At present, the development of new agents is based on experimental optimisation procedures. It has been shown, however, that the design process may be enhanced by adopting a theoretical approach (Stride 2005) and this will be demonstrated further in this thesis.

The attachment of targeting species to CAP shells is also a rapidly expanding area of research (c.f. e.g. Klibanov *et al* 1999; May *et al* 2000), and recently the possibility of producing CAPs with crumpled shells has been investigated in order to increase the surface area available and hence the likelihood of attachment (Klibanov *et al* 2004). An increase in the rate of attachment has been demonstrated although the effect of crumpling upon the acoustic response of the CAP has not yet been examined. Again, as mentioned in Chapter 1, it has been suggested that there may be other therapeutic applications for CAPs, in addition to drug delivery. As yet there have been no reported attempts at designing agents for these procedures. However, it has been shown that the heating effect generated by CAPs may be determined by the properties of the CAP shell (Stride and Saffari 2004a) and the implications of this for CAP safety and design will be discussed in Chapter 5.

2.4 Summary

The aim of this review has been to examine the existing theoretical and experimental evidence to clarify the extent to which contrast agents are currently understood and to identify areas requiring further research. It has been shown that, whilst there have been extensive investigations of the behaviour of free bubbles, the results are often inapplicable to CAPs, owing to the presence of the encapsulating shell. At present, the characterisation of existing shell materials is somewhat limited, both in terms of the models used and the experimental data available. Similarly, there has been relatively little investigation of the effect of the surrounding fluid upon CAP behaviour and upon the propagation of the incident and radiated sound fields. The effects of multiple scattering within a CAP population have also received little attention and there remains a considerable degree of controversy regarding the mechanisms of CAP destruction. In terms of CAP design, whilst new contrast agents have been developed for a wide range of applications, there has been have been no attempts to optimise CAP performance theoretically. The aim of the subsequent chapters is to address these areas.

3

Theoretical Characterisation

3.1 Overview

In order to improve contrast agent effectiveness, an accurate model of CAP behaviour is required to enable different designs and/or insonation schemes to be investigated. As described in Chapter 2, a number of models describing the response of a single, coated gas bubble to an imposed sound field have been developed (Fox and Herzfeld 1954; Glazman 1983; de Jong *et al* 1992; Church 1995; Khismatullin *et al* 2002; Morgan *et al* 1999). All of these treatments are limited to some degree by the assumptions upon which they rely and in the absence of reliable experimental data for shell characterisation it is not possible to assess their relative worth. The aim of this chapter is to derive a generalised model, of which the models mentioned above represent specific forms. The individual terms will then be examined to determine the most appropriate form of the model for a particular set of conditions.

3.2 Formulation of generalised model for a single CAP

In common with previous treatments, the CAP is modeled as a spherical volume of gas enclosed by a stabilising outer layer and surrounded by liquid (figure 3.1). For the sake of consistency, the notation used in the previous chapter has been retained, whereby R_1 and R_2 are the inner and outer radii of the CAP, ρ is density, u is radial velocity, p is pressure, t is time, $\mathbf{T}$ is the stress tensor with components T_{rr}, $T_{\theta\theta}$ etc. and r, θ and ϕ represent spherical polar coordinates with their origin at the CAP centre.

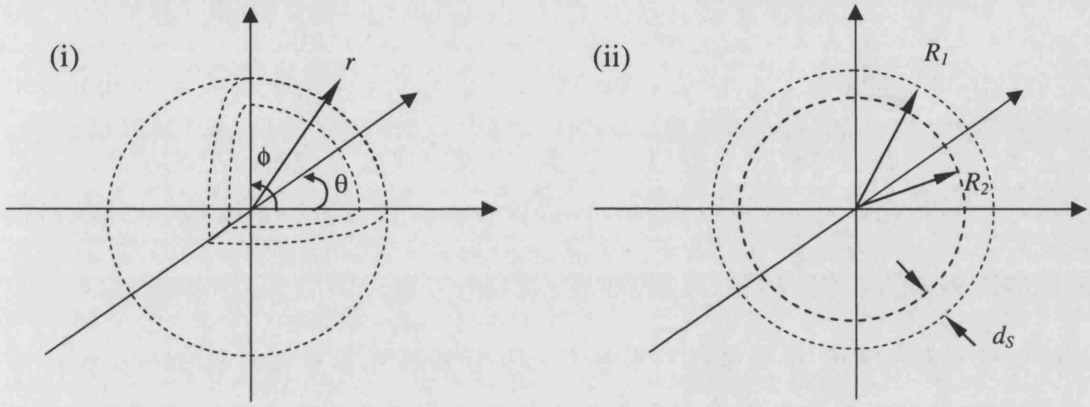

Figure 3.1: Schematic representation of a CAP (i) Three-dimensional view indicating coordinate system (ii) Cross-sectional view indicating dimensions.

Assuming spherical symmetry, conservation of momentum (Landau and Lifshitz 1987) yields

$$\rho\left(\frac{\partial u}{\partial t}+u\frac{\partial u}{\partial r}\right)+\frac{\partial p}{\partial r}=\frac{\partial T_{rr}}{\partial r}+\frac{2T_{rr}-T_{\theta\theta}-T_{\phi\phi}}{r}. \qquad (3.1)$$

Similarly, from conservation of mass

$$\frac{\partial \rho}{\partial t}+\rho\frac{\partial u}{\partial t}+u\frac{\partial \rho}{\partial r}+\frac{2\rho u}{r}=0. \qquad (3.2)$$

Integrating equation 3.1 over the three regimes for the gas, shell and surrounding liquid gives

$$\int_0^{R_1}\left[\rho_G\left(\frac{\partial u}{\partial t}+u\frac{\partial u}{\partial r}\right)+\frac{\partial p}{\partial r}=\frac{\partial T_{G,rr}}{\partial r}+\frac{2T_{G,rr}-T_{G,\theta\theta}-T_{G,\phi\phi}}{r}\right]dr$$
$$+\int_{R_1}^{R_2}\left[\rho_S\left(\frac{\partial u}{\partial t}+u\frac{\partial u}{\partial r}\right)+\frac{\partial p}{\partial r}=\frac{\partial T_{S,rr}}{\partial r}+\frac{2T_{S,rr}-T_{S,\theta\theta}-T_{S,\phi\phi}}{r}\right]dr \qquad (3.3)$$
$$+\int_{R_2}^{\infty}\left[\rho_L\left(\frac{\partial u}{\partial t}+u\frac{\partial u}{\partial r}\right)+\frac{\partial p}{\partial r}=\frac{\partial T_{L,rr}}{\partial r}+\frac{2T_{L,rr}-T_{L,\theta\theta}-T_{L,\phi\phi}}{r}\right]dr=0$$

where subscripts *G*, *S* and *L* represent the gas, shell and liquid respectively.

If it is assumed, for the present, that the density, elasticity and viscosity of the filling gas will be considerably smaller than those of the solid shell or the surrounding fluid, then the first integral in equation 3.3 may be neglected. Similarly, if the surrounding fluid is considered to be infinite, i.e. the presence of boundaries such as blood vessel walls and other CAPs is ignored, there is no need to modify the third integral. The validity of these assumptions will be discussed shortly.

If the presence of other CAPs in the fluid is ignored, then, at the frequencies relevant for medical ultrasound (1-20 MHz), the speed of the CAP wall (≈10 m/s) will be much smaller than the speed of sound in either the shell or the surrounding fluid (≈1500 m/s) (see section 3.4.1). The densities ρ_s and ρ_L may therefore be treated as constants and hence from equation 3.2

$$u(r,t)r^2 = const. = R_1^2(t)\dot{R}(t) \qquad (3.4)$$

The surface energy associated with the two interfaces on either side of the shell may be found approximately as

$$E_{1or2} = \sigma_{1or2}A_{1or2} + \frac{\xi_{1or2}}{A_{1or2}} = \sigma_{1or2}4\pi R_{1or2}^2 + \frac{\xi_{1or2}}{4\pi R_{1or2}^2} \qquad (3.5)$$

where $A_{1\ or\ 2}$ represents the interfacial area, $\sigma_{1\ or\ 2}$ the surface tension and $\xi_{1\ or\ 2}$ the resistance to compression of the inner and outer surfaces respectively (Boal 2002).

For thermodynamic equilibrium to be maintained, there must be a balance between the variations in surface energy, the work done associated with viscoelastic stresses in the shell and the pressure work associated with changes in CAP volume.

For example, for the inner surface of the CAP the pressure work for a small change in volume $\delta V = 4\pi R_1^2 \delta R$ is given by

$$p\delta V = \left(p_G(R_1,t) - p_S(R_1,t)\right)4\pi R_1^2 \delta R \tag{3.6}$$

The corresponding change in surface energy is given by

$$\delta E = 8\pi R_1 \sigma_1(R_1,t)\delta R_1 + 4\pi R_1^2 \frac{\partial \sigma_1}{\partial R_1}\delta R_1 + \frac{\delta R_1}{4\pi R_1^2}\frac{\partial \xi_1}{\partial R_1} - \frac{2\xi_1(R_1,t)\delta R_1}{4\pi R_1^3} \tag{3.7}$$

and the work associated with stresses in the shell by

$$T_{rr}\delta A = \left(T_{S,rr}(R_1,t) - T_{G,rr}(R_1,t)\right)4\pi R_1^2 \delta R. \tag{3.8}$$

Likewise for the outer surface

$$p\delta V = \left(p_S(R_2,t) - p_L(R_2,t)\right)4\pi R_2^2 \delta R \tag{3.9}$$

$$\delta E = \left(\begin{array}{l} 8\pi R_2 \sigma_2(R_2,t)\delta R_2 + 4\pi R_2^2 \dfrac{\partial \sigma_2}{\partial R_2}\delta R_2 \\ \quad + \dfrac{\delta R_2}{4\pi R_2^2}\dfrac{\partial \xi_2}{\partial R_2} - \dfrac{2\xi_2(R_2,t)\delta R_2}{4\pi R_2^3} \end{array}\right) \tag{3.10}$$

$$T\delta A = \left(T_{L,rr}(R_2,t) - T_{S,rr}(R_2,t)\right)4\pi R_2^2 \delta R \tag{3.11}$$

Thus, dividing through by $4\pi R_{1or2}^2 \delta R$ and letting $\xi'_{1or2} = \dfrac{\xi_{1or2}}{16\pi^2}$, the boundary conditions for either side of the shell may be written as

$$\begin{aligned} p_G(R_1,t) = {} & p_S(R_1,t) - T_{S,rr}(R_1,t) \\ & + \frac{2\sigma_1(R_1,t)}{R_1} + \frac{\partial \sigma_1}{\partial R_1} + \frac{1}{R_1^4}\frac{\partial \xi'_1}{\partial R_1} - \frac{2\xi'_1(R_1,t)}{R_1^5} \end{aligned} \tag{3.12}$$

$$\begin{aligned} p_S(R_2,t) = {} & T_{S,rr}(R_2,t) + p_L(R_2,t) - T_{L,rr}(R_2,t) \\ & + \frac{2\sigma_2(R_2,t)}{R_2} + \frac{\partial \sigma_2}{\partial R_2} + \frac{1}{R_2^4}\frac{\partial \xi'_2}{\partial R_2} - \frac{2\xi'_2(R_2,t)}{R_2^5} \end{aligned} \tag{3.13}$$

Substituting from equations 3.4, 3.12 and 3.13 into equation 3.3 gives

$$R_1\ddot{R}_1\left(1+\left(\frac{\rho_L-\rho_S}{\rho_S}\right)\frac{R_1}{R_2}\right)+\dot{R}_1^2\left(\frac{3}{2}+\left(\frac{\rho_L-\rho_S}{\rho_S}\right)\left(\frac{4R_2^3-R_1^3}{2R_2^3}\right)\frac{R_1}{R_2}\right)$$
$$=\frac{1}{\rho_S}\left(\begin{array}{l} p_G-p_\infty(t)-\dfrac{2\sigma_1}{R_1}-\dfrac{\partial\sigma_1}{\partial R_1}-\dfrac{1}{R_1^4}\dfrac{\partial\xi_1'}{\partial R_1}+\dfrac{2\xi_1'}{R_1^5}-\dfrac{2\sigma_2}{R_2}-\dfrac{\partial\sigma_2}{\partial R_2}-\dfrac{1}{R_2^4}\dfrac{\partial\xi_2'}{\partial R_2}+\dfrac{2\xi_2'}{R_2^5} \\ +\displaystyle\int_{R_1}^{R_2}\left[\frac{2T_{S,rr}-T_{S,\theta\theta}-T_{S,\phi\phi}}{r}\right]dr+\int_{R_2}^{\infty}\left[\frac{2T_{L,rr}-T_{L,\theta\theta}-T_{L,\phi\phi}}{r}\right]dr \end{array}\right) \quad (3.14)$$

This may be rewritten as

$$R_1\ddot{R}_1\left(1+\left(\frac{\rho_L-\rho_S}{\rho_S}\right)\frac{R_1}{R_2}\right)+\dot{R}_1^2\left(\frac{3}{2}+\left(\frac{\rho_L-\rho_S}{\rho_S}\right)\left(\frac{4R_2^3-R_1^3}{2R_2^3}\right)\frac{R_1}{R_2}\right)$$
$$=\frac{1}{\rho_S}\left(p_G-p_\infty(t)+f_\sigma+f_{Ls}+f_{Lv}+f_{Ss}+f_{Sv}+f_{b_{rad}}+f_{b_{th}}\right) \quad (3.15)$$

where f_{Sv}, f_{Ss}, f_{Lv} and f_{Ls}, correspond to the integrals for stress in the shell and fluid

$$f_{Sv}+f_{Ss}=\int_{R_1}^{R_2}\left[\frac{2T_{S,rr}-T_{S,\theta\theta}-T_{S,\phi\phi}}{r}\right]dr$$

$$f_{Lv}+f_{Ls}=\int_{R_2}^{\infty}\left[\frac{2T_{L,rr}-T_{L,\theta\theta}-T_{L,\phi\phi}}{r}\right]dr$$

f_σ represents the terms relating to surface forces

$$f_\sigma=-\frac{2\sigma_1}{R_1}-\frac{\partial\sigma_1}{\partial R_1}-\frac{1}{R_1^4}\frac{\partial\xi_1'}{\partial R_1}+\frac{2\xi_1'}{R_1^5}-\frac{2\sigma_2}{R_2}-\frac{\partial\sigma_2}{\partial R_2}-\frac{1}{R_2^4}\frac{\partial\xi_2'}{\partial R_2}+\frac{2\xi_2'}{R_2^5}$$

and the two additional factors, f_{brad} and f_{bth}, represent re-radiation and thermal damping respectively.

In its present form equation 3.15 represents a generalised model for CAP behaviour. The existing models (de Jong *et al* 1992; Church 1995 etc.) represent specific cases, according to the ways in which the last eight terms are defined. The advantage of this new approach is that it enables the appropriate function to be selected for a particular set of conditions. The aim of the following sections is to define each function according to the conditions relevant to specific applications.

3.3 Primary assumptions

There are a number of assumptions implicit in the derivation of equation 3.15. First of all, it was assumed that spherical symmetry would be maintained during CAP oscillation. The additional complexity involved in incorporating the shell into a non-linear analysis of spherical harmonics was not thought to be justified, since experimental observations (Dayton *et al* 1999; Chomas *et al* 2001) indicate that non-spherical CAP oscillations do not exhibit the well-ordered modes considered in the existing work on free bubbles (e.g. Longuet-Higgins 1989 a & b). An alternative would be to use an approximate technique such as finite element modelling. However, results for the spherically symmetric case would still be required in order to validate this type of analysis. This will be discussed again in Chapter 6.

The second assumption was that there would be no changes in the CAP properties, such as equilibrium radius or shell thickness, and that the CAPs would not be destroyed during oscillation. Clearly, this places a limit on the amplitudes of oscillation which may be considered and this limit will be quantified in section 3.6. Finally, external forces such as gravity, and *in vivo* effects such as phagocytosis, were neglected on the grounds that their effects would be small compared with those included in equation 3.15 and/or because they could not be accurately quantified. Effects falling into the latter category will also be discussed again in later chapters.

3.4 The filling gas

3.4.1 Influence upon CAP behaviour

As mentioned above, the densities and viscosities of the gases typically used for CAPs are very low compared with those of the surrounding fluid and typical shell materials (table 3.1).

Fluid	Density	Viscosity	Reference
	(kgm^{-3})	(Pas)	
air	1.24	1.8×10^{-5}	Kaye and Laby (1995)
perfluropropane	8.0	1.45×10^{-5}	Kaye and Laby (1995)
plasma (mammalian blood)	1030	0.0015	Duck (1990)
serum albumin	1100	1.77	de Jong *et al* (1994)

Table 3.1: Densities and viscosities for relevant fluids at 20° C and atmospheric pressure.

Under the conditions relevant to medical ultrasound applications, therefore, the inertial and viscous contributions of the gas will be negligible. For example, for an insonation frequency of 5 MHz and a radial amplitude of 10% R_{o1}, the wall velocity will be approximately $\dot{R}_1 \approx \frac{0.1R_{o1}}{2\pi/4\omega} = \frac{0.2\omega R_{o1}}{\pi} = 8$ m/s.

Following Prosperetti *et al* (1988) and examining the order of each term in equation 3.1 for the gas

$$\rho\frac{\partial u}{\partial t} \approx \rho_G \frac{\omega\dot{R}_1}{2\pi}, \qquad \rho u\frac{\partial u}{\partial r} \approx \rho_G \frac{\dot{R}_1^{\,2}}{R_1}, \qquad \frac{\partial p}{\partial r} \approx \frac{\Delta p_G}{R_1} \qquad \text{and} \qquad \nabla.\mathbf{T} \approx \frac{\mu_G \dot{R}_1}{R_1^{\,2}}$$

From table 3.1, the last term will be very small for all relevant gases and CAP diameters.

Therefore $$\rho_G \frac{\omega\dot{R}_1}{2\pi} + \rho_G \frac{\dot{R}_1^{\,2}}{R_1} + \frac{\Delta p_G}{R_1} = 0 \quad \text{and} \quad -\frac{\Delta p_G}{p_G} = \frac{\rho_G \dot{R}_1}{p_G}\left(\frac{\omega R_1}{2\pi} + \dot{R}_1\right) \approx 0.01$$

The influence of the gas upon CAP behaviour is thus described solely by the term representing the internal pressure, $p_G(t)$, on the right hand side of equation 3.15.

3.4.2 Quasistatic behaviour

For the assumption of quasistatic behaviour to be valid, it is necessary that the pressure inside the CAP can be considered to be uniform at all times, i.e. that the rate of equalization must be large compared with the insonation frequency. Prosperetti *et al* (1988) define a characteristic wavelength, λ_G, for pressure variations in the gas as the product of the period of the sound wave and the speed of sound in the gas. The latter may be found as (Landau and Livshitz 1987)

$$c_G \approx \sqrt{\left(\frac{p_G}{\rho_G}\right)} \tag{3.16}$$

At resonance

$$\lambda_G = \frac{2\pi}{\omega_o}\sqrt{\left(\frac{\gamma p_o}{\rho_G}\right)} \tag{3.17}$$

where ω_o is the approximate resonance frequency for the CAP obtained from a simplified form of equation 2.17.

$$\omega_o = \sqrt{\left(\frac{3\gamma p_o}{\rho_L R_{o1}^2}\right)} \tag{3.18}$$

Thus

$$\lambda_G = 2\pi R_{o1}\sqrt{\left(\frac{\rho_L}{3\rho_G}\right)} \tag{3.19}$$

The ratio of liquid to gas density, and hence of the wavelength to radius, is large for the range of fluids given in table 3.1, e.g. for air and plasma $\lambda_G/R_{o1} = 103$. Hence the pressure variations inside the CAP may be regarded as negligible.

3.4.3 Ideal gas behaviour

An ideal gas behaves according to the equation

$$pV = BT \tag{3.20}$$

where p is pressure, V is the volume of the gas, T is the absolute temperature and B is the gas constant.

Departure from ideal gas behaviour may be described in terms of a compressibility factor Q defined as

$$Q = \frac{PV}{BT} \tag{3.21}$$

where Q = 1 describes an ideal gas (Cengel and Boles 1989).

For the amplitudes of oscillation considered above, the ratios of pressure and temperature to the respective critical values for commonly used filling gases correspond to compressibility factors close to unity (table 3.2), i.e. ideal gas behaviour may be assumed for the conditions relevant to CAPs.

Gas	Critical temperature	Critical pressure	Q @ 40°C, 0.1 MPa
	(K)	(MPa)	
air (nitrogen)	126.2	3.39	0.997
perfluoropropane	345.1	2.68	0.980
sulphur hexafluoride	318.6	3.67	0.974

Table 3.2: Critical temperatures, pressures and compressibility factors for typical CAP filling gases (Cengel and Boles 1989).

3.4.4 Polytropic behaviour

In each of the CAP models discussed in Chapter 2, the behaviour of the filling gas has been assumed to be polytropic, i.e. that compression and expansion can be described by the equation

$$pV^{\kappa} = constant. \tag{3.22}$$

In order for this to be valid, the thermal diffusivity of the filling gas must remain constant during oscillation. For very small free bubbles at very high amplitudes this may not be the case (Leighton 1994) owing to the effects of the high Laplace pressure (equation 2.29) upon the gas properties. In the case of a CAP, however, this pressure is balanced by the stress in the encapsulating shell, as shown in equation 3.13. Hence, it may be assumed that any variations in thermal diffusivity will be sufficiently small for the polytropic index to be considered constant.

It has also been assumed that the vapour pressure inside the CAP will be negligible. This is based on the fact that the majority of CAPs are manufactured under gas saturated conditions (Becher and Burns 2000) and the encapsulating shell would be expected to inhibit inwards diffusion after the CAPs have been formed. To the author's knowledge, however, this has not been confirmed by experimental analysis of CAP contents and may not be a valid assumption for CAPs which are formed *in vivo* (e.g. Echovist). This matter will be re-examined in Chapter 6.

According to data cited by Church (1995), albumin shells are sufficiently permeable over long time periods for the initial pressure inside the CAP to be equal to that of the surroundings i.e. $p_G(0) = p_o$. This is likely to be a reasonable assumption for all CAPs, given the fact that all known CAPs will eventually disappear as a result of diffusion. Hence, from equation 3.22, the time dependent pressure in the gas may be defined as

$$p_G(t) = p_o\left(\frac{R_{o1}}{R_1}\right)^{3\kappa} \tag{3.23}$$

3.4.5 Isothermal behaviour

The value of the polytropic constant κ may vary between 1 and γ, where γ is the ratio of specific heats for the gas. These values represent the extremes of isothermal and adiabatic behaviour respectively. It has already been shown above that the thermal gradients generated in the gas will be negligible under the relevant insonation conditions. In addition, the ratio of gas diffusivity to frequency $\sqrt{\left(\frac{2\pi D_G}{\omega_o}\right)}$ will be large for CAPs ($>> R_{o1}$) (e.g. for air D_G = 2.3 x 10^{-5}m^2/s) and the specific heat capacity and thermal conductivity of plasma are sufficiently high for the surrounding fluid to be treated as a heat sink (4180 J/kg-°C and 0.58 Wm^{-1}K^{-1} respectively). It is therefore reasonable to assume that compression and expansion will be isothermal, i.e. $\kappa = 1$.

Equation 3.23 implies that, since $\oint pdV = 0$, there will be no thermal dissipation over the course of a complete oscillation, i.e. that $f_{b_{rad}} = 0$. In spite of this, some previous investigators, e.g. de Jong *et al* (1992), have included an approximate thermal

damping factor (equation 2.6) in their models. As shown in figure 3.2, if the magnitude of this factor is compared with that corresponding to viscous damping for free bubbles, it may be seen that the viscous term is greater by several orders of magnitude over the range of diameters and frequencies relevant to CAPs. In the case of a CAP, it would be expected to be even greater, since the viscosity of the encapsulating shell is likely to be larger than that of the surrounding fluid (table 3.1).

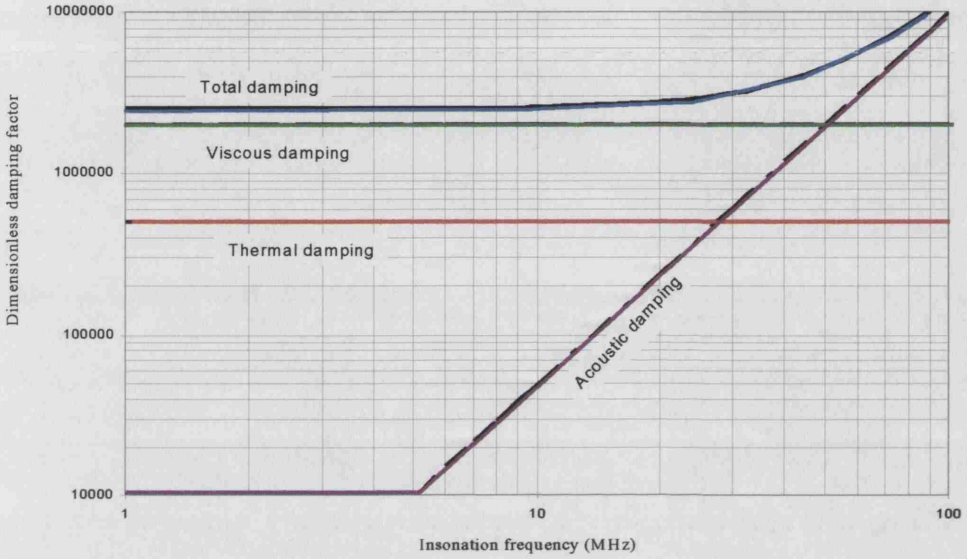

Figure 3.2: Comparing the magnitude of the approximate damping factors (Devin 1959) for a free bubble of radius 1 μm.

This would appear to confirm that, if it is valid to assume isothermal behaviour, it is also valid to ignore thermal damping. However, the evidence presented in figure 3.2 is based on an analysis which is inherently inconsistent, since, if polytropic behaviour is assumed, then necessarily, $f_{b_{rad}} = 0$. It can be confirmed rigorously that thermal damping is negligible by solving the equations for conservation of mass and energy coupled to equation 3.15.

$$\frac{d\rho}{dt} + \rho \nabla \cdot u = 0 \tag{3.24}$$

$$\nabla \cdot (K \nabla T) = \frac{\gamma}{(\gamma - 1)} \frac{p}{T} \left(\frac{\partial T}{\partial t} + u \frac{\partial T}{\partial r} \right) - \frac{dp}{dt} \tag{3.25}$$

The details of this work are shown in Appendix Bi. Representative results for an albumin-coated CAP at resonance are shown in figure 3.3.

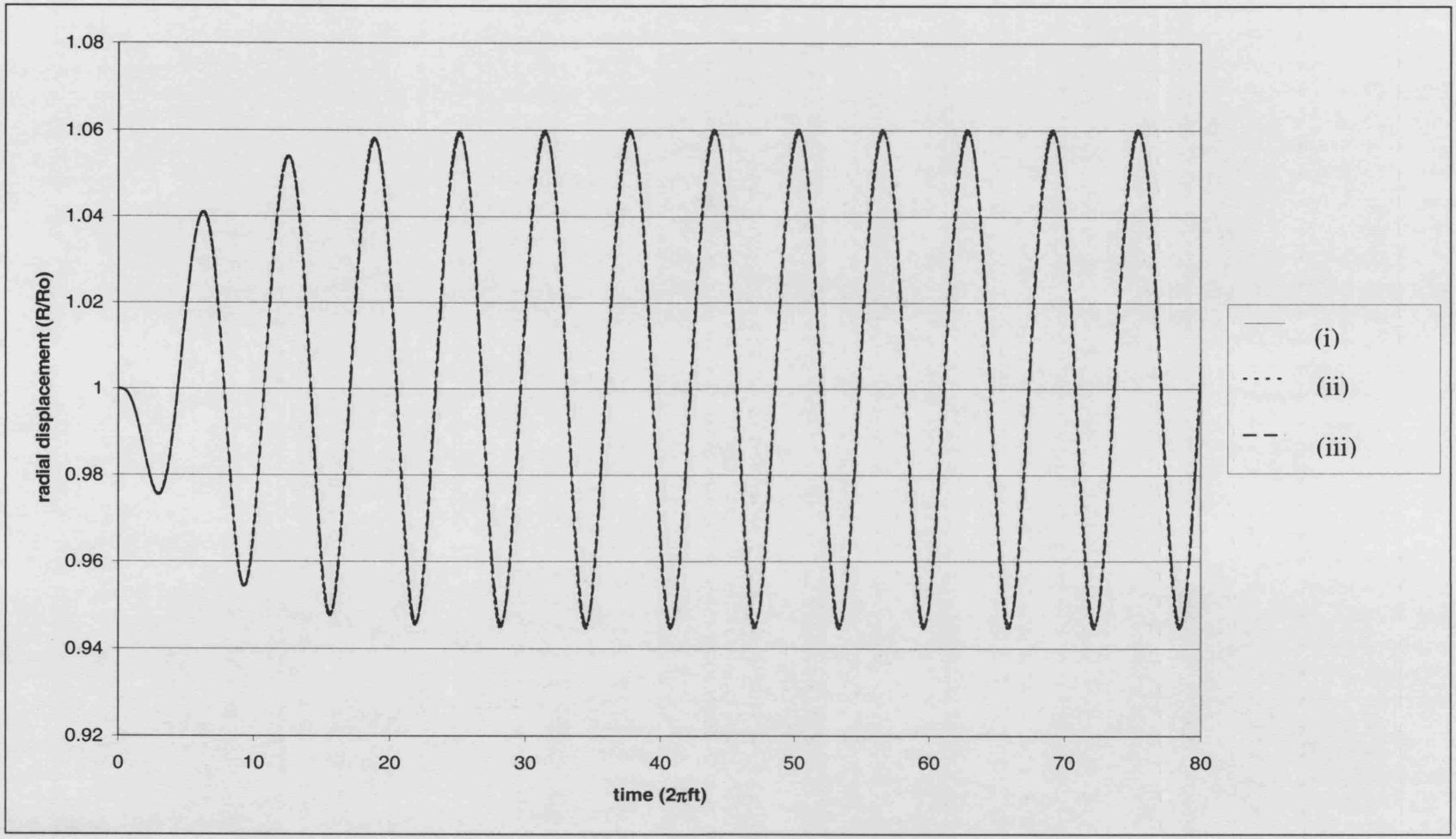

Figure 3.3: Demonstrating the influence of thermal damping upon the amplitude of oscillation of a resonant Albunex® CAP insonified at 3 MHz and 0.1 MPa. (i) no correction for thermal damping (ii) including an approximate thermal damping factor (iii) full solution of equations 3.24 and 3.25.

3.5 The encapsulating shell

3.5.1 Influence upon CAP behaviour

The presence of the encapsulating shell is clearly of great significance in terms of stabilising the CAP against dissolution. Moreover, it has a central role in drug delivery applications, since it both provides a substrate to which drugs or targeting species can be attached and influences the threshold for CAP destruction. It also has an important function in determining the CAP's dynamic and hence acoustic response. This will be shown in detail in Chapter 5. Accurate modelling of the shell material is thus essential and it is inappropriate to treat CAPs as free bubbles, as has been the case in a number of previous studies (e.g. Hilgenfeldt *et al* 2000; Chin and Burns 2000). The aim of the following sections is to derive suitable definitions of the functions f_{Ss} and f_{Sv}.

3.5.2 Shell compressibility

Strictly speaking, the term $f_{b_{rad}}$ in equation 3.15 refers to the damping effect arising not only from the compressibility of the surrounding fluid, but also from that of the encapsulating shell. However, the thickness of the shell is very small relative to the acoustic wavelength in e.g. air or plasma for frequencies of 1-10 MHz (1-100 nm vs. 30 μm -1.5 mm). Its effect upon the propagation of the radiated sound field will thus be negligible and the sound field may be treated as emanating from the outer wall of the CAP. In addition, the significance of shell compressibility can be determined from the Mach number, i.e. the ratio of $\dot{R}$ to the speed of sound in the shell (Massey 1989). Therefore, since the maximum velocity of the CAP wall was estimated as above to be approximately 10 m/s and the speed of sound in the shell material will be of the order of that in the surrounding fluid (Duck 1990), $\frac{\dot{R}}{c_S} \approx 10^{-2}$. Thus, any additional damping effect due to shell compressibility would be expected to be insignificant.

3.5.3 Shell solubility

It is clearly desirable that CAPs should eventually be eliminated safely from the body. Over a time span of a few hours, therefore, the shell material should dissolve, particularly if the CAPs are subject to processes such as phagocytosis. It can be assumed, however, that over the time span associated with insonation, there will be no significant changes in the shell properties. For example, Glazman (1984) shows that the dissolution of protein and phospholipid films may be regarded as negligible for bubbles oscillating at frequencies greater than 10^5 Hz. His analysis neglects the possibility of chemical interactions which might occur in the case of a CAP between the shell and, e.g., blood constituents *in vivo* and this area may warrant investigation. As mentioned in Chapter 2, however, the existing evidence would seem to indicate that CAPs are chemically inert (e.g. Podell *et al* 1999) and a more detailed examination would be outside the scope of this thesis.

3.5.4 Shell permeability

It was assumed above that, prior to insonation, the pressure inside the CAP would be equal to the ambient pressure $p_G(0) = p_o$. Clearly, this implies that the shell is not completely impermeable. Once again, however, on the timescale corresponding to the frequencies used in medical ultrasound, gas diffusion may be regarded as negligible, provided it can be assumed that the shell remains intact (see section 3.6). As discussed in Chapter 2, it has been reported by various authors (e.g. Sboros *et al* 2000) that albumin, phospholipid and polymer-coated CAPs, do not shrink significantly when exposed to low insonation pressures (<200 kPa) for periods of up to 30 minutes. This concurs with the author's own observations discussed in Chapters 4 and 6. Rapid diffusion was only observed at higher insonation pressures, following shell disruption.

It would be possible, in a numerical formulation, to define R_o, d_o, and the shell material parameters as functions of time, according to the relevant rates of diffusion, and/or dissolution. This might be appropriate if the total time spent by a CAP *in vivo* were being considered, in which case the timescale could not be treated as short compared with the rates of dissolution and diffusion. There might also be changes in the shell parameters produced by fatigue, due to the repetitive stretching and compression and/or the variation in temperature experienced by the shell during

oscillation. To determine the appropriate functions, however, would require a large amount of data regarding both CAP properties and conditions *in vivo*. This is not available at present. Moreover, since the ultimate aim of this work is to improve CAP design, it is justifiable to consider a hypothetical material for which properties such as chemical inertness and low permeability can be specified.

3.5.5 Shell uniformity

In order to satisfy the assumption of spherical symmetry, it is necessary to assume that the shell will be uniform in terms of thickness and material homogeneity in the ϕ and θ directions. This assumption has yet to be justified experimentally, since information regarding the tolerances on CAP dimensions is not available from the manufacturers and, to the author's knowledge, this has not been investigated independently. This is predominantly a manufacturing consideration, however, and so, again, uniformity would seem to be a reasonable assumption for the purposes of design. The effects of radial variation in material properties, e.g., due to the presence of an oil layer for drug delivery applications, will be investigated in Chapter 5.

3.5.6 Viscoelastic response

As described in Chapter 2, various materials have been used for coating CAPs, from palmitic acid to cyanoacrylates. Viscoelastic models provide a convenient means of describing such materials (Fung 1993; Boal 2002) but it is important to select the appropriate model and parameters for a particular type of shell. For CAP design, the model must provide a sufficiently general definition of f_{Ss} and f_{Sv} to enable a wide range of materials to be investigated, including those exhibiting non-linear viscoelastic behaviour. In this case it cannot be assumed that the trace of the stress tensor **T** in equation 3.15 will be zero and the shell functions will therefore be of the form

$$f_{Ss} + f_{Sv} = 2\int_{R_1}^{R_2} \frac{T_{S,rr} - T_{S,\theta\theta}}{r}\, dr \qquad (3.26)$$

Again from spherical symmetry $\qquad T_{\phi\phi} = T_{\theta\theta}. \qquad (3.27)$

There are several models available for describing this type of material. One of the most general is that due to Green and Rivlin (1957).

$$\mathbf{T}(t) = \int_{-\infty}^{t} \{\mathbf{I}\psi_1 tr(\mathbf{M}_1) + \psi_2 \mathbf{M}_1\} d\tau_1 + \int_{-\infty}^{t}\int_{-\infty}^{t} \{\mathbf{I}\psi_3 tr(\mathbf{M}_1)tr(\mathbf{M}_2) + \mathbf{I}\psi_4 tr(\mathbf{M}_1\mathbf{M}_2) + \mathbf{I}\psi_5 tr(\mathbf{M}_2) + \psi_6 \mathbf{M}_1\mathbf{M}_2\} d\tau_1 d\tau_2 + \ldots \quad (3.28)$$

where $\tau_{1,2}$ are time variables of integration, **I** is the identity matrix and $\mathbf{M}_{1,2}$ are the time derivatives of the strain tensor with respect to $\tau_{1,2}$ etc. Functions $\psi_{1,2}$ etc. must be determined experimentally for a particular material.

Incorporating equation 3.28 into equation 3.15 generates a system of differential equations which can be solved numerically, as will be shown in Chapter 5. This form of equation 3.15 is also suitable for modelling large amplitude deformations. In spite of its potential for describing complex material behaviour, however, equation 3.28 is of limited value until functions $\psi_{1,2}$ etc. can be specified. Thus, the main difficulty in applying equation 3.28 to existing contrast agents is obtaining reliable experimental data. Indeed, without the necessary data, all treatments of the shell may be shown to be mathematically equivalent, as demonstrated in Appendix B.ii.

Fortunately, for the purposes of CAP design this is a comparatively minor obstacle. The aim of the design process is to establish the optimum CAP characteristics for a particular application and to determine how these may be achieved. The absence of data for existing CAPs is thus relatively insignificant as $\psi_{1,2}$ etc. may, within reason, be specified by the designer. The derivation of suitable functions for $\psi_{1,2}$ will be examined in Chapter 5. Before this can be done, however, it is important to investigate the mechanisms and thresholds for CAP destruction.

3.6 Shell destruction

3.6.1 Shell stress analysis

In order to satisfy the assumption that the shell remains intact during CAP oscillation, it is necessary to examine and quantify the conditions leading to CAP destruction. In contrast to the "wall" of a free bubble, the shell of a CAP is a solid or at least semi-solid structure. As discussed in Chapter 2, optical experiments (e.g. Dayton *et al.* 1999) indicate that, under certain conditions, CAP destruction occurs as a result of shell rupture, i.e. that the stresses produced within the shell exceed its strength. The aim of this section is to determine the shell stresses associated with a variety of insonation conditions for different types of CAP and to compare them with experimental observations made by previous researchers. It should be noted, that, *in vivo,* a CAP may be subjected to a range of stresses, for example shear stresses due to microstreaming or due to being deformed in narrow blood vessels. In this investigation, however, only the stresses due to ultrasound excitation will be considered.

In order to maintain consistency with the available experimental data, it is necessary to assume a linear viscoelastic model. The elastic component of stress in this case is given by

$$T_{S,rr(elast.)} = (\lambda_s + 2G_S)\left(\frac{\partial \varepsilon_{rr}}{\partial r}\right) + 2\lambda_s\left(\frac{\varepsilon_{rr}}{r}\right) \tag{3.29}$$

where λ_s and G_s are the Lamé constants for the shell material and ε_{rr} is the component of the strain tensor in the radial direction for small displacements (Reissmann and Pawlik 1980) which is given by

$$\varepsilon_{rr} = \left(\frac{R_1^2}{r^2}\right)(R_1 - R_{1e}). \tag{3.30}$$

Linear viscous damping is proportional to the first derivative of velocity, so the viscous component of stress will be

$$T_{S,rr\,(vis.)} = 2\mu_s \frac{\partial u}{\partial r} = \frac{-4\mu_S R_1^{\,2} \dot{R}}{r^3}. \tag{3.31}$$

For spherical polar coordinates, the effective stress is defined as

$$T_{eff} = \sqrt{\frac{1}{2}\left(\left(T_{rr} - T_{\phi\phi}\right)^2 + \left(T_{\phi\phi} - T_{\theta\theta}\right)^2 + \left(T_{rr} - T_{\theta\theta}\right)^2\right)} = \frac{3T_{rr}}{2} \qquad (3.32)$$

As above, for the linear case, the direct components of the stress tensor **T** may be related by

$$T_{rr} = -\left(T_{\phi\phi} + T_{\theta\theta}\right) \quad and \quad \left(T_{\phi\phi} = T_{\theta\theta}\right) \qquad (3.33)$$

Thus the effective stress is given by

$$T_{S,eff} = -6\left(\frac{R_1^2}{r^3}\right)\left(G_S\left(R_1 - R_{1e}\right) + \mu_S \dot{R}_1\right). \qquad (3.34)$$

3.6.2 Selection of parameters

As indicated in Chapter 2, the majority of the experimental studies of CAP destruction have been performed using CAPs having either albumin shells, such as Albunex® and Optison®, or phospholipid coatings such as Sonovue® and MP1950. The simulations were therefore based on these types of agent. In the absence of better data, the approximate values for the shear modulus and viscosity of human serum albumin obtained by de Jong *et al* (1992) were used for Albunex® and Optison® (table 3.3). The parameters published by Gorce *et al* (2000) for Sonovue® were used for the phospholipid-coated CAPs. The CAP dimensions were taken from the data supplied by the manufacturers (table 3.3).

Parameter	Symbol	Albunex®/Optison®	Sonovue®/MP1950	
Shear modulus	G_s	88.8	122	MPa
Density	ρ_s	1100	1000	kgm^{-3}
Viscosity	μ_s	1.77	2.5	Pas
Inner radius	R_1	3.635	1.0	μm
Inner surface tension	σ_2	0.005	0.005	Nm^{-1}
Thickness	d_e	15	1.5	nm
Outer surface tension	σ_1	0.04	n/a	Nm^{-1}

Table 3.3: Parameters used for the analysis of CAP shell stresses.

The properties of the surrounding fluid were taken to be those of water (ρ_S = 1000 kgm^{-3}; μ_S = 0.001 Pas) since the experimental results with which the simulations were to be compared were all obtained *in vitro*, in distilled water or saline solution. For these fluids the assumption of Newtonian behaviour is approximately valid, (Fung 1993), and thus

$$T_{L,rr} = 2\mu_L \frac{\partial u}{\partial r} \qquad \text{so} \qquad 3\int_{R_2}^{\infty} \frac{T_{L,rr}}{r} = -4\mu_L \frac{R_1^2 \dot{R}_1}{R_2^3} \tag{3.35}$$

The justification for neglecting thermal damping has already been given. Similar arguments for neglecting acoustic damping will be given in section 3.7.

Again, for the sake of consistency with the models used to obtain the shell parameters, variations in surface tension were also ignored, i.e.

$$f_\sigma = -\frac{2\sigma_1}{R_1} - \frac{2\sigma_2}{R_2}. \tag{3.36}$$

In the absence of detailed information regarding the sound fields used in the aforementioned experiments and given the uncertainty in the other model parameters, the simplest representation of the imposed sound field as a continuous sinusoid was used: $p_\infty = p_o + p_A Sin(\omega t)$ for insonation pressures and frequencies ranging from 0.02 to 2 MPa and 0.5 to 5 MHz respectively (p_o = 0.1 MPa). Tests with typical diagnostic pulse forms having the same centre frequencies and maximum pressures, indicated that the effect upon the peak amplitudes of oscillation and hence upon the results and conclusions of the work was not significant (Appendix B.iii). This was an interesting finding, since it demonstrated that the transient part of a CAP's response is less important than that of a free bubble (again see Appendix B.iii).

The form of equation 3.15 used for the simulations may be expressed as

$$\begin{aligned} &R_1\ddot{R}_1\left(1+\left(\frac{\rho_L-\rho_S}{\rho_S}\right)\frac{R_1}{R_2}\right)+\dot{R}_1^2\left(\frac{3}{2}+\left(\frac{\rho_L-\rho_S}{\rho_S}\right)\left(\frac{4R_2^3-R_1^3}{2R_2^3}\right)\frac{R_1}{R_2}\right) \\ &=\frac{1}{\rho_S}\left(\begin{array}{l} p_o\left(\frac{R_1}{R_2}\right)^3 - p_o - p_A Sin(\omega t) - \frac{2\sigma_1}{R_1} - \frac{2\sigma_2}{R_2} \\ -\frac{4\mu_L R_1^2 \dot{R}_1}{R_2^3} - \frac{4V_S G_S}{R_2^3}\left(1-\frac{R_{1e}}{R_1}\right) - \frac{4\mu_S V_S \dot{R}_1}{R_1 R_2^3} \end{array}\right) \end{aligned} \tag{3.37}$$

3.6.3 Solution

In order to facilitate its solution, equation 3.38 was non-dimensionalised according to the following scheme

$$[\text{mass}] = [p_o R_{o1}/\omega^2] \qquad [\text{length}] = [R_{o1}]$$

$$[\text{time}] = [1/\omega]$$

It was then solved numerically, using purpose-written code (Appendix B.iv) implementing a fourth-order Runge-Kutta method, to ensure that the full CAP response was obtained. The radial displacement, velocity and acceleration of the shell wall were determined as functions of time for the range of parameters indicated above. The effective stress was found from equation 3.35 for the inner shell surface where the stress would be highest. The peak tensile and compressive stresses were identified for each set of conditions.

For validation purposes, the results were compared firstly with those produced by the Matlab® solver function *ode45* (Matlab® 6.13, The Mathworks Inc.), and secondly with results previously published by Leighton (1989) for unencapsulated bubbles. In the latter case, the model was run with $G_S = \mu_S = \sigma_2 = d_S = 0$, $\rho_S = 1000$ kgm^{-3} and $\sigma_1 = 0.07$ Nm^{-1} whereby equation 3.38 reduces to the RPNNP equation (2.2). The calculation error was monitored by repeating each test with a time step of half the length and ensuring that the differences were negligible.

3.6.4 Results

The variation in radial shell stress with time is shown in figure 3.4 for the three agents Albunex®, MP1950 and Optison®, insonified at 2.25 MHz and 0.3 MPa. The corresponding values of peak displacement, stress and acceleration for these conditions and the range of pressures and frequencies tested are given in tables 3.4-3.6.

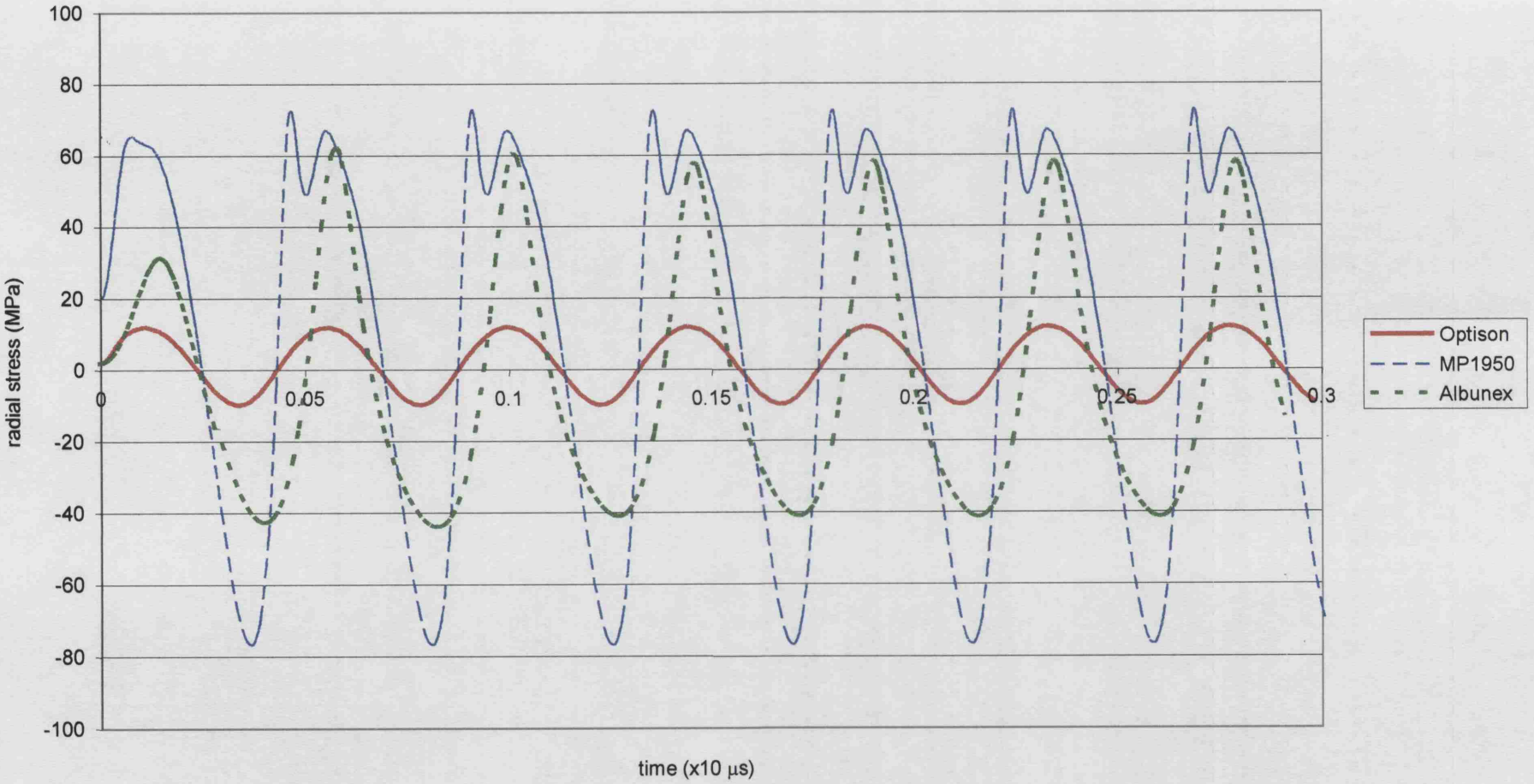

Figure 3.4: Variation in radial stress with time for CAPs insonated at 2.25 MHz and 0.3 MPa.

Frequency	Pressure	R_{max}	R_{min}	$T_{eff\ comp.}$	$T_{eff\ tens.}$
MHz	MPa	%	%	MPa	MPa
2.25	0.3	14.4	-13.4	93.6	65.9
2.25	0.4	17.4	-13.9	100.4	79.7
2.25	2	187.6	-56.6	18792.7	1264.7
5	2	59.8	-34.3	373.7	210.7

Table 3.4: Peak radial displacements and stresses for an Albunex® CAP.

Frequency	Pressure	R_{max}	R_{min}	$T_{eff\ comp.}$	$T_{eff\ tens.}$
MHz	MPa	%	%	MPa	MPa
0.5	0.4	434.4	-62.4	11359.1	595.4
0.5	0.2	9.9	-5.6	75.7	38.8
2.25	0.3	22.1	-8.0	109.4	115.2
2.25	0.7	226.7	-54.3	5039.4	523.5

Table 3.5: Peak radial displacements and stresses for an MP1950 CAP.

Frequency	Pressure	R_{max}	R_{min}	$T_{eff\ comp.}$	$T_{eff\ tens.}$
MHz	MPa	%	%	MPa	MPa
0.5	0.4	4.5	-3.3	21.7	20.4
2.25	0.3	3.3	-2.6	18.1	14.9
2.25	0.7	9.6	-5.4	34.9	46.2

Table3.6: Peak radial displacements and stresses for an Optison® CAP.

3.6.5 Discussion

The results shown in figure 3.4 indicate that, even at moderate insonation pressures (0.3 MPa), the stresses in a CAP shell may be extremely high: between 15-95 % and 50-105 % of the shear modulus, in tension and compression respectively. To the author's knowledge, neither the tensile strength of denatured serum albumin, nor that of a phospholipid monolayer has been accurately determined. Indeed, it may be inappropriate to attempt to characterise these types of material in terms of such a quantity. As an approximate comparison, however, the maximum tensile strength for a thermoplastic polymer is typically between 10 and 50 MPa (≈ 10% modulus), between 40 and 90 MPa for a thermoset (≈ 5% modulus) and between 1 and 20 MPa for an elastomer (≈ 90% modulus) (Callister 1994). The rupture strain for a phospholipid membrane is 2-5% (Boal 2002).

Thus, even allowing for some uncertainty as to the exact nature of the material, it would seem unlikely that the shell could sustain the stresses predicted by the model for insonation pressures of more than a few hundred kilopascals. There would appear, therefore, to be two possibilities. The first is that the stresses predicted by the model are realistic estimates of those which would be experienced by a CAP shell in practice. This being so, CAP destruction would be expected at pressures of a few hundred kilopascals. The second possibility is that the model does not accurately represent the behaviour of the shell material, in which case discrepancies between the theoretical and experimental results would be expected. To determine which of these conclusions is correct, it is necessary to review the experimental evidence discussed in Chapter 2.

The results obtained by Dayton *et al* (1999) suggest that certain types of CAP are significantly affected at insonation pressures of a few hundred kilopascals. They observed that the appearance of an Albunex® CAP tethered to a polystyrene plate was significantly altered after insonation by a single pulse of several[1] hundred kilopascals and centre frequency 2.25 MHz. Over a course of ten pulses (PRF 100 Hz), its appearance changed completely from "coarse and wrinkled" to "smooth and spherical." This was interpreted as an indication that the shell had been somehow disrupted, with the result that surface tension effects had become dominant. The CAP

[1] Reflections from the plate would have altered the local acoustic pressure incident upon the CAP compared with that measured using a hydrophone in a large volume of fluid.

was also seen to shrink, suggesting that the disruption of the shell had enabled some of the air inside to diffuse out into the surrounding fluid. Later results obtained by the same group (Dayton *et al* 1999) confirmed the formation of a defect leading to the release of gas, at pressures of 0.4 MPa, via a process of "sonic-cracking" as discussed in Chapter 2. Frinking *et al* (1999) similarly identified a threshold pressure for shell destruction for Quantison® of 0.2 MPa, over the frequency range 2-5 MHz.

At 2 MPa (2.25 MHz and 100 Hz PRF) the disappearance of the received echo in Dayton *et al*'s experiment indicated that the CAP was destroyed within a single pulse. The rapid destruction is perhaps not surprising. Strictly, oscillations with amplitudes larger than 10% of the initial radius are outside the range of validity for the model (Reissman and Pawlik 1980). However, even allowing for errors in the precise values, it is clear from tables 3.4-6 that the effective stress at this insonation pressure would be high enough to damage almost any material, and that the shell would be destroyed long before this level was reached.

At a higher centre frequency of 5 MHz, less extreme changes in the shell were observed. This would also be expected, given the increased distance from resonance, and it concurs qualitatively with the smaller radial displacements and stresses predicted by the model for this pressure and frequency (table 3.4). Quantitatively, however, the predicted stresses are still extremely high, and a rather more dramatic response might have been expected than the progressive change in the received echo actually observed. The increase in amplitude, duration and bandwidth would nonetheless be concordant with some form of disruption reducing the restraining effect of the shell. Moreover, there were a number of factors which could have affected the CAP response. These include the shielding effect discussed in Chapter 2 and the fact that the CAPs were tethered to the base plate which could have restricted their ability to respond.

In contrast to the albumin-shelled CAPs, no changes in either the appearance or the received echoes were detectable over the first 10 pulses for MP1950 CAPs, even when the pressure was increased to 0.7 MPa (Dayton *et al* 1999). After a longer (unspecified) time, a reduction in the diameter of the CAPs was noticed and subsequent work by Chomas *et al* (2001) indicated that this took place in steps coincident with the arrival of each new pulse. This could be interpreted as an

indication that lipid shells are disrupted under these conditions, allowing gas to escape, but that the nature of the material is such that defects can be repaired. Alternatively, it may be that the permeability of a phospholipid shell is so small that the large pressure gradient achieved during CAP compression is needed for outward diffusion of the gas to be noticeable.

This is an area requiring further examination. It is certainly the case that phospholipid monolayers are different from albumin/polymer shells in terms of their microstructure. The former consists of a single layer of phospholipid molecules aligned so that their polar "heads" all point outwards into the surrounding fluid[2] and their non-polar "tails" point in towards the gas inside the bubble (figure 3.5). The molecules are bound together by secondary (van de Waals) bonds, which are continuously being broken and reformed. As a result, the molecules can slip over each other, allowing the layer to deform without wrinkling and to form pores when stretched beyond their equilibrium spacing (Boal 2002).

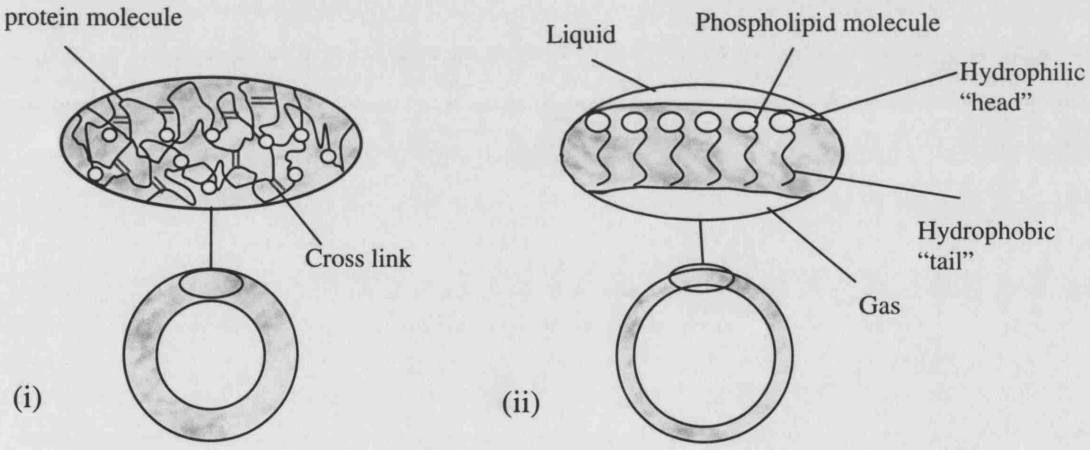

Figure 3.5: Schematic illustration of the contrasting microstructures of (i) polymer (albumin) and (ii) phospholipid shells.

In the form used for CAPs, serum albumin and other polymer shells, consist of layers of much larger molecules cross-linked by covalent bonds, which prevent continuous deformation so that the shell is more likely to buckle and/or rupture (figure 3.5). This difference would explain why defect formation was observed with Albunex® and Optison® but not MP1950, as well as the ability of the latter to "repair" itself after disruption.

[2] assuming it is polar; in a non-polar fluid the alignment would be reversed.

In light of the fact that different types of shell break down in different ways, it may be more appropriate to quantify the destruction limits for phospholipid-coated CAPs in terms of strain rather than stress. This is common for biological membranes, as mentioned above. A percentage area extension is defined, beyond which pores in the membrane are unable to close (Boal 2002). Determining the precise value of this extension is difficult. Molecular modelling techniques are not yet capable of predicting these values theoretically and experimental measurements must therefore be made for individual membranes. Whilst "phospholipid" has been used in a generic sense in this discussion, different types of membrane may be expected to exhibit different properties. Nevertheless, the value of 2-5% given by Boal (2002) for a "typical" phospholipid membrane would appear to concur with the experimental evidence cited here for CAP destruction and provides a useful limit for the purposes of CAP design.

3.6.6 Conclusions

It would seem from the results examined above that both of the conclusions proposed at the start of this discussion apply to some extent. There is certainly evidence for CAP disruption at relatively low insonation pressures, but it is also clear that the model does not provide a complete description of CAP behaviour. Given the uncertainty regarding the shell parameters available for existing CAPs, only a preliminary estimate may be obtained for the maximum stresses or strains which may be sustained, and the corresponding radial amplitudes. However, whilst this is clearly an area requiring further investigation, it is possible to define some approximate criteria on which to base subsequent design work. Both the results of the simulations and existing experimental data indicate that CAP destruction will occur at insonation pressures exceeding 200-300 kPa. This corresponds to effective shell stresses of between 10-50 MPa at which polymeric materials would be expected to fail; and to area extensions of more than 5% which would be expected to result in the rupture of phospholipid membranes. For the remainder of the work, therefore, an approximate destruction threshold for the radial amplitude of $2\%R_{o1}$ will be assumed.

3.7 The surrounding fluid

3.7.1 Assumptions

The majority of the existing models consider the CAP surrounded by an infinite, static, homogenous and Newtonian fluid. This would appear to be a poor description of blood, however, which flows within the confines of blood vessels, which is known to behave in a Non-Newtonian manner (Fung 1993) and which contains a high volume fraction of cells (40%) whose size is comparable with that of a CAP. The definitions of f_{Ls} and f_{Lv} and the associated assumptions therefore require some careful consideration.

3.7.2 Infinite extent

Fluid enclosed by the walls of a blood vessel clearly cannot be considered to be truly infinite. In certain situations, however, it is a reasonable approximation. For example, in a large blood vessel, whose diameter is two or more orders of magnitude greater than that of a CAP (i.e. >100 μm), the influence of the wall upon CAP behaviour will be relatively small. This is because the radial velocity of the fluid at this distance will be negligible: from the assumption of fluid incompressibility

$$u = \frac{\dot{R}_1 R_1^2}{r^2}. \qquad (3.38)$$

At distances far from the CAP, e.g. $r = 10 R_1$ this gives $u = 0.01 \dot{R}_1$.

In a capillary, whose diameter is likely to be similar to that of a CAP (8-10 μm), this will not be the case and this discussion will therefore be confined to larger blood vessels. The presence of blood cells and other CAPs will be discussed in sections 3.7.5 and 3.9 respectively.

3.7.3 Fluid incompressibility

The fact that the fluid surrounding the CAPs is capable of transmitting a sound field implies that it must have some degree of compressibility. The extent to which this affects the behaviour of an individual CAP, however, depends upon the amount of energy it re-radiates as sound and the associated damping effect. As explained in Chapter 2 there are a number of equations describing the behaviour of free bubbles which either include simple approximations or provide a rigorous treatment of

acoustic re-radiation damping (e.g. Keller and Miksis 1980). These may be modified to include a basic description of an encapsulating shell for modelling CAPs (e.g. Morgan 2000). All of these models, however, may be expressed in the form of equation 3.15 where f_{brad} represents the additional terms relating to acoustic damping. For example

$$\rho_L\left(R\ddot{R}+\frac{3}{2}\dot{R}^2\right)=\left(p_o+\frac{2\sigma}{R}+\frac{2\chi_S}{R_o}\right)\left(1-\frac{3\kappa\dot{R}}{c_L}\right)\left(\frac{R_o}{R}\right)^{3\kappa}-\frac{4\mu_L\dot{R}}{R}$$
$$-\frac{2\sigma}{R}\left(1-\frac{\dot{R}}{c_L}\right)-\frac{2\chi_S}{R}\left(1-\frac{3\dot{R}}{c_L}\right)\left(\frac{R_o}{R}\right)^2-\frac{12\mu_S d_S\dot{R}}{R(R-d_S)}-p_\infty(t) \qquad (2.11)$$

may be expressed as

$$\rho_L\left(R\ddot{R}+\frac{3}{2}\dot{R}^2\right)=\underbrace{\left(p_o+\frac{2\sigma}{R}+\frac{2\chi_S}{R_o}\right)\left(\frac{R_o}{R}\right)^{3\kappa}}_{p_G}-p_\infty(t)-\underbrace{\left(\frac{2\sigma}{R}\right)}_{f_\sigma}-\underbrace{\left(\frac{12\mu_S d_S\dot{R}}{R(R-d_S)}\right)}_{f_{Sv}}-\underbrace{\left(\frac{4\mu_L\dot{R}}{R}\right)}_{f_{Lv}}$$
$$-\underbrace{\left(\frac{2\chi_S}{R}\left(\frac{R_o}{R}\right)^2\right)}_{f_{Ss}}-\underbrace{\left(\frac{3\kappa\dot{R}}{c_L}\left(p_o+\frac{2\sigma}{R}+\frac{2\chi_S}{R_o}\right)\left(\frac{R_o}{R}\right)^{3\kappa}-\frac{2\sigma}{R}\frac{\dot{R}}{c_L}-\frac{3\dot{R}}{c_L}\frac{2\chi_S}{R}\left(\frac{R_o}{R}\right)^2\right)}_{f_{brad}}$$

As may be seen, each of the terms represented by f_{brad} depends upon the ratio between the velocity of the CAP wall $\dot{R}$ and the acoustic velocity of the surrounding liquid c_L. Following the reasoning shown above for the shell, for the amplitudes of oscillation corresponding to non destructive behaviour ($\approx 1\% R_{o1}$) and the relevant insonation frequencies ($\approx$5 MHz), the velocity of the CAP wall must be of the order of 4 x 5 x 10^6 x 0.01 R_{o1} = 0.8 m/s. Therefore the ratio $\frac{\dot{R}}{c} \approx 5 \times 10^{-4}$, will be much less than unity. Hence the magnitude of f_{brad} will be negligible compared with the remaining terms in the equation. This may also be seen from a comparison of the approximate damping factors defined by Devin (1959), as demonstrated in figure 3.2.

3.7.4 Static

The maximum average flow velocity for blood in vessels having diameters 1-10 mm is approximately 10^{-2} m/s (Guyton and Hall 1990). Therefore, the distance traveled over the course of a single 3 cycle pulse with centre frequency 1 MHz is 3 x $1/10^6$ x 10^{-2} = 3 x 10^{-6} x 10^{-2} = 3 x 10^{-8} m. This is negligible compared with the diameter of the CAP (>10^{-6} m). Similarly, 10^{-2} m/s is small compared with the velocity estimated for the CAP wall above. The influence of microstreaming upon CAP behaviour has not been included in the analysis although this will be discussed again in Chapter 6.

3.7.5 Newtonian behaviour

3.7.5.1 Fluid models

As mentioned above, the majority of the existing models consider the fluid surrounding the CAPs to be Newtonian. In the majority of cases, however, the CAPs will be suspended in blood once they have been injected. The aim of this work was to investigate the influence of blood cells upon the dynamic, and hence acoustic, response of a CAP and to determine the most appropriate means of modelling the suspending medium for the purposes of CAP design.

The existing evidence is somewhat inconclusive. As described in Chapter 2, some recent theoretical studies have considered the behaviour of CAPs in non-Newtonian fluids (Khismatullin and Nadim 2002; Allen & Roy 2000a; 2000b), but it is not clear to what extent their results apply to whole blood, as opposed to plasma or more solid tissue. Experiments examining the effect of blood cells upon the motion of CAPs under the influence of acoustic radiation forces have also been reported, (Chelly *et al* 2002) but, to the author's knowledge, there have been no experimental studies of the effects upon CAP acoustic response.

Interestingly, in spite of the conditions *in vivo* described above and notwithstanding the speculation of various authors (e.g. Khismatullin and Nadim 2002), there are a number of reasons why the presence of blood cells may be relatively insignificant in terms of its effect upon CAP dynamics. Firstly, as will be shown in Chapter 5, the influence of the surrounding fluid upon CAP response is small compared with that of the encapsulating shell. The effect of varying the properties of the surrounding fluid therefore, would also be expected to be small.

Secondly, the non-Newtonian nature of blood observed in rheological experiments is produced by the "rolling" motion of cells as they are transported on a scale that is large compared with the CAP diameter (Fung 1993; Snabre and Mills 1999). Owing to the similarity in size between CAPs and cells, the radial motion of the CAP wall produced by insonation would not be expected to set up this type of flow. Instead, much smaller deformations of the nearby cells would be expected. The fluid inside a blood cell is very similar to the surrounding plasma (Fung 1993) and the elasticity of the membrane around each cell is small (Boal 2002). Thus the difference between the behaviour of CAPs in plasma or in whole blood would not be expected to be very great. Thirdly, blood cells are relatively poor back-scatterers of ultrasound. This is precisely the reason for the development of ultrasound contrast agents. Consequently, the effect of cells upon the incident ultrasound field would be expected to be small, particularly compared with the effect of other CAPs.

On the basis of the above it may be postulated that, for the purposes of modelling CAP dynamics, it is justifiable to treat the surrounding fluid as homogeneous and Newtonian. Indeed, in the absence of reliable experimental data it may be more appropriate to do so than to attempt more sophisticated treatments. The following sections contain details of the new modelling work which was carried out to determine the validity of this postulate. The supporting experimental work is described in Chapter 4.

3.7.5.2 A new model for CAP dynamics in whole blood

As indicated above, it was considered inappropriate to employ treatments developed for comparatively large scale non-Newtonian flows, owing to the similarity in size between blood cells and CAPs. It was proposed instead that the cells surrounding a CAP should be modelled as a concentric outer layer (figure 3.6), having viscous and elastic properties corresponding to those of red blood cells for small deformations.

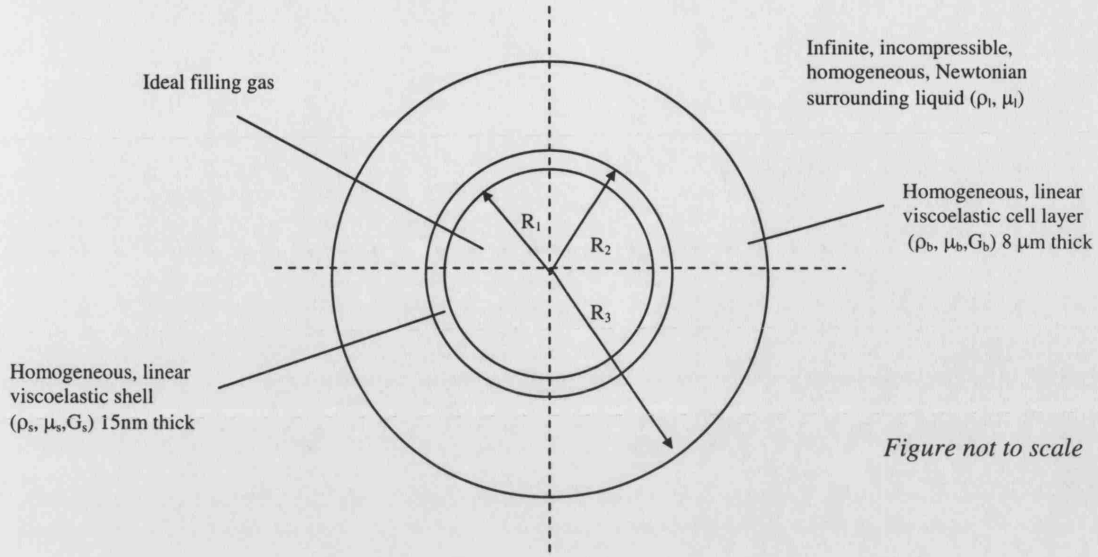

Figure 3.6: Schematic of blood cells surrounding a CAP modelled as a concentric outer layer.

Under the insonation conditions typically used in ultrasound examinations, the radiation forces generated by CAP oscillation would not be sufficient to cause clustering of blood cells around individual CAPs (Appendix A.iii). However, given the relative volume fractions of CAPs and cells *in vivo*, it is reasonable to assume that CAPs would be closely surrounded by cells, even in the absence of significant secondary radiation forces. Moreover, in terms of the magnitude of cell influence, this model should represent the limiting case and is therefore appropriate for a preliminary examination.

Since the primary interest of this work was the effect of the cells upon CAP oscillation, the CAP itself was modelled as described in section 3.6, and the fluid surrounding the cell layer was considered to be infinite, homogeneous and Newtonian. This assumption was justified on the basis that the fluid closest to the CAP, i.e. the cell layer, will have the greatest influence upon its behaviour and the modelling of the fluid further away from the CAP is therefore less important. It has already been shown above that the velocity of the surrounding fluid, and hence the viscous stress, will be small at distances greater than a few CAP radii. The inertial contribution will be unaffected since the density of the intercellular fluid is almost identical to that of plasma (Fung 1993).

A similar procedure to that described in section 3.2 was adopted, but in this case it was necessary to integrate equation 3.1 over three regions of interest: shell, cell layer and surrounding fluid

$$\rho_S\left[R_1\ddot{R}_1\left(1-\frac{R_1}{R_2}\right)+\dot{R}_1^2\left(\frac{3}{2}+\frac{R_1^4}{2R_2^3}-\frac{2R_1}{R_2}\right)\right]+\rho_L\left[R_1\ddot{R}_1\frac{R_1}{R_3}+\dot{R}_1^2\left(\frac{2R_1}{R_3}-\frac{R_1^4}{2R_3^3}\right)\right]$$
$$+\rho_B\left[R_1\ddot{R}_1\left(\frac{R_1}{R_2}-\frac{R_1}{R_3}\right)+\dot{R}_1^2\left(\frac{R_1^4}{2R_3^4}-\frac{2R_1}{R_3}+\frac{2R_1}{R_2}-\frac{R_1^4}{2R_2^4}\right)\right]$$
$$=p_S(R_1,t)-p_S(R_2,t)+p_B(R_2,t)-p_B(R_3,t)+p_L(R_3,t)-p_L(\infty,t) \qquad (3.39)$$
$$+T_{S,rr}(R_2,t)-T_{S,rr}(R_1,t)+T_{B,rr}(R_3,t)-T_{B,rr}(R_2,t)+T_{L,rr}(\infty,t)-T_{L,rr}(R_3,t)$$
$$+\int_{R_1}^{R_2}\frac{3T_{S,rr}}{r}dr+\int_{R_2}^{R_3}\frac{3T_{B,rr}}{r}dr+\int_{R_3}^{\infty}\frac{3T_{L,rr}}{r}dr$$

The corresponding boundary conditions for continuity of stress at each interface are given by

$$p_G(R_1,t)=p_S(R_1,t)-T_{S,rr}(R_1,t)+\frac{2\sigma_1}{R_1} \qquad (3.40)$$

$$p_S(R_2,t)=p_B(R_2,t)+T_{S,rr}(R_2,t)-T_{B,rr}(R_2,t)+\frac{2\sigma_2}{R_2} \qquad (3.41)$$

$$p_B(R_3,t)=p_L(R_3,t)+T_{B,rr}(R_3,t)-T_{L,rr}(R_3,t)+\frac{2\sigma_3}{R_3} \qquad (3.42)$$

Substituting these into equation 3.39, the right hand side is reduced to

$$p_G(R_1,t)-\frac{2\sigma_1}{R_1}-\frac{2\sigma_2}{R_2}-\frac{2\sigma_3}{R_3}-p_L(\infty,t)+\int_{R_1}^{R_2}\frac{3T_{S,rr}}{r}dr+\int_{R_2}^{R_3}\frac{3T_{B,rr}}{r}dr+\int_{R_3}^{\infty}\frac{3T_{L,rr}}{r}dr$$

As explained above $p_G(t)=p_o\left(\frac{R_{o1}}{R_1}\right)^3$,

$$T_{L,rr}=\frac{-4\mu_L R_1^2\dot{R}_1}{r^3} \quad \text{and} \quad T_{S,rr}=-4\left(\frac{R_1^2}{r^3}\right)\left(G_S(R_1-R_{1e})+\mu_S\dot{R}_1\right)$$

Similarly the stress in the linear viscoelastic layer representing the blood cells may be expressed as

$$T_{B,rr} = -4\left(\frac{R_1^2}{r^3}\right)\left(G_B(R_1 - R_{1e}) + \mu_B \dot{R}_1\right) \qquad (3.43)$$

The validity of this equation and the provenance of G_b and μ_b is discussed shortly.

The final equation of motion for the CAP then becomes

$$\begin{aligned}
&\rho_S\left[R_1\ddot{R}_1\left(1-\frac{R_1}{R_2}\right)+\dot{R}_1^2\left(\frac{3}{2}+\frac{R_1^4}{2R_2^3}-\frac{2R_1}{R_2}\right)\right]+\rho_L\left[R_1\ddot{R}_1\frac{R_1}{R_3}+\dot{R}_1^2\left(\frac{2R_1}{R_3}-\frac{R_1^4}{2R_3^3}\right)\right]\\
&+\rho_B\left[R_1\ddot{R}_1\left(\frac{R_1}{R_2}-\frac{R_1}{R_3}\right)+\dot{R}_1^2\left(\frac{R_1^4}{2R_3^4}-\frac{2R_1}{R_3}+\frac{2R_1}{R_2}-\frac{R_1^4}{2R_2^4}\right)\right] \qquad (3.44)\\
&=p_o\left(\frac{R_{o1}}{R_1}\right)^3-\frac{2\sigma_1}{R_1}-\frac{2\sigma_2}{R_2}-\frac{2\sigma_3}{R_3}-p_\infty(t)-\frac{4\mu_L R_1^2\dot{R}_1}{R_3^3}\\
&-4R_1^2\left(\frac{V_{s1}}{R_2^3R_1^3}\right)\left(G_S(R_1-R_{1e})+\mu_S\dot{R}_1\right)-4R_1^2\left(\frac{V_{s2}}{R_2^3R_3^3}\right)\left(G_B(R_1-R_{1e})+\mu_B\dot{R}_1\right)
\end{aligned}$$

The nature of the sound field incident upon an individual CAP and the extent to which it is affected by blood cells is discussed in the section 3.8. For the purposes of this work, the sound field was based upon the model of an imaging pulse given by Lord *et al* (1990) whereby

$$p_{inc}(t) = p_A\left(1-\cos\left(\frac{\omega t}{m}\right)\right)\left(1-\sin\left(\frac{\omega t}{m}\right)\right)\cos(\omega t)\sin(\omega t) \qquad (3.45)$$

for $$0 \le \frac{\omega t}{m} \le 2\pi$$

In this case m was chosen to be 5. Again, however, since the purpose of this investigation was to compare CAP response in different surrounding fluids, the precise nature of the insonating field was unimportant.

3.7.5.3 Solution

Equation 3.44 was non-dimensionalised and solved as described in section 3.6. Results were obtained for a CAP suspended in plasma with and without a surrounding cell layer. Properties for Albunex® (table 3.2) were again used in the simulations, since it was only the comparative behaviour in plasma and blood that was of interest. Thus, as indicated above for the sound field, the exact values were unimportant. The properties for plasma were taken from results published by Duck (1990). The properties for the cell layer were derived from data published by Boal (2002) based on the measurements of Evans and Waugh (1977) (table 3.7). Plots of the results were prepared using Matlab® R.12 (The Mathworks, Natick MA).

	Parameter	Symbol	Value	Unit
Cell layer (blood)	Shear modulus	G_B	500 ± 50	Pa
	Density	ρ_B	1050 ± 5	kgm^{-3}
	Viscosity	μ_B	0.006 ± 0.001	Pas
	Thickness	d_B	8 ± 0.5	μm
Liquid (plasma)	Density	ρ_L	1030 ± 5	kgm^{-3}
	Viscosity	μ_L	0.0015 ± 0.0001	Pas
	Surface tension	σ_1	0.04	Nm^{-1}

Table 3.7: Average properties for plasma and blood used in the simulations.

A range of insonation frequencies was used, corresponding to resonant, sub-resonant and super-resonant regimes. There is some controversy over the definition of resonance for contrast agent suspensions. "Resonance frequency" is used here in its loosest sense to denote the frequency at which attenuation is maximised. This frequency was estimated approximately by running the model for different insonation frequencies. The insonation pressure was varied within the range of pressures (0.05 - 0.1 MPa) defined in section 3.6 for which a CAP would be expected to remain intact. The radial amplitude, velocity and acceleration were recorded since it would be these variables which would ultimately determine the scattered pressure signal.

3.7.5.4 Results

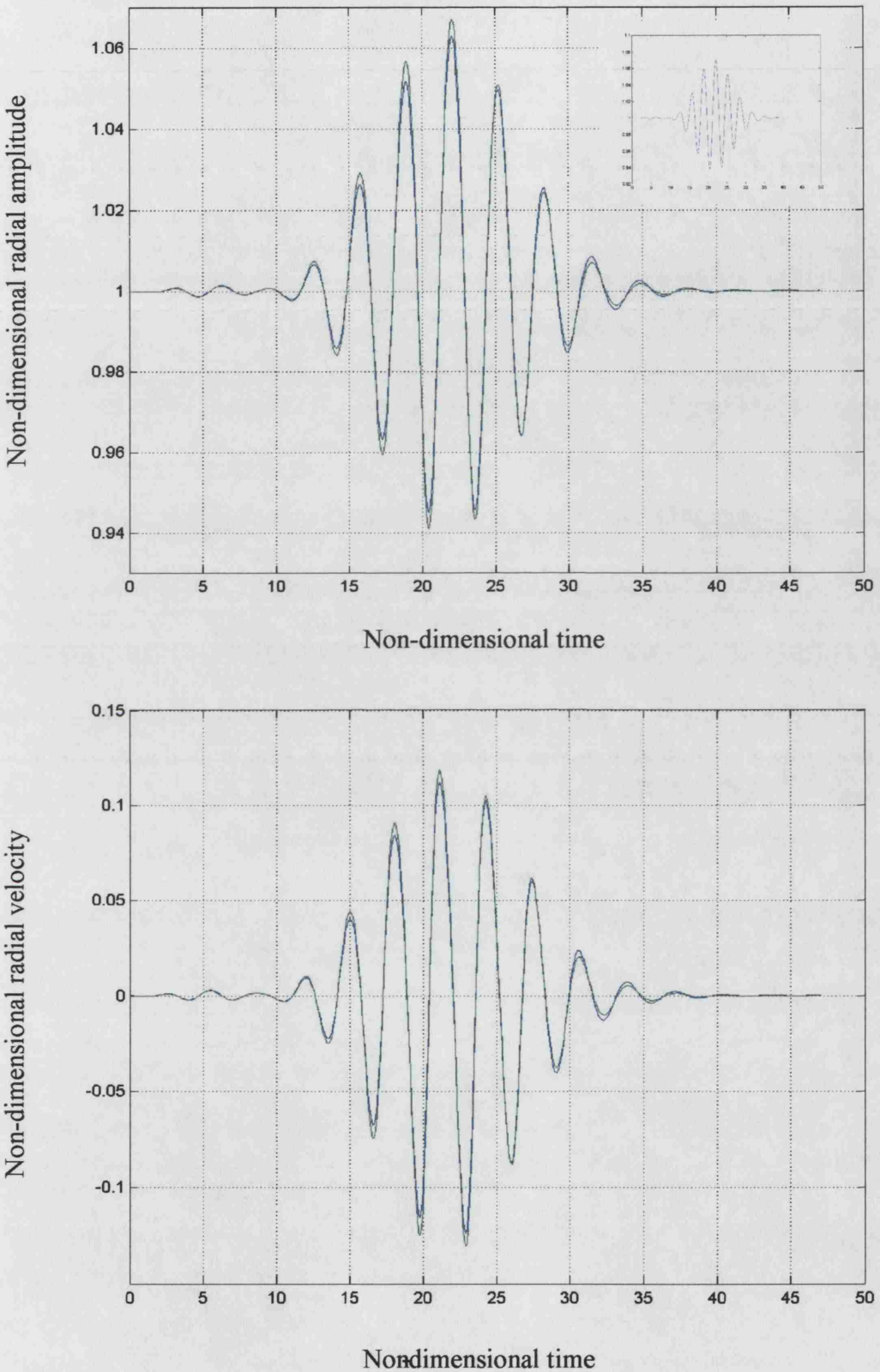

Figure 3.7: (a) Comparison between the variation in CAP radius with time during insonation at 3 MHz 0.1 MPa in plasma and whole blood (inset shows pressure waveform for insonating pulse). (b) Comparison between the variation in CAP radial velocity with time during insonation at 3 MHz 0.1 MPa in plasma (green) and whole blood (blue).

3.7.5.5 Discussion

In accordance with the predictions made in the previous section, the results from the numerical solution of equation 3.44 indicated that the effect of an additional viscoelastic layer upon CAP oscillations was relatively small. This is demonstrated in figure 3.7 for the resonant case (3 MHz, 0.1 MPa). The motion of the CAP wall was slightly dampened by the presence of the cell layer, as would be expected, owing to its higher viscosity, but no other significant effects were observed. For the non-resonant cases the effects were even smaller. Assuming the published parameters are accurate, it would appear that cell elasticity is too small to noticeably affect CAP oscillation and that it is the encapsulating shell which dominates CAP behaviour. There is good reason to suppose the published cell elasticity is reliable since it is known that cells are able to deform easily in order to pass along narrow blood vessels (Fung 1993). Thus, in terms of CAP design, whilst the additional damping provided by blood cells should be taken into account when selecting an appropriate input pressure, the presence of cells in the surrounding fluid would indeed appear to be small.

This conclusion is of course based upon the results of a comparatively simple model and there are a number of questions which must be answered before it may reasonably be accepted. In particular, the validity of considering a continuous layer must be examined. Firstly, if blood cells are not bound to the surface of a CAP then they will only offer resistance to CAP expansion and not compression, although given the small cell elasticity, the consequent increase in non-linearity would be expected to be very small. Secondly, the hypothesised arrangement of cells and CAPs in large blood vessels has yet to be observed experimentally. If the arrangement of cells around the CAP was not naturally close packed, plasma would flow *between* the cells during CAP oscillation. This would cause the cells to deform in a different direction and thus give rise to additional resistive forces not predicted by the current model. There might also be other interactions, chemical etc. between cells and CAPs which could affect the dynamics of the latter. Consideration of these effects should, however, be suspended until the experimental results have been examined for indications of unpredicted phenomena. This will be done in Chapter 4.

3.8 The sound field

3.8.1 Influence upon CAP behaviour

As will be demonstrated further in Chapter 5, the sound field is an important determinant of CAP behaviour. This is due, firstly, to the fact that CAPs resonate at frequencies within the diagnostic range and, secondly, to the fact that their response may vary considerably at different insonation pressures. This thesis is not concerned specifically with the design of the incident field, which would constitute a major piece of research in itself. The assumptions relating to the nature of the input waveform and its propagation through the CAPs' surroundings, however, do need to be examined.

3.8.2 Uniformity of pressure around the CAP

The term $p_\infty(t)$ in equation 3.15 represents the pressure in the fluid at distances far from the CAP wall and comprises the hydrostatic pressure p_o and the imposed sound field. At the frequencies typically used in medical imaging (1-10 MHz) the wavelength of sound in plasma (0.15 - 1.5 mm) is considerably larger than the diameter of a CAP (2-10 μm). In a homogeneous liquid, therefore, the pressure at the CAP wall may be considered to be spatially uniform at any point in time and any curvature of the wave fronts may be ignored. As mentioned in the previous section, blood cells will not give rise to significant scattering compared with CAPs, owing to their being filled with liquid rather than gas, and should therefore have a relatively negligible effect upon the incident field. Hence, this assumption may also be made for blood. Blood vessel walls may modify the incident field, and this effect may be significant particularly in narrow vessels, but for the reasons given in section 3.3 their influence has been neglected for the purposes of this work. The influence of other CAPs will be considered in detail in section 3.9.

3.8.3 Propagation effects

A diagram illustrating the range of effects potentially influencing the incident and radiated sound fields is shown in figure 3.8.

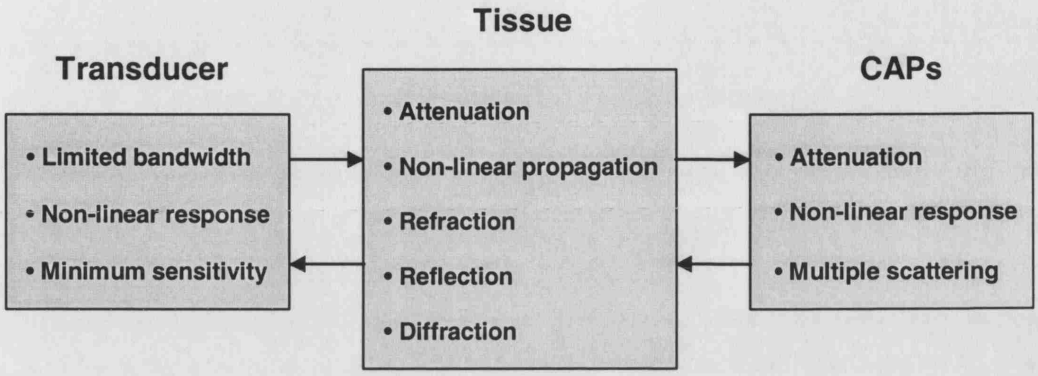

Figure 3.8: Flow chart indicating the factors affecting the incident and radiated sound fields.

The work in this thesis is mainly concerned with the incident and radiated sound fields in the immediate vicinity of a CAP. If CAPs are to be designed to produce a particular signal, however, it is important to consider the limits imposed by the available bandwidth and the sensitivity of medical transducers. Similarly, it is necessary to determine the degree to which the signal will be attenuated and/or distorted in passing through the surrounding tissue. These factors will be discussed again and quantified in Chapter 5.

Attenuation may be enhanced as a result of non-linear propagation leading to an increase in the harmonic content of the signal, as discussed in Chapter 2. As indicated in section 2.2.3.3, however, Kvikliene *et al* (2004) have shown that the effects of non-linear propagation upon CAP response were only observable for CAPs having diameters greater than 2.5 μm and for insonation pressures greater than 0.4 MPa. This is outside the range of pressure over which CAPs may be assumed to remain intact and may therefore be regarded as a minor influence upon the sound fields considered in the remainder of this thesis. The problem of multiple scattering and its effects upon CAP response and attenuation are addressed in the next section.

3.9 Multiple scattering

3.9.1 Aims and objectives

As mentioned previously, the existing models for the behaviour of ultrasound contrast agents consider single, isolated contrast agent particles (CAPs) suspended in infinite media. In order to predict the behaviour of a CAP population, there are assumed to be no interactions between individual CAPs, and the results for single CAPs are simply summed, after being weighted according to the size distribution in the suspension. However, given that the effectiveness of CAPs is due to the fact that they are strong back-scatterers of ultrasound, it would seem reasonable to suppose that at certain concentrations and frequencies there will be multiple scattering between CAPs which will affect the overall response of the population. This supposition is supported by a number of experimental studies (e.g. Marsh *et al* 1997, Chen *et al* 2002) in which discrepancies between measurements and the predictions from single CAP theories are identified. If contrast agent behaviour is to be fully understood, it is essential to determine the conditions under which CAP multiple scattering should be taken into account.

The specific objectives of this section are:

- To derive linear multiple scattering models for CAP suspensions to identify approximately the conditions under which the effects of multiple scattering are likely to be significant.
- To develop a non-linear multiple scattering model to investigate the phenomenon in CAP suspensions at higher insonation pressures.

3.9.2 Linear multiple scattering in CAP suspensions

The first part of the work will be concerned with the problem of linear multiple scattering using two of the models described in Chapter 2: those of Foldy (1945)

$$K_{eff}^2 = k_L^2 + 4\pi nf \tag{2.27}$$

and Henyey (1999)

$$K_{eff}^2 = k_L^2 + 4\pi nF \qquad \text{where} \qquad F = \left(\frac{1}{f}k_L - K_{eff}\right)^{-1} \tag{2.28}$$

Equations 2.27 and 2.28 may be used for suspensions of any type of particle, including CAPs, provided an appropriate scattering function, *f*, can be defined. As explained previously, for low amplitude oscillations corresponding to linear behaviour, the pressure radiated by a CAP subject to sinusoidal excitation may be approximated as

$$p_s = \frac{\rho_L R_{o1}^2 \dot{R}_1 \omega}{r} e^{i\left(\frac{\pi}{2} - k_L r\right)} = f \frac{p_{inc}(t)}{r} e^{-ik_L r} \qquad (2.15)$$

The scattering function may therefore be obtained by solving the equation of motion for the CAP for $\dot{R}_1$ and substituting this into equation 2.15.

Since the models are valid for linear scattering only, it is necessary to use the linearised version of equation 3.15 to obtain $\dot{R}_1 = R_{o1}\dot{x}$

$$\ddot{x} + \delta_d \dot{x} + \omega_o^2 x = -\frac{p_A \sin(\omega t)}{\rho_S R_{o1}^2 \alpha} \qquad (2.16)$$

Thus
$$p_s = \left(\frac{\rho_L R_{o1}}{\rho_S \alpha \left(\left(\frac{\omega_o^2}{\omega^2} - 1 \right)^2 + \frac{\delta_d^2}{\omega^2} \right)} \right) \frac{p_A i \sin(\omega t + \phi)}{r} e^{-ik_L r} \qquad (3.46)$$

and the scattering function for a CAP is therefore given by

$$f = \frac{\rho_L R_{o1} \left(\left(\frac{\omega_o^2}{\omega^2} - 1 \right) - i \frac{\delta_d}{\omega^2} \right)}{\rho_S \alpha \left(\left(\frac{\omega_o^2}{\omega^2} - 1 \right)^2 + \frac{\delta_d^2}{\omega^2} \right)} \qquad (3.47)$$

Equations 2.27 and 2.28 were used with equation 3.47 to calculate the attenuation coefficients for CAP suspensions of varying concentration and mean radii over a range of insonation frequencies. As before, properties for Albunex® were used (table 3.3) to enable comparison with previous results.

Assuming linear propagation, the wave number for a given medium is, by definition, complex: $K_{eff} = \mathrm{Re}(K_{eff}) + i\mathrm{Im}(K_{eff})$, and the attenuation coefficient may be found from the imaginary component as

$$a = 20\log_{10}(e)\ \mathrm{Im}(K_{eff}) \tag{3.48}$$

From equation 2.27

$$K_{eff}^2 = k_L^2 + 4\pi nf = \mathrm{Re}\left(K_{eff}^2\right) + i\,\mathrm{Im}\left(K_{eff}^2\right) = k_L^2 + \frac{4\pi n\left(\mathrm{Re}(f) - i\,\mathrm{Im}(f)\right)}{\mathrm{Re}(f)^2 + \mathrm{Im}(f)^2} = \left|K_{eff}^2\right| e^{i\arg\left(K_{eff}^2\right)}$$

$$K_{eff} = \mathrm{Re}\left(K_{eff}\right) + i\,\mathrm{Im}\left(K_{eff}\right) = \sqrt{\left|K_{eff}^2\right| e^{i\arg\left(K_{eff}^2\right)}}$$

$$\mathrm{Im}(K_{eff}) = \sqrt{\left|K_{eff}^2\right|}\sin\left(\frac{\arg\left(K_{eff}^2\right)}{2}\right) \tag{3.49}$$

The same principle may be applied to equation 2.28, although in this case $\mathrm{Im}(K_{eff})$ must be obtained numerically from the resulting cubic equation.

$$K_{eff}^2 = k_L^2 + 4\pi nF = X + iY = k_L^2 + 4\pi n\left(\frac{1}{\left(\mathrm{Re}(f) + i\,\mathrm{Im}(f)\right)} - i\left(X + iY - k_L\right)\right)^{-1} \tag{3.50}$$

For comparison, the attenuation coefficient was also found assuming no multiple scattering, using the summation method adopted by de Jong *et al* (1992) described in Chapter 2 whereby

$$a = 10\log_{10} e \int_0^\infty s_{ext}\, n(R_1)\, dR_1 \tag{2.24}$$

and

$$s_{ext} = \frac{\left\langle P_{vis} \right\rangle_t}{I_i} = \frac{4\pi\omega^2 \rho_L c_L \delta_d}{\rho_S \alpha\left(\left(\omega_o^2 - \omega^2\right)^2 + \delta_d^2 \omega^2\right)} \tag{2.26}$$

The results are shown in figures 3.9-11.

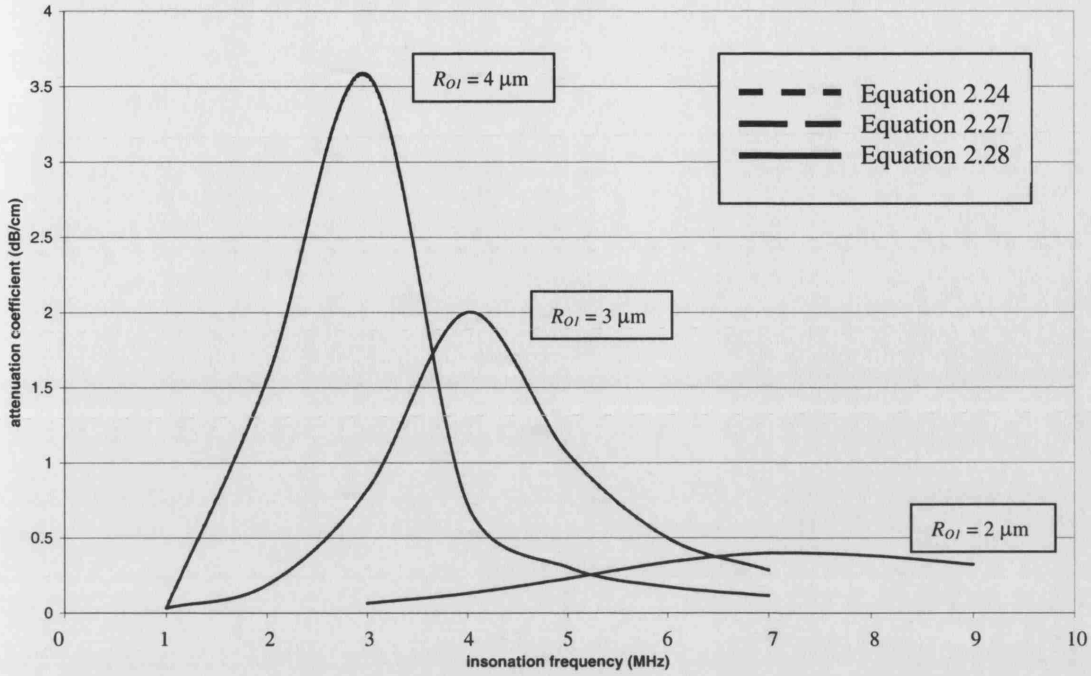

Figure 3.9: Variation in attenuation with frequency and CAP radius for Albunex® suspensions in water with concentrations of 10^4 CAPs/ml, as predicted by equations 2.24, 2.27 and 2.28.

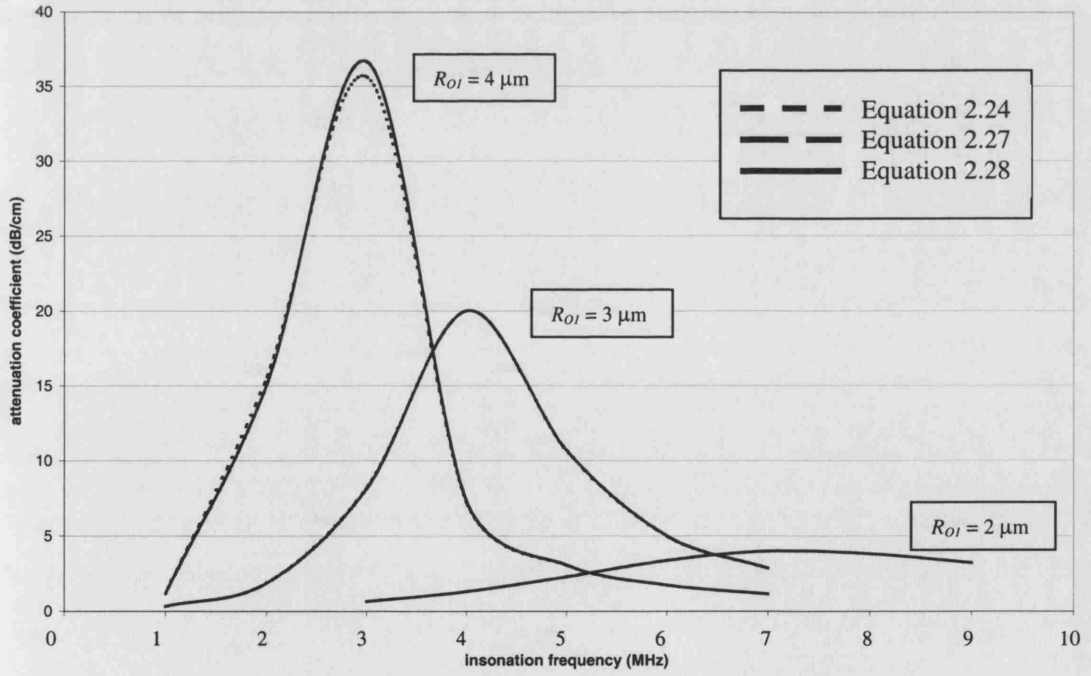

Figure 3.10: Variation in attenuation with frequency and CAP radius for Albunex® suspensions in water with concentrations of 10^5 CAPs/ml, as predicted by equations 2.24, 2.27 and 2.28.

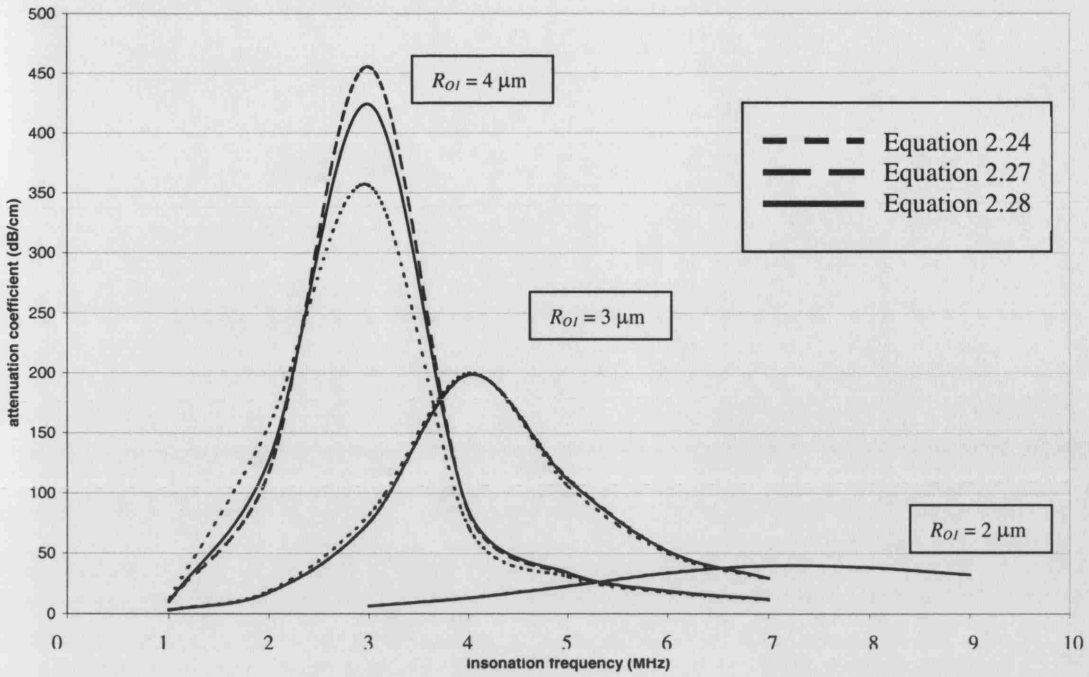

Figure 3.11: Variation in attenuation with frequency and CAP radius for Albunex® suspensions in water with concentrations of 10^6 CAPs/ml, as predicted by equations 2.24, 2.27 and 2.28.

Figure 3.9 indicates that, at a concentration of 10^4 CAPs/ml, the effects of multiple scattering should be negligible, and equations 2.27, 2.28 and 2.24 are then of equal value provided small amplitude linear behaviour can be assumed. This would appear to be supported by the existing experimental evidence (e.g. Marsh *et al* 1997) as will be discussed below. At 10^5 CAPs/ml (figure 3.10) there is some discrepancy between the predictions of equation 2.24 and those of equations 2.27 and 2.28 at the peak of the curve for the largest CAP radius (R_{o1} = 4 μm). This implies that a small degree of multiple scattering may be expected between the larger CAPs in the distribution at this concentration when they are excited at their resonance frequencies.

At 10^6 CAPs/ml (figure 3.11) the discrepancies between the curves for equations 2.24, 2.27 and 2.28 are much more significant, implying that there would be a higher incidence of multiple scattering over a wider range of CAP radii. Moreover, the differences between the results for equation 2.27 and equation 2.28, indicate that higher orders of scattering may also be expected. The initial concentrations of contrast agent suspensions, as supplied by their manufacturers, are of the order of 10^9 CAPs/ml. Clearly the suspensions will be diluted upon injection into the body, and this will be discussed further later, but it would appear that the possibility of multiple scattering cannot be dismissed without further investigation. First, however, the non-linearity of CAP behaviour must be taken into account.

3.9.3 Non-linear multiple scattering

As discussed in Chapter 2, a number of models for non-linear multiple scattering in liquids containing free bubbles have been derived (Van Wijngaarden 1968; Commander & Prosperetti 1989). None of the existing models, however, consider the effect of an encapsulating shell and the majority of the results published relate to linear behaviour only. The aim of this section is to present a new model, derived according to the reasoning of Van Wijngaarden and Caflisch, which includes the effects of an encapsulating shell and which can be solved numerically in order to examine the effects of multiple scattering upon non-linear CAP behaviour. The derivation is shown below.

Assuming spherical symmetry, conservation of mass in spherical polar coordinates gives

$$\frac{\partial \rho_{eff}}{\partial t} + \nabla.\left(\rho_{eff}\mathbf{u}\right) = 0 \tag{3.51}$$

Where subscript *eff* denotes the effective medium (i.e. fluid + CAPs), ρ is density and **u** is radial velocity.

The volume fraction of CAPs in the mixture is

$$\beta = \frac{4}{3}\pi R_2^3 n \approx \frac{4}{3}\pi R_1^3 n \tag{3.52}$$

where n is the number of CAPs per unit volume. As will be shown below, n may be defined so that equation 3.52 is valid for an arbitrary size distribution.

Since $\rho_L >> \rho_G$, and $\beta << 1$, so

$$\rho_{eff} \approx \rho_G\beta + \rho_L(1-\beta) \approx \rho_L(1-\beta) \tag{3.53}$$

The contribution from the CAP shells has been ignored owing to its small value and the fact that ρ_L is similar to ρ_S (table 3.2).

Thus

$$\frac{1}{\rho_L}\frac{\partial \rho_L}{\partial t} + \nabla.\mathbf{u} - \frac{1}{1-\beta}\frac{d\beta}{dt} = 0 \tag{3.54}$$

If there is no fragmentation or coalescence of the CAPs over the time period considered then the number of CAPs will remain constant and

$$\frac{\partial n}{\partial t} + n\nabla.\mathbf{u}_C = 0 \tag{3.55}$$

Where $\mathbf{u}_C$ is the velocity of the CAP wall.

Differentiating equation 3.52 and substituting from equation 3.55 gives

$$\frac{d\beta}{dt} = \frac{4}{3}\pi\left(3R_1 n\frac{\partial R_1}{\partial t} + R_1^3\frac{\partial n}{\partial t}\right) = \frac{4}{3}\pi\left(3R_1 n\frac{\partial R_1}{\partial t} + R_1^3\left(n\nabla.\mathbf{u}_c\right)\right) \tag{3.56}$$

Substituting this into equation 3.54 gives

$$\frac{1}{\rho_L}\frac{\partial \rho_L}{\partial t} + \nabla.\mathbf{u} - \frac{4\pi}{3(1-\beta)}\left(3R_1 n\frac{\partial R_1}{\partial t} + R_1^3\left(n\nabla.\mathbf{u}_c\right)\right) = 0. \tag{3.57}$$

Since $O(\mathbf{u}) \approx O(\mathbf{u}_c)$ so $\beta\nabla.\underline{\mathbf{u}}_c << \nabla.\mathbf{u}$ and thus $\frac{d\beta}{dt} \approx \frac{\partial\beta}{\partial t}$.

equation 3.57 may hence be simplified to

$$\frac{1}{\rho_L}\frac{\partial \rho_L}{\partial t} + \nabla.\mathbf{u} - \frac{\partial\beta}{\partial t} = 0 \tag{3.58}$$

and using $\frac{dp}{d\rho_L} = c_L^2$ this may be expressed as

$$\frac{1}{\rho_L c_L^2}\frac{\partial p}{\partial t} + \nabla.\mathbf{u} - \frac{\partial\beta}{\partial t} = 0. \tag{3.59}$$

From conservation of momentum

$$\frac{\partial}{\partial t}\left(\rho_{eff}\mathbf{u}\right) + \nabla.\left(\rho_{eff}\mathbf{u}\right)\mathbf{u} = \rho_{eff}\frac{\partial \mathbf{u}}{\partial t} + \nabla.\left(\rho_{eff}\mathbf{u}\right)\mathbf{u} - \nabla.\left(\rho_{eff}\mathbf{u}\right)\mathbf{u} \approx \rho_L\frac{\partial \mathbf{u}}{\partial t} = -\nabla p. \tag{3.60}$$

The effective medium is assumed to be homogeneous and ρ_L and c_L to be constant over the range of pressures and frequencies. Thus, using equation 3.6 to eliminate $\mathbf{u}$ in equation 3.59 gives

$$\frac{1}{c_L^2}\frac{\partial^2 p}{\partial t^2} - \nabla^2 p = \rho_L\frac{\partial^2\beta}{\partial t^2} \tag{3.61}$$

If β is defined for an arbitrary size distribution $h(R_{o1},y)$ then

$$\beta = \frac{4}{3}\pi \int_0^\infty R_1^3(R_{o1}, y, t)h(R_{o1}, y)dR_{o1} \tag{3.62}$$

and

$$\frac{\partial^2 \beta}{\partial t^2} = 4\pi \int_0^\infty \left(2R_1 \left(\frac{\partial R_1}{\partial t} \right)^2 + R_1^2 \frac{\partial^2 R_1}{\partial t^2} \right) h(R_{o1}, y)dR_{o1} \tag{3.63}$$

To solve equation 3.63, and hence equation 3.61, a further equation of motion defining R_1 is needed. Equation 3.37 is suitable for this purpose, since the results shown in figures 3.9-3.11 were obtained using equation 3.37 in its linearised form.

$$\begin{aligned} & R_1\ddot{R}_1\left(1+\left(\frac{\rho_L-\rho_S}{\rho_S}\right)\frac{R_1}{R_2}\right)+\dot{R}_1^2\left(\frac{3}{2}+\left(\frac{\rho_L-\rho_S}{\rho_S}\right)\left(\frac{4R_2^3-R_1^3}{2R_2^3}\right)\frac{R_1}{R_2}\right) \\ & =\frac{1}{\rho_S}\left(\begin{array}{l} p_o\left(\frac{R_1}{R_2}\right)^3-p_\infty-\frac{2\sigma_1}{R_1}-\frac{2\sigma_2}{R_2} \\ -\frac{4\mu_L R_1^2\dot{R}_1}{R_2^3}-\frac{4V_sG_s}{R_2^3}\left(1-\frac{R_{e1}}{R_1}\right)-\frac{4\mu_sV_s\dot{R}_1}{R_1R_2^3} \end{array}\right) \end{aligned} \tag{3.37}$$

Equation 3.45 was again used as the model of the imaging pulse and, as discussed previously, acoustic damping has been neglected in equation 3.37. This is consistent with the assumption of constant density in the surrounding fluid made above. It is also a reasonable approximation for CAP behaviour at the relatively low concentrations and insonation pressures considered. For these conditions the ratio of CAP wall velocity to sound speed in the effective medium will always be much less than unity (Appendix B.v), and the value of f_{brad} will remain negligible compared with the viscous dissipation term as in figure 3.2. Clearly, however, if the model is to be developed to simulate higher pressures and concentrations this will no longer be the case, and methods for including acoustic damping in the model will be discussed below.

The solution for the simple case of a monodisperse, homogeneous CAP suspension was considered in one dimension. Equation 3.37 is coupled to equation 3.61 via $p_\infty(t)$, the pressure in the effective medium. Equation 3.61 must therefore be discretised so that the pressure p_i is evaluated at each point y_i along the direction of transmission.

$$\frac{1}{c_L^2}\frac{\partial^2 p_i}{\partial t^2} - \nabla^2 p_i = 4\rho_L \pi n\left[2R_1\dot{R}_1^2 + R_1^2\ddot{R}_1\right]_i \tag{3.64}$$

Replacing the derivatives by standard finite difference approximations (Collatz 1960) gives

$$\frac{p_{j+1,i} - 2p_{j,i} + p_{j-1,i}}{c_L^2\Delta t^2} - \frac{p_{j,i+1} - 2p_{j,i} + p_{j,i-1}}{\Delta y^2} = 4\rho_L \pi n\left[2R_1\dot{R}_1^2 + R_1^2\ddot{R}_1\right]_{j,i} \tag{3.65}$$

Subscripts i and j represent discretisation in space and time respectively.
Rearranging equation 3.65 for $p_{j,i}$ gives

$$\begin{aligned} p_{j,i} = {} & 2p_{j-1,i} - p_{j-2,i} + c_L^2\Delta t^2\left(\frac{p_{j-1,i+1} - 2p_{j-1,i} + p_{j-1,i-1}}{\Delta y^2}\right) \\ & + 4\rho_L \pi n c_L^2 \Delta t^2\left[2R_1\dot{R}_1^2 + R_1^2\ddot{R}_1\right]_{j-1,i} \end{aligned} \tag{3.66}$$

Equations 3.37 and 3.66 were non-dimensionalised as described earlier. Equation 3.66 was then evaluated using purpose written code simultaneously implementing a fourth order Runge-Kutta procedure for solving equation 3.37 at each point in space and time (Appendix B.iv).

Initial conditions representing an initially quiescent fluid were taken as:

$$p_{0,i} = p_o \qquad \textit{and} \qquad p_{1,i} = p_o \tag{3.67}$$

Boundary conditions representing a plane source of sound at y = 0 and undisturbed fluid at y = $N\Delta y$. were taken as:

$$p_{j,0} = p_o + p_A \quad \textit{and} \quad p_{j,N} = p_o \tag{3.68}$$

N was selected to ensure that $N\Delta y$ was greater than the distance propagated by the wave during the time period $M\Delta t$ considered. Similarly the latter was selected so that $M\Delta t$ was greater than the pulse length.

It was necessary to consider both accuracy and computation time in selecting Δy. For the sake of the former it was necessary for Δy to be smaller than the smallest wavelength considered ($\approx 1.5 \times 10^{-4}$ m) and for the subsequent selection of Δt to satisfy the Von Neumann criterion (Collatz 1960). The maximum values for Δy and Δt were therefore chosen to be 1.5×10^{-5} m and 1.0×10^{-8}s respectively and these were reduced proportionately until the difference between the results for Δy and Δt and $\Delta y/2$ and $\Delta t/2$ was found to be less than 2%. It was recognised that this method only provided a first order means of ensuring numerical stability. Nevertheless, its validity was supported by making further checks of the results for $\Delta y/4$ and $\Delta t/4$, and for different transmission distances (i.e. different values of M and N) to ensure that the differences in the calculated attenuation coefficients remained small. The agreement with the results from linear theory described below also provided corroboration.

The results are shown in figures 3.12 and 3.13. It should be noted that this approach is similar in some respects to that adopted in a recent treatment of free bubbles (Leighton 2004). However, the work presented here was completed independently prior to publication of the above, and whilst both treatments follow the reasoning of Van Wijngaarden (1968), Caflisch (1985) and Commander and Prosperetti (1989) in their description of the effective medium they differ fundamentally in their description of the scatterers. The present work considers microbubbles surrounded by encapsulating shells which, as mentioned above, behave very differently from free bubbles having diameters of a few millimetres.

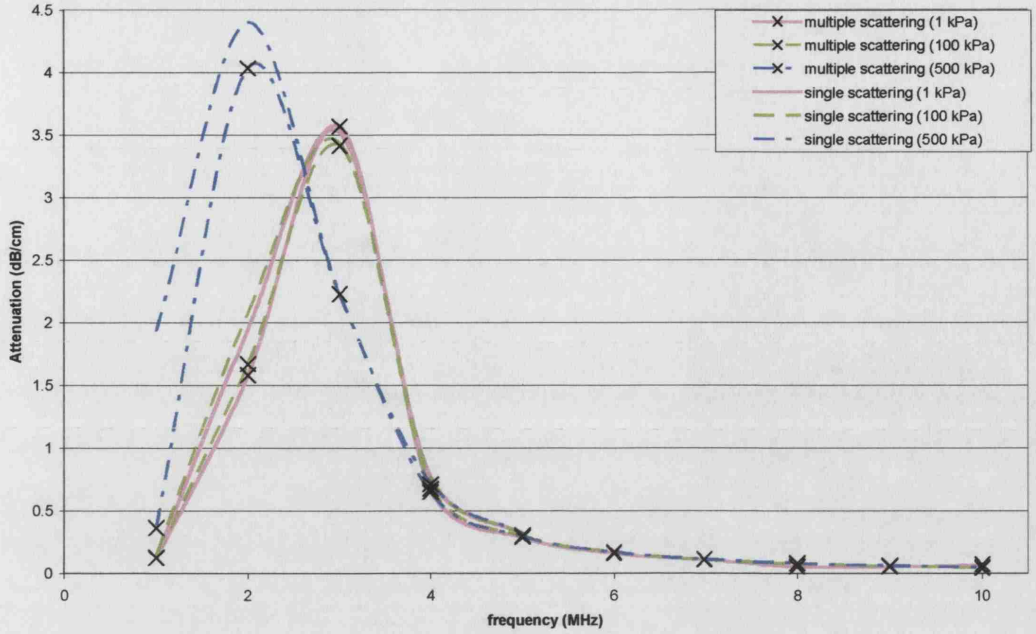

Figure 3.12: Comparison between single and multiple scattering models (equations 2.27 and 3.66) for Albunex® suspensions of 4 μm radii CAPs in water with concentrations of 10^4 CAPs/ml. Variation in attenuation with insonation frequency and pressure.

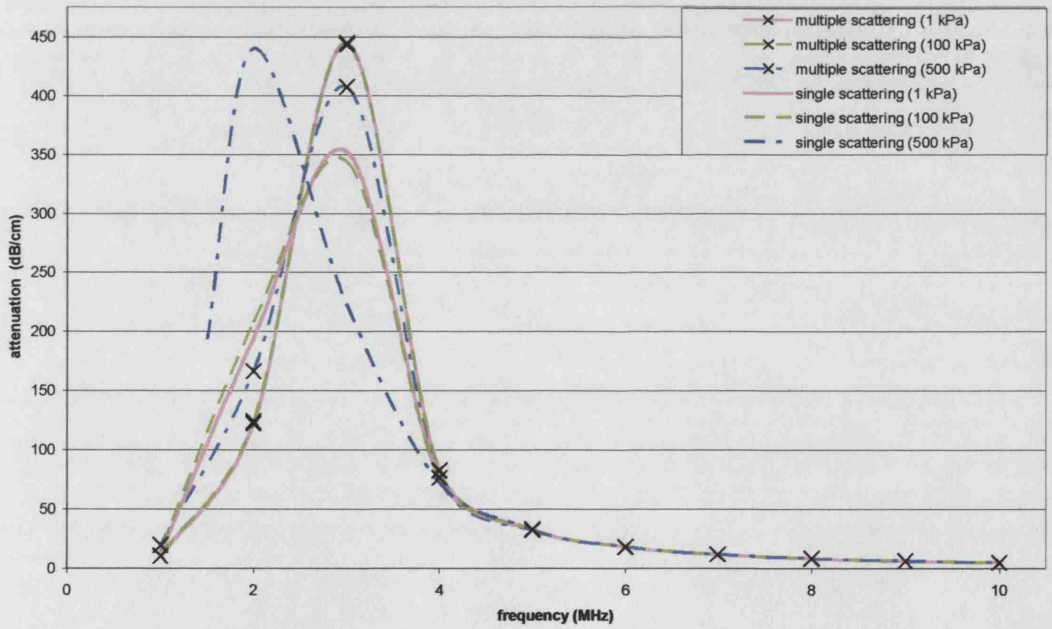

Figure 3.13: Comparison between single and multiple scattering models (equations 2.27 and 3.66) for Albunex® suspensions of 4 μm radii CAPs in water with concentrations of 10^6 CAPs/ml. Variation in attenuation with insonation frequency and pressure.

As shown in figures 3.12 and 3.13, there was found to be excellent agreement between the results of equation 3.66 and equation 2.27 (Foldy 1945) for the range of CAP radii (2-4 μm) and concentrations (10^4-10^6 CAPs/ml) investigated at low insonation pressures (10 kPa). This was as expected, since equation 2.27 may be derived from equation 3.61 in the linear limit, and it confirmed the ability of the new model to accurately predict linear multiple scattering. The small discrepancies observable may be explained by the difference in the incident frequency spectrum for pulsed and continuous wave excitation.

It was found that these discrepancies became negligible when longer bursts of sinusoidal excitation were modelled. However, the additional computing time required to carry out all the simulations with sinusoidal excitation was prohibitive. As shown previously in figure 3.11, at the highest concentration (10^6 CAPs/ml) there was a much more noticeable difference between the results from equations 2.27 and 2.28 (Henyey 1999) due to the fact that higher orders of scattering are only accounted for by the latter. Methods for incorporating higher order scattering into equation 3.66 will be discussed later.

Figures 3.12 and 3.13 show how the attenuation in CAP suspensions may be expected to vary with insonation pressure. To enable single and multiple scattering models to be compared at different pressures, results were plotted from equation 3.66 and from a numerical solution of equation 3.37. For the latter, attenuation was found from equation 2.24 with s_{ext} being found from numerical integration of the dissipated power[3] over the course of a single pulse

$$s_{ext} = \frac{\langle P_{vis} \rangle_t}{I_i} \text{ where } P_{vis} = P_{S,vis} + P_{L,vis} \tag{2.25}$$

$$P_{S,vis} = \int_{R_1}^{R_2} \frac{-48\pi\mu_S R_1^4 \dot{R}_1}{r^4} dr = \frac{16\pi V_S \mu_S R_1 \dot{R}_1^2}{R_2^3} \tag{3.69}$$

$$P_{L,vis} = \int_{R_2}^{\infty} \frac{-48\pi\mu_L R_1^4 \dot{R}_1}{r^4} dr = \frac{16\pi\mu_L R_1^4 \dot{R}_1^2}{R_2^3} \tag{3.70}$$

[3] Further details regarding the derivation of equations 3.69 and 3.70 may be found in Appendix Diii.

As expected, the results for the lower insonation pressure mimicked those shown in figures 3.9-11. With increasing pressure, however, the results from the single scattering model showed a downwards shift in the frequency at which the attenuation was maximised and an increase in the value of the maximum. This may be attributed to the increase in prominence of the non-linear components of the CAP response with increasing pressure. The same effect was also seen in the results from the multiple scattering model (figures 3.12-3.1.3). However, it was considerably less pronounced than was the case for the single scatterer model (equation 2.24). This may be explained in terms of the modification of the incident field "seen" by each CAP as a result of multiple scattering. Qualitatively, the presence of harmonics in the fields radiated by neighbouring CAPs would skew the incident spectrum towards higher frequencies. This would counteract the downwards shift due to increasing pressure. The potential consequences of using single scatterer models to interpret experimental results are discussed in Chapter 4.

The new model overcomes several of the limitations associated with equations 2.27, 2.28 and 2.24. It is valid for the same range of concentrations as equation 2.27 (Foldy 1945) so that, unlike equation 2.24 (Medwin 1977), it may be used to predict CAP behaviour when multiple scattering effects are observable. Unlike equations 2.27 and 2.28, however, it is valid for insonation pressures at which CAPs undergo non-linear oscillations. In addition, the treatment of the pressure radiated by the CAP is more realistic than that given by equation 2.15 which models the CAP as a rigid sphere and is therefore only valid at very low amplitudes of oscillation. It also enables the effects of different types of insonation, e.g. different pulse shapes, to be examined because it must be solved numerically.

Equation 3.66 is still limited in terms of the maximum concentration for which it can be used. For the assumption of an effective medium to be valid, it is necessary to assume that the average pressure field incident upon any one CAP is large compared with that radiated by its immediate neighbour. Assuming it is valid to take $n^{-1/3}$ as the average distance between CAPs, then for the linear case this imposes the following condition (Commander and Prosperetti 1989):

$$\frac{\omega R_{o1}}{n^{-1/3}\sqrt{\left(\left(\omega_o^2-\omega^2\right)^2+4\delta_d^2\omega^2\right)}} \ll 1 \qquad (3.71)$$

This may be used as an approximate gauge for the validity of equation 3.66. Clearly the condition is most severe at the resonance frequency when $\omega = \omega_o$ for a given R_0. The limiting concentrations for each CAP radius are shown in table 3.8.

Radius (microns)	Limiting concentration (CAPs/ml)
2	6.87×10^8
3	3.34×10^7
4	3.91×10^6

Table 3.8: Limiting concentrations for which equation 3.66 is valid.

Equation 3.66 is analogous to equation 2.27 in that only one additional scattering from each CAP is considered. Equation 2.28 is valid for higher concentrations than either equation 2.27 or equation 3.66 because it considers higher orders of scattering. For equation 3.66 to be valid at higher concentrations, it would be necessary to estimate the speed of sound for the effective medium, rather than treat it as a constant equal to the sound of speed in the surrounding fluid. This could be done iteratively, improving the estimate for c_{eff} upon each run of the model. For consistency it would also be necessary to include an acoustic damping factor in equation 3.37, which would itself depend upon the sound speed in the effective medium. Before this work is carried out, however, it is important to determine whether the effects of multiple scattering indicated by the above results can be observed experimentally, and hence whether the additional complexity and computing time is in fact warranted. This is the topic of the next chapter.

3.10 Summary

In this chapter a new generalised model for CAP behaviour has been derived and the assumptions underlying individual terms have been examined in order to define a suitable equation for subsequent design work. It has been shown that, for the range of insonation pressures and frequencies used in diagnostic imaging, it is valid to assume that the filling gas will behave isothermally and that thermal damping may be neglected. It has also been shown that the encapsulating shell may be treated as incompressible, impermeable and insoluble over time periods considered and that its behaviour may be described using a non-linear viscoelastic constitutive equation. The selection of a suitable equation will be examined in Chapter 5. A threshold for CAP destruction has been defined, based on a new analysis of the stresses generated in the shell during oscillation and a review of the existing experimental data. This indicates that the amplitude of radial oscillation should not exceed of 2% of the initial CAP radius.

It has been shown that the pressure surrounding the CAP may be regarded as uniform, provided the CAPs remain spherically symmetric and are sufficiently far from tissue interfaces (>10 R_{o1}) and other CAPs. The influence of non-linear propagation upon the incident and radiated fields will be small for the range of pressures to be considered. Similarly, it is valid to assume for these conditions that the surrounding fluid may be regarded as incompressible and static. The results from simulations using a new model for a CAP surrounded by blood cells indicate that the influence of cells upon CAP behaviour is relatively small and may be neglected for the purposes of CAP design. The validity of this conclusion will be assessed experimentally in Chapter 4. New models for linear and non-linear multiple scattering in CAP suspensions have also been derived and used to determine the range of concentrations for which this phenomenon is likely to be significant. The findings from this work will also be compared with experimental results in the next chapter.

4

Experimental Validation

4.1 Overview

In the previous chapter, new modelling work was presented describing the behaviour of a single CAP suspended in blood. The results indicated that the presence of blood cells was a relatively minor consideration in terms of CAP design. A new model was also derived for the multiple scattering of ultrasound in a CAP population. This enabled the range of concentrations over which multiple scattering would be expected to be significant to be determined for particular CAP properties and insonation conditions. It also indicated how the attenuation coefficient would be expected to vary with increasing concentration in CAP suspensions. In order to test the validity of this work, the simulation results need to be compared with experimental data. The aim of this chapter is to describe the experiments conducted in order to obtain suitable data and to examine the implications of the results with regard to the accuracy of the models and their application to CAP design.

4.2 The behaviour of ultrasound contrast agents in whole blood

4.2.1 Aims and objectives

The degree to which a pulse of ultrasound is attenuated in passing through a CAP suspension will depend upon the dynamic response of the CAPs and hence upon any interactions between the CAPs and their surroundings. It should therefore be possible to deduce whether or not blood cells have a significant effect upon CAP behaviour by comparing the attenuation of ultrasound in plasma and in whole blood with and without CAPs present. In the absence of any significant CAP/cell interaction, the same difference in attenuation between plasma and blood would be expected in both cases.

The sources of attenuation in plasma and blood are summarised in table 4.1. It is the absorption and scattering losses which should be affected primarily by any CAP/cell interaction. This might be due to direct damping of CAP oscillations by surrounding cells, to modification of the incident field due to scattering or to a hitherto unrecognised mechanism. The other sources of attenuation mentioned in table 4.1 should remain constant since they are essentially apparatus dependent. There will be slight differences in the losses through the reflecting plate (c.f. figure 4.1), but these should be small since the suspending fluid (plasma) remains the same. The diffraction losses will vary between the different media but these effects may be compensated for as described in Appendix C.i. The dependence of the attenuation coefficient upon the insonation pressure will be discussed later.

	Fluid			
Source of attenuation	Plasma (no cells)	Whole blood	Suspension of CAPs in plasma	Suspension of CAPs in whole blood
Fluid absorption	•	•	•	•
Losses through reflecting plate	•	•	•	•
Diffraction	•	•	•	•
Transducer losses	•	•	•	•
Cell absorption		•		•
Cell scattering		•		•
CAP absorption			•	•
CAP scattering			•	•

Table 4.1: Mechanisms of attenuation in plasma and whole blood, with and without contrast agent.

4.2.2 Apparatus

A schematic of the experimental apparatus is shown in figure 4.1. The test medium was contained in a clear polymethylmethacrylate cylinder (inner diameter 39 mm, wall thickness 3 mm) adhesively joined to a stainless steel plate and sealed. The dimensions of the cylinder were selected so as to avoid interference from the cylinder walls and to provide sufficient depth of fluid for the selected transmission distances d_1 and d_2 (which were varied in the range 2.25 cm to 5.5 cm). The latter were chosen to ensure adequate separation of the incident and reflected pulses (for a pulse of 4 cycles pulse length = 1500 x 4 /5 x 10^6 = 1.2 x 10^{-3} m). Stainless steel was used to provide a good impedance contrast with the fluid, and hence a high reflection coefficient, and to avoid any contamination of the fluid due to chemical reaction.

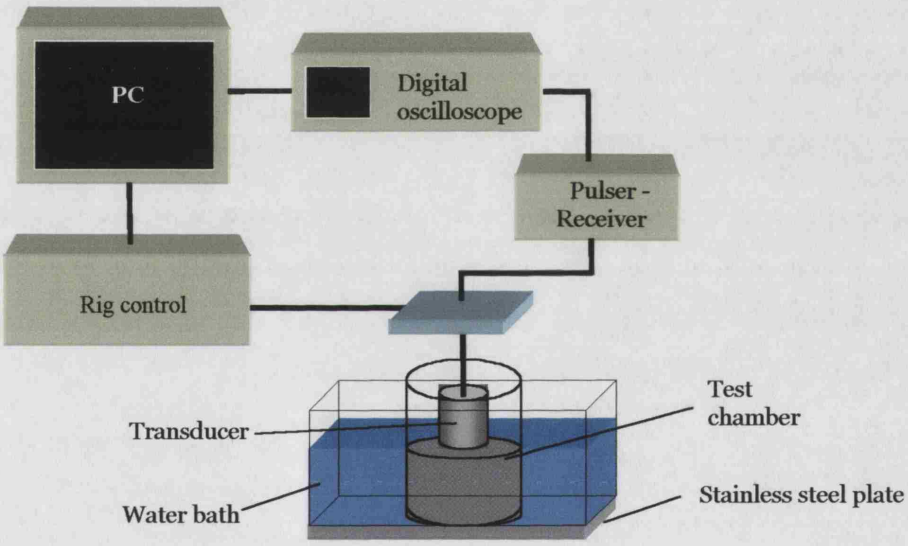

Figure 4.1: Schematic of the experimental apparatus.

Since the behaviour of contrast agents, and ultrasound attenuation measurements in general, are extremely sensitive to temperature, all the experiments were conducted at room temperature and the test cylinder was immersed in a water bath to reduce the effect of temperature fluctuations. For the same reason all the instruments used for handling the test samples were kept immersed in the bath when not in use. These considerations were thought to outweigh the advantages of performing the experiments at *in vivo* temperatures. The temperature in the test cylinder was monitored continuously using a digital thermometer (model 650-419, RS Components, Corby, Northhants, UK).

The contrast agent Optison® (Amersham PLC Bucks. UK) was selected on the basis that its having an albumin shell would enable reasonable comparisons between theory and experiment. The properties as specified by the manufacturer are shown in table 4.2.

Shell	Human serum albumin
Filling gas	Octafluoropropane
Mean radius	2.25 μm
Maximum radius	16 μm (93% less than 10 μm)
Concentration	5-8 x 10^8 CAPs/ml prior to dilution

Table 4.2: Properties of Optison® (Amersham PLC, Amersham, Bucks., UK).

Optison® suspensions were prepared according to the manufacturer's instructions and diluted to concentrations of 10^3 CAPs/ml with blood or plasma according to the experiment. This relatively low concentration was used for two reasons. Firstly, a high cell:CAP ratio was required, in order to maximise the probability of CAP/cell interaction. Secondly, it was desirable to reduce significant multiple scattering between CAPs in order to minimise additional sources of attenuation which might distort the results. The CAP size distribution for Optison® was determined using a particle sizer (Malvern Mastersizer 2000, Malvern, UK) as shown in figure 4.2.

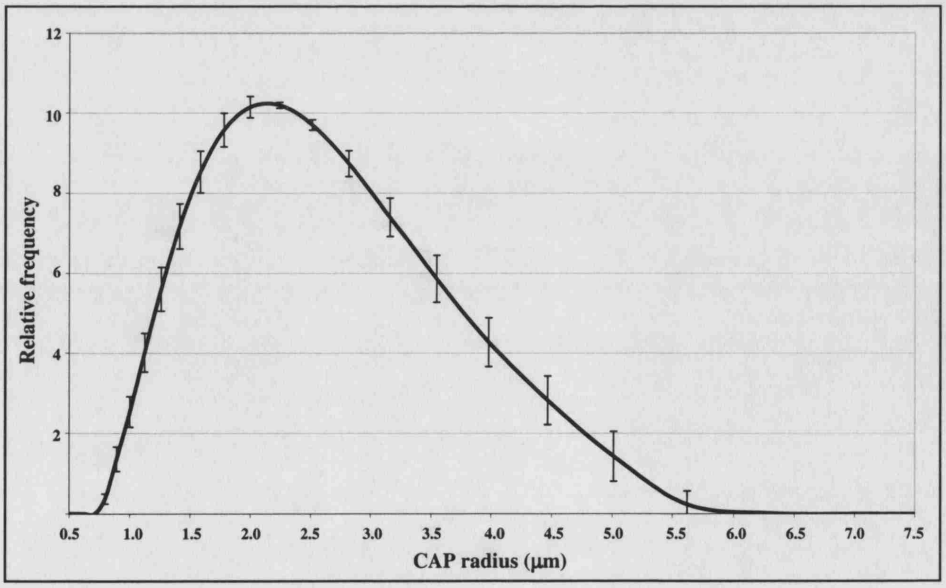

Figure 4.2: Size distribution determined for Optison®.

Thirty six day-old whole human blood from a single donor was obtained from the UCL Hospital transfusion service and handled in accordance with their guidelines. The test samples were examined using an optical microscope (Vickers 6199T @ 40 x 10 magnification) to verify that the majority of blood cells were still intact. The plasma for the experiments was prepared by centrifuging the blood from half of the samples to ensure continuity of properties. The centrifuge (Eppendorf 5810 R) was run for 10 minutes at 2500 relative centrifugal force (RCF) and the plasma was re-examined using the optical microscope to confirm that the cells had been removed.

The samples were insonified using a bespoke broadband transducer having a nominal centre frequency of 5 MHz, diameter 20 mm and a 3 dB bandwidth of 5 MHz. This was selected in order to cover the range of frequencies over which the larger CAPs in the suspension would be expected to exhibit maximum response, and in which it would seem reasonable to expect any CAP/cell interaction to occur. At higher frequencies the attenuation and sensitivity to certain types of error (c.f. section 4.2.4.2) would have been too great for accurate measurements to be made. At lower frequencies, the amplitude of the CAP response would have been smaller and thus the likelihood of CAP/cell interaction reduced.

As shown in figure 4.1, the transducer was activated using a pulser/receiver unit (Panametrics model 5055 PR) which was set to give an output peak negative pressure in water of approximately 50 kPa. The exact pressure was determined using a needle hydrophone as described below. According to the results shown in the previous chapter (section 3.6) this pressure should have been low enough both to avoid rapid CAP destruction and to suppress the excitation of any higher harmonics in the CAP response. This was desirable in order to minimise the time and pressure dependence of the attenuation measurements, and because low insonation pressures corresponded to the behaviour considered in the model.

The hydrophone measurements were performed using a needle hydrophone (Precision Acoustics model 698) with a 0.2 mm tip which was scanned across the transducer face in 0.2 mm steps at different planes to capture the beam profile (Appendix C.ii). The angular tolerance for the hydrophone was 0 dB for $\pm 10^{o}$ over the measured bandwidth. The signals from the transducer were captured using a digital oscilloscope (LeCroy 9310M Dual 300 MHz) connected to a PC.

4.2.3 Procedure

The apparatus was set up as shown in figure 4.1. The vertical distance between the face of the transducer and the reflecting plate was measured in two ways to reduce the risk of error. Firstly, the number of revolutions of the leadscrew from a known starting position on the precision scanning rig was recorded and, secondly, a direct measurement was made using Vernier callipers. The plane of the transducer face was brought parallel with the reflecting plate using the adjusting screws on the rig and transducer holder. The correct level was initially determined using spirit levels on the rig and subsequently checked by ensuring that the amplitude of the first echo from the base plate was maximised on the oscilloscope (corresponding to an uncertainty of $\pm 1.5^{o}$).

To minimise the influence of external factors, each complete set of experiments was performed on the same day. Preliminary measurements were made prior to the main experiment using rape seed oil in order to assess the sensitivity of the apparatus. For each fluid, the test cylinder was filled to a depth of 6 cm and time allowed for the temperature to stabilise. Broadband pulses were transmitted at a pulse repetition frequency of 0.6 kHz and the first and second echoes from the reflecting plate captured at 1 Giga-sample per second. The separation of the echoes was also measured by recording the positions of both the first zero crossing and the peak negative pressure, so as to compensate for any distortion of the signal.

These measurements were repeated with the transducer at two positions below the starting position of 5.5 cm (figure 4.3). The motor powering the rig was switched off whilst the measurements were being made in order to avoid signal interference. At each position three traces were captured and the cylinder temperature recorded. Between captures the fluid samples were mixed by plunging a 1 ml syringe which was fixed to the inside of the cylinder to ensure an even distribution of CAPs and/or cells and to equalise the fluid temperature by removing any localised heating from the transducer.

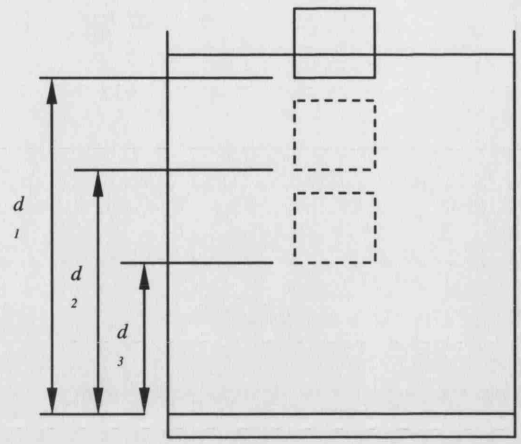

Figure 4.3: Diagram showing transducer positions and transmission distances d_1, d_2, d_3.

For each sample, two sets of measurements were made from slightly different starting positions, so that six sets of measurements for each pair of distances were obtained. This was done to enable averaging and because the variation in the signals would provide a measure of the uncertainty in the results. Between each test the cylinder was cleaned and then left in the water bath to allow the temperature to stabilise before the next sample was added. A summary description of the samples is given in table 4.3.

Sample name	Volume (ml)	Preparation	CAP concentration (CAPs/ml)
Oil	72	As received.	0
Plasma	72	Centrifuged for 10 mins @ 2500 RCF.	0
Blood	72	As received.	0
Plasma/CAP	72	Centrifuged as above with addition of CAP suspension.	10^3
Blood/CAP	72	As received with addition of CAP suspension.	10^3

Table 4.3: Summary of fluid test samples.

4.2.4 Analysis

4.2.4.1 Attenuation Coefficients and velocity

The captured signals were processed in Matlab®. Each signal was normalised with respect to its mean value and its frequency spectrum obtained via fast Fourier transform. The amplitudes at 3.0, 4.0 and 5.0 MHz were determined and the mean average amplitude calculated for each transducer position. The attenuation coefficient was then found for each pair of transducer positions as

$$a = \frac{10\log_{10} e}{2(d_i - d_j)} \ln \left| \frac{A_j}{A_i} \frac{A_{di}}{A_{dj}} \right| \qquad i = 1,2; j = 1,2,3; i < j \qquad (4.1)$$

where A is the average measured amplitude from the frequency spectrum and A_d is the diffraction correction factor (Appendix C.i). The subscripts i and j refer to individual transducer positions. The mean average attenuation coefficient and corresponding standard deviation were then found for each fluid. Similarly the acoustic velocity for each fluid was found as

$$c = \frac{2d_i}{t_2 - t_1} \qquad (4.2)$$

where t_2-t_1 is the separation in time of the first and second echoes from the reflecting plate. Again the mean average and standard deviation were calculated for each set of measurements.

4.2.4.2 Uncertainty Analysis

The potential sources of uncertainty were identified as follows:

i) Measurement uncertainty

The uncertainty in the amplitude measurements δA_i was estimated from the variation between the different traces taken at each position, since these should, in theory, have been identical. For the transducer/plate separation, the uncertainty δd_i was taken to be half the smallest division of the scale used to measure the initial separation. Added to this was the appropriate multiple of the uncertainty in the screw thread (see (iv) below) corresponding to the number of steps taken from the initial position. The uncertainty in the pulse separation measurements δt was similarly taken to be half the smallest division on the measurement scale.

The corresponding theoretical uncertainties in the attenuation coefficient (δa) and acoustic velocity (δc) were then found as:

$$\begin{aligned}\delta a &= \frac{\partial a}{\partial A}\delta A + \frac{\partial a}{\partial A_d}\delta A_d + \frac{\partial a}{\partial d}\delta d \\ &= \frac{1}{2d}\left(\frac{A_d}{A}\delta A \frac{\partial A}{A_d}\delta A_d - \frac{1}{d}\ln|AA_d|\delta d\right)\end{aligned} \tag{4.3}$$

$$\delta c = \frac{\partial c}{\partial d_i}\delta d_i + \frac{\partial c}{\partial t}\delta t = \frac{2}{t}\delta d_i + \frac{2d}{t^2}\delta t \tag{4.4}$$

where $\delta A = \frac{A_j \delta A_i}{A_i^2} + \frac{\delta A_j}{A_i}$, $\delta A_d = \frac{A_{di}\delta A_{dj}}{A_{dj}^2} + \frac{\delta A_{di}}{A_{dj}}$ and $\delta d = \delta d_i + \delta d_j$,

The uncertainty associated with the diffraction correction factor δA_d was primarily related to the uncertainty in the value of c. δA_d could not be derived analytically owing to the complexity of the diffraction correction function (Appendix C.i). The maximum allowable precision in A_d was therefore estimated by varying c according to the calculated δc and then according to the observed standard deviation and noting the corresponding variation in A_d.

ii) Diffraction

As indicated above, the attenuation measurements were corrected to compensate for diffraction by a factor A_d. The method is described in Appendix C.i.

iii) Levelling

The measured signal amplitudes were found to be extremely sensitive to the angle between the plane of the transducer face and that of the reflecting plate surface. This angle, which ideally should have been zero, could not be measured accurately with the apparatus used, and the relative levels of the transducer and plate had to be judged by eye, as described previously. Consequently it was not possible to quantify the associated uncertainty. It was confirmed, however, using spirit levels that there was no change in the angle between the plate and transducer upon altering their separation. The effect of any levelling error upon the relative attenuation measurements, and hence upon the main results of the experiment, should therefore have been minimal.

iv) Temperature

Every effort was made to maintain the apparatus at a constant temperature but inevitably some heat was generated during the experiment. The estimated effects of the measured temperature rises based on published data for blood (Duck 1990) are shown in table 4.4.

Temperature	°C	20	30	40		Approx. gradient	
Velocity	m/s	1555	1571	1592		2.0	m/s/°C
Attenuation (@ 10 MHz)	dB/cm	2.90	2.7	2.5		-0.02	dB/cm/°C

Table 4.4: variation in acoustic velocity and attenuation with temperature in blood (Duck 1990).

In addition to the effect upon the fluid properties, changes in the ambient temperature were found to affect the pitch of the screw controlling the transducer/plate separation. This had been measured previously at a much lower temperature so that the initial (discarded) calculations of a were subject to large errors. Once the screw had been recalibrated for the higher room temperature, however, the changes due to the relatively small short term fluctuations were found to be negligible.

v) Destruction

In the event of substantial CAP destruction, the amplitude of the observed signal at a particular transducer position would have been expected to increase with time as the attenuating effect of the CAP diminished. No such changes were observed in any of the tests, however, implying that the insonation pressure was sufficiently low to avoid significant CAP destruction within the measurement time.

vi) Drift

Similarly, the continuity of the observed signal at each transducer position indicated that the CAP suspension was adequately mixed over the course of the experiment and any errors due to CAP segregation were small.

vii) Transducer surface contamination

Care was taken to remove all visible bubbles from the surface of the transducer and there was no evidence of CAPs sticking preferentially to the surface, either visually or in terms of intermittently enhanced attenuation.

viii) Numerical processing errors

A sensitivity analysis indicated that the uncertainties due to quantisation of the measured signals and calculation of the FFT were small compared with those from other sources.

4.2.5 Results

The principal results from the investigation are summarised in this section. The complete set of results is included in Appendix F.

			Max uncertainty	Max standard deviation
Acoustic velocity	(m/s)	1413	32.1	11.7
Attenuation coefficient	(dB/cm)	0.54	0.01	0.008

Table 4.5: Results for calibration experiment with rape seed oil at 29°C.

Frequency	Additional attenuation due to the presence of blood cells		Difference	Max Uncertainty	Max Standard Deviation
	No CAPs	With CAPs			
(MHZ)	(dB/cm)	(dB/cm)	(dB/cm)	(dB/cm)	(dB/cm)
3.0	0.35	0.35	-0.00001	0.004	0.010
4.0	0.47	0.47	-0.00013	0.010	0.009
5.0	0.58	0.58	0.00021	0.019	0.011

Table 4.6: Average change in attenuation produced by the presence of blood cells with and without contrast agent present.

Fluid		Plasma	Blood	Plasma/CAP	Blood/CAP
Temperature	(°C)	30.6	29.4	30.9	30.9
Acoustic velocity	(m/s)	1528	1564	1529	1562
Max Standard Deviation	(m/s)	3.48	3.19	3.00	3.89
Max Uncertainty	(m/s)	32.2	32.8	25.3	37.6

Table 4.7: Average acoustic velocities measured for the fluid samples.

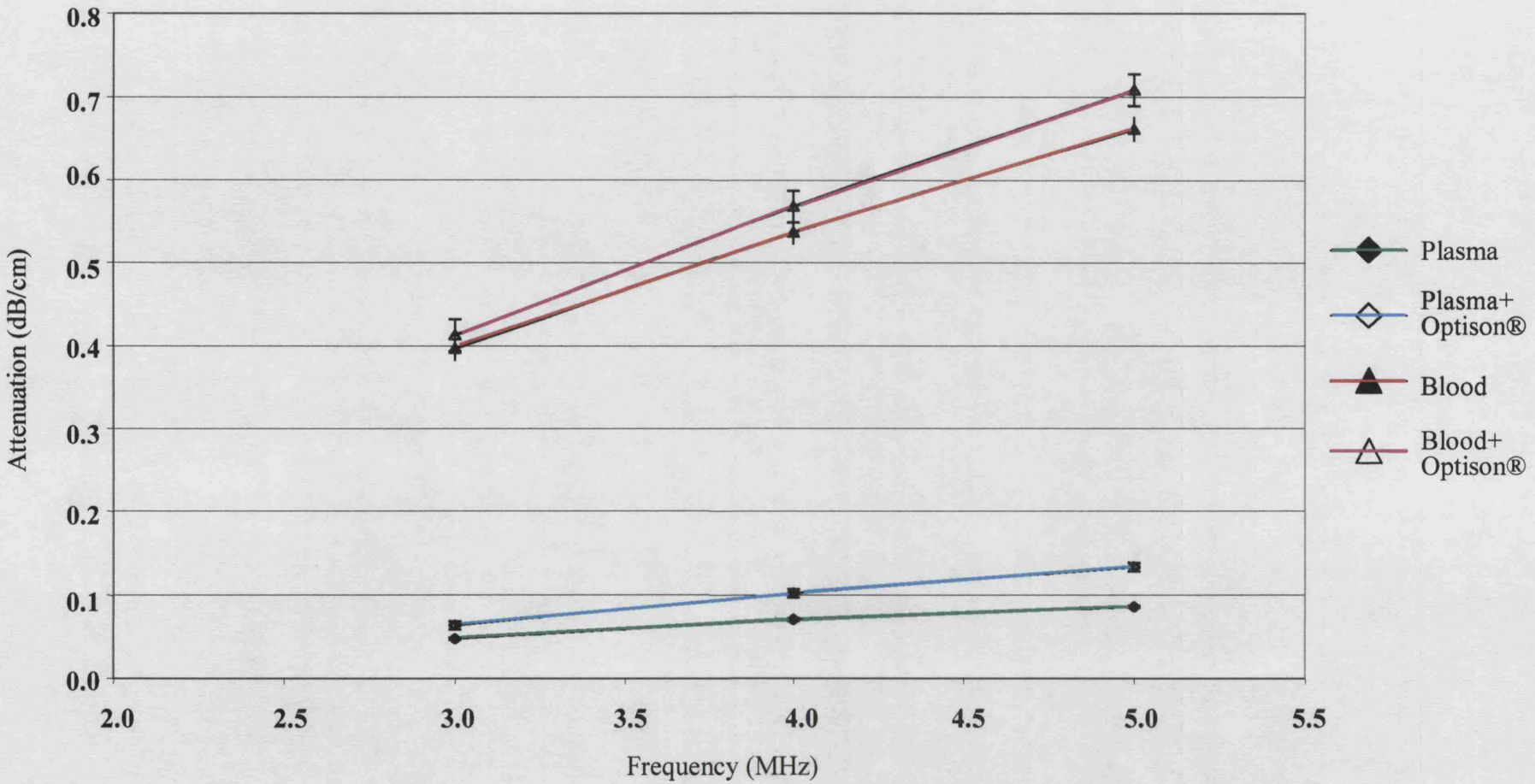

Figure 4.4: Average broadband attenuation measurements for (i) plasma (30.6°C), (ii) CAP suspension in plasma (30.9°C), (iii) blood (29.4°C), (iv) CAP suspension in blood (30.9°C). Error bars indicate experimental uncertainty.

4.2.6 Discussion

The attenuation coefficients calculated for the rape seed oil, plasma and blood (tables 4.5 and 4.6) were in good agreement with published values for these fluids (e.g. Duck 1990). Similarly, the measured velocities were also found to correlate well with previous measurements (tables 4.5 and 4.7). Any differences may be explained in terms of the different temperatures at which the previous experiments were conducted and variability in the properties of blood/plasma between individuals e.g. % haematocrit. This was not measured in these experiments since the absolute values of attenuation were not the primary values of interest and these variations would not be expected to significantly affect the behaviour of CAPs in plasma or whole blood. As shown in the previous section, the predicted uncertainties in the measurements were less than 5% of the values themselves, with only two exceptions. More importantly, the standard deviations in the measurements were lower than the predicted uncertainties in all cases. On the basis of the above, it may be concluded that the accuracy of the experiment was adequate for the purposes of this investigation.

It should be emphasised that it was only the relative degree of attenuation between the fluid samples which was of interest in this experiment. The accurate prediction of the absolute values for the attenuation coefficient in CAP suspensions is, as indicated in Chapter 3, a much more complex problem owing to the uncertainties in the CAP parameters. The effect of CAPs upon the measured acoustic velocity was found to be smaller than the standard deviation for the measurements and did not show a clear trend (table 4.7). This was as expected, since, according to the results shown in the previous chapter (figure 3.9), the CAP concentration used was too low for a significant change to be observed. Consequently the dispersive nature of the fluid samples was not investigated. If dispersion had been significant, a change in the shape of the pulse and frequency spectrum would have been observed between the first and second echoes due to the differing velocities of individual frequency components. This was not seen (Appendix Cii).

The main concern of this investigation was to determine whether the presence of blood cells has a significant effect upon CAP behaviour. As shown in table 4.6, the change in attenuation due to the cells was found to be very similar with and without CAPs present over the range of frequencies tested. The differences were

considerably smaller than either the predicted uncertainty or the standard deviation in the attenuation measurements. There was a larger difference in the change in acoustic velocity between the plasma and whole blood samples. Again though this was found to be less than the expected uncertainty in the measurements and could not therefore be interpreted as evidence of CAP/cell interaction.

Clearly a smaller experimental uncertainty in the velocity measurements would have been desirable, and it might have been advantageous to have used a higher CAP concentration, since the change in attenuation produced by the addition of the CAPs was somewhat close to the predicted uncertainty. Unfortunately, neither of these modifications could have been implemented with the apparatus available and, as discussed previously, there were reasons why using a low CAP concentration was considered to be appropriate. Notwithstanding these criticisms, the results do appear to support the conclusion of the theoretical study: that the effect of interaction between CAPs and blood cells is small in terms of its effect upon CAP acoustic response. This in turn implies that blood cells are not a major consideration in terms of CAP design.

There are a number of caveats associated with this conclusion. Firstly, the effect of anti-coagulants upon the viscoelastic properties of red blood cells was not examined. However, it is unlikely that any changes would be significant compared with the differences between the properties of cells and CAP coatings. As will be shown further in the next chapter, it is this which is important in terms of CAP response. Secondly, the results were obtained using relatively low insonation pressures. It should not be assumed automatically that the same results would be obtained at higher pressures such as those used for destructive imaging modes. Further modelling of CAP destruction, as indicated in Chapter 3, followed by further experiments, would be required in order to assess this. Thirdly, the results only apply to albumin-shelled CAPs and should not be used to draw conclusions about the behaviour of, e.g. free bubbles in the bloodstream without further investigation. For the purposes of this thesis, the results for albumin-shelled CAPs are the most relevant since, as will be shown in the next chapter, the nature of the encapsulating shell can have a very strong influence upon CAP behaviour. This is the case with albumin-shelled CAPs and is a feature which may be exploited for CAP design.

The positive slope of the curves in figure 4.4 would seem to suggest, at first, that the CAPs were not excited at their resonance frequencies. If they had been then, intuitively, a peak in the attenuation coefficient would have been expected. However, for small CAP radii, such as are present in Optison®, the sharpness of the resonance peak is greatly decreased. This is due to the fact that shell thickness does not vary with radius and hence the relative degree of viscous damping is increased for smaller CAPs. There is also some discrepancy between the frequency at which the amplitude of CAP oscillation is greatest and that at which the attenuation coefficient is maximised. According both to theory and previous experimental results (Shi and Forsberg 2000; Chen *et al* 2002), the range of insonation frequencies used in the experiment should have coincided with the regime in which the amplitude of CAP oscillation was greatest. Hence the probability of interaction between CAPs and cells should have been maximised.

There may have been an additional reason for the lack of an attenuation peak in figure 4.4. As discussed in Chapter 2, the attenuation of contrast agent suspensions has been found to be dependent upon insonation pressure as well as frequency. Consequently, the attenuation-frequency curve obtained from broadband measurements depends not only upon the attenuative properties of the medium but also upon the amplitude distribution of the input spectrum. The curve may be distorted compared with that which would be obtained by narrowband measurements at a single insonation pressure, so that the resonance peak is obscured. This could potentially explain why there was found to be some discrepancy between figure 4.4 and the attenuation curves obtained by Shi and Forsberg (2000). The latter investigators were, however, using different suspending fluids and concentrations of Optison®, and without details of the size distributions and temperature within the measurement volume a valid comparison of results cannot be made.

It should also be emphasised that it was only the effect of the presence of blood cells upon CAP acoustic response that was investigated and not the reverse. There is substantial experimental evidence to suggest that cells are affected by the presence of oscillating CAPs, albeit at higher insonation pressures than those considered here. For example, Khanna *et al* (2003) examined the effect of ultrasound exposure upon red blood cells in the presence of Optison® CAPs at an insonation pressure of 0.98 MPa and a CAP/cell ratio of 5:1. In agreement with the results obtained in this

investigation, and in spite of using much higher pressures and concentrations, they observed no differences in the acoustic emissions from the CAP/cell suspensions compared with those containing pure contrast agent. They did, however, observe haemoglobin release and other changes in the appearance of the cells indicating that they had been quite severely affected.

4.2.7 Conclusion

The experimental results support the conclusion of the theoretical results (section 3.7) that the presence of blood cells in a contrast agent suspension does not have a significant effect upon the acoustic response. This implies that it is justifiable to model the surrounding fluid as homogeneous and Newtonian for the purposes of CAP design, particularly if the influence of the encapsulating shell upon CAP response is large. It should be noted that only the low pressure response of albumin-shelled CAPs was investigated and the results should not be used to predict the behaviour of CAPs at high insonation pressures, at which CAP destruction might be significant. Similarly, the effect of CAP/cell interaction upon blood cells was not examined and no conclusions regarding contrast agent safety should be drawn.

4.3 Multiple scattering

4.3.1 Aim

As discussed in Chapter 2, experimental evidence for multiple scattering has already been reported. Marsh *et al* (1997) performed attenuation and phase velocity measurements in suspensions of Albunex® and found that the peak attenuation was underestimated by equation 2.24 for suspensions with concentrations greater than 10^6 CAPs/ml. This finding would appear to support the predictions of section 3.9.2. There are, however, a number of factors to consider in assessing the reliability of this evidence. For example, the measurements were reported as being highly sensitive to temperature and the heat generated during the experiment would have been expected to increase with increasing concentration. Thus, there would have been a variation in the attenuation of the different test samples, regardless of whether or not multiple scattering was taking place. From existing data (Duck 1990), the additional heating would in fact have been expected to reduce the measured attenuation, but a separate experiment to confirm that this is the case in Albunex® suspensions would be needed to remove the uncertainty.

In comparing their experimental results with theory, Marsh *et al* assumed that the Albunex® CAPS would behave linearly. However, at the insonation pressures used (0.2-0.3 MPa), detectable non-linear behaviour would have been expected and this would have increased the apparent attenuation at the fundamental frequency. It is not clear that this could explain the enhancement in attenuation at higher concentrations, however, since, in the absence of multiple scattering, the generation of higher harmonics should not be a function of concentration. As mentioned previously, the values of the shell parameters derived by Marsh *et al* were also rather different from those derived for the same agent (Albunex®) by de Jong *et al* (1992) (table 2.1) and were found to be inconsistent between different sets of results from the same experiment. These discrepancies inevitably call into question the reliability of the model and/or the experimental technique and hence that of the results and their interpretation. Thus, additional results are required for corroboration.

Owing to the uncertainty in the value of CAP shell parameters and in their uniformity within a given population, it would be impractical to attempt a quantitative comparison between the results shown in figures 3.9-3.13 and those obtained experimentally. However, it should be possible to determine the nature of the relationship between concentration and attenuation in CAP suspensions without these values. This was the aim of the experiment described below.

4.3.2 Apparatus

In terms of objective, the experiment was similar to that conducted by Marsh *et al* (1997). Broadband transmission measurements were made of the attenuation of ultrasound in CAP suspensions of varying concentration. There were a number of differences in the apparatus and procedure, however, which were introduced with the aim of reducing uncertainty. Two different types of CAP were used: a commercial diagnostic contrast agent, Optison® (Amersham PLC, BUCKS, UK) and a blowing agent[1] Expancel® (Casco Products AB, Sundsvall, Sweden). Their respective properties are shown in table 4.8

	Optison®	Expancel®
Shell material	Human serum albumin	Copolymer (acrylonitrile; vinylidene chloride)
Filling gas	Octafluoropropane	Isobutane
Mean radius	2.25 μm	12 μm
Maximum radius	16 μm (93% less than 10 μm)	100 μm

Table 4.8: Manufacturer specifications for Optison® and Expancel®.

As in the previous experiments, Optison® was selected as having similar shell properties, but greater stability, than Albunex® owing to its containing a gas of higher molecular weight than air. It was intended that this should lessen the handling problems experienced by Marsh *et al.* The aim in selecting Expancel® was to examine whether similar behaviour would be observed with CAPs having a different coating material and size distribution. Size distribution measurements were again performed using a Malvern Mastersizer (2000 series, Malvern, UK). The results for each type of CAP are shown in figure 4.5.

[1]Encapsulated gas-filled particles, similar to ultrasound contrast agents, used for increasing the bulk of polymer melts in various manufacturing processes.

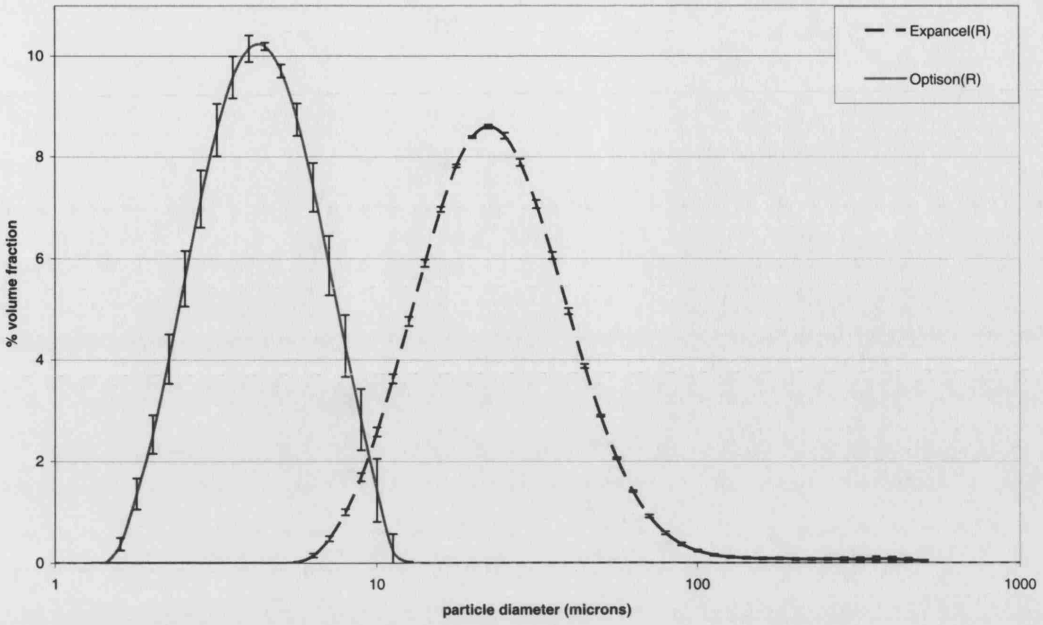

Figure 4.5: Size distribution data for Optison® and Expancel®.

The attenuation measurements were made using a pair of broadband unfocused transducers (Panametrics 5108R) each having a nominal centre frequency of 5 MHz, diameter 20 mm and a 3 dB bandwidth of 3 MHz. As in the previous experiment, the transducers were activated using a pulser/receiver unit (Panametrics model 5055 PR) set to give a transmitted peak negative pressure in water of approximately 50 kPa. This was again measured using a needle hydrophone as described in Appendix C.ii. The pressure was lower than that used by Marsh *et al* (1997) and would have been low enough both to avoid rapid CAP destruction and to reduce the presence of significant higher harmonics in the CAP response.

The use of a lower insonation pressure also reduced the likelihood of distortion of the results due to non-linear propagation, which would have increased the harmonic content of the received signal. The absence of significant harmonic content was verified by examination of the signal frequency spectra. Likewise, the lack of variation in the received signal over the measurement time confirmed that CAP destruction and drift was also minimal. It was found that if the experiments were repeated after the suspensions had been left standing for several minutes a reduction in the measured attenuation was seen. Consequently care was taken to ensure that the time between preparing the suspensions and capturing the signals was kept constant and as short as possible.

In order to reduce the effect of temperature fluctuations, all the measurements were again conducted at room temperature in a large water bath (length 45 mm, width 25 mm, height 25 mm). The instruments used for handling the test samples were also kept immersed in the bath when not in use. A container was designed to the hold the CAP suspensions (figure 4.6). This was constructed from a section of PMMA (polymethylmethacrylate) tubing (inner diameter 60 mm, wall thickness 5 mm, length 30 mm) with acoustic "windows," made from polyethylene film (thickness 50 μm), at either end. The tubing was held between two square aluminium plates into which recessed circular holes had been cut to allow access to the ends of the tubing and hold it in place. The plates were bolted together to ensure a tight seal. A hole was cut in the wall of the tubing and sealed with a Newplast® (Newclay, Newton Abbot, UK) plug in which two polyethylene tubes were embedded to enable the container to be filled and emptied. The container was located on the base of the tank between two fixed blocks to ensure accurate positioning for each test.

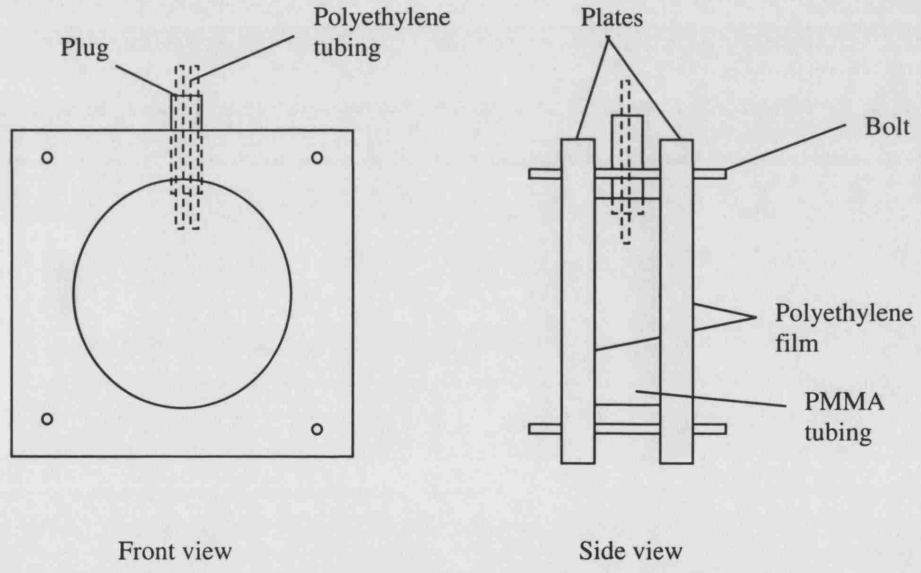

Figure 4.6: Schematic of the measurement chamber used for the multiple scattering experiments.

Holders for the transducers were also constructed. The holder for the receiving transducer was positioned on the base of the tank at a known distance from the suspension container. The transmitting transducer was connected to a precision scanning rig to enable accurate positioning with respect to the container and receiver. The distance between the transducers and the container was measured as in section 4.2 above.

The holder for the transmitter was designed to enable the axes of the transducers to be aligned. The correct alignment was determined, prior to the experiment by adjusting the position of the transmitter in water until the amplitude of the received signal was maximised.

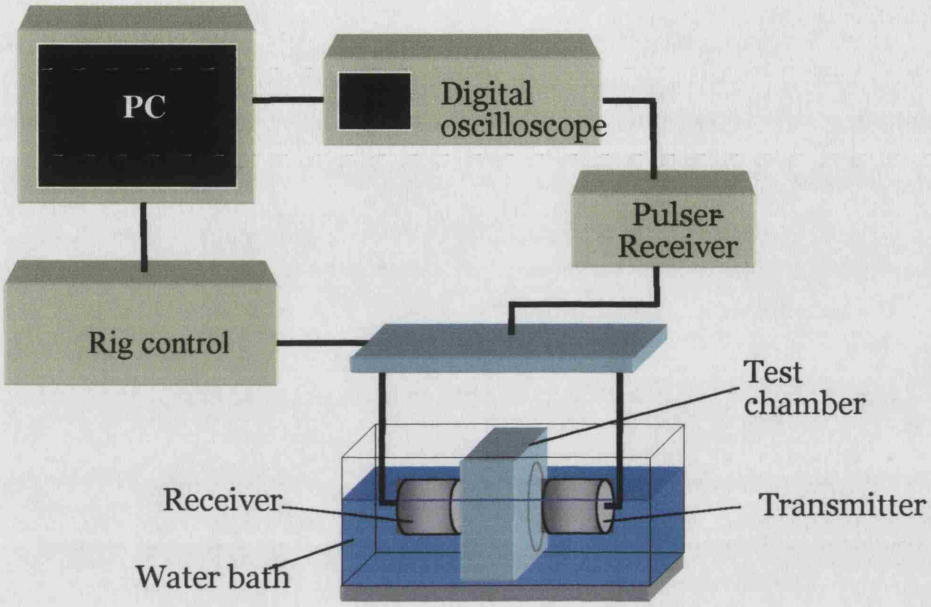

Figure 4.7: Schematic of the experimental apparatus.

4.3.3 Procedure

The apparatus was set up as shown in figure 4.7. Again, each complete set of experiments was performed on the same day in order to minimise the influence of external factors. The Optison® suspensions were prepared according to the manufacturers instructions on the product insert. The Expancel® suspensions were prepared by dispersing a known volume (1.55×10^{-4} m^3) of product in 300 ml distilled water. The measurement container was also filled with distilled water at room temperature and a 1 ml syringe with a 20 gauge needle used to transfer the appropriate volumes of each suspension to the container to yield the concentrations indicated in figures 4.9 and 4.10. A fine wire with a looped end was inserted into the container via one of the polyethylene tubes to enable the suspension to be gently stirred. This was done continuously whilst the measurements were being taken. The temperature in the container was also monitored continuously using a digital thermometer (model 650-419, RS Components, Corby, Northhants, UK).

As before, broadband pulses were transmitted at a pulse repetition frequency of 0.6 kHz and captured at 1 Giga-sample per second. For each test, measurements were made first in the water bath without the container present, and then through the suspension. This was done in order to reduce further the influence of effects such as temperature fluctuations upon the results. Three pulses were captured for each concentration and the process repeated with fresh samples to give a total of six measurements for each test. The chamber was rinsed thoroughly with distilled water in between tests.

4.3.4 Analysis

The captured signals were processed in Matlab®. Each signal was normalised with respect to its mean value and its frequency spectrum obtained via fast Fourier transform. The amplitudes at 4.0, 5.0 and 6.0 MHz were determined and the attenuation coefficient found, as described above, using equation 4.1. In this case A_1 is the average amplitude in water for that frequency, A_2 the average amplitude with the container present and d the length of the container. The mean average attenuation coefficient and corresponding standard deviation were then found for each concentration, from which the experimental uncertainty was estimated. Similarly, the acoustic velocity for each test with and without the container present was found in water as

$$c_L = \frac{d + y_1 + y_2}{t_2 - t_1} \tag{4.5}$$

and in the suspension as

$$c_{eff} = \frac{d}{t_2 - t_1 - c_L(y_1 + y_2)} \tag{4.6}$$

where t_2-t_1 is the transmission time for the captured pulse and y_2 and y_1 are the distances between the container and the two transducers. Again the mean average and standard deviation were calculated for each set of measurements and an uncertainty analysis was performed as described above.

It was intended initially that a diffraction correction factor should be applied to the results as described in Appendix C.i. However, the differences in the measured velocities for water and for the suspensions (table 4.9) were found to be too small compared with the experimental uncertainty to justify this. This was somewhat unexpected given the variation in the values of $\mathrm{Im}(K_{eff})$ from equations (5) and (8) at the higher concentrations. However, since these equations were derived on the assumption that the velocity would remain constant and equal to c_L, this was not an accurate means of predicting the variation in velocity. Moreover, given that the transmission distances were small compared with those used in the previous experiment and with the near field distance (33 cm) the magnitude of the correction factors would have been relatively small (Appendix C.i).

4.3.5 Results

The principal results are shown in this section. The complete set is included in Appendix F.

Expancel® concentration	mean velcocity	standard deviation	Optison® concentration	mean velcocity	standard deviation
(CAPs/ml)	(m/s)	(m/s)	(CAPs/ml)	(m/s)	(m/s)
0	1505	1.7	0	1507	2.1
121000	1506	2.2	5000	1505	3.0
243000	1497	3.0	50500	1506	2.2
364000	1498	2.6	707000	1506	2.4
485000	1497	2.2	1010000	1506	3.1
607000	1500	3.1	2020000	1508	1.8

Table 4.9: Acoustic velocity measurements for Optison ® and Expancel® suspensions.

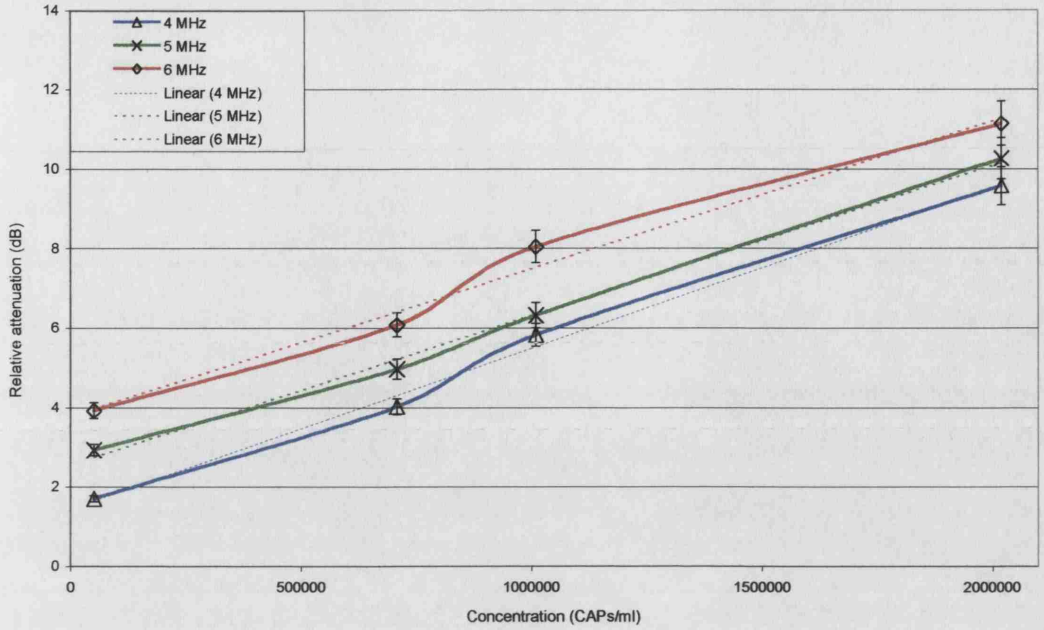

Figure 4.8 Variation in attenuation with concentration for suspensions of Optison® in distilled water.

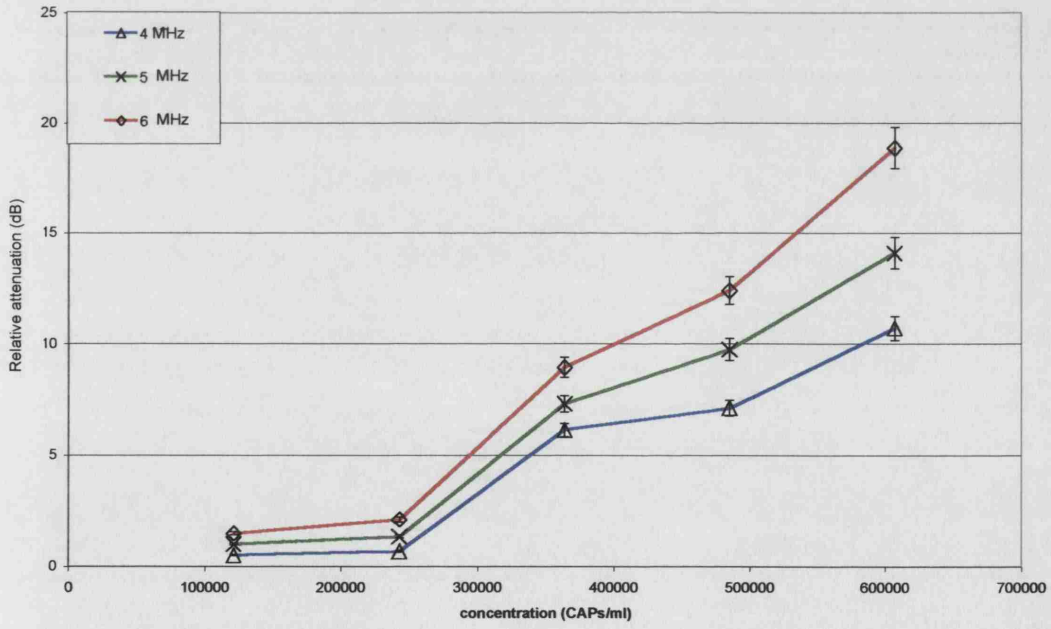

Figure 4.9: Variation in attenuation with concentration for suspensions of Expancel® in distilled water.

4.3.6 Discussion

As shown in figure 4.8, attenuation was seen to vary linearly with concentration for Optison® over the 3 dB bandwidth at an insonation pressure of 50 kPa. The deviation from a linear fit is shown in the figure. A linear relationship might have been expected from the theoretical results shown in the previous chapter. Assuming that the shell parameters for Optison® would be similar to those determined for Albunex® (table 2.1), then the majority of the Optison® CAPs would have been smaller than the resonant size for the range of frequencies used. Consequently, the effects of multiple scattering would have been small. Indeed, as shown in figures 3.9-3.11, the discrepancy between the results from the single and multiple scattering models is practically negligible at resonance for the 2 μm radius CAPs even at the highest concentrations. These findings are in agreement with the results obtained by Marsh *et al* (1997) for Albunex® at non-resonant frequencies.

As will be discussed shortly, the results for Optison® were intended to be representative of diagnostic conditions for this agent. The aim in repeating the experiment with Expancel® was to investigate whether multiple scattering could be observed with CAPs having different shell properties and larger diameters. As shown in figure 4.9, the relationship between attenuation and concentration for this agent was found to be non-linear. This was as predicted by equations 2.27, 2.28 and 3.66 (figures 3.10-3.12).

The shell parameters for Expancel® are not known at present, and given the doubt which has been cast upon the technique employed by de Jong *et al* (1992), they cannot be determined without alternative means of investigation. Nevertheless, the fact that attenuation was found to increase non-linearly would seem to indicate that at least a proportion of the population was resonant over the range of frequencies used. This again concurs with the results of Marsh *et al* (1997) who found that the attenuation in Albunex® suspensions was underpredicted by equation 2.24 over the resonance regime.

Notwithstanding the qualitative agreement between the experimental and theoretical results, there remains a degree of uncertainty which warrants further discussion. As mentioned above, it was assumed that the shell parameters for Optison® and Albunex® would be similar, given that they describe the same material. However,

further investigation is required in order to confirm this and to determine the appropriate values for Expancel®. Similarly, it was necessary to assume that any variability in the shell parameters would be constant between samples. The similarity between the results from different samples indicated that this assumption was valid. This is an area requiring further examination, however, since such variability could account for the differences in the response of individual CAPs observed by Postema *et al* (2003) and could contribute to the pressure dependence of attenuation in CAP suspensions. If there were found to be significant variability, the CAP concentration n would effectively become a function of pressure in equation 3.66. This will be discussed again in Chapter 6.

On account of these uncertainties it was not possible to attempt a quantitative comparison between the experimental and theoretical results, nor was it practical to investigate CAP behaviour at higher insonation pressures. Marsh *et al* (1997) did report that increasing insonating pressure caused a downwards shift in the frequency of the attenuation peak, accompanied by an increase in amplitude. This was as predicted in figures 3.12 and 3.13, but in order to confirm this finding, more accurate experiments would be required than could be performed with the existing apparatus. For example, an improved method for measuring the propagation speed would be required. Nevertheless, it is still worthwhile considering the implications of multiple scattering for the characterisation and applications of ultrasound contrast agents based on the findings of this work.

As shown above, multiple scattering would be expected to affect the attenuation and velocity of ultrasound in a CAP suspension. The important question is whether or not the effects would be significant at the concentrations found *in vivo*. Unfortunately, the values of these concentrations are not simple to estimate. If the injected volume of contrast agent is dispersed uniformly then, assuming an average human adult blood volume of 5 litres, the average concentration will be reduced from 10^9 CAPs/ml to approximately 10^5 CAPs/ml. In this case the effects of multiple scattering would be expected to be minimal as demonstrated in figure 3.9. If, on the other hand, the CAPs are not dispersed evenly, the local concentration could remain much higher in which case multiple scattering effects might be observed.

In diagnostic applications, this could limit the maximum contrast enhancement achievable with increasing dose and prevent deep structures from being imaged, owing to the rise in attenuation through the suspension. This could also affect the percentage of CAPs destroyed in a drug delivery application, since part of the population would be effectively shielded from the incident field by the other CAPs closer to the probe. The effect of multiple scattering upon the speed of propagation and frequency spectrum could also introduce errors into measurements of blood velocity. Further investigation is required in order to determine the magnitude of these effects.

The most significant implications of multiple scattering relate to CAP characterisation experiments. The shell parameters shown in table 2.1 were derived from measurements of the attenuation and back scattering coefficients from a suspension of Albunex® (de Jong *et al* 1992) and similar techniques have been applied to determine the properties of other agents (Gorce and Scheneider 2000, Marsh *et al* 1997). According to the results obtained above, at the concentrations used e.g. by Gorce and Scheneider ($>10^5$ CAPs/ml), their measurements could have been affected by multiple scattering. Hence, using a single scattering model for interpretation would have been inappropriate. This is in addition to the fact that the shell models used may not have been accurate and that there may have been considerable variability between individual CAPs, as discussed previously.

On account of the uncertainty in the variability of CAP properties, improving the multiple scattering model, as suggested in Chapter 3, would not enable more accurate CAP characterisation using acoustic techniques. It might be useful for improving the design of diagnostic procedures, for example, estimating the additional error introduced into blood velocity measurements, but this would only be the case if the variation in the *in vivo* concentration could be accurately determined. Alternative techniques are needed, as will be discussed in Chapter 6.

The implications for CAP design are perhaps less significant. It is clear that at high concentrations the signal radiated by a CAP population will be different from that predicted using a single CAP model and this should perhaps be taken into account when designing a CAP to produce a particular response. However, it would not be feasible to control the concentration of a CAP suspension *in vivo*, and would

therefore be impractical to design CAPs to produce a response as a population. A more realistic approach would be to design a CAP to produce a highly distinctive response so that high concentrations would not be required. This would have the additional benefits of reducing the quantity of agent required and avoiding the shielding problems discussed in Chapter 2 which might affect therapeutic applications. The design of such a CAP will be the subject of the next chapter.

4.3.7 Conclusions

The results from linear modelling of ultrasound propagation in CAP suspensions indicate that multiple scattering effects may be observed at the concentrations found *in vivo* if the CAPs are of sufficient diameter and are excited at their resonance frequency. These findings have been supported qualitatively by low pressure broadband attenuation measurements in suspensions of two different types of CAPs. It was found that attenuation increased linearly with concentration in suspensions containing small, non-resonant CAPs and non-linearly in those containing larger, resonant CAPs. Unfortunately, a quantitative comparison could not be made owing to the uncertainty in the properties of the CAP shells.

It is clear from the results that the effects of multiple scattering should be taken into account for CAP characterisation experiments based on acoustic techniques. Accurate determination of the *in vivo* concentrations for CAP suspensions is needed in order to assess the significance of multiple scattering for medical applications. With regard to CAP design, it was concluded that the aim should be to reduce the need for high concentrations and hence the distorting effects associated with multiple scattering as well as the additional expense and potential safety risks.

4.4 Summary

The aim of this chapter was to compare the theoretical predictions discussed in Chapter 3 with experimental results, in order to assess the validity of the new models. In particular, the influence of blood cells upon CAP behaviour and the significance of multiple scattering in CAP populations were investigated. In both cases, the results obtained were found to support the conclusions of the theoretical work. Firstly, it was found that the presence of blood cells in a contrast agent suspension did not appear to have a significant effect upon the acoustic response. This implies that it is justifiable to model the surrounding fluid as homogeneous and Newtonian for the purposes of CAP design. Secondly, it was found that multiple scattering effects could be observed at the concentrations which might be expected *in vivo,* when CAPs of sufficient diameter were excited at their resonance frequency. It was concluded that the aim in CAP design should be to reduce the need for high concentrations and hence the distorting effects associated with multiple scattering as well as the additional expense and potential safety risks. The application of these findings to CAP design will be the subject of the next chapter.

5

Design for diagnostic applications

5.1 Overview

The aim of the previous two chapters has been to derive and validate a new model which provides a description of CAP behaviour over a wide range of conditions. In this chapter, the model will be used to investigate how CAPs may be designed to improve their effectiveness for particular applications. After an initial discussion of the requirements for an ultrasound contrast agent, a sensitivity analysis will be carried out to identify the most significant factors controlling CAP behaviour. The specific requirements for diagnostic applications will then be considered and designs formulated to meet those needs. The new model will be used to simulate the response of the different CAPs to identify the most effective designs. Scale models of the selected CAP designs will then be tested in order to assess their effectiveness experimentally. Finally, the manufacturing requirements and safety considerations for the new CAPs will be discussed.

5.2 Outline of design requirements

The first step in any design process is to define the requirements for a particular application. In the case of diagnostic imaging, the aim is to obtain a satisfactory image of the region of interest, quickly, safely and, if possible, economically. In terms of equipment costs and portability, scanning time and patient risk, ultrasound is superior to alternative imaging techniques such as CT and MRI. In terms of image quality, however, it is generally inferior, and the requirement for a contrast agent is to lessen this disadvantage by increasing the reflectivity of a particular feature compared with that of the surrounding tissue. As explained in Chapter 1, gas bubbles are effective contrast agents for three reasons. Firstly, they have a high compressibility compared with blood cells. Secondly, they respond non-linearly to ultrasound excitation. Thirdly, they are resonant at diagnostic frequencies. Thus, whilst the discovery of microbubble contrast agents was in fact accidental, in design terms, they represent the ideal choice for ultrasound contrast enhancement.

In therapeutic applications the aim is to target treatment, be it a drug or a physical effect such as heating, to a specific region of the body in order to minimise unwanted side effects. There is a wider range of factors to consider in assessing the optimality of microbubbles for this purpose. For example, in addition to ensuring the survival of the CAP *in vivo*, the CAP coating may be required to act as an anchor site for certain species, according to the type of therapy to be delivered and/or the target area. There may also be differing requirements regarding the shape of the CAP. Spheres have a low ratio of surface area to volume, whereas to increase the probability of a particle adhering to a target, a large surface area is desirable. Notwithstanding the question of optimality, however, CAPs are undoubtedly an effective means of delivering therapy, particularly if there is an additional requirement for imaging, for example, to trace the passage of the CAPs to the target site. The fact that they can be destroyed using ultrasound is also an advantage since it enables drug delivery to be localized.

This chapter will focus mainly upon the diagnostic applications of CAPs. Before, examining how CAP design may be improved, however, it is important to determine which factors are the most significant in controlling CAP behaviour.

5.3 Sensitivity analysis

5.3.1 Formulation

Equation 3.15 contains a number of factors f_{Sv}, f_{Ss}, f_{Lv}, f_{Ls}, f_{brad}, f_{bth}, p_G and p_∞, which must be defined according to the particular conditions being considered. In the preceding chapters it has been demonstrated that, provided the analysis is restricted to the behaviour of CAPs in relatively large blood vessels, the surrounding fluid may be regarded as incompressible and Newtonian.

Thus $f_{brad} = f_{Ls} = 0$ and $2T_{L,\theta\theta} = 2T_{L,\phi\phi} = -T_{L,rr} = T_{L,rr} = 2\mu_L \dfrac{\partial u}{\partial r}$

and hence $$f_{Lv} = 3\int_{R_2}^{\infty} \frac{T_{L,rr}}{r} dr = -4\mu_L \frac{R_1^2 \dot{R}_1}{R_2^3}. \qquad (5.1)$$

It has also been shown that, for the conditions relevant to diagnostic imaging, the behaviour of the filling gas may be regarded as isothermal

$$\text{i.e.} \quad f_{bth} = 0 \qquad \text{and} \qquad p_G(t) = p_o\left(\frac{R_{o1}}{R_1}\right)^3. \qquad (5.2)$$

The remaining terms to be defined are those relating to the sound field (p_∞) and the encapsulating shell (f_{Sv} and f_{Ss}). As demonstrated in Chapter 3 these may be replaced by a wide range of functions. In order to proceed with the analysis, it is necessary to make some preliminary simplifying assumptions from which initial definitions of the above terms can be derived. The validity of these assumptions will be reviewed subsequently.

If, as in section 3.6, the shell is initially assumed to be a homogeneous, linear viscoelastic solid layer with finite thickness, then for strains <2% R_{o1} simple definitions of f_{Ss} and f_{Sv} can be used

$$f_{Ss} = \frac{-4G_S(R_1 - R_{1e})\left(R_2^3 - R_1^3\right)}{R_2^3 R_1} \qquad (5.3)$$

$$f_{Sv} = -4\mu_S \dot{R}_1 \left(\frac{R_2^3 - R_1^3}{R_2^3 R_1}\right) \qquad (5.4)$$

At low insonation pressures and low CAP concentrations, distortion due to non-linear propagation and multiple scattering effects will be small. For the purposes of this preliminary analysis, therefore, the incident field may be modelled as a simple sinusoid

$$p_\infty(t) = p_o + p_A \sin(\omega t). \qquad (5.5)$$

Substituting from the above into equation 3.15 gives

$$\begin{aligned} &R_1\ddot{R}_1\left(1+\left(\frac{\rho_L-\rho_S}{\rho_S}\right)\frac{R_1}{R_2}\right)+\dot{R}_1^2\left(\frac{3}{2}+\left(\frac{\rho_L-\rho_S}{\rho_S}\right)\left(\frac{4R_2^3-R_1^3}{2R_2^3}\right)\frac{R_1}{R_2}\right) \\ &=\frac{1}{\rho_S}\left(\begin{array}{l} p_o\left(\frac{R_1}{R_2}\right)^3-p_o-p_A Sin(\omega t)-\frac{2\sigma_1}{R_1}-\frac{2\sigma_2}{R_2} \\ -\frac{4\mu_L R_1^2\dot{R}_1}{R_2^3}-\frac{4V_S G_S}{R_2^3}\left(1-\frac{R_{1e}}{R_1}\right)-\frac{4\mu_S V_S\dot{R}_1}{R_1R_2^3} \end{array}\right) \end{aligned} \qquad (5.6)$$

This is equivalent to equation 3.37. To determine the factors having the most significant effect upon CAP behaviour, equation 5.6 may be rearranged in terms of the wall acceleration $\ddot{R}_1$, and broken down into six components representing: pressure (*PF*), the inertia of the shell and the surrounding fluid (*IF*), the acoustic pressure (*AF*), fluid viscosity (L_vF), shell viscosity (S_vF), and shell stiffness (S_sF).

$$\ddot{R}_1 = PF - IF - AF - L_vF - S_vF - S_sF \qquad (5.7)$$

where

$$\begin{aligned} \ddot{R}_1 =& \underbrace{\frac{p_o}{X}\left(\left(\frac{R_1}{R_2}\right)^3-1\right)}_{PF}-\underbrace{\rho_S\dot{R}_1^2\left(\frac{3}{2}+\left(\frac{\rho_L-\rho_S}{\rho_S}\right)\left(\frac{4R_2^3-R_1^3}{2R_2^3}\right)\frac{R_1}{R_2}\right)}_{IF} \\ &-\underbrace{\left(\frac{p_A Sin(\omega t)}{X}\right)}_{AF}-\underbrace{\frac{4\mu_L R_1^2\dot{R}_1}{XR_2^3}}_{L_vF}-\underbrace{\frac{4\mu_S V_S\dot{R}_1}{XR_1R_2^3}}_{S_vF}-\underbrace{\frac{4V_S G_S}{XR_2^3}\left(1-\frac{R_{1e}}{R_1}\right)-\frac{2}{X}\left(\frac{\sigma_1}{R_1}+\frac{\sigma_2}{R_2}\right)}_{S_sF} \end{aligned} \qquad (5.8)$$

and

$$X = \rho_S R_1\left(1+\left(\frac{\rho_L-\rho_S}{\rho_S}\right)\frac{R_1}{R_2}\right) \qquad (5.9)$$

This type of analysis is similar to that carried out by Flynn (1964) to investigate the nature of free bubble cavitation behaviour.

5.3.2 Procedure

Equation 5.8 may be solved numerically as described previously in Chapter 3 and the size of the acceleration factors compared to determine their relative importance. As before, the properties of the surrounding fluid were taken to be those of plasma (table 3.7) and the initial simulations were performed using the properties for Albunex® at resonance (table 3.3) to provide a set of results against which subsequent results could be compared. A range of insonation frequencies was used, corresponding to the resonant, sub-resonant and super-resonant regimes (1-5 MHz). The insonation pressure was varied within the range of pressures (0.05 - 0.1 MPa) for which the CAP could be expected to remain intact and for which equations 5.3 and 5.4 would be valid.

Tests were then carried out for different radii, shell thicknesses and shell parameters, including those corresponding to a free bubble. For each set of conditions, the relative magnitudes of the acceleration factors were compared. Subsequently, the effect upon the radial amplitude, velocity and acceleration of a 20% variation in each of the model parameters was examined for a range of initial conditions. The results are shown in figures 5.1-5.16.

5.3.3 Results

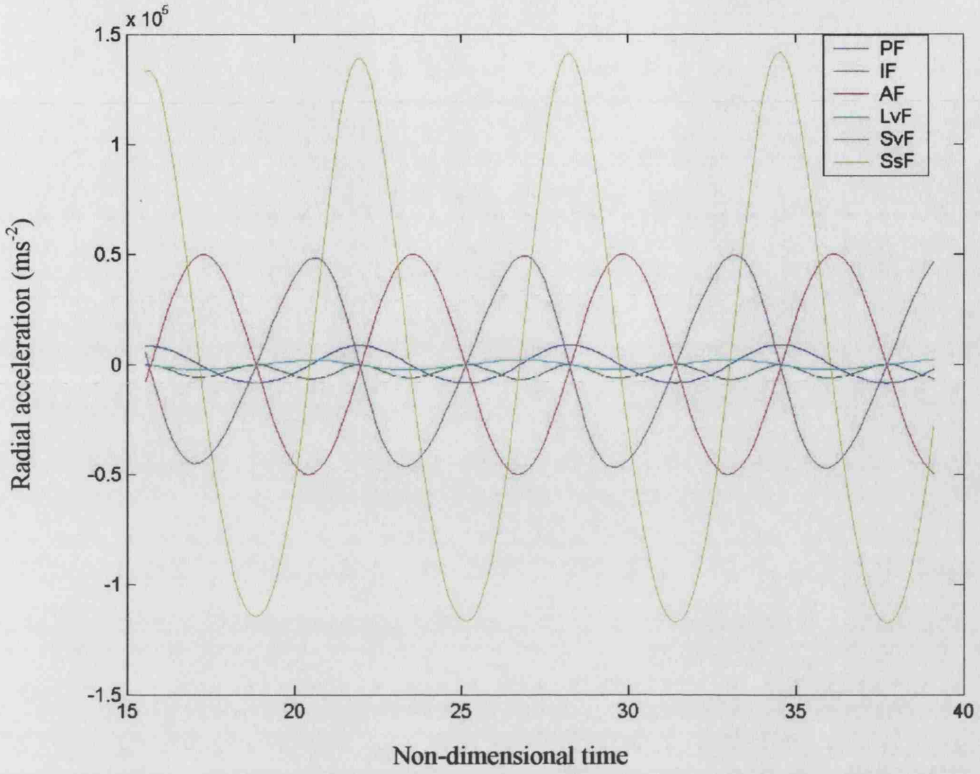

Figure 5.1: Acceleration factor plot for a 3.635 μm radius Albunex® CAP insonated at 3 MHz and 50 kPa.

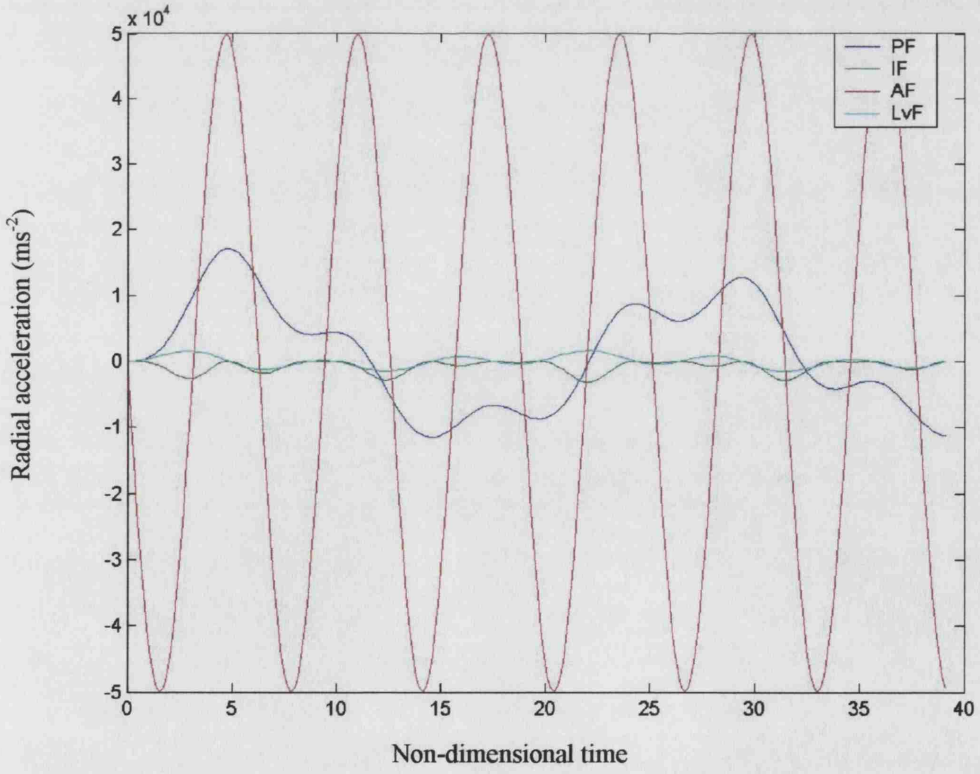

Figure 5.2: Acceleration factor plot for a 3.635 μm radius free bubble insonated at 1 MHz and 50 kPa.

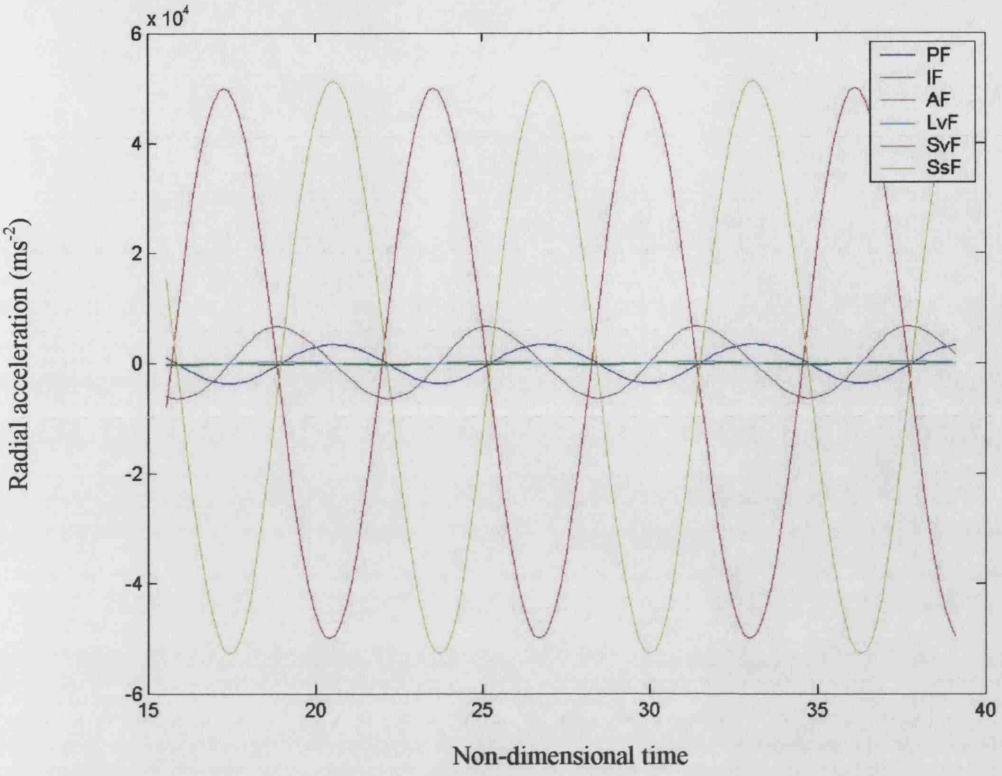

Figure 5.3: Acceleration factor plot for a 3.635 μm radius Albunex® CAP insonated at 1 MHz and 50 kPa.

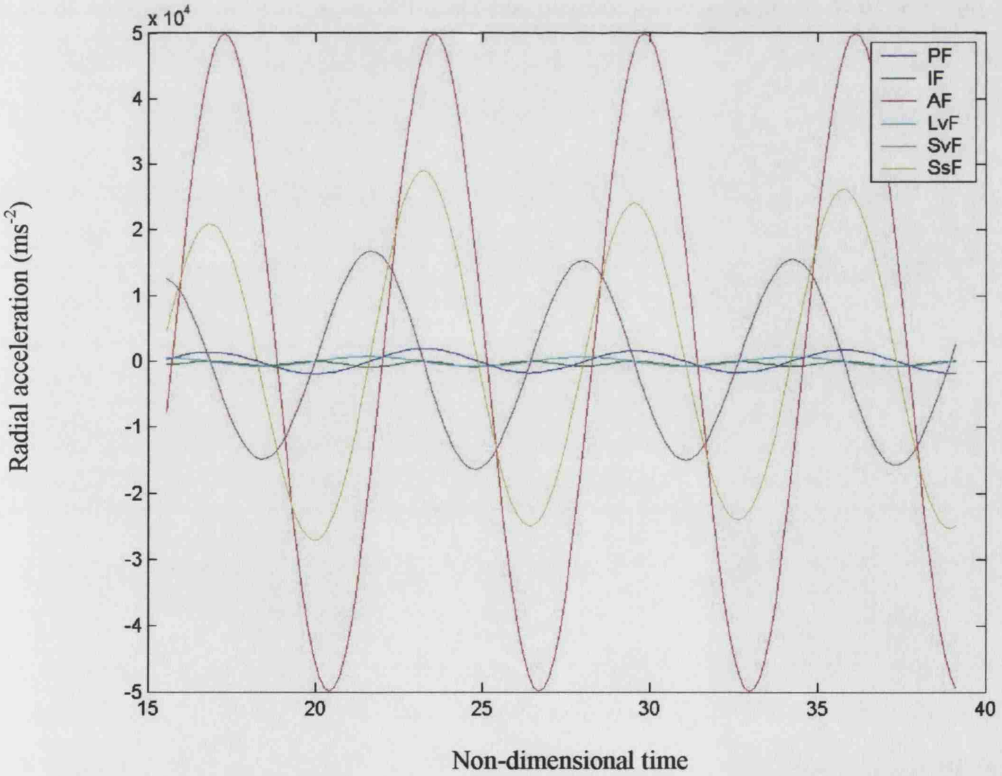

Figure 5.4: Acceleration factor plot for a 3.635 μm radius Albunex® CAP insonated at 5 MHz and 50 kPa.

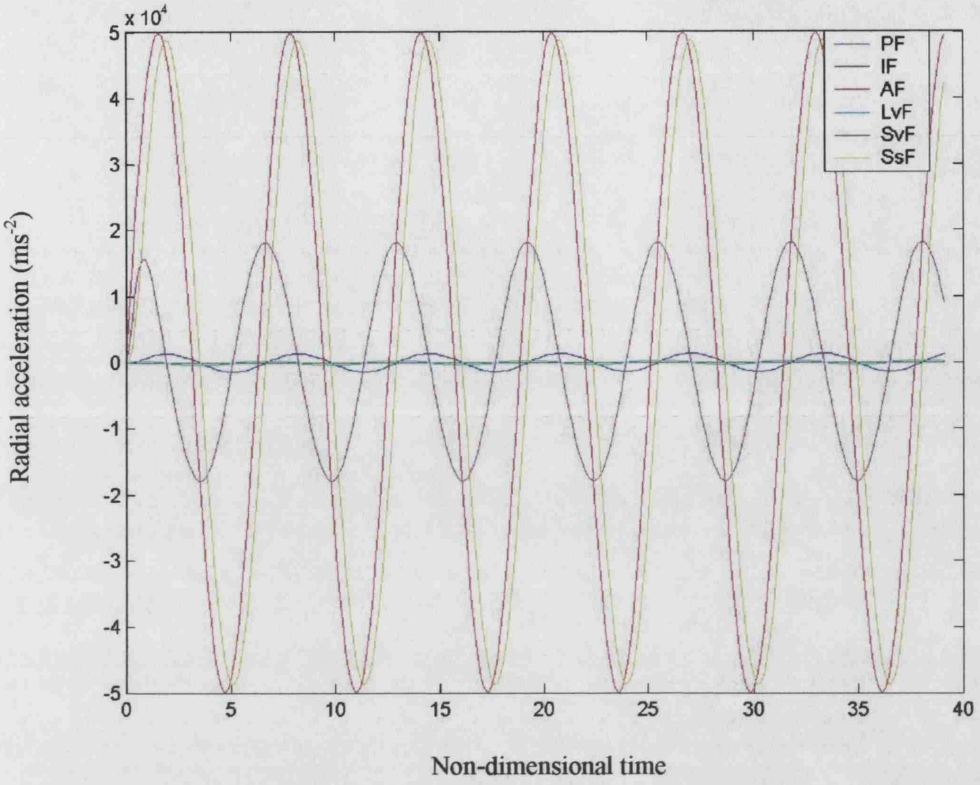

Figure 5.5: Acceleration factor plot for a 1.5 μm radius Albunex® CAP insonated at 3 MHz and 50 kPa.

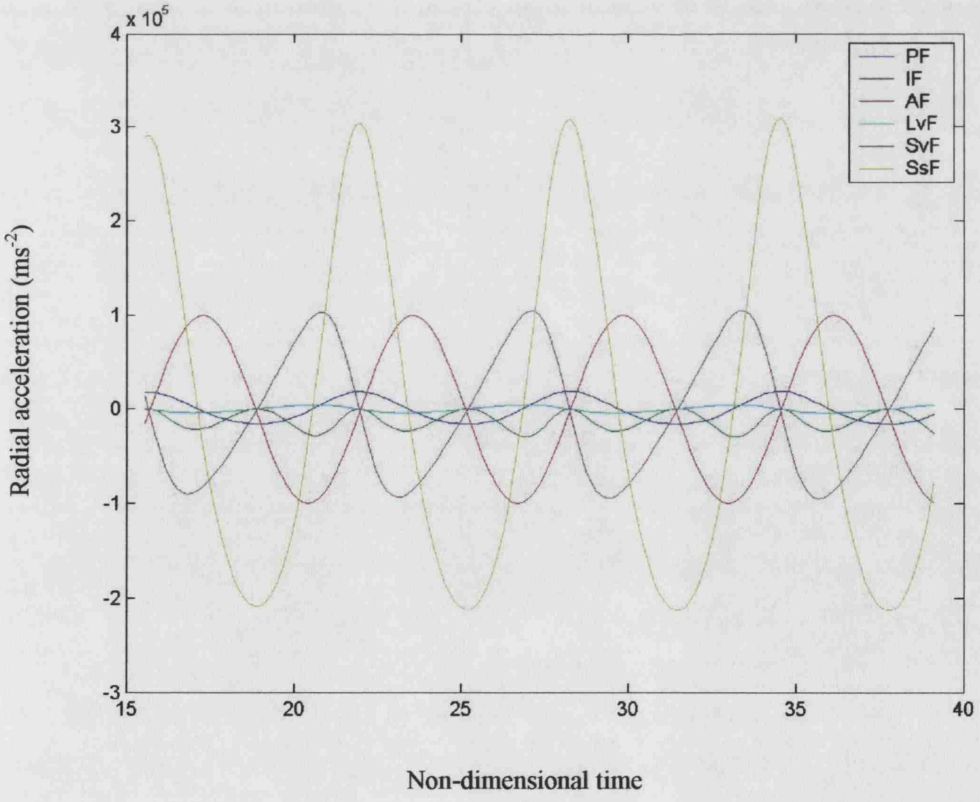

Figure 5.6: Acceleration factor plot for a 3.635 μm radius Albunex® CAP insonated at 3 MHz and 100 kPa.

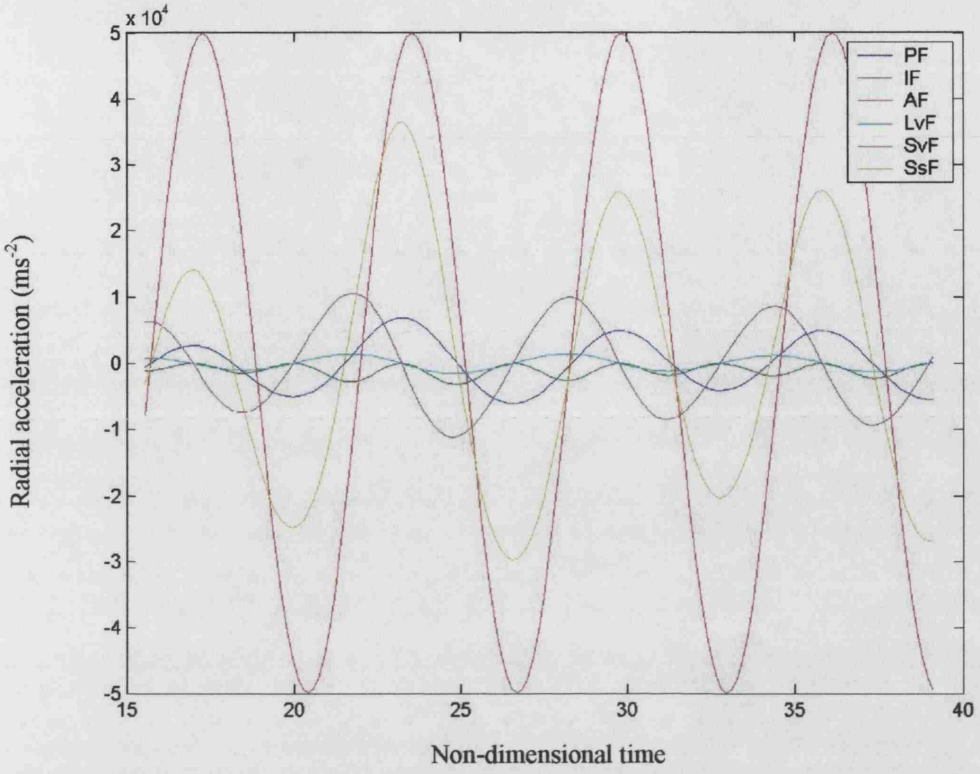

Figure 5.7: Acceleration factor plot for a 3.635 μm radius albumin-shelled CAP having a 5 nm thick shell, insonated at 3 MHz and 50 kPa.

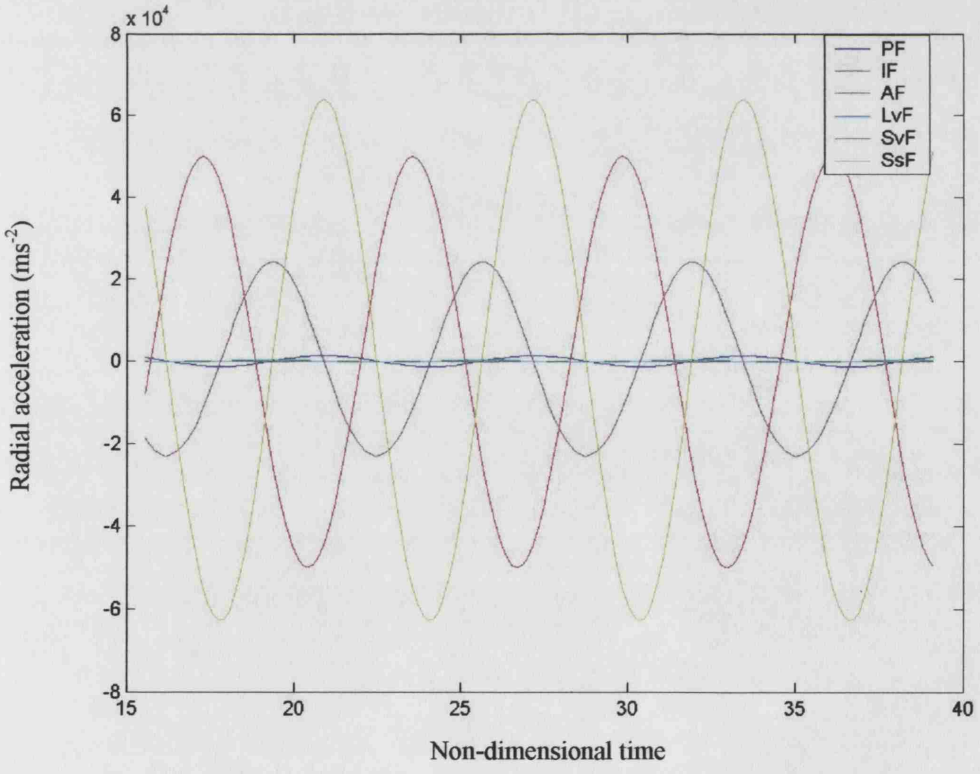

Figure 5.8: Acceleration factor plot for a 3.635 μm radius albumin-shelled CAP having a 50 nm thick shell, insonated at 3 MHz and 50 kPa.

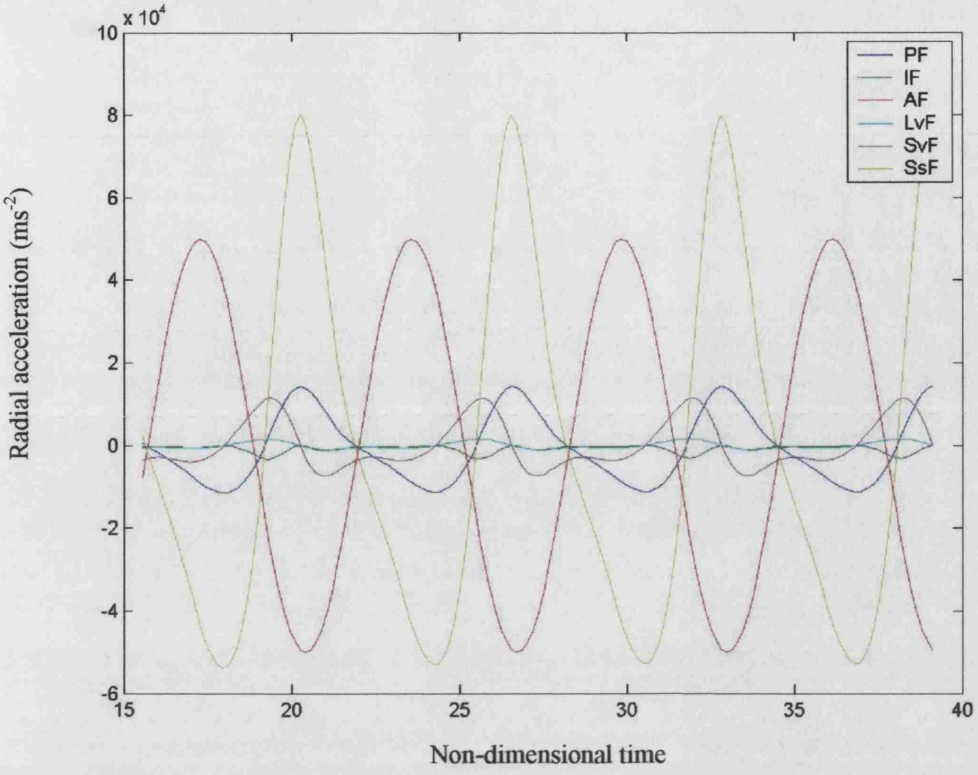

Figure 5.9: Acceleration factor plot for a 3.635 μm radius albumin-shelled CAP having a 5 nm thick shell, insonated at 1 MHz and 50 kPa.

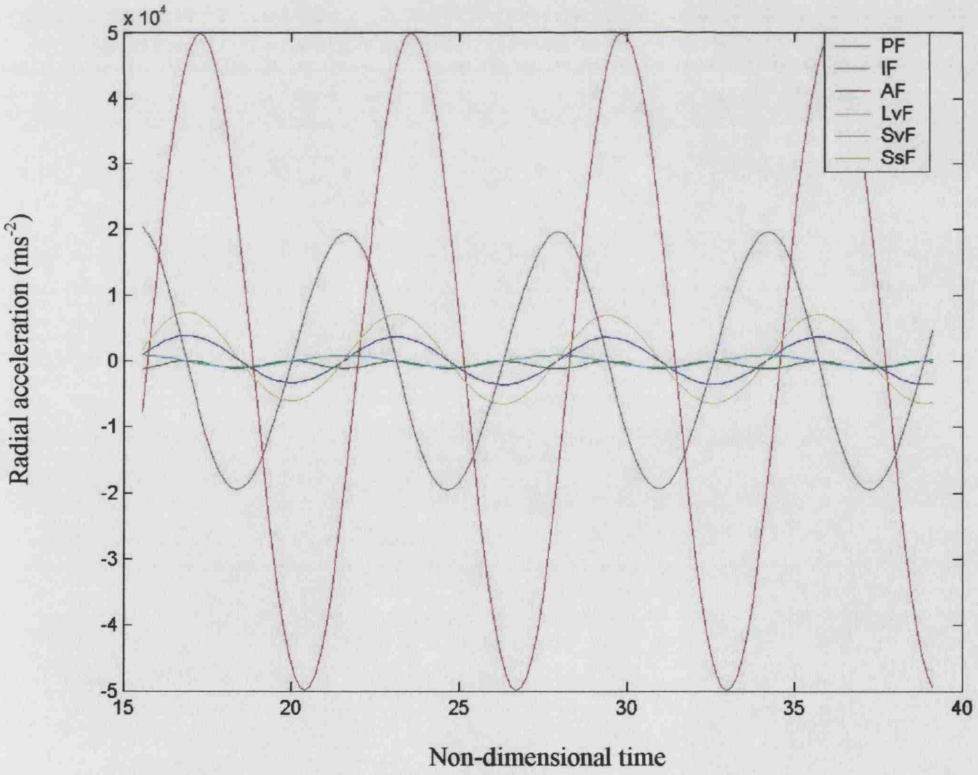

Figure 5.10: Acceleration factor plot for a 3.635 μm radius CAP having a shear modulus of 10 MPa, shear viscosity of 1.77 Pas and a shell thickness of 15 nm, insonated at 3 MHz and 50 kPa.

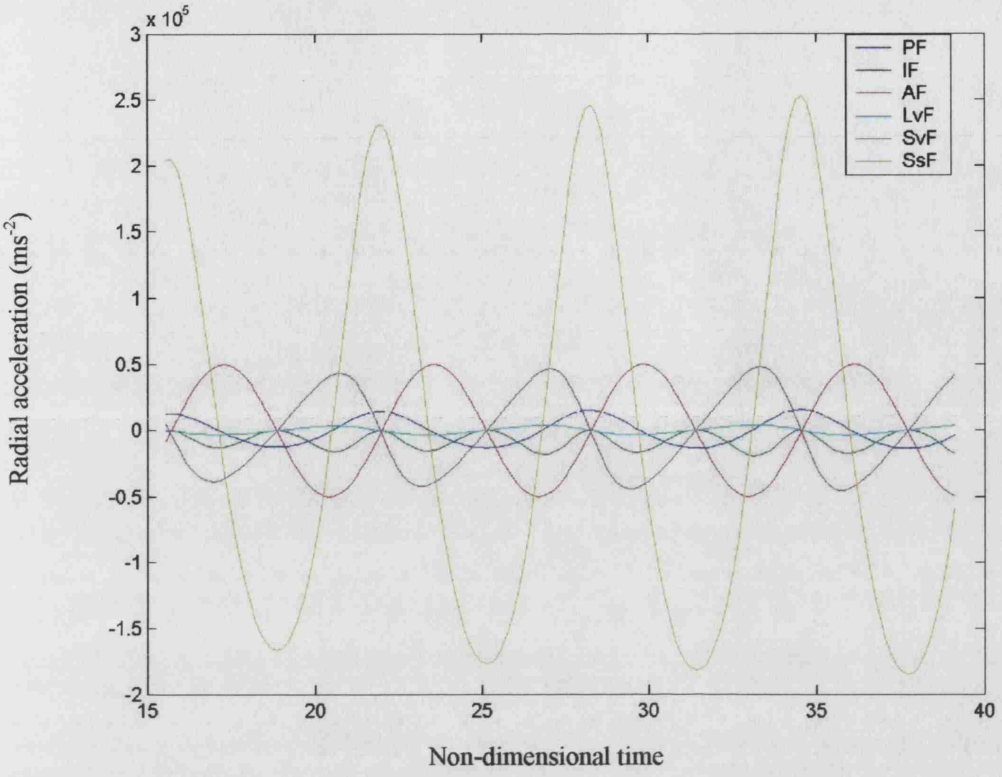

Figure 5.11 Acceleration factor plot for a 3.635 μm radius CAP having a shear modulus of 88.8 MPa, shear viscosity of 1.0 Pas and a shell thickness of 15 nm, insonated at 3 MHz and 50 kPa.

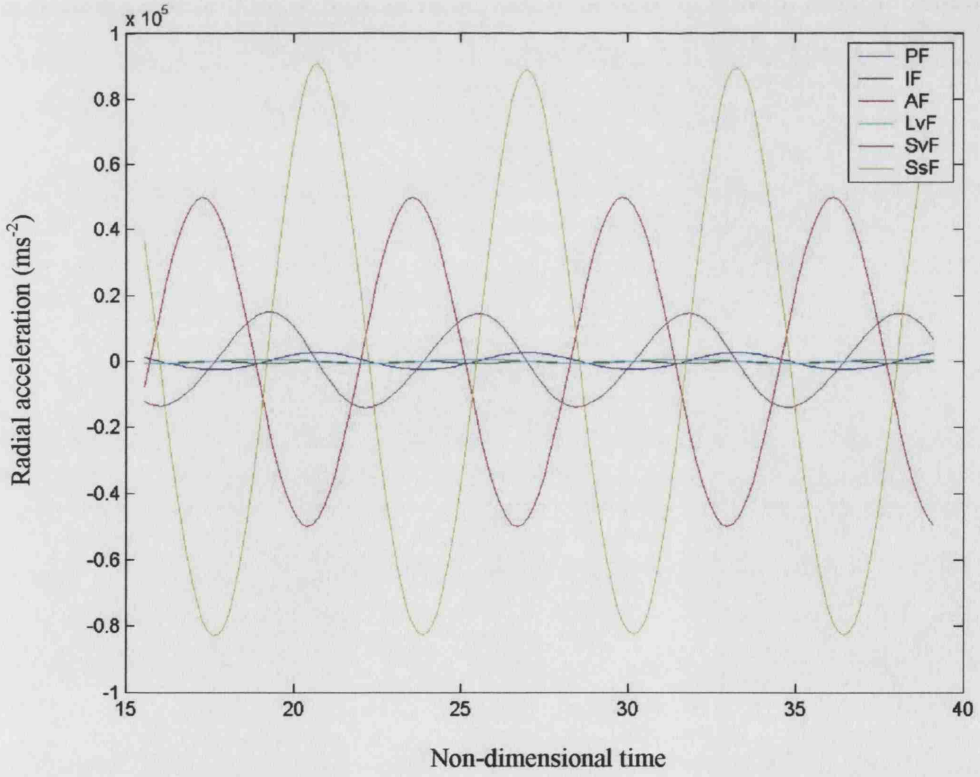

Figure 5.12: Acceleration factor plot for a 3.635 μm radius CAP having a shear modulus of 200 MPa, shear viscosity of 1.77 Pas and a shell thickness of 15 nm, insonated at 3 MHz and 50 kPa.

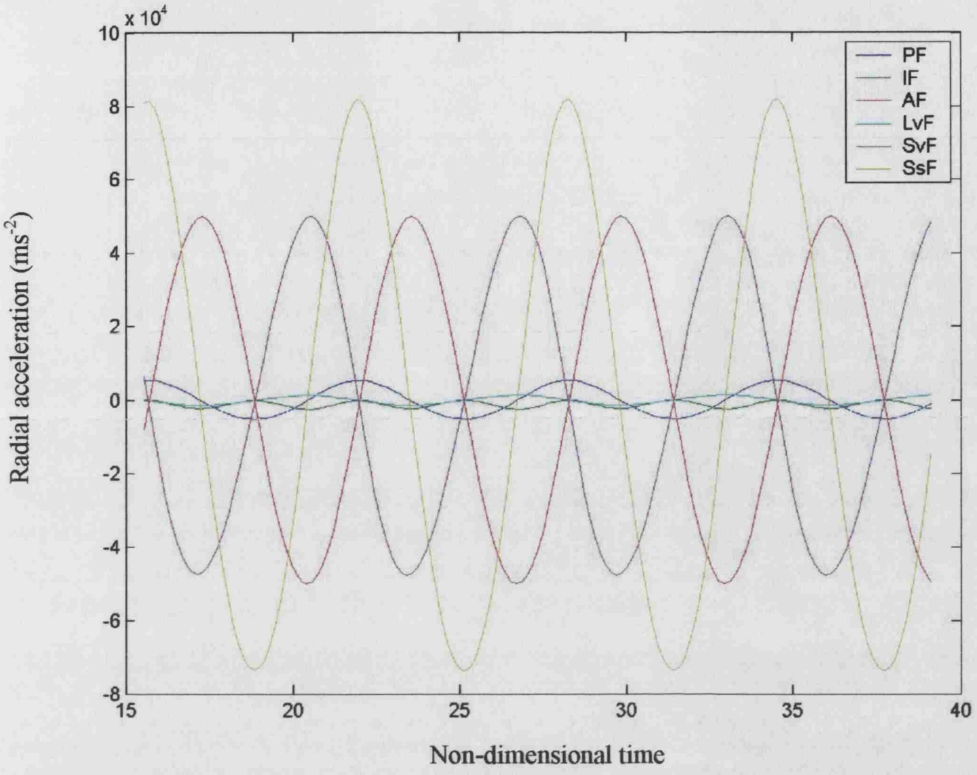

Figure 5.13: Acceleration factor plot for a 3.635 μm radius CAP having a shear modulus of 88.8 MPa, shear viscosity of 3.0 Pas and a shell thickness of 15 nm, insonated at 3 MHz and 50 kPa.

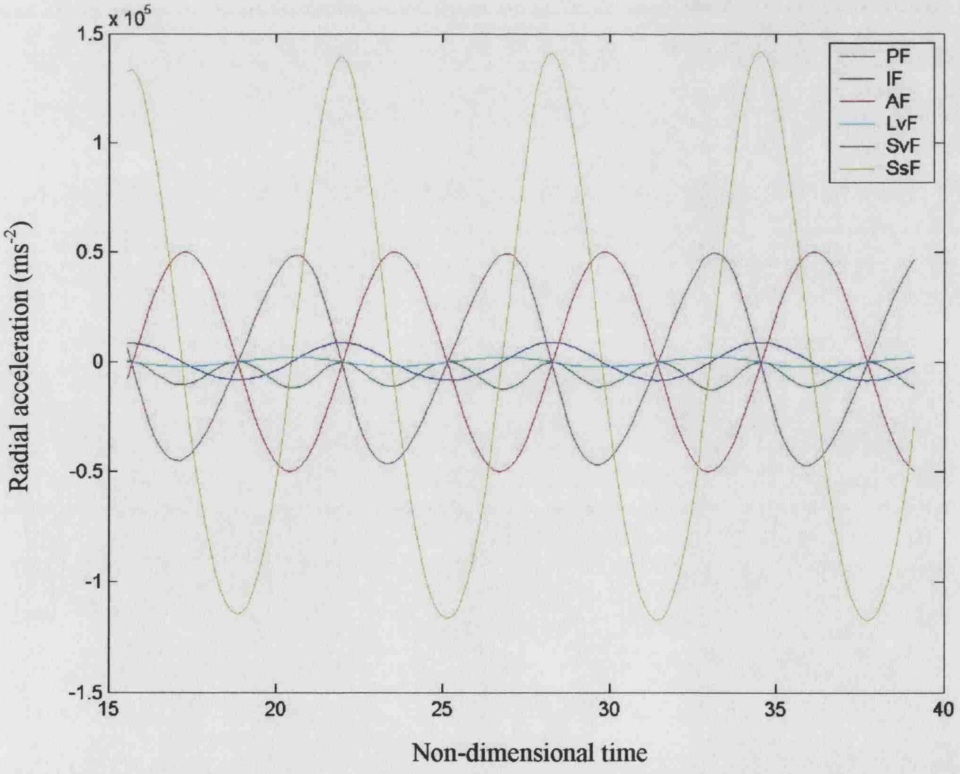

Figure 5.14: Acceleration factor plot for a 3.635 μm radius CAP having a shear modulus of 88.8 MPa, shear viscosity of 1.77 Pas, density of 2000 kgm^{-3} and a shell thickness of 15 nm, insonated at 3 MHz and 50 kPa.

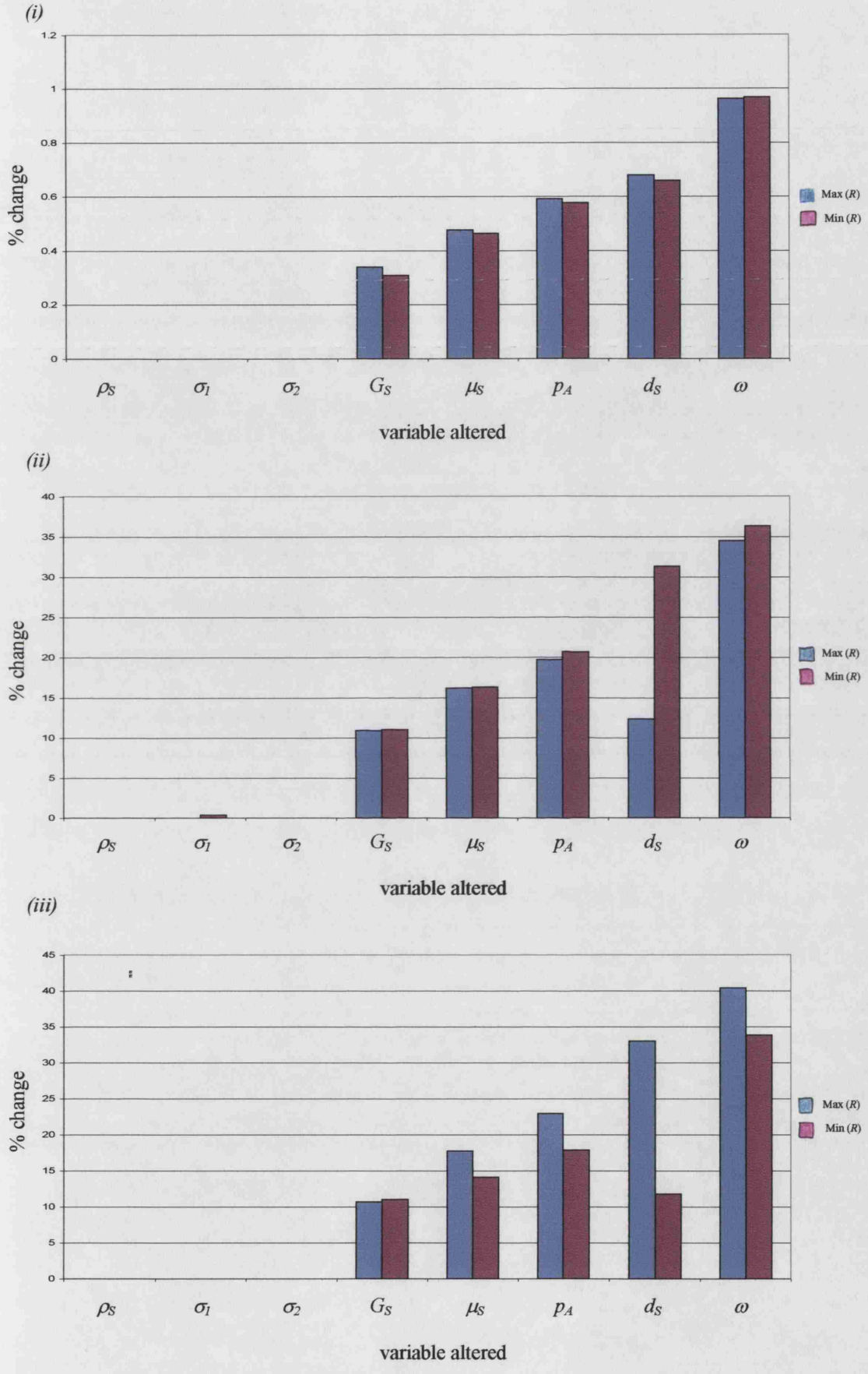

Figure 5.15: Demonstrating the sensitivity of (i) radial amplitude (ii) radial velocity and (iii) radial acceleration to variations of 20% in each of the model parameters for a 3.635 μm radius Albunex® CAP insonated at 3 MHz and 50 kPa.

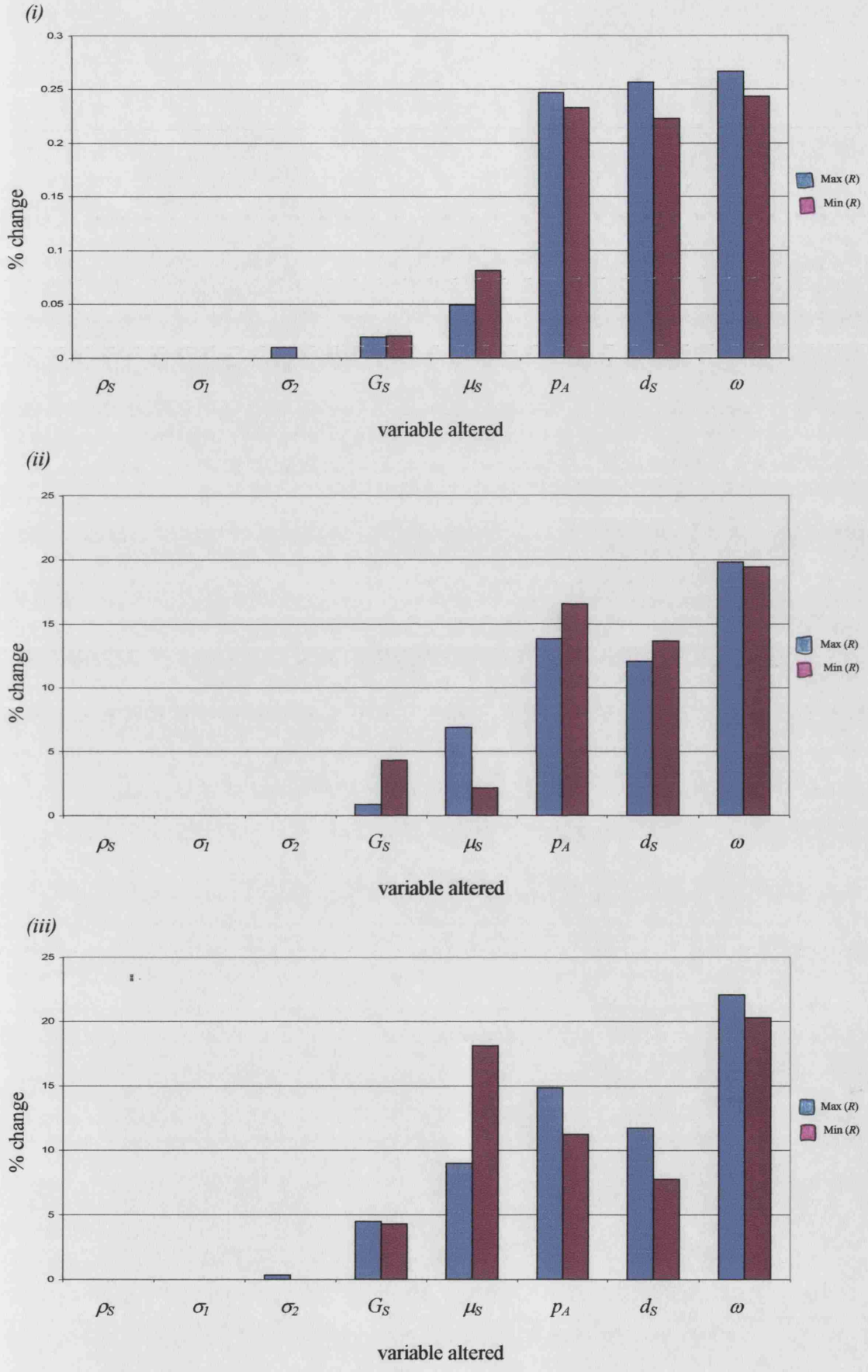

Figure 5.16: Demonstrating the sensitivity of (i) radial amplitude (ii) radial velocity and (iii) radial acceleration to variations of 20% in each of the model parameters for a 3.635 μm radius Albunex® CAP insonated at 1 MHz and 50 kPa.

5.3.4 Discussion

5.3.4.1 Acceleration factors

A comparison of figures 5.1 and 5.2 indicates that the factors controlling the behaviour of a CAP may differ considerably from those controlling the behaviour of a free bubble. Whilst the latter is primarily determined by either the pressure or inertia factors, CAP response is dominated by the factors relating to the stiffness and viscosity of the encapsulating shell. This finding has a number of implications. For example, it calls into question the validity of relating results obtained from work on free bubbles, to CAPs. This is particularly relevant for the assessment of contrast agent safety, which has in many cases been based on results derived from free bubble models (c.f. e.g. Nyborg 2001). This will be discussed further in section 5.8. For the purposes of design, however, the main conclusion is the importance of the shell as a feature requiring accurate modelling and offering opportunities for modifying CAP response. Similarly, the relatively large amplitude of the acoustic pressure factor indicates that the sound field should also be a focus for modelling and design.

The results shown in figure 5.1 relate to an Albunex® CAP excited at resonance. Figures 5.3 and 5.4 demonstrate the effects of lowering and increasing the insonation frequency respectively. In both cases the shell stiffness and acoustic pressure factors remain the most significant, but their relative amplitudes are altered, with the latter becoming dominant at non-resonant frequencies[1]. The same effect was seen when the radius of the CAP was altered, since this was equivalent to examining non-resonant conditions for a different size of CAP (figure 5.5). Similarly, varying the thickness of the CAP shell was found to increase the relative significance of the acoustic pressure factor at 3 MHz (figures 5.7 & 5.8), whereas, at the new resonance frequency for the CAP, the shell stiffness factor was still dominant (figure 5.9).

Reducing the shell stiffness, G_S, was found to increase the relative amplitudes of the shell viscosity and acoustic pressure factors (figure 5.10) for both the resonant and non-resonant cases. Likewise, reducing the shell viscosity, μ_S, increased the relative amplitude of the shell stiffness factor (figure 5.11). Clearly, in the limit, as G_S and μ_S are reduced, the behaviour of the CAP will approach that of a free bubble.

[1] It is, of course, the shell properties which determine the resonance frequency, so in this respect it could be argued that the shell is still the ultimate determinant of CAP behaviour.

As would be expected, increasing G_S and μ_S was found to increase the relative amplitudes of the shell stiffness and viscosity factors respectively (figures 5.12 and 5.13). This was found to be the case at all insonation frequencies tested, although the effects were most pronounced at resonance. An interesting comparison may be made between the amplitude of the shell viscosity factor and that corresponding to the surrounding fluid. This is another respect in which CAP behaviour differs from that of a free bubble, for which viscous effects are relatively small (figure 5.2). The implications of this for the safety of contrast agents are discussed further in Appendix D.iii.

It was found that varying the incident pressure within the range for which CAPs could be expected to remain intact did not affect the relative amplitude of the different factors to any great extent (figure 5.6). Also, although increasing the shell density, ρ_S, was found to increase the amplitude of the inertial factor slightly at resonance (figure 5.14), the effect was not sufficient for *IF* to be considered significant compared with the shell and acoustic pressure factors. For non-resonant frequencies the effects of altering ρ_S were barely observable.

5.3.4.2 Sensitivity

The results in figure 5.15 indicate that CAP response is most sensitive to changes in the shell and sound field parameters (d_S, ω, p_A). This reinforces the findings discussed above that the shell and acoustic pressure factors are the most significant in terms of CAP design. At the resonant frequency (3 MHz) it was the frequency and shell thickness to which the radial amplitude, velocity and acceleration were found to be most sensitive, followed by the pressure and shell parameters. This might have been expected, since variations in frequency would determine whether or not the CAP was resonating and hence whether or not its response would be maximised. Moreover, the amplitude of the response would be expected to change most rapidly around resonance, as would be the case with any system. At the lower, non-resonant frequency, CAP response would be expected to vary more gradually with frequency and hence would be more sensitive to the insonating pressure and shell stiffness, as was seen in figure 5.16.

The location of the resonance frequency, and hence the CAP response, would be expected to be more sensitive to variations in thickness than to variations in other parameters such as, G_S, μ_S, owing to the nature of the relationship between these variables. This may be seen from equation 2.17 for the linear natural frequency of a CAP, which provides an approximate estimate of the resonance frequency.

$$\omega_o^2 = \left[3\kappa p_o - \frac{2\sigma_1}{R_{o1}} - \frac{2\sigma_2 R_{o1}^3}{R_{o2}^4} + \frac{4V_S G_S}{R_{o2}^2}\left(1+z\left(1+\frac{3R_{o1}^3}{R_{o2}^3}\right)\right)\right]\left(R_{o1}^2\rho_S\alpha\right)^{-1} \qquad (2.17)$$

It is clear that ω_o^2 has a much stronger dependence upon the ratio R_{o1}:R_{o2} and hence upon the shell thickness than upon G_S.

Before the implications of these findings are discussed further, the validity of the sensitivity analysis itself must be examined. The assumptions relating to the filling gas and the surrounding fluid have already been shown to be valid for the conditions being considered. The question remains as to whether the results obtained using relatively simple models of the encapsulating shell and the sound field can be used to draw general conclusions about CAP behaviour, or whether using a more advanced model would produce different results.

With regard to the sound field, it has already been shown that the pressure surrounding the CAP may be regarded as uniform, provided the presence of nearby boundaries is ignored and sufficiently low concentrations are considered. The effects of using pulsed as opposed to continuous wave insonation are demonstrated in figure 5.17. As may be seen, the relative amplitudes of the different factors are not substantially different from those in figure 5.1. It is possible that a complex pulse form, such as a chirp, could alter the results, since it would contain a range of frequencies, some of which would not correspond to the CAP resonance frequency. This should perhaps be considered when investigating how CAP insonation schemes should be optimised, but does not affect the validity of the findings of the present analysis.

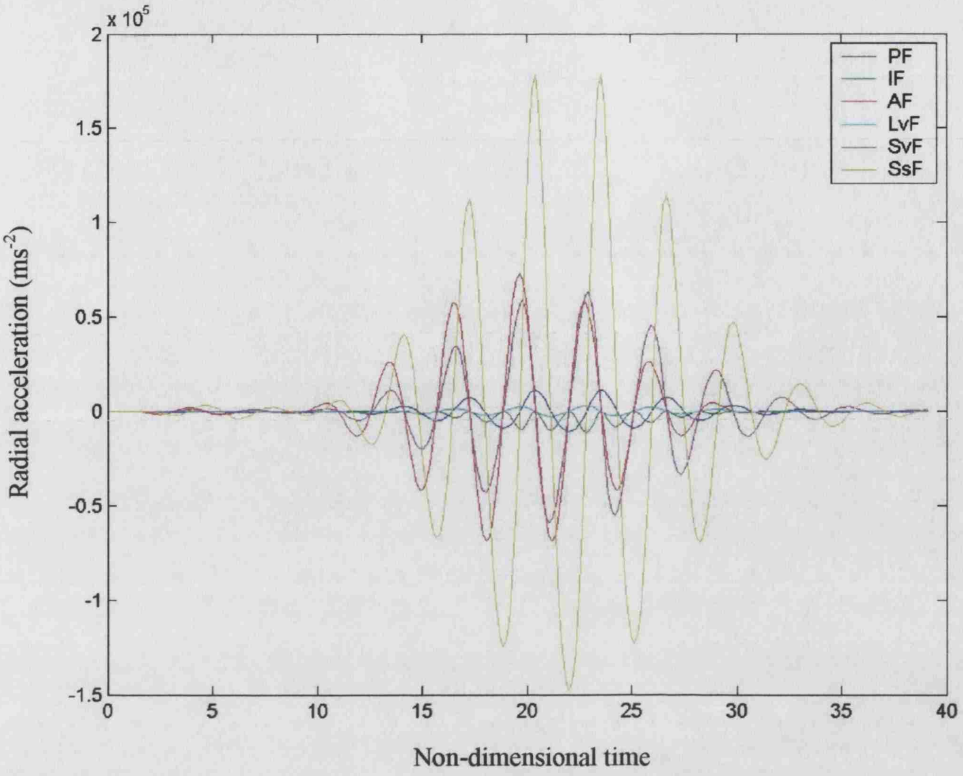

Figure 5.17: Acceleration factors for an Albunex® CAP insonated at 3 MHz and 50 kPa with a 6 cycle pulse (equation 3.45).

If a more advanced treatment of the encapsulating shell were to be used, e.g. for modelling larger amplitudes of oscillation, then the significance of the inertia factor, *IF*, would be expected to increase. This is due to the dependence of *IF* upon the square of the radial velocity (equation 5.8) and has been shown to be the case with free bubbles approaching the cavitation threshold (Flynn 1964). However, at the amplitudes at which *IF* would be expected to become comparable with S_sF, shell destruction would be likely to occur and thus equation 5.8 would be invalidated.

There is no intrinsic reason why a more complex shell model should affect the amplitude of S_sF, unless the material parameters were selected to describe a very thin and/or weak shell. For the purposes of design, the most important thing which the sensitivity analysis demonstrates is that CAP behaviour *can* be controlled by the properties of the shell, if these are selected appropriately. Before the selection of appropriate properties is investigated, however, the requirements for improving CAP effectiveness should be considered in more detail.

5.4 Design specifications

Having established the suitability of microbubbles for diagnostic and therapeutic applications in a general sense in section 5.2, the design of the CAPs themselves must now be examined more closely. For diagnostic applications, the three main requirements for an ultrasound contrast agent are:

- Detectability – CAPs should produce as large a contrast effect as possible for a given dose.
- Longevity – CAP survival times should be sufficient to enable imaging of the required region.
- Safety – CAPs should pose no risk to the patient.

For existing contrast agents these are conflicting requirements. In order to achieve a large contrast effect, and thereby minimise the dose required, the scattered signal from the CAPs must be distinct from that generated by tissue. At present, the most effective way of obtaining a distinctive signal is to use a high insonation pressure (Mechanical Index, MI). This not only increases the amplitude of the CAP signal and the proportion of CAPs excited, but also causes the CAPs to behave non-linearly. In theory, the non-linear components in the overall scattered signal will be due primarily to this behaviour. Thus, by using an appropriate imaging technique such as pulse inversion, which isolates these components, much of the noise from the surrounding tissue can be eliminated.

However, using a high MI also increases the likelihood of CAP destruction. This may be desirable for certain types of imaging, but it requires larger and/or more frequent doses to be administered and is clearly unacceptable if, for example, drug carrying CAPs are being imaged away from the target site. Moreover, at high MI the potential for harmful bio-effects is necessarily increased, and the effects of non-linear propagation through the surrounding tissue will become noticeable. The latter will limit the maximum CAP:tissue signal ratio that may be achieved.

The possibility of designing CAPs in order to overcome these problems is discussed in the next section. There are some further requirements to consider, however, which are general to all applications.

An ideal CAP should:

- Respond predictably and reproducibly
- Have a well defined destruction threshold
- Locate preferentially in the area required
- Be economical to produce
- Be convenient to administer
- Eventually disintegrate or be eliminated from the body

The reproducibility of CAP response, the ease with which CAPs can be administered and their cost, will be determined primarily by the manufacturing process. It should perhaps be noted at this point that the main disadvantage of ultrasound contrast agents is the fact that the need to administer them increases the time, skill and resources required for performing a scan. Since this must be offset against the benefits of contrast agents, it is important that manufacturing requirements are considered in the design process. This will be discussed again in section 5.8. The remaining requirements depend upon the selection of the shell material which will be considered next.

5.5 Design formulation

5.5.1 Principle

In order to meet the requirements for the ideal CAP set out in section 5.4, an improvement in CAP detectability at low insonation pressures is needed. The most obvious means of achieving this would be to increase the harmonic content of the signal radiated by the CAPs. The presence of harmonics in the CAP signal is due to the fact that, for equal peak positive and negative insonation pressures, the amplitude of CAP oscillations will be greater during expansion than during compression ($|R_{max}|>|R_{min}|$). Therefore, if the ratio $|R_{max}|:|R_{min}|$ could be increased, the harmonic content and hence CAP detectability could be enhanced. It is clear from the previous discussion that the most effective way of modifying CAP response is likely to relate to the CAP shell.

5.5.2 Shell model

Clearly, more advanced constitutive equations than equations 5.3 and 5.4 are required in order to examine the effects of different types of shell material and their potential for enhancing CAP non-linearity. In reality, the behaviour of most materials is non-linear to some extent and linear approximations are often used merely for the sake of mathematical convenience. In the remainder of this section different types of non-linear material behaviour will be examined in order to define suitable functions for f_{Ss} and f_{Sv}.

5.5.2.1 Elastic solids

i) One of the simplest examples of a non-linear material is one for which the elastic modulus is constant with strain but has a different value depending upon whether or not the material is in tension and compression (figure 5.18). Materials displaying this behaviour include certain metal alloy crystals and biological tissues (c.f. section 5.6).

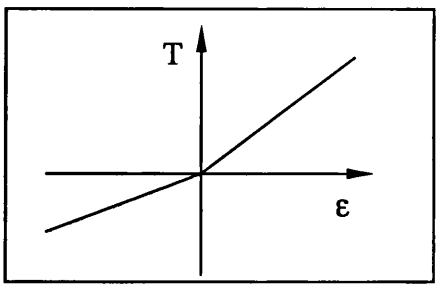

$$\mathbf{T}=\begin{cases}\mathbf{E}_1\boldsymbol{\varepsilon},\boldsymbol{\varepsilon}\geq 0\\ \mathbf{E}_2\boldsymbol{\varepsilon},\boldsymbol{\varepsilon}<0\end{cases} \qquad (5.9)$$

Figure 5.18: Stress-strain relation for an elastic solid in tension and compression.

ii) Similar behaviour is shown by elasto-plastic materials for which the modulus changes above a certain limiting "yield" stress (figure 5.19). This describes a wide range of materials including most metals and crystalline polymers.

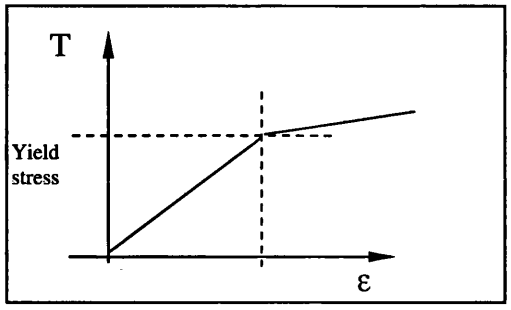

$$\mathbf{T} = \begin{cases} \mathbf{E}_1 \boldsymbol{\varepsilon}, \boldsymbol{\varepsilon} < \boldsymbol{\varepsilon}_y \\ \mathbf{E}_2 \boldsymbol{\varepsilon}, \boldsymbol{\varepsilon} \geq \boldsymbol{\varepsilon}_y \end{cases} \qquad (5.10)$$

Figure 5.19: Stress-strain relation for an elasto-plastic solid, showing the elastic limit in tension.

iii) In fully non-linear elastic materials, primarily polymers, the modulus varies as a function of the strain (figure 5.20).

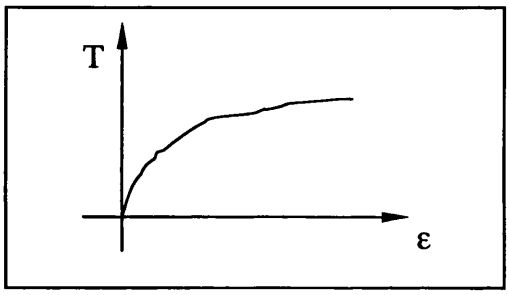

$$\mathbf{T} = \mathbf{E}(\boldsymbol{\varepsilon})\boldsymbol{\varepsilon} \qquad (5.11)$$

Figure 5.20: Stress-strain relation for a non-linear elastic solid.

5.5.2.2 Viscous fluids

i) Analogous to the non-linear elastic material is the pseudoplastic fluid, whose viscosity falls with increasing shear rate (figure 5.21). C and n are material constants.

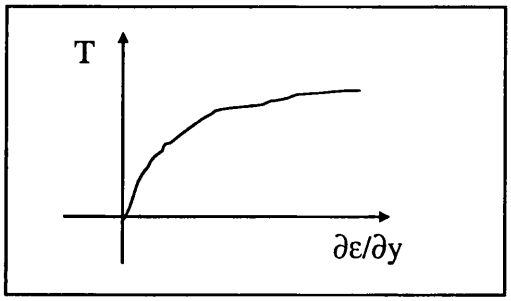

$$\mathbf{T} = \mu_S \left(\frac{\partial \boldsymbol{\varepsilon}}{\partial y} \right) \frac{\partial \boldsymbol{\varepsilon}}{\partial y} = C \left[\frac{\partial \boldsymbol{\varepsilon}}{\partial y} \right]^{n-1} \frac{\partial \boldsymbol{\varepsilon}}{\partial y}, n < 1 \qquad (5.12)$$

Figure 5.21: Stress-strain rate relation for a pseudo-plastic fluid.

ii) Conversely, in dilatant fluids, viscosity increases with increasing shear rate (figure 5.22). Again C and n are material constants.

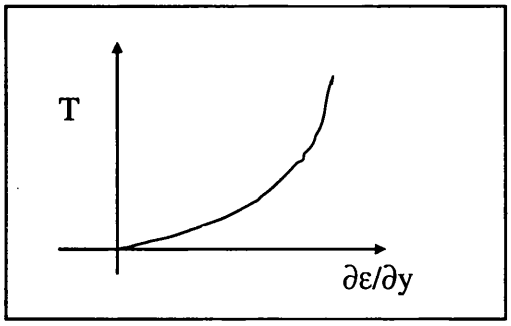

$$\mathbf{T} = \mu_s\left(\frac{\partial \boldsymbol{\varepsilon}}{\partial y}\right)\frac{\partial \boldsymbol{\varepsilon}}{\partial y} \qquad (5.13)$$
$$= C\left[\frac{\partial \boldsymbol{\varepsilon}}{\partial y}\right]^{n-1}\frac{\partial \boldsymbol{\varepsilon}}{\partial y}, n<1$$

Figure 5.22: Stress-strain rate relation for a dilatant fluid.

5.5.2.3 Viscoelastic materials

As discussed in section 3.5.6, in non-linear viscoelastic materials stress is related to strain by a factor which is itself a function of both strain and time (figure 5.23).

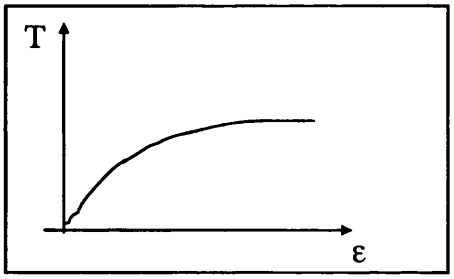

$$\mathbf{T} = \mathbf{E}(\boldsymbol{\varepsilon}, t)\boldsymbol{\varepsilon} \qquad (5.14)$$

Figure 5.23: stress-strain relation for a non-linear viscoelastic material.

This type of behaviour can be viewed as a combination of the characteristics described by equations 5.9-5.13 and may be described in general form by equation 3.28. It is displayed most noticeably by polymeric materials.

$$\mathbf{T}(t) = \int_{-\infty}^{t}\{\mathbf{I}\psi_1 tr(\mathbf{M}_1)+\psi_2\mathbf{M}_1\}d\tau_1$$
$$+\int_{-\infty}^{t}\int_{-\infty}^{t}\{\mathbf{I}\psi_3 tr(\mathbf{M}_1)tr(\mathbf{M}_2)+\mathbf{I}\psi_4 tr(\mathbf{M}_1\mathbf{M}_2)+\mathbf{I}\psi_5 tr(\mathbf{M}_2)+\psi_6\mathbf{M}_1\mathbf{M}_2\}d\tau_1 d\tau_2+... \qquad (3.28)$$

The aim of the next section is to investigate CAP behaviour for different definitions of the functions $\mathbf{M}_1$ and $\mathbf{M}_2$.

5.5.3 Model definition

5.5.3.1 Shell

In this section the range of non-linear material characteristics discussed above (equations 5.9-5.14) will be used to re-define f_{Ss} and f_{Sv}.

From equations 5.12 and 5.13 the viscous stress may be written as

$$T_{S,rr(vis)} = 2\mu_S a\left(\frac{2R_1^2\left|\dot{R}_1\right|}{r^3}\right)^n \quad \text{where} \quad a=\begin{cases}1, \dot{R}_1 > 0\\ -1, \dot{R}_1 < 0\end{cases} \tag{5.15}$$

Since the shell must be comparatively thin to allow the CAP to deform when passing through narrow blood vessels, it is reasonable to assume that G_S and μ_S are constant throughout the shell at a particular instant.

The shell factors may thus be found as

$$f_{Ss}+f_{Sv} = 3\int_{R_1}^{\infty}\frac{T_{rr}}{r}dr = -\frac{4\mu_L\dot{R}_1R_1^2}{R_2^3} - \frac{2a\mu_S V_s}{n}\left(\frac{2\left|\dot{R}_1\right|}{R_2^3R_1}\right)^n - \frac{4V_sG_s}{R_2^3}\left(1-\frac{R_{1e}}{R_1}\right) \tag{5.16}$$

If n is set to unity and G_S and μ_S are held constant, these expressions reduce to equations 5.3 and 5.4. However, it is possible to model very different, non-linear, shell behaviour by varying n and exchanging the constants G_S and μ_S for functions based on those defined in equations 5.9 - 5.13. For the purposes of this investigation the following functions for shell stiffness were used sequentially in equation 5.16

$$G_s(R_1)=\begin{cases}G_{s1}, R_1 \geq R_{e1}\\ G_{s2}, R_1 < R_{e1}\end{cases} \tag{5.17}$$

$$G_s(R_1)=\begin{cases}G_{s1}, R_1 < R_{e1}\\ G_{s2}, R_1 \geq R_{e1}\end{cases} \tag{5.18}$$

$$G_s(R_1) = G_{s1}R_1^m \tag{5.19}$$

$$G_s(R_1) = Ae^{bR_1} \tag{5.20}$$

The effect of variable shell viscosity was gauged by altering the value of m and substituting the following for μ_S.

$$\mu_s(R_1) = \mu_{s1} R_1^x \tag{5.21}$$

$$\mu_s(R_1) = Ce^{hR_1} \tag{5.22}$$

It has been shown in section 5.3 that the effect of changing shell density and inner and outer surface tensions is relatively small and these values were therefore kept constant.

As demonstrated above, the nature of CAP behaviour will be determined mainly by the proximity of the insonation frequency to CAP resonance frequency. The absolute values of the shell parameters used for this investigation were therefore comparatively unimportant, and it was reasonable to use the values for Albunex® from table 3.3 for G_{S1} and μ_{S1}.

5.5.3.2 Sound field

Once again, to enable any non-linearity in the CAP response to be clearly observed, the excitation was assumed to be continuous and sinusoidal i.e. $p_\infty = p_o + p_A Sin(\omega t)$ Simulations were carried out for both resonant and non-resonant conditions to investigate the full range of CAP behaviour. Where G_s varied between two values, two sets of tests were made, based on the corresponding pair of resonance frequencies. Since one of the aims of this work was to determine whether a detectable signal could be obtained without disrupting the CAP, the insonation pressures were selected according to the tensile strain criterion defined in Chapter 3.

The overall form of equation 3.15 used may be expressed as

$$\begin{aligned} &R_1\ddot{R}_1\left(1+\left(\frac{\rho_L-\rho_S}{\rho_S}\right)\frac{R_1}{R_2}\right)+\dot{R}_1^2\left(\frac{3}{2}+\left(\frac{\rho_L-\rho_S}{\rho_S}\right)\left(\frac{4R_2^3-R_1^3}{2R_2^3}\right)\frac{R_1}{R_2}\right) \\ &=\frac{1}{\rho_S}\left(\begin{array}{l} p_o\left(\frac{R_1}{R_2}\right)^3-p_o-p_A Sin(\omega t)-\frac{2\sigma_1}{R_1}-\frac{2\sigma_2}{R_2} \\ -\frac{4\mu_L R_1^2\dot{R}_1}{R_2^3}-\frac{4V_S G_S(R_1)}{R_2^3}\left(1-\frac{R_{1e}}{R_1}\right)-\frac{4\mu_S(R_1)V_S\dot{R}_1}{R_1R_2^3} \end{array}\right) \end{aligned} \tag{5.23}$$

5.5.3.3 Radiated pressure

The main interest of this investigation was the effect of the shell characteristics upon the radiated pressure. From Appendix A.ii, this may be expressed as

$$p_s(R_2) = \rho_L\left(R_2\ddot{R}_2 - \frac{3\dot{R}_2^2}{2}\right) - p_\infty \qquad (5.24)$$

p_s was evaluated at (R_2) since only the harmonic content was required for the analysis described below. The propagation of the radiated field will be discussed later.

5.5.4 Procedure

The use of non-linear material constitutive equations for f_{Ss} and f_{Sv} requires that equation 5.23 should be solved numerically. This would be desirable, in any case, to enable the full response of the CAP to be examined. For each set of conditions defined below, the solution of equation 5.23 was obtained as described previously. The results were used to calculate the radiated pressure using equation 5.24. From this, the signal frequency spectrum was derived via fast Fourier transform. All calculations were performed in Matlab™ 5.3 using purpose written code (Appendix D.i). The details of the tests were as follows:

A Albunex®

A reference set of results was obtained using the parameters for Albunex® (i.e. $G_S = G_{S1}$, $n = 1$ and $\mu_S = \mu_{S1}$ at all times) at the linear resonance frequency (3 MHz) and at sub and super-resonant frequencies (1 MHz, and 6 MHz). Results were also obtained for predominantly elastic and predominantly viscous shells by setting G_S and μ_S respectively to negligibly low values.

B Asymmetric G_S

G_S was varied according to equation 5.17 with $G_{S2} = xG_{S1}$ and $x = 2$, $x = 3$. Tests were carried out at the linear resonance frequencies corresponding to G_{S1} and each value of G_{S2}, and off resonance at 1 MHz. Viscosity was kept constant at μ_{S1}, with $n = 1$.

C Asymmetric G_S

G_S was varied according to equation 5.18 with $G_{S2} = xG_{S1}$ and $x = 2$, $x = 3$, $x = 0.5$, $x = 0.8$. Tests were carried out at the linear resonance frequencies corresponding to G_{S1} and each value of G_{S2}, and off resonance at 1 MHz. Viscosity was kept constant at μ_{S1}, with $n = 1$.

D Non-linear elastic solid

G_S was varied according to equation 5.19 with $m = 1$. Tests were carried out at the linear resonance frequency corresponding to G_{S1} and off resonance at 1 MHz. Viscosity was kept constant at μ_{S1}. with $n = 1$, and then at a negligibly low value.

E Non-linear elastic solid

G_S was varied according to equation 5.19 with $m = -1$. Tests were carried out at the linear resonance frequency corresponding to G_{S1} and off resonance at 1 MHz. Viscosity was kept constant at μ_{S1}. with $n = 1$, and then at a negligibly low value.

F Non-linear elastic solid

G_S was varied according to equation 5.20 with $A = = e^{-b}$ and $b = \pm 1,2$. Tests were carried out at the linear resonance frequency corresponding to G_{S1} and off resonance at 1 MHz. Viscosity was kept constant, first at μ_{S1}.with $n = 1$, and then at a negligibly low value.

G Non-linear viscous fluid

μ_S was varied according to equation 5.21 with $x = 1$, n =1. Tests were carried out at the linear resonance frequency corresponding to G_{S1} and off resonance at 1 MHz. Stiffness was kept constant, first at G_{S1}, and then at a negligibly low value (for the latter 1MHz corresponded to the resonance frequency and 3 MHz to the off resonance condition).

H Non-linear viscous fluid

G_S was varied according to equation 5.21 with x = -1, n = 1. Tests were carried out at the linear resonance frequency corresponding to G_{S1} and off resonance at 1 MHz. Stiffness was kept constant, first at G_{S1}, and then at a negligibly low value (for the latter 1MHz corresponded to the resonance frequency and 3 MHz to the off resonance condition).

J Dilatant fluid

Viscosity was varied according to equation 5.22 with x = 0, $\mu_S=\mu_{S1}$ and n = 1.1. Tests were carried out at the linear resonance frequency corresponding to G_{S1} and off resonance at 1 MHz. Stiffness was kept constant, first at G_{S1}, and then at a negligibly low value (for the latter 1MHz corresponded to the resonance frequency and 3 MHz to the off resonance condition).

K Pseudoplastic fluid

Viscosity was varied according to equation 5.22 with x = 0, $\mu_S=\mu_{S1}$ and n = 0.8 & 0.9. Tests were carried out at the linear resonance frequency corresponding to G_{S1} and off resonance at 1 MHz. Stiffness was kept constant, first at G_{S1}, and then at a negligibly low (for the latter 1MHz corresponded to the resonance frequency and 3 MHz to the off resonance condition). In this case sub-resonant insonation at 500 kHz was also simulated.

L Non-linear viscous fluid

μ_S was varied according to equation 5.22 with $C = e^{-h}$ and $h = \pm 1,2$. Tests were carried out at the linear resonance frequency corresponding to G_{S1} and off resonance at 1 MHz. Stiffness was kept constant, first at G_{S1}, and then at a negligibly low value.

For each of the tests (A-L) results were obtained over an interval beginning at time t = 0s and lasting for 2π periods of the insonation frequency. Plots were prepared of the time variation in radial displacement, radial velocity and radiated pressure and of the frequency spectrum. Those sets of results for which the frequency spectrum contained significant harmonic components (>10% fundamental) were identified and subjected to further analysis as described below.

5.5.5 Analysis

As discussed previously, the minimisation of shell strain was assumed to be desirable for the majority of applications. In terms of acoustic response, however, the "ideal" contrast agent can only be defined, in detail, within the context of a particular application. A number of different features were therefore considered in assessing the results, as follows:

- The number of harmonics present in the frequency spectrum (figure 5.24)
- The presence of sub- or ultra-harmonics in the spectrum
- The amplitude of the radiated pressure (figure 5.25)
- The ratio of harmonic to fundamental signal power (figure 5.26)
- The quality factors of the harmonic components (figure 5.27)

The significance of these features in terms of CAP effectiveness, and the manufacturing of non-linear CAPs will be addressed in section 5.8.

5.5.6 Results

The selected sets of results were ranked according to the above criteria as shown in table 5.1. Details of the corresponding test conditions are shown in table 5.2. Ideally, assessment of signal detectability should be based on the sensitivity of the equipment to be used, but in the absence of suitable data the results were compared with those obtained for Albunex®, which is known to be effective as a contrast agent. Results for Albunex® have been included in figures 5.24-5.27 and table 5.1 for comparison. The complete set of results has been included in Appendix F for reference.

Feature of interest	*Test(s) with Highest Value Results*				
Number of harmonics	Ciii	Biii			
Fractional harmonics	Ki				
Fundamental power	Bii				
2nd harmonic power	Cii				
3rd harmonic power	Bii				
4th harmonic power	Biii				
Fundamental quality factor	Cii				
2nd harmonic quality factor	Ciii	Cii	Ci	Bi	Di
3rd harmonic quality factor	Ciii	Cii			
4th harmonic quality factor	Ciii	Ci	Bi		
2nd harmonic:fundamental ratio	Ciii				
3rd harmonic:fundamental ratio	Di				
4th harmonic:fundamental ratio	Ciii				

Table 5.1: Results ranked according to the criteria set out in section 5.5.5.

Test Code	G_S (tension)	G_S (compression)	μ_s	p_A	$\omega/2\pi$
	MPa	MPa	Pas	MPa	MHz
Ai	88.8	88.8	1.77	0.02	3
Aii	88.8	88.8	1.77	0.1	1
Bi	177.6	88.8	1.77	0.1	1
Bii	266.4	88.8	1.77	0.05	3
Biii	266.4	88.8	1.77	0.1	1
Ci	88.8	177.6	1.77	0.05	1
Cii	88.8	266.4	1.77	0.05	3
Ciii	88.8	266.4	1.77	0.05	1
Di	Scaled with R	Scaled with R	0.000177	0.05	1
Ki	88.8	88.8	n=0.9	0.05	1
Kii	0	0	n=0.8	0.005	0.5

Table 5.2: Summary of test conditions for results shown in table 5.1

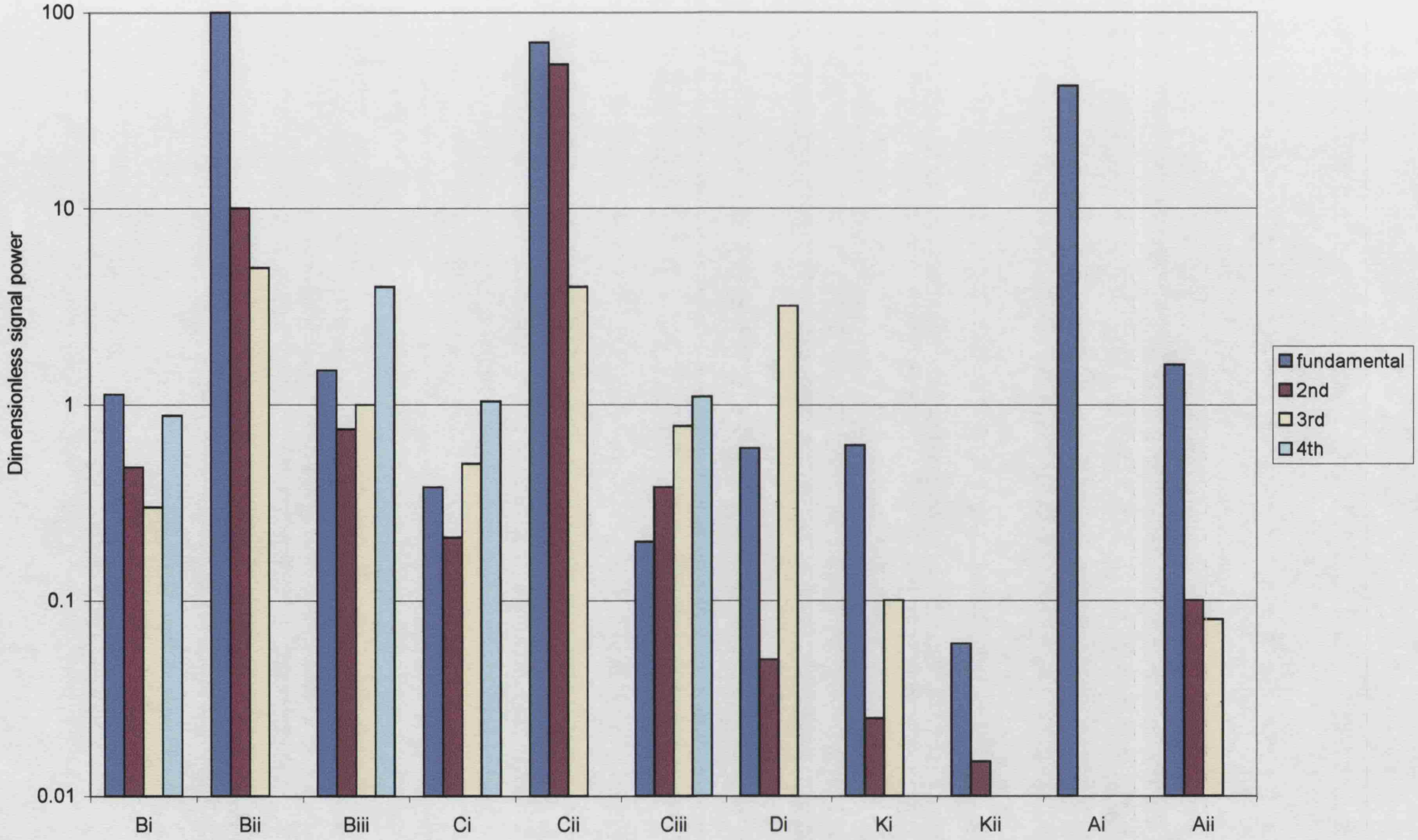

Figure 5.24: Comparing the frequency spectra components for Albunex® and non-linear-shelled CAPS

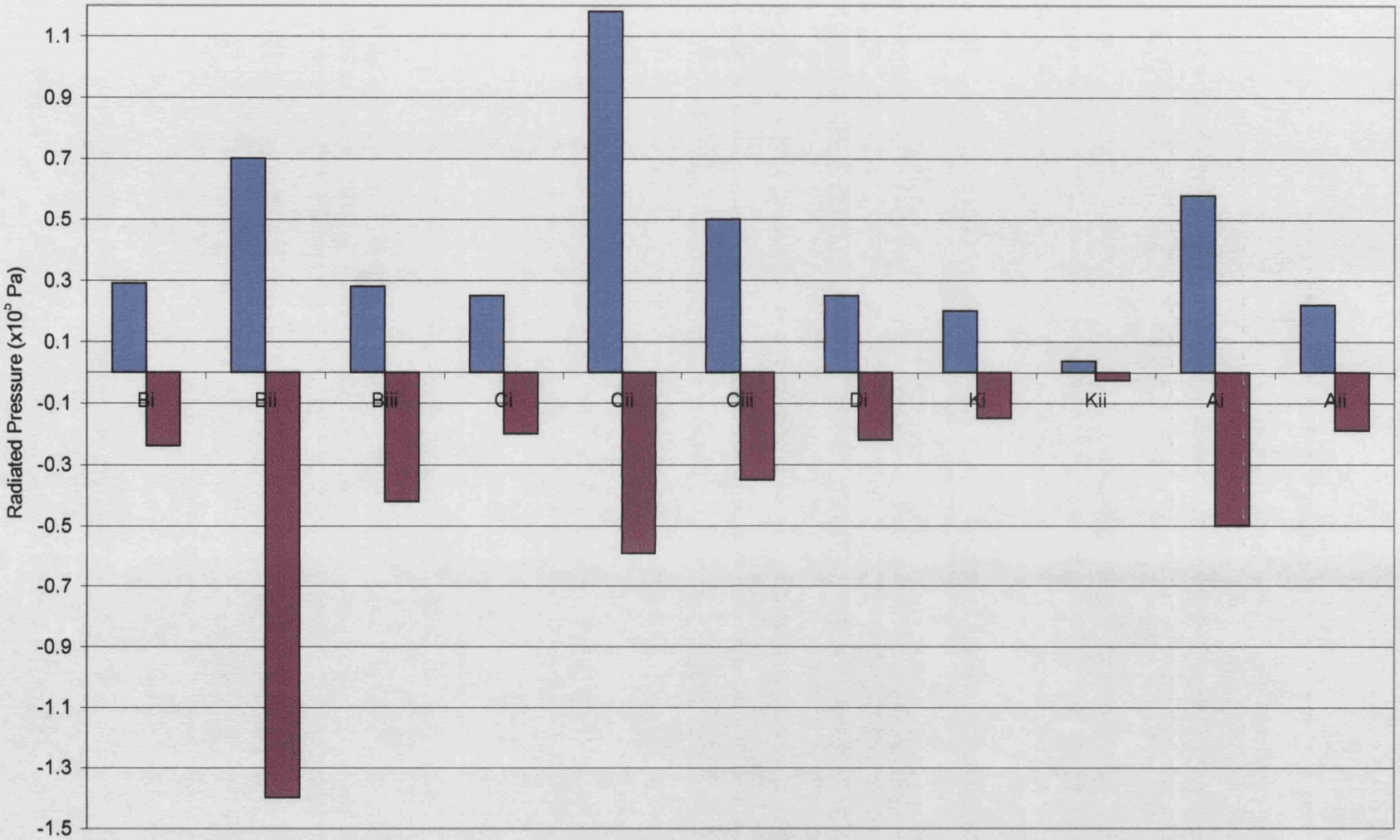

Figure 5.25: Comparative radiated pressure amplitudes for Albunex® and non-linear-shelled CAPS (blue bars indicate expansion and red bars compression).

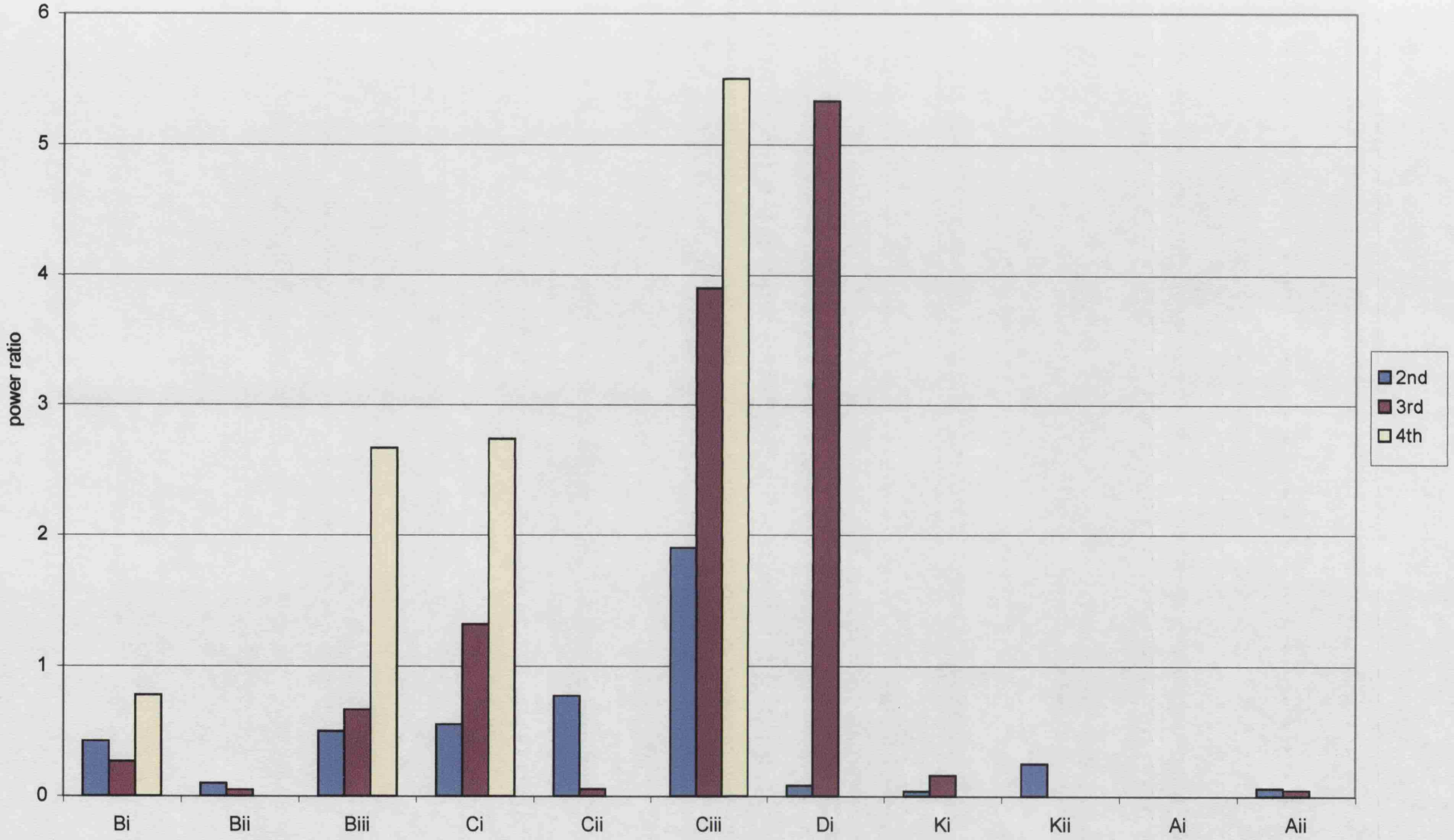

Figure 5.26: Ratios of harmonic to fundamental signal component power for Albunex® and non-linear-shelled CAPS

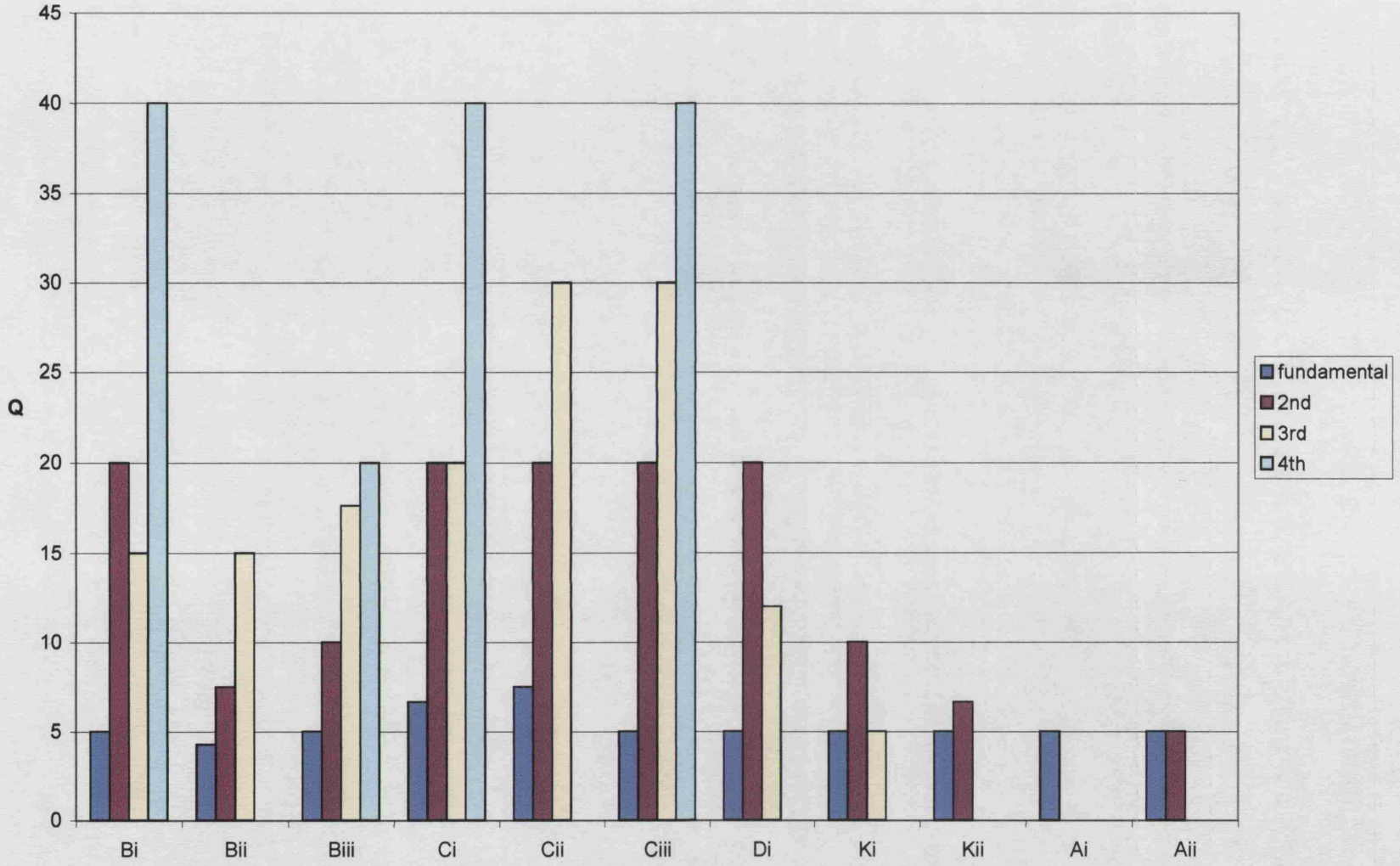

Figure 5.27: Quality factors for signal components from Albunex® and non-linear-shelled CAPS.

5.5.7 Discussion

The results shown in the previous section suggest that, by selecting a suitable shell material, it is indeed theoretically possible to obtain a non-linear acoustic response from a CAP at low amplitudes of oscillation. If the frequency spectra of the non-linear-shelled CAPs are compared with those of Albunex®, it may be seen that the harmonic content is significantly increased at both resonant and non-resonant frequencies (figure 5.24). With the exception of the fluid-shelled CAP in test (Kiv)Kii, the radiated pressure from the non-linear CAPs is of the same order of magnitude as that from Albunex® (figure 5.25). Similarly, the quality factors of the individual signal components are also comparable with those for Albunex® and in several cases substantially higher (figure 5.27). Since Albunex® is known to perform effectively as a contrast agent, these comparisons indicate that a non-linear-shelled CAP should do likewise.

As discussed in Chapter 1, the presence of harmonic components in a CAP signal enables it to be distinguished from signals due to reflections from the surrounding tissue and/or other background noise. The larger the number of harmonics, the more likely it is that one or more of the components will be unique to the CAPs. Moreover, the higher the frequency used for detecting the CAPs, the higher will be the resolution in the final images, although the degree of improvement possible will be limited by the increased attenuation suffered by high frequency signals. Sub-harmonic and ultra-harmonic components may offer even greater advantages in terms of signal to noise ratio since they are less likely to originate from sources other than the CAPs.

Table 5.1 indicates which type of contrast agent would be the most suitable for a particular application, in terms of the features defined in section 5.5.5. It is clear from these results that the greatest effect on the acoustic response was produced by varying the shear modulus. This concurs with the results of section 5.3 which identified the shell factor as the dominant influence in equation 5.8. The highest number of harmonic components was observed in test Ciii, in which the CAP was excited below its resonant frequency, and for which the shell shear modulus was higher in compression than in tension by a factor of 3. The highest ratios of harmonic to fundamental component power were also observed under these conditions.

These findings might have been expected from the explanation of CAP non-linearity given above. Increasing the compression modulus of the shell would have enhanced the ratio of expansion to contraction for the CAP, and hence the non-linearity of its response. Increasing the shear modulus in tension (test B) would also have affected the asymmetry of the oscillation, but in the opposite sense. Thus the effect would have been offset by the CAP's natural asymmetry. This explains why the harmonic content of the spectra in tests Bi and Bii was less than that in tests Ci and Ciii. A higher harmonic content would have been expected in tests Biii and Ciii than in tests Bi and Ci respectively, since the difference in the tensile and compressive moduli was higher.

The ease with which individual signal components may be detected also depends upon their bandwidth and separation in the frequency spectrum. If the bandwidth is too broad, i.e. the quality factor is too low, the signal will not be satisfactorily filtered and the spatial resolution in the image will suffer. It should be noted, however, that using a narrow bandwidth could impair axial resolution, although this problem may be overcome to some extent by using coded harmonics and subtracting rather than filtering out the unwanted components, as described in Chapter 1. It would appear from figure 5.27 that high quality factors are obtained away from resonance when there is a large difference in the shear modulus in tension and compression (tests Bi, Biii, Ci and Ciii). The physical reason for this is unclear at present. There was found to be no correlation between the variation in quality factor and shell viscosity, radial velocity or insonation frequency and there was no change in the fluid parameters. It is hoped that the explanation may be found in future work (c.f. Chapter 6).

Whichever signal component is used for imaging, it must be of sufficient amplitude to be detected by the receiving transducer outside the body. The absolute amplitude of the signal is therefore important, and in this respect the "best" results were obtained by exciting the CAPs at their resonant frequencies (figure 5.25, tests Bii & Cii). However, when a system is in resonance, the majority of the radiated signal power will be concentrated at the insonation frequency, because that is the frequency at which the system would naturally vibrate. If higher harmonics were to be used for imaging, a lower, sub-resonant insonation frequency would be more effective, as shown in figure 5.15. Similarly, the ratio of harmonic to fundamental component power would appear to be higher at sub-resonant frequencies (figure 5.26). As

mentioned previously, optimisation of the insonation scheme was not a concern of this thesis although this will be discussed again in Chapter 6. The main finding from this investigation is that there would appear to be good evidence that a non-linear-shelled CAP would produce a satisfactory non-linear response at low insonation pressures. How this may be achieved in practice, is examined the following next sections.

5.6 CAP design

The conclusion from the previous section was that the most effective way of increasing CAP detectability at low pressures is to modify the shell so that its response is asymmetric in tension and compression ($|R_{max}| > |R_{min}|$). Both the structure and the material of the shell may be modified and there are several possible approaches. Considering first the material, there are a number of materials which naturally display this type of behaviour. The response of TiNi crystals, for example, has long been recognised as being asymmetric in tension and compression (Gall *et al* 1999). Clearly, this type of material is unsuitable for coating CAPs, but similar behaviour has also been demonstrated for materials such as cartilage (Provenzano *et al* 2002) and other natural polymers.

The reported tensile and compressive moduli for these materials are derived from relatively large samples and may relate to material structure on a scale which is large compared with the thickness of a CAP coating. However, it may be possible to imitate these structures on a much smaller scale. The inclusion of cholesterol molecules in a cell membrane for example has been shown to produce a highly non-linear increase in its resistance to deformation (Boal 2002). Since the coatings of phospholipid CAPs are very similar in composition to cell membranes, it would seem feasible that they could be similarly engineered. A detailed discussion of such procedures would beyond the scope of this thesis, but there are alternative means by which enhanced non-linear behaviour may be achieved which will be discussed here.

Firstly, by varying its thickness over the CAP surface, the shell may be constructed so that it will buckle in compression. This will have a similar effect to increasing the ratio of compressive to tensile modulus, since a buckled shell will not compress to the same degree as one which remains smooth (Matan *et al* 2002). Similarly, there are other ways in which the structure of the shell may be designed to alter its relative

resistance to tension and compression. For example, if the shell were made up of two separate, unbonded layers having different elastic moduli and/or thicknesses (figure 5.28) then the minimum radius would be determined by the stiffer, inner layer whilst the maximum radius would be controlled by the more flexible outer layer.

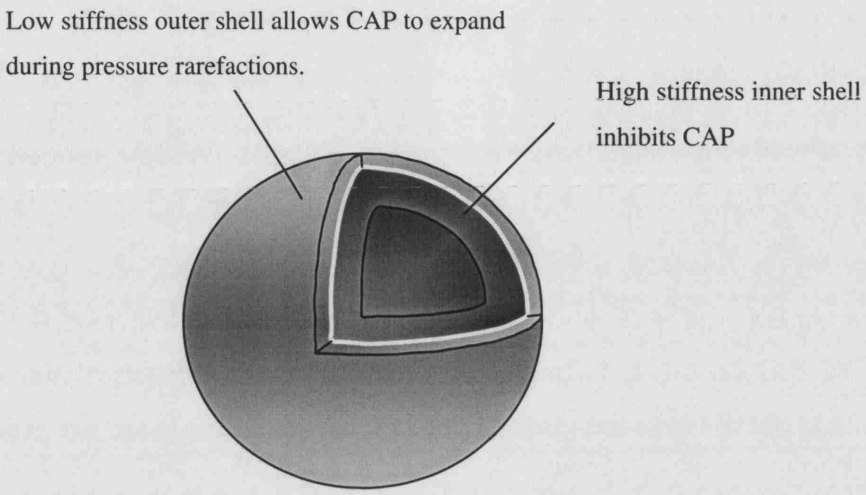

Figure 5.28: Schematic illustration of how the structure of a CAP could be modified to enhance non-linear behaviour at low insonation pressures.

An alternative would be to have a rigid frame work inside the CAP, again not bonded to the shell, which would have no effect upon CAP expansion but which would prevent the CAP from shrinking during compression (figure 5.29).

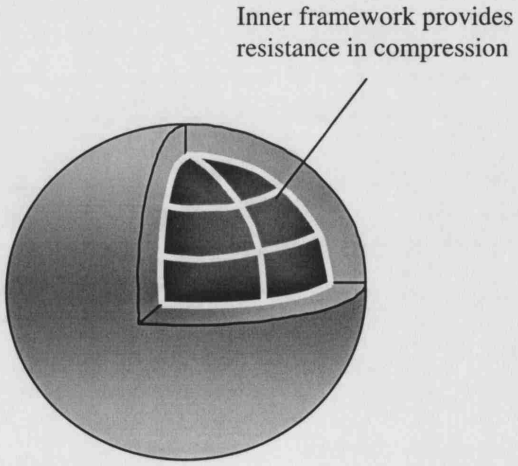

Figure 5.29: Schematic illustration of an alternative CAP design.

A third possibility would be to include a viscous layer underneath the shell in which solid particles could be suspended. The particles would be able flow freely during expansion, but would be pressed together during compression and thus obstruct further motion (figure 5.30). The effectiveness of these designs will be assessed in the next section.

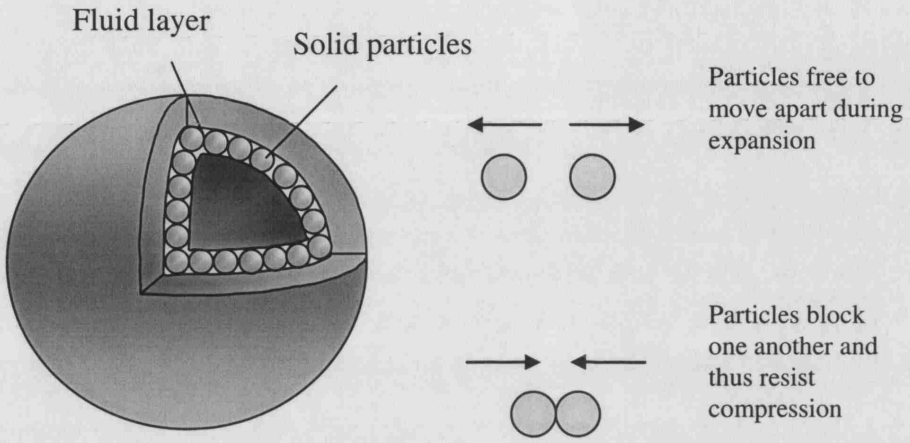

Figure 5.30: Schematic illustration of another alternative CAP design.

5.7 Experimental demonstration of feasibility

5.7.1 Aim

The aim of the experiment was to determine whether the designs proposed in the previous section would produce a significant increase in the ratio $|R_{max}|:|R_{min}|$ compared with existing CAPs.

5.7.2 Apparatus

Owing to the constraints of time, and the availability of suitable equipment and expertise, it was not possible to manufacture microbubbles with the shell structures described in section 5.5. In order to examine the effectiveness of the designs therefore, scale models were constructed for use in the experiments.

Hollow latex spheres were used as the basis for the model CAPs. These were dip-cast using an inflatable former whose internal surface was coated with Hi-float™ to prevent loss of volume over the drying period. The former was rotated after dipping to remove excess solution and avoid large inhomogeneities in thickness. The spheres were made up of 5 layers of latex (Magnacraft, Midhurst, UK) with 24 hours drying time allowed between each casting. A small cylindrical projection on each sphere enabled it to be sealed and provided an anchor point for positioning the models (figure 5.32).

Each sphere was tested as described below to provide a set of reference measurements. Models were then produced for the three designs as follows:

(i) A wire frame was constructed from 6 steel hoops soldered together. The diameter of the hoops was chosen to be the same as the initial diameter of the spheres (10 cm). The frame was then inserted into the first sphere prior to sealing.

(ii) An additional sphere was cast with 15 layers of latex to provide a stiffer inner shell which was inserted into the second sphere.

(iii) The internal surface of the third sphere was coated with hydrolysed sucrose solution in to which polypropylene beads (8 mm diameter) had been mixed so that the beads were almost touching when the sphere was at its equilibrium radius.

The pressure variation to which a CAP would be subjected in a sound field was simulated by placing the spheres inside a bell jar (20 cm diameter, 30 cm height Nalgene®, Rochester, USA) and varying the pressure inside the jar using a vacuum pump (Speedivac 2 A134-51-912, BOC Edwards, Crawley, UK). A graduated transparent screen was placed in front of the bell jar at a fixed distance of 15 cm to enable the variation in the radius of the spheres to be measured. The results were recorded using a digital camera (Nikon E2000). A schematic of the apparatus is shown in figure 5.31.

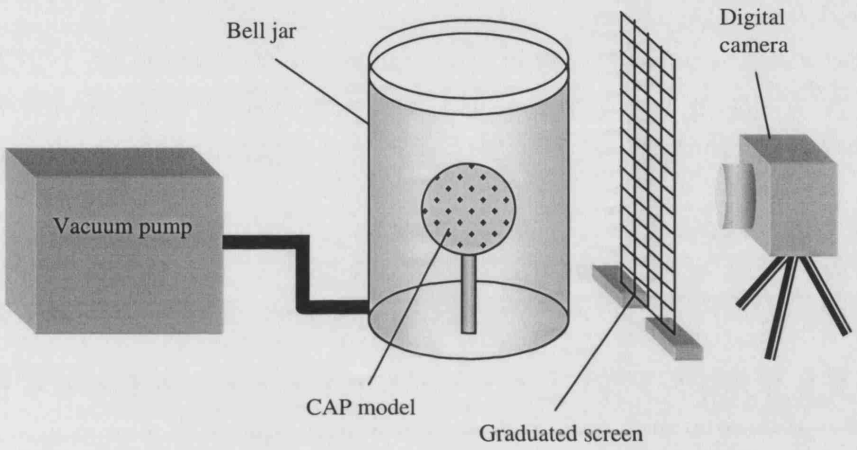

Figure 5.31: Schematic of the experimental apparatus.

5.7.3 Procedure

Each sphere was inflated to a diameter of 10 cm and sealed by knotting the cylindrical projection. The models were then placed inside the bell jar in turn and anchored by clamping the knotted part in a crocodile clip which was attached to a fixed vertical metal bar in the centre of the jar. For each model, the pressure in the jar was varied using the vacuum pump as indicated in table 5.3. The pressure measurements were made using the gauge located on the pump. To avoid any discrepancies between tests due to hysteresis or fatiguing of the spheres, the pressure was varied in the same way for each test, being first reduced and then increased. The diameter of the spheres was recorded at specific pressures (table 5.3) both directly, using the graduated screen, and photographically.

Owing to the need to seal and anchor the models it was not possible to maintain perfect spherical symmetry during the tests. Indeed, it was not possible with the casting technique used to manufacture models which were perfectly spherical. However, since the main aim of the experiment was to identify any differences in the degree of expansion and compression exhibited by the models, lack of spherical symmetry was not a serious concern, provided measurements of both the vertical and horizontal diameters were made. Moreover, as mentioned above, each sphere was tested prior to modification to provide a set of measurements with which to compare the results for each design and thus minimise the effects of any differences between the spheres due to manufacturing. For design (iii), an additional test was made after the hydrolysed sucrose solution had been applied to the model but before the addition of the beads, to determine whether the solution itself had any effect upon the ratio $|R_{max}|:|R_{min}|$.

The variation in model diameter with pressure was determined from the photographs for each test as indicated in figure 5.32. The ratios of maximum to minimum diameter were then calculated for each, as shown in the next section.

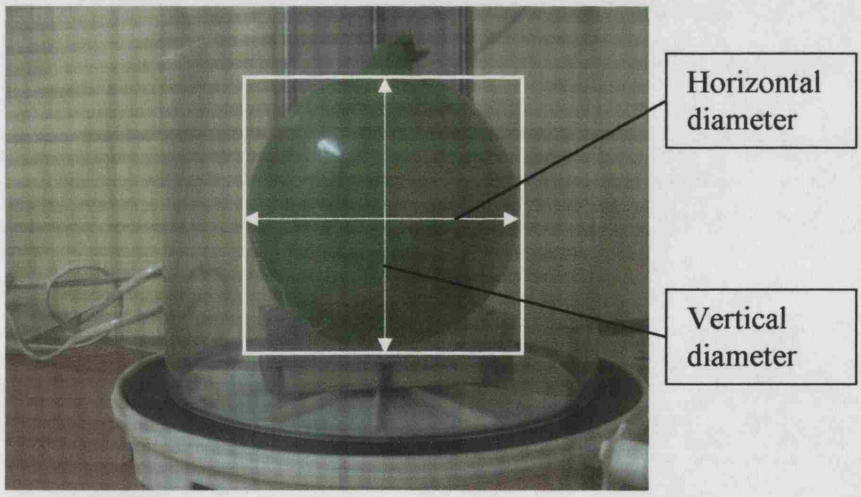

Figure 5.32: Illustrating the analysis of the photographic results.

	Horizontal diameter at -10 kPA	*Vertical diameter at -10 kPA*	*Horizontal diameter at 0 kPA*	*Vertical diameter at 0 kPA*	*Horizontal diameter at 10 kPA*	*Vertical diameter at 10 kPA*	*Amplitude ratio*	
Model	(cm)	(cm)	(cm)	(cm)	(cm)	(cm)	horizontal	vertical
sphere (i) unmodified	3.55	3.60	2.90	2.95	2.70	2.63	3.25	2.03
sphere (i) with wire frame	3.80	3.80	3.10	3.10	3.05	3.05	14.00	14.00
sphere (ii) unmodified	3.55	3.60	2.90	2.95	2.70	2.63	3.25	2.03
sphere (ii) with inner sphere	3.80	3.85	3.10	3.10	2.95	2.90	4.67	3.75
sphere (iii) unmodified	3.55	3.60	2.90	2.95	2.70	2.63	3.25	2.03
sphere (iii) with viscous layer	4.60	4.10	3.80	3.38	3.40	3.00	2.00	1.89
sphere (iii) with viscous layer and beads	4.20	3.70	3.65	3.10	3.60	3.05	11.00	12.00

Table 5.3: Measured diameters and amplitude ratios for each design (measurements refer to photographs rather than actual size).

Increase in amplitude ratio	*vertical*	*horizontal*
sphere (i) with wire frame	10.75	11.97
sphere (ii) with inner sphere	1.42	1.72
sphere (iii) with viscous layer and beads	9.00	10.11

Table 5.4: Improvement in amplitude ratio produced by each design compared with the unmodified CAP model.

5.7.5 Discussion

Table 5.4 indicates that the most effective design in terms of increasing the ratio of maximum to minimum radial amplitude was design (i) in which radial compression was inhibited by the presence of a wire frame. This was perhaps unsurprising since, in theory, a solid frame could prevent CAP compression entirely, giving rise to an infinite amplitude ratio. The fact that this was not observed in the experiment was due to the fact that the wire frame was not completely rigid and, indeed, this would probably be the case were such a CAP to be manufactured. Design (ii), containing a thicker inner layer, could be regarded as a version of design (i), since, in the limit, the inner layer could be made so stiff as to constitute a solid frame. In this case the inner layer was clearly insufficiently thick to greatly enhance the amplitude ratio. This indicates that it might be better to use different materials with contrasting stiffnesses for the two layers in order to avoid having to use very large thicknesses.

In terms of enhancing the amplitude ratio, design (iii), which incorporated a layer of beads in a viscous liquid under the outer shell was found to be almost as effective as design (i). This was an encouraging result, since there would be fewer safety implications associated with a CAP based on this design. For example, a potential objection to design (i) would be that the presence of a rigid layer or frame would prevent the CAP from deforming when passing through a narrow blood vessel. This would increase the risk of the CAP causing an embolism. The presence of a viscous inner layer containing beads, however, would not inhibit the type of deformation involved in passing through a narrow vessel, since this would not involve a reduction in shell surface area, only a change in shape[2]. Safety considerations will be discussed further in section 5.8.2.

[2] This is analogous to the case of a red blood cell, which is not significantly compressible, but which can deform in order to pass through narrow capillaries (Fung 1993).

It is perhaps legitimate to query the validity of this experiment. There is clearly a substantial difference between measuring the radial amplitude of a large latex sphere exposed to low frequency pressure variations, and examining the response of a coated microbubble to an ultrasound field. Nevertheless, the results do demonstrate that substantial asymmetry in radial amplitude between compression and expansion can be produced by relatively simple modifications in CAP structure. If the results were dependent upon the viscoelastic properties of the shell material, it would be justifiable to question the value of scaled experiments, since it would be important to consider the relationship between the material time constants and the insonation frequency. However, there is no reason to suppose that effects due to changes in CAP structure should not be as effective at ultrasonic frequencies as at low frequencies; although naturally this needs to be demonstrated before the effectiveness of the designs can be truly confirmed.

In terms of uncertainty, the simplicity of the experiment was such that there were relatively few sources of potential error. The differences in the measurements shown in table 5.3 were considerably greater than the uncertainty associated with measuring the model diameters from the photographs (±0.005 cm). The positioning of the camera, the graduated screen and the bell jar was not altered during the experiment and the questions relating to the symmetry of the models have already been discussed. The pressure inside the bell jar was not checked independently during the experiment. However, even if the absolute values taken from the gauge were slightly inaccurate, the range of pressures to which each model was subjected would have been the same since same procedure was adopted for all tests. Perhaps the most important question is whether or not it would be possible to manufacture microbubble CAPs according to these designs in practice. This is the subject of the next section.

5.8 Evaluation

5.8.1 Manufacturing feasibility

Methods for manufacturing coated microbubbles, both for use as contrast agents and for industrial applications have been developed over the past three decades. Recently techniques for producing CAPs with multiple coatings for incorporating drug layers or targeting species have also been devised (Point Biomedical 2004). It would seem feasible therefore, that the proposed designs could be produced using existing technology. Further research would clearly be required in order to identify the most suitable materials, particularly for design (iii), which would both satisfy the design requirements and not present any problems as regards the toxicity and/or degradability of the CAPs. It seems unlikely that this would present a serious obstacle, however.

So far the design process has concentrated upon modifying the response of a single CAP, with the implicit assumption that all of the CAPs in a population will behave in the same way. However, owing to the small thickness of the shell, the assumption of material homogeneity, both throughout the shell of a single CAP and across a population, should perhaps be questioned. As noted previously, variability in CAP properties presents a problem for characterisation and it would also affect the certainty with which the response of an engineered CAP could be predicted. For example, figures 5.15 and 5.16 demonstrate that CAP response is extremely sensitive to variations in shell thickness.

Considerable variation in the behaviour of ostensibly identical CAPs has been observed with existing agents (Postema *et al* 2003) using high speed photography. The same authors also noted a wide variation in the fraction of CAPs in a given population which responded to the incident sound field. Such variation could lead to an increase in the size of contrast agent dose required to produce a given level of enhancement and would make optimisation of the insonation scheme extremely difficult. The implication is that the level of control over CAP parameters provided by the manufacturing process may need to be examined.

Similarly, it is important that the destruction thresholds should be well defined, both to ensure that CAPs remain intact when required and so that the delivery of treatment can be optimised. For example, it would be desirable both to minimise the pressure required for destruction, and to maximise the number of CAPs destroyed in the target area. In theory it should be possible to introduce defects into the shell in order to control the insonation pressure at which rupture occurs, although this is clearly dependent upon the level to which shell homogeneity can be controlled.

There are some further issues to consider. The long term stability of CAPs without insonation will be affected by the shell. For example, the permeability and solubility of the shell material will determine the length of time over which the CAP will degrade. This may restrict the choice of materials to some extent and there may be further constraints relating to the material's chemical properties if targeting species are to be attached to the shell or if a drug layer is to be included (c.f. Appendix D.ii). Requirements for therapeutic applications may also affect CAP structure. For example, a buckled shell offers an increased surface area for the same radius compared with a smooth CAP, and hence an increased area available for adhesion. Methods for producing CAPs with permanently buckled shells have been developed for this purpose (Klibanov *et al* 2003).

The choice of filling gas will also affect the long term stability of the CAP. If the shell is gas permeable and/or soluble, then the rate at which the CAP dissolves will depend upon the solubility of the gas as well as the durability of the shell. Clearly, any shrinkage of the CAPs due to dissolution will affect their acoustic response and this may be important for some applications. In addition there may be some safety issues relating to very low solubility gases. If free bubbles are able to persist after the CAP shells have degraded they could potentially coalesce to form a large bubble capable of causing an embolism. Finally, the possibility of chemical interaction between the filling gas and the shell material or any therapeutic compounds may need to be considered.

5.8.2 Safety considerations

It has been assumed above that the risk of bio-effects would be minimised by ensuring small amplitude oscillations. This is in agreement with the existing experimental evidence (Mornstein 1997, Nyborg 2001). However, it is worthwhile considering the potential mechanisms for CAP related bio-effects in relation to the new designs. Firstly, the materials would need to be selected so that the risk of toxicity or of exciting significant immune response *in vivo*, would be minimised. As mentioned above, it would be important to ensure the CAPs were sufficiently small and flexible to avoid causing an embolism. Similarly, the shell should prevent CAPs from coalescing to form a larger body. The selection of the filling gas is also important in this regard. Although higher molecular weight gases improve CAP stability by dissolving more slowly in the blood, their ability to persist as free bubbles after shell destruction increases the risk of coalescence.

The risk of inertial cavitation and its associated effects such as microjetting and the production of toxic chemicals, should be low at the insonation pressures considered in this work. The thresholds for free bubbles under these conditions, for example those defined by Flynn (1964) which require that the inertial factor in equation 5.8 is greater than the pressure factor at the start of bubble compression, would not be exceeded. Moreover, the corresponding thresholds for CAPs would be expected to be much higher owing to the dominant effect of the CAP shell (figure 5.1). As mentioned previously, microjetting has apparently been observed at much lower insonation pressures than would be expected (Postema *et al* 2004). This requires further investigation, however, to determine whether potentially dangerous jet velocities may indeed be produced below the cavitation threshold or whether the pressures in the experiment were in fact higher than expected.

Similarly, further examination of the speeds to which CAPs are accelerated as a result of radiation forces should be made *in vivo*. Potentially, a CAP could reach sufficient speeds to rupture a neighbouring cell upon impact (Dayton *et al* 1999) but the obstructions presented by large concentrations of blood cells or of other CAPs have not been taken into account. The same is true of the microstreaming currents set up around an oscillating CAP. These have been shown to have sufficient velocity to produce potentially harmful shearing stresses (e.g. Wu 2002), albeit at higher pressures than were considered in this work, but no study has been carried out in

which *in vivo* conditions have been considered. Where *ex vivo/in vivo* experiments have demonstrated CAP-enhanced tissue damage (e.g. Dalecki 1997) it has not been possible to positively identify the underlying mechanism specifically.

A further safety concern relating to CAPs is the heating effect produced during oscillation. Whilst it is true that the temperatures inside a CAP or bubble may be very high during compression, it has been shown in Appendix B.i that relatively little energy is conducted into the surroundings. The majority of the energy is reabsorbed during CAP/bubble expansion. There are, however, additional heating mechanisms which may present a greater risk. These are discussed in the Appendix D.iii. As concluded by Mornstein (1997), Nyborg (2001) and a number of other reviews of the subject, there is, as yet, no conclusive evidence that contrast agents produce harmful bio-effects. It is, however, an area requiring further theoretical, experimental and clinical studies, particularly as new CAPs are produced.

5.8.4 Further considerations

Whilst the development of a new contrast agent based on the designs discussed above is clearly at a very early stage, a brief discussion of the demand for improvements in CAP design is perhaps warranted. The previous sections have presupposed the need for more effective contrast agents, based on the fact that existing contrast agents have been developed mainly by trial and error and the fact that their design *could* be improved. This does not necessarily equate to high demand or commercial success, however. Existing ultrasound contrast agents are relatively expensive and increasing the complexity of their design might be regarded as injudicious, even if the technology to produce them is well established. On the other hand, there is undoubtedly a need to improve the imaging of, e.g. the blood vessel networks surrounding cancerous tumours (e.g. Balci *et al* 1999) and CAPs have additional benefits to offer. They are able to deliver treatment to the disease site and, potentially, they may be used destroy the fragile vessels, thus starving the tumour of blood. Moreover, as well as being cheaper and safer, ultrasound is the only method suitable for imaging certain features, such as blood flow velocity. It could also be argued that by improving CAP effectiveness, demand would be increased which would reduce manufacturing costs. Thus, whilst further assessment of demand would certainly be required, it would seem that future development of the design work would be justified.

5.9 Summary

The aim of this chapter has been to demonstrate how ultrasound contrast agents may be designed in order to improve their suitability for particular applications. It has been shown that analytical techniques may be applied to identify the most important factors for modelling and design, and that this knowledge may be used to determine how the material and/or structure of the encapsulating shell could be selected in order to enhance the non-linearity of CAP oscillations at low insonation pressures. The new model developed in Chapters 3 and 4 was used to simulate the behaviour of a range of new designs in order to assess their effectiveness. Experiments were then conducted, using scale models of the most successful designs to test their effectiveness in practice. The results indicated that CAP structure could indeed be modified successfully to increase the degree of non-linear behaviour by the addition of an inner layer with increased resistance to compression. Finally, the feasibility of manufacturing a new contrast agent and the implications for patient safety were examined.

6

Conclusions

6.1 Overview

The overall aim of the work described in this thesis was to improve the characterisation of ultrasound contrast agent particles (CAPs) and use the results obtained to design more effective agents. The first aim of this chapter is to review the objectives set out in Chapter 1, to assess the degree to which these have been accomplished and summarise the contributions of the work. The second aim is to examine those areas requiring further investigation and to discuss any new problems identified as a result of the work, together with possible means of addressing them.

6.2 Contributions

In this section the achievements of the work will be compared with the list of aims set out in Chapter 1 in order to assess the degree to which new contributions have been made.

The planned review of previous theoretical and experimental work on ultrasound contrast agents was made in Chapter 2. In Chapter 3, a new generalised model for CAP behaviour was derived to enable a wider range of conditions to be simulated than was possible with existing models. Definitions for the individual terms in the model were then developed, based on a rigorous examination of the underlying assumptions. First of all, it was demonstrated that the behaviour of the filling gas could be regarded as isothermal and that thermal damping could be neglected for the range of gases commonly used for CAPs and for the range of insonation pressures and frequencies over which CAPs could be assumed to remain intact.

The modelling of the encapsulating shell was then examined and it was shown that, under typical insonation conditions, the shell material could be regarded as insoluble, impermeable, incompressible and uniform. The linear constitutive equation used in existing models was replaced by a non-linear viscoelastic material function suitable for a much wider range of materials and larger amplitudes of oscillation. This was followed by an investigation of the role of the shell in CAP destruction based on an analysis of the stresses generated in the shell during CAP oscillation. The results were compared with existing experimental data and used to define the range of amplitudes and corresponding insonation conditions for which CAPs could be expected to remain intact. The potential for CAPs to undergo inertial cavitation was also discussed.

The next subject to be addressed was the influence of the surrounding fluid upon CAP behaviour, and a new model was derived for a CAP surrounded by red blood cells. The results of the simulations indicated that, owing to the small elasticity of cell membranes, it was justifiable to treat the surrounding fluid as homogeneous and Newtonian for the purposes of CAP design. This was subsequently verified by new experimental data obtained as described in Chapter 4. It was also shown that, under the conditions relevant to diagnostic imaging, the surrounding fluid could be regarded as both static and incompressible.

It was demonstrated that, at low CAP concentrations, the wavelength of ultrasound in blood would be sufficiently large compared with the diameter of a CAP for the pressure surrounding the CAP to be regarded as uniform over the range of insonation frequencies used for diagnostic imaging. The problems associated with CAP behaviour at higher concentrations were addressed by the development of a new model for multiple scattering in CAP suspensions. Both linear and non-linear scattering were modelled in order to identify the concentrations and insonation conditions under which this phenomenon would become significant. These findings were also supported by the results of new experiments described in Chapter 4.

In Chapter 5, the new model was applied to the problem of improving CAP design. A sensitivity analysis was carried out in order to identify the main factors controlling CAP response. It was shown that, contrary to the assumptions made in numerous previous investigations, CAP behaviour may differ significantly from that of a free bubble and is determined primarily by the nature of the encapsulating shell. The main objective of the subsequent design work was therefore to determine how the shell could be modified in order to improve CAP effectiveness.

A review of the requirements for ultrasound contrast agents indicated that the aim should be to enhance the degree of non-linear behaviour at low insonation pressures. This would improve CAP detectability, whilst reducing the risk of CAP destruction or harmful bio-effects. A number of designs were developed on this basis and their relative effectiveness assessed theoretically and experimentally using scale models. The manufacturing and safety considerations for the most effective designs were then discussed. The results indicated that the structure of the CAP shell could indeed be modified to enhance non-linear behaviour and that a new agent could be produced on this basis.

6.3 Further work

It was shown in the previous section that each of the objectives set out in Chapter 1 has been achieved and that a number of additional discoveries have been made as a result of the work. However, as indicated at various stages throughout the thesis, there are many areas requiring further investigation. The aim of this section is to summarise those areas.

Perhaps the greatest area of uncertainty, which has been discussed at several points in the thesis, is the lack of reliable experimental data relating to the properties of the encapsulating shell. Whilst this problem was avoided to some extent in the preceding chapters by the use of hypothetical shell functions, it remains an important issue for accurate CAP characterisation. It seems likely that the most practical approach would be to use a range of different measurement techniques to determine G_S and μ_S, or the equivalent quantities, and compare the results.

Suitable techniques might include micropipette aspiration, which is a well established technique for measuring the properties of biological cells (Evans 1983), and manipulation using optical tweezers. In both cases a variable pressure could be exerted upon a portion of the shell and the variation in displacement recorded photographically using an optical microscope. It might also be possible to modify the technique used in Chapter 5 with the CAP scale models, and to vary the hydrostatic pressure in the liquid surrounding a CAP. Again the change in CAP radius with pressure could be recorded photographically for different rates of pressurisation. The results would indicate whether or not there is a difference between the shell properties measured for a part of the shell and those for the CAP as a whole.

The results of these experiments could be compared with those obtained by recording the acoustic response from a single CAP in an ultrasound field and, if possible, with optical measurements of the radial amplitude of oscillation made using a high speed camera. It might also be useful to compare the results with properties derived from scattering and attenuation measurements for CAP populations using the curve-fitting methods employed by e.g. de Jong *et al* (1992) in order to determine the error associated with the latter method. Additionally, these techniques could be used to determine the thresholds for shell destruction, in terms of a limiting stress or strain,

over which there is similar uncertainty. Likewise, the degree of variability in CAP properties within a population, discussed in Chapter 3, could be investigated.

Allied to the problem of shell characterisation is the lack of information regarding the properties of biological tissue. In order to make a reliable assessment of the ability of CAPs to produce harmful bio-effects, details of the thresholds for both mechanical and thermal damage for different types of tissue are needed. For example, when considering the behaviour of CAPs in narrow blood vessels, it is important to know the extent to which a blood vessel wall may be stretched before it ruptures, in order to determine the maximum amplitude of oscillation allowable. This information is not available at present.

Of similar importance is the need to investigate the inverse problem of how the presence of a blood vessel affects CAP behaviour. The modelling described in this thesis was necessarily restricted to large blood vessels in which the influence of vessel walls could be neglected. In a narrow capillary, however, this is clearly not a valid assumption. Accurate characterisation of CAP behaviour within the confines of a blood vessel would be extremely important if CAPs were to be designed to produce a particular response for imaging, e.g. in the narrow vessel network surrounding a cancerous tumour. It would also be important in order to optimise the use of CAPs for therapeutic applications such as destroying atherosclerotic plaques.

It is likely that the presence of a vessel wall, or indeed any boundary, would invalidate the assumption of spherical symmetry upon which the new model developed in Chapter 3 depends. Numerical methods, such as finite element analysis would therefore be required to investigate CAP behaviour and the effects upon the radiated field under these conditions. A numerical model could also be used to assess the effect of inhomogeneities in the shell and phenomena such as buckling, which have been observed experimentally (e.g. Chomas *et al* 2001). This would be important in order to make further investigation of the mechanisms of CAP destruction, which represent another large area of uncertainty. Large amplitude oscillations and shell destruction could be modelled in order to investigate the fragmentation processes observed by e.g. Dayton *et al* (1999). It might be necessary to review the assumptions relating to the behaviour of the filling gas under these conditions and replace the polytropic model (equation 3.23) with a suitable equation

of state such as the Van der Waals' equation. It might also be necessary to remove the assumption of negligible mass transfer in order to model outwards diffusion of the filling gas and/or inwards diffusion of liquid vapour. As mentioned above, this work would need to be accompanied by experimental determination of the thresholds for shell destruction.

The ability to manufacture CAPs would also be central to advancing the design work. Whilst it was concluded in Chapter 5 that it would be feasible to produce contrast agents based on the proposed designs, it is clear that this process would involve several stages. First of all it would be necessary to develop a prototype. This would require a potentially extended period of *in vitro* testing and design modification to achieve the desired characteristics. Once the results of the *in vitro* tests were deemed to be satisfactory they would need to be followed by *ex vivo* and eventually *in vivo* experiments to demonstrate the effectiveness of the new agent. It would also be important to refine the manufacturing process and investigate methods of controlling quantities such as particle uniformity to ensure that the correct response was obtained. Finally, assuming all of the above stages could be completed successfully, a full assessment of the marketability of the new agent and clinical trials would be required.

A further factor which should play a part in the design process is the selection of the insonation scheme. Whilst the optimisation of the incident field was not considered in this thesis it is clearly an area of great importance. A detailed theoretical examination of the relationship between the frequency content of the incident pulse and CAP response should be made to determine the most effective insonation scheme for a particular shell design. As indicated in Chapter 5, the most useful response in terms of CAP detection may not necessarily be obtained at the resonance frequency. The results of this work would need to be validated experimentally. In addition, the attenuation and distortion of the incident and radiated fields in the surrounding tissue would need to be taken into account in selecting a suitable input signal. This would need to be examined for a wider range of conditions than considered in this thesis. It would also be useful to determine the sensitivity of a commercial medical scanner in order to quantify the minimum pressure amplitude required for the CAP response.

6.4 Summary

It has been shown in this chapter that the aims and objectives defined at the start of the work have been achieved. In particular, a new model for CAP behaviour under a wide range of conditions has been derived, using a combination of theoretical analysis and experimental validation. The model has been used to develop designs for a new contrast agent, which has improved detectability at low insonation pressures. The effectiveness of the designs has been demonstrated experimentally using scale models. Areas for future work have also been identified in this chapter. These include improving the characterisation of CAP shell materials, identifying the damage thresholds for biological tissue, determining the influence of blood vessel walls upon CAP behaviour, further investigation of the mechanisms of CAP destruction and further development of a new contrast agent.

Similarly, it is important that the destruction thresholds should be well defined, both to ensure that CAPs remain intact when required and so that the delivery of treatment can be optimised. For example, it would be desirable both to minimise the pressure required for destruction, and to maximise the number of CAPs destroyed in the target area. In theory it should be possible to introduce defects into the shell in order to control the insonation pressure at which rupture occurs, although this is clearly dependent upon the level to which shell homogeneity can be controlled.

There are some further issues to consider. The long term stability of CAPs without insonation will be affected by the shell. For example, the permeability and solubility of the shell material will determine the length of time over which the CAP will degrade. This may restrict the choice of materials to some extent and there may be further constraints relating to the material's chemical properties if targeting species are to be attached to the shell or if a drug layer is to be included (c.f. Appendix D.ii). Requirements for therapeutic applications may also affect CAP structure. For example, a buckled shell offers an increased surface area for the same radius compared with a smooth CAP, and hence an increased area available for adhesion. Methods for producing CAPs with permanently buckled shells have been developed for this purpose (Klibanov *et al* 2003).

The choice of filling gas will also affect the long term stability of the CAP. If the shell is gas permeable and/or soluble, then the rate at which the CAP dissolves will depend upon the solubility of the gas as well as the durability of the shell. Clearly, any shrinkage of the CAPs due to dissolution will affect their acoustic response and this may be important for some applications. In addition there may be some safety issues relating to very low solubility gases. If free bubbles are able to persist after the CAP shells have degraded they could potentially coalesce to form a large bubble capable of causing an embolism. Finally, the possibility of chemical interaction between the filling gas and the shell material or any therapeutic compounds may need to be considered.

5.8.2 Safety considerations

It has been assumed above that the risk of bio-effects would be minimised by ensuring small amplitude oscillations. This is in agreement with the existing experimental evidence (Mornstein 1997, Nyborg 2001). However, it is worthwhile considering the potential mechanisms for CAP related bio-effects in relation to the new designs. Firstly, the materials would need to be selected so that the risk of toxicity or of exciting significant immune response *in vivo*, would be minimised. As mentioned above, it would be important to ensure the CAPs were sufficiently small and flexible to avoid causing an embolism. Similarly, the shell should prevent CAPs from coalescing to form a larger body. The selection of the filling gas is also important in this regard. Although higher molecular weight gases improve CAP stability by dissolving more slowly in the blood, their ability to persist as free bubbles after shell destruction increases the risk of coalescence.

The risk of inertial cavitation and its associated effects such as microjetting and the production of toxic chemicals, should be low at the insonation pressures considered in this work. The thresholds for free bubbles under these conditions, for example those defined by Flynn (1964) which require that the inertial factor in equation 5.8 is greater than the pressure factor at the start of bubble compression, would not be exceeded. Moreover, the corresponding thresholds for CAPs would be expected to be much higher owing to the dominant effect of the CAP shell (figure 5.1). As mentioned previously, microjetting has apparently been observed at much lower insonation pressures than would be expected (Postema *et al* 2004). This requires further investigation, however, to determine whether potentially dangerous jet velocities may indeed be produced below the cavitation threshold or whether the pressures in the experiment were in fact higher than expected.

Similarly, further examination of the speeds to which CAPs are accelerated as a result of radiation forces should be made *in vivo*. Potentially, a CAP could reach sufficient speeds to rupture a neighbouring cell upon impact (Dayton *et al* 1999) but the obstructions presented by large concentrations of blood cells or of other CAPs have not been taken into account. The same is true of the microstreaming currents set up around an oscillating CAP. These have been shown to have sufficient velocity to produce potentially harmful shearing stresses (e.g. Wu 2002), albeit at higher pressures than were considered in this work, but no study has been carried out in

which *in vivo* conditions have been considered. Where *ex vivo/in vivo* experiments have demonstrated CAP-enhanced tissue damage (e.g. Dalecki 1997) it has not been possible to positively identify the underlying mechanism specifically.

A further safety concern relating to CAPs is the heating effect produced during oscillation. Whilst it is true that the temperatures inside a CAP or bubble may be very high during compression, it has been shown in Appendix B.i that relatively little energy is conducted into the surroundings. The majority of the energy is reabsorbed during CAP/bubble expansion. There are, however, additional heating mechanisms which may present a greater risk. These are discussed in the Appendix D.iii. As concluded by Mornstein (1997), Nyborg (2001) and a number of other reviews of the subject, there is, as yet, no conclusive evidence that contrast agents produce harmful bio-effects. It is, however, an area requiring further theoretical, experimental and clinical studies, particularly as new CAPs are produced.

5.8.4 Further considerations

Whilst the development of a new contrast agent based on the designs discussed above is clearly at a very early stage, a brief discussion of the demand for improvements in CAP design is perhaps warranted. The previous sections have presupposed the need for more effective contrast agents, based on the fact that existing contrast agents have been developed mainly by trial and error and the fact that their design *could* be improved. This does not necessarily equate to high demand or commercial success, however. Existing ultrasound contrast agents are relatively expensive and increasing the complexity of their design might be regarded as injudicious, even if the technology to produce them is well established. On the other hand, there is undoubtedly a need to improve the imaging of, e.g. the blood vessel networks surrounding cancerous tumours (e.g. Balci *et al* 1999) and CAPs have additional benefits to offer. They are able to deliver treatment to the disease site and, potentially, they may be used destroy the fragile vessels, thus starving the tumour of blood. Moreover, as well as being cheaper and safer, ultrasound is the only method suitable for imaging certain features, such as blood flow velocity. It could also be argued that by improving CAP effectiveness, demand would be increased which would reduce manufacturing costs. Thus, whilst further assessment of demand would certainly be required, it would seem that future development of the design work would be justified.

5.9 Summary

The aim of this chapter has been to demonstrate how ultrasound contrast agents may be designed in order to improve their suitability for particular applications. It has been shown that analytical techniques may be applied to identify the most important factors for modelling and design, and that this knowledge may be used to determine how the material and/or structure of the encapsulating shell could be selected in order to enhance the non-linearity of CAP oscillations at low insonation pressures. The new model developed in Chapters 3 and 4 was used to simulate the behaviour of a range of new designs in order to assess their effectiveness. Experiments were then conducted, using scale models of the most successful designs to test their effectiveness in practice. The results indicated that CAP structure could indeed be modified successfully to increase the degree of non-linear behaviour by the addition of an inner layer with increased resistance to compression. Finally, the feasibility of manufacturing a new contrast agent and the implications for patient safety were examined.

References

Akhatov, I. Vakhitova, N. Galeyeva, G. *et al* (1997) Weak oscillations of a gas bubble in a spherical volume of compressible liquid. Journal of Applied Mathematics and Mechanics 6:921-930.

Allen, J. & Roy, R. (2000) Dynamics of gas bubbles in viscoelastic fluids I. Linear viscoelasticity. Journal of the Acoustical Society of America 107:3167-3178.

Allen, J. & Roy, R. (2000) Dynamics of gas bubbles in viscoelastic fluids. II. Non-linear viscoelasticity. Journal of the Acoustical Society of America 108:1640-1651.

Allen, J. Kruse, D. & Ferrara, K. (2001) Shell Waves and Acoustic Scattering from Ultrasound Contrast Agents. IEEE Transactions on Ultrasonics, Ferroelectrics & Frequency Control 48:409-418.

Apfel, R. & Holland, C. (1991) Gauging the likelihood of cavitation from short-pulse-low-duty cycle diagnostic ultrasound. Ultrasound in medicine & biology 17:179-185.

Avetisyan, I. (1977) Stabilisation of gas bubbles in water. Soviet Physics. Acoustics 23:285-288.

Balci, N. Semelka R. Patt, R. *et al* (1999) Complex renal cysts: findings on MR imaging. American Journal of Roentgenoltoy 172:1495-1500.

Bao, S. Thrall, B. & Miller, D. (1997) Transfection of a reporter plasmid into cultured cells by sonoporation in vitro. Ultrasound in Medicine & Biology 23:953-959.

Becher, H. & Burns, P. (2000) Handbook of Echocardiography. Frankfurt: Springer-Verlag.

Besant, W. (1859) Hydrostatics and Hydrodynamics. Cambridge: Deighton Bell.

Bleeker, H. Shung, K. & Bamhart, J. L. (1990) On the application of ultrasonic contrast agents for blood flowmetry and assessment of cardiac perfusion. Journal of Ultrasound in Medicine 9:461-471.

Blake, J. Tahib, B. & Doherty, G. (1986) Transient cavities near boundaries. Part 1: rigid boundary. Journal of Fluid Mechanics 170:479-497.

Boal, D. (2002) Mechanics of the cell. Cambridge: Cambridge University Press.

Borsboom, J. Chin, C. & de Jong, N. (2003) Non-linear coded excitation method for ultrasound contrast imaging. Ultrasound in Medicine and Biology 29:285-292.

Bouakaz, A. Frigstad, S. Ten Cate, F. *et al* (2002) Super harmonic imaging: a new technique for improved contrast detection Ultrasound in Medicine and Biology 28:59–68.

Brujan, E. (2004) The role of cavitation microjets in the therapeutic applications of ultrasound. Ultrasound in Medicine & Biology 30:381-387.

Caflisch, R. Miksis, M. Papanciolaou, G. *et al* (1985) Effective equations for wave propagation in bubbly liquids. Journal of Fluid Mechanics 153:259-273.

Callister, W. (1994) Materials science and engineering. New York: John Wiley.

Cengel, Y. & Boles, M. (1989) Thermodynamics: An Engineering Approach. International Edition: McGraw-Hill.

Choice MS Inc. (2003) Choice Medical Systems Inc., Available from <http://www.choicemedical.com>.

Collatz, L. (1960) Numerical treatment of differential equations. 3rd ed. Berlin: Springer.

Chahine, G. (1993) Cavitation dynamics at microscale level. Journal of Heart Disease 3:102-116.

Chelly, N. Yamakoshi, Y. Sawada, Y. *et al* (2002) Effects of red blood cells on ultrasonic wave microbubble trapping. Japanese Journal of Applied Physics 41: 3145-4146.

Chen, W. Matula, T. & Crum, L. (2000) Behaviour of ultrasound contrast agents near the fragmentation threshold. Journal of the Acoustical Society of America 108:2547.

Chen, Q. Zagzebski, J. Wilson, T. *et al* (2002) Pressure-dependent attenuation in ultrasound contrast agents, Ultrasound in Medicine & Biology 8:1041-1051.

Chin, C. & Burns, P. (2000) Predicting the acoustic response of a microbubble population for contrast imaging in medical ultrasound. Ultrasound in medicine & Biology 26:1293-1300.

Chomas, J. Dayton, P. Allen, J. *et al* (2001) Mechanisms of contrast agent destruction. IEEE Transactions on Ultrasonics, Ferroelectrics and Frequency Control 48:232 –248.

Church, C. (1988) Prediction of rectified diffusion during nonlinear bubble pulsations at biomedical frequencies. Journal of the Acoustical Society of America 83:2210-2217.

Church, C. (1995) The effects of an elastic solid surface layer on the radial pulsations of gas bubbles. Journal of the Acoustical Society of America 97:1510-1520.

Church, C. & Carstensen, E. (2001) Stable Inertial Cavitation. Ultrasound in Medicine & Biology 27:1435-1437.

Coakley, W. & Nyborg, W. (1978) In: Ultrasound, its Applications in Medicine and Biology. Part 1. Ed. Fry, F. Oxford: Elsevier Scientific.

Commander, K. & Prosperetti, A. (1989) Linear pressure waves in bubbly liquids: Comparison between theory and experiments. Journal of the Acoustical Society of America 85:732-746.

Crum, L. (1975) Bjerknes forces on bubbles in a stationary sound field. Journal of the Acoustical Society of America 57:1363-1370.

Crum, L. (1979) Surface oscillations and jet development in pulsating bubbles. Journal of Physics C8:285-288.

Crum, L. (1984) Rectified diffusion. Ultrasonics 22:215-223

D'Agostino, L. & Brennen, C. (1988) Acoustical absorption and scattering cross-sections of spherical bubble clouds. Journal of the Acoustical Society of America 84: 2126-2134.

Dalecki, D. Raeman, C. Child, S. *et al* (1997) Hemolysis in vivo from exposure to pulsed ultrasound. Ultrasound in Medicine & Biology 23:307-313.

Dayton, P. Morgan, K. Klibanov, A. *et al* (1997) A preliminary evaluation of the effects of primary and secondary radiation forces on acoustic contrast agents. IEEE Transactions on Ultrasonics, Ferroelectrics and Frequency Control 44:1264 –1281.

Dayton, P. Morgan, K. Klibanov, A. *et al* (1999) Optical and acoustical observations of the effects of ultrasound on contrast agents. IEEE Transactions on Ultrasonics, Ferroelectrics and Frequency Control 46:220–236.

Dayton, P. Chomas, J. Lum, A. *et al* (2000) Acoustical and physical dynamics of phagocytosed microbubble contrast agents. Proceedings of the IEEE Ultrasonics Symposium 2: 1877-1880.

Dayton, P. Chomas, J. Lum, A. *et al* (2001) Optical and Acoustical Dynamics of Microbubble Contrast Agents inside Neutrophils. Biophysical Journal 80: 1547-1556.

de Jong, N. Hoff, L. Skotland, T. *et al* (1992) Absorption and scatter of encapsulated gas filled microspheres: theoretical considerations and some measurements. Ultrasonics 30:95-103.

de Jong, N. Cornet, R. & Lancée, C. (1994) Higher harmonics of vibrating gas-filled microspheres. Part one: simulations. Ultrasonics 32:447-453

de Jong, N. Cornet, R. & Lancée, C. (1994) Higher harmonics of vibrating gas-filled microspheres. Part two: measurements. Ultrasonics 32:455-459

Devin, C. (1959) Survey of thermal, radiation and viscous damping of pulsating air bubbles in water. Journal of the Acoustical Society of America 31:1654.

Duck, F. (1990) Physical Properties of tissue: a comprehensive reference book. London: Academic press.

Duck, F. (2002) Nonlinear acoustics in diagnostic ultrasound. Ultrasound in Medicine & Biology 28:1-18.

Dufrene, Y. Boland, T. Schneider, J. *et al* (1998) Characterisation of the physical properties of model biomembranes at the nanometer scale with the atomic force microscope. Faraday Discussions of the Chemical Society 111:79-94.

Epstein, P. & Plesset, M. (1950) On the stability of gas bubbles in liquid-gas solutions. Journal of Chemical Physica 18:1505 – 1509.

Evans, E. (1983) Bending elastic modulus of red blood cell membrane derived from buckling instability in micropipet aspiration tests. Biophysical Journal 43:27-30.

Feigenbaum, H. Stone, J. Lee, D. *et al* (1970) Identification of ultrasound echoes from the left ventricle by use of intracardiac injections of indocyanine green. Circulation 41 615-621.

Feinstein, S. Ten Cate, F. Zwehl, W. *et al* (1984) Two-dimensional contrast echocardiography. I: in vitro development and quantitative analysis of echo contrast agents. Journal of the American College of Cardiology 3: 14-20.

Flynn, H. (1964) Physics of acoustic cavitation in liquids. In: Mason, W. (ed) Physical Acoustics 1B. Academic Press, pp 85.

Foldy, L. (1945) The multiple scattering of waves I. General theory of isotropic scattering by randomly distributed scatterers. Physical Review 67:107-119.

Forsberg, F. Ro, R. Potoczek, M. *et al* (2004) Assessment of angiogenesis: implications for ultrasound imaging. Ultrasonics 42:325-330.

Forsberg, F. Basude, R. Liu, J. *et al* (1999) Effect of filling gases on the backscatter from contrast microbubbles: theory and in vivo measurements - development of a novel contrast agent for diagnostic ultrasound. Ultrasound in Medicine & Biology 25:1203-1211.

Fox, F. & Herzfeld, J. (1954) Gas bubbles with organic skin as cavitation nuclei. Journal of the Acoustical Society of America 26:984-989.

Frinking, P. & de Jong, N. (1997) Modelling of ultrasound contrast agents. Proceedings of the IEEE Ultrasonics Symposium 1:1601–1604.

Frinking, P. & de Jong, N. (1998) Acoustic Modelling of Shell-Encapsulated Gas Bubbles. Ultrasound in Medicine & Biology 24:523-533.

Frinking, P. Cespedes, E. & de Jong, N. (1998) Multi-pulse ultrasound contrast imaging based on a decorrelation detection strategy. Proceedings of the IEEE Ultrasonics Symposium 1:1787-1790.

Frinking, P. de Jong, N. & Cespedes, E. (1999) Scattering properties of encapsulated gas bubbles at high ultrasound pressures. Journal of the Acoustical Society of America 105:1989-1996.

Frinking, P. Bouakaz, A. Kirkhorn, J. *et al* (2000) Ultrasound contrast imaging: current and new potential methods. Ultrasound in Medicine & Biology 26:965-975.

Fung, Y. (1993) Biomechanics: Mechanical Properties of living tissues. New York: Springer-Verlag.

Gall, K. Sehitoglu, H. Chumlyakov, Y. *et al* (1999) Tension compression asymmetry of the stress-strain response in aged single cystal and polycrystalline NiTi. Acta Materialia 47:1203-1217.

Gilmore, F. (1952). The collapse and growth of a spherical bubble in a viscous compressible liquid. California Institute of Technology: Hydrodynamics Laboratory Report No. 26-4.

Glazman, R. (1983) Effects of adsorbed films on gas bubble radial oscillations. Journal of the Acoustical Society of America 74:980-986.

Glazman, R. (1984) Damping of bubble oscillations induced by transport of surfactants between the adsorbed film and the bulk solution. Journal of the Acoustical Society of America 76:890-896.

Gorce, J. Arditi, M. & Schneider, M. (2000) Influence of bubble size distribution on the echogenicity of ultrasound contrast agents: A study of SonoVue. Investigative Radiology 35:661-671.

Gracewski, S. Miao, H. Dalecki, D. *et al* (2004) Simulation of an acoustically excited bubble near a simulated "cell," Journal of the Acoustical Society of America 115: 256.

Gramiak, R. & Shah, P. (1968) Echocardiography of the aortic root. Investigative Radiology 3:356-366.

Gramiak, R. Shah, P. & Kramer, D. (1969) Ultrasound cardiography: contrast studies in anatomy and function. Radiology 92: 939-948.

Green, E. & Rivlin, R. (1957) The mechanics of non-linear materials with memory. Arch Rational Mech. Anal. 1:1-21.

Guyton, A. & Hall, J. (1996) Textbook of medical physiology. 10th Ed. London: Saunders.

Harvey, C. Pilcher, J. Eckersley, R. *et al* (2002) Advances in ultrasound. Clinical Radiology 57:157-177.

Helfer, E. Harlepp, S. Bourdieu, L. *et al* (2001) Viscoelastic properties of actin-coated membranes. Physical Review E 63:021904.

Henyey, F. (1999) Corrections to Foldy's effective medium theory for propagation in bubble clouds and other collections of very small scatterers. Journal of the Acoustical Society of America 105:2149-2154.

Herring, C. (1941) Theory of the pulsations of the gas bubble produced by an underwater explosion. O.S.R.D. Rep. No. 236.

Hilgenfeldt, S. Lohse, D. & Zomack, M. (1998) Response of bubbles to diagnostic ultrasound: a unifying theoretical approach. European Physical Journal B 4:247-255.

Hilgenfeldt, S. Lohse, D. & Zomack, M. (2000) Sound scattering and localised heat deposition of pulse-driven microbubbles. Journal of the Acoustical Society of America107:3530-3539.

Hoff, L. Sontum, P. & Hovem, J. (2000) Oscillations of polymeric microbubbles: Effect of the encapsulating shell. Journal of the Acoustical Society of America 107:2272- 2280.

Hoff, L. Sontum, P. & Hoff, B (1996) Acoustic Properties of Shell-Encapsulated, Gas-Filled Ultrasound Contrast Agents. Proceedings of the IEEE Ultrasonics Symposium 2:1441-1444.

Hope Simpson, D. Chin, C. & Burns, P. (1999) Pulse inversion Doppler: a new method for detecting non-linear echoes from microbubble contrast agents. IEEE Transactions on Ultrasonics, Ferroelectrics & Frequency Control . 46:372-382

Humphrey, V. (2000) Nonlinear propagation in ultrasonic fields: measurements, modelling and harmonic imaging. Ultrasonics 38:267-272.

Israelachvili, J. (2003) Intermolecular and surface forces. 3rd ed. San Diego: Academic Press.

Kamiyama, N. Moriyasu, F. Mine, Y. *et al* (1999) Analysis of flash echo from contrast agent for designing optimal ultrasound diagnostic systems - In vitro and in vivo observations. Ultrasound in Medicine & Biology 25:411-420.

Kaye, G. & Laby, T. (1995) Tables of physical and chemical constants. 16th ed. London: Longman.

Keller, J. & Miksis, M. (1980) Bubble oscillations of large amplitude. Journal of the Acoustical Society of America 68:628-633.

Khanna, S. Nazar, N. Amso, S. *et al* (2003)Contrast agent bubble and erythrocyte behavior in a 1.5-MHz standing ultrasound wave. Ultrasound in Medicine & Biology 29:1463-1470.

Khismatullin D, & Nadim A. Radial oscillations of encapsulated microbubbles in viscoelastic liquids. Phys. Fluids. 2002; 14:3534-3557.

Khismatullin, D. (2001) Acoustic cavitation bio-effects. Available from: www.geocities.com/dkhismatullin/drug.htm [Accessed 10/10/01].

Kim, D. & Needham, D. (2003) Lipid bilayers and monolayers: characterization using micropipet manipulation techniques. In: Hubbard A, ed. Encyclopaedia of surface and colloid science. New York: Marcel Dekker.

Kirkwood, J. & Bethe, H. (1942). The pressure wave produced by an underwater explosion. O.S.R.D., Rep. 588.

Klibanov, A. Ferrara, K. Hughes, M. *et al* (1998) Direct microscopic observation of the dynamic effects of ultrasound on ultrasonic contrast microspheres. Investigative Radiology 33:863-870.

Klibanov, A. Hughes, M. Villanueva, F. *et al* (1999) Targeting and ultrasound imaging of microbubble-based contrast agents. MAGMA 8:177-84.

Klibanov, A. Rychak, J. Takalkar, A. *et al* (2004) Targeting of microbubbles: in vitro flow chamber studies. In: de Jong N (ed) Proc. 9th European symposium on ultrasound contrast imaging. Thursday 22nd January 17:00.

Krasovitski, B. & Kimmel, E. (2001) Gas bubble pulsation in a semi-confined space subjected to ultrasound. Journal of the Acoustical Society of America 109:891-898.

Kremkau, F. Gramiak, R. Carstensen, E. *et al* (1970) Ultrasonic detection of cavitation at catheter tips. American Journal of Roentgenology, Radium Therapy & Nuclear Medicine 110:177-183.

Kudo, N. Miyaoka, T. Kuribayashi, K. *et al* (2000) Study of the mechanism of fragmentation of a microbubble exposed to ultrasound using a high speed observation system. Journal of the Acoustical Society of America 108:2547.

Kvikliene, A. Jurkonis, R. Ressner, M. *et al* (2004) Modelling of nonlinear effects and the response of ultrasound contrast micro bubbles: simulation and experiment. Ultrasonics 42:301–307.

Lamb, H. (1879) A treatise on the mathematical theory of the motion of fluids. Cambridge: The University Press.

Lamb, H. (1924) Hydrodynamics. 4th ed. Cambridge: Cambridge University Press.

Landau, L. & Lifshitz, E. (1959) Fluid Mechanics. London: Pergamon Press Ltd.

Lauterborn, W. (1976) Numerical investigation of non-linear oscillations of gas bubbles in liquids. Journal of the Acoustical Society of America 59:283-293.

Lauterborn, W. & Bolle, H. (1975) Experimental investigation of cavitation-bubble collapse in the neighbourhood of a solid boundary. Journal of Fluid Mechanics 72: 391-399.

Lauterborn, W. & Parlitz, U. (1987) On the bifurcation structure of bubble oscillators. Proceedings of the XII International Symposium on Non-Linear Acoustics: 71-80.

Leighton, T. (1989) Transient excitation of insonated bubbles. Ultrasonics 27:50-53.

Leighton, T. (1994) The Acoustic Bubble. London: Academic Press.

Leighton, T. (1995) Bubble Population phenomena in acoustic cavitation. Ultrasonics Sonochemistry 2:s123-s136.

Lewin, P. (2004) Quo vadis medical ultrasound? Ultrasonics 42:1-7.

Mornstein, V. (1997) Cavitation-induced risks associated with contrast agents used in ultrasonography. European Journal of Ultrasound 5:101-111.

Lloyd, P. & Berry, M. (1967) Wave propagation through an assembly of spheres IV: Relations between different multiple scattering theories. Proceedings of the Physical Society 91:678-688.

Longuet-Higgins, M. (1989) Monopole emission of sound by asymmetric bubble oscillations, part 1: Normal modes. Journal of Fluid Mechanics 201: 525-541.

Longuet-Higgins, M. (1989) Monopole emission of sound by asymmetric bubble oscillations, part 2: An initial value problem. Journal of Fluid Mechanics 201:543-565.

Lord, W. Ludwig, R. & You, Z. (1990) Developments in ultrasonic modelling with finite element analysis. Journal of Non-destructive Evaluation 9:129.

Machado, J. & Valente, J. (2003) Ultrasonic scattering cross sections of shell encapsulated gas bubbles immersed in a viscoelastic liquid: first and second harmonics. Ultrasonics 41:605-613.

Marmottant, P. & Hilgenfeldt, S. (2003) Controlled vesicle deformation and lysis by single oscillating bubbles. Nature 423:153-6.

Marsh, J. Hall, C. & Hughes, M. (1997) Broadband through-transmission signal loss measurements of Albunex® suspensions at concentrations approaching in vivo doses. Journal of the Acoustical Society of America 101:115-1161.

Matan, K. Williams, R. Witten, T. *et al* (2002) Crumpling a Thin Sheet. Physical Review Letters 88.

Massey, B. (1989) Mechanics of fluids. 6th ed. London: Chapman and Hall.

May, D. Dayton, P. Chomas, J. *et al* (2000) Ultrasound contrast agents used for localized drug delivery. Proceedings of the IEEE Ultrasonics Symposium 2:1429 - 1432.

Medwin, H. (1977) Counting bubbles acoustically: a review. Ultrasonics 15:7-13.

Moran, C. Anderson, T. Sboros, V. *et al* (1998) Quantification of the enhanced backscatter phenomenon from an intravenous and an intra-arterial contrast agent - stabilization and simulations of cyclic changes of size and content. Ultrasound in Medicine & Biology 24:871-880.

Moran, C. Anderson, T. Pye, S. *et al* (2000) Quantification of microbubble destruction of three fluorocarbon-filled ultrasonic contrast agents. Ultrasound in Medicine and Biology 26:629-639.

Morgan, K. Allen, J. Chomas, J. *et al* (1999) Experimental and theoretical analysis of individual contrast agent behaviour. Proceedings of the IEEE Ultrasonics Symposium 2:1685 –1688.

Naude, C. & Ellis, A. (1961) On the mechanism of cavitation damage by non-hemispherical cavities in contact with a solid boundary. ASME. Journal of Basic Engineering 83:648-656.

Neppiras, E. (1980) Acoustic cavitation. Physics Reports; 61; 159-251.

Noltingk, B. & Neppiras, E. (1950). Cavitation produced by ultrasonics. Proceedings of the Physical Society B63:674-685.

Neppiras, E. & Noltingk, B. (1951) Cavitation produced by ultrasonics: theoretical conditions for the onset of cavitation. Proceedings of the Physical Society B 64B:1032-1038.

Nyborg, W. (2001) Biological Effects of Ultrasound: Development of Safety Guidelines. Part II: General Review. Ultrasound in Medicine & Biology 27:301-333.

Omta, R. (1987) Oscillations of a cloud of bubbles of small and not so small amplitude. Journal of the Acoustical Society of America 82:1018-1033.

Plesset, M. (1949) The dynamics of cavitation bubbles. Transactions of the Americal Society of Mechanical Engineers: Journal of Applied Mechanics 16:228.

Plesset, M. & Chapman, R. (1971) Collapse of an initially spherical vapour cavity in the neighbourhood of a solid boundary. Journal of Fluid Mechanics 47:283-290.

Podell, S. Burrascano, C. & Mehlhaff, P. (1999) Physical and biochemical stability of Optison®, an injectable ultrasound contrast agent. Biotechnology and Applied Biochemistry 30:213-223.

Poliachik, S. Chandler, W. Mourad, P. *et al* (1999) Effect of high-intensity focused ultrasound on whole blood with and without microbubble contrast agent. Ultrasound in Medicine & Biology 25:991-998.

Poritsky, H. (1952) Proceedings of the first US National Congress in Applied Mechanics (ASME) 813.

Postema, M. Bouakaz, A. Chin, C. *et al* (2003) Simulations and measurements of optical images of insonified ultrasound contrast microbubbles. IEEE Transactions on Ultrasonics, Ferroelectrics & Frequency Control 50:523-535.

Postema, M. van Wamel, A. Lancee, C. *et al* (2004) Ultrasound induced encapsulated microbubble phenomena. Ultrasound in Medicine & Biology. 30:827-840.

Prosperetti, A. Crum, L. & Commander, K. (1988) Nonlinear bubble dynamics. Journal of the Acoustical Society of America 83:502-514.

Provenzano, P. Lakes, R. Corr, D. *et al* (2002) Application of non-linear viscoelastic models to describe ligament behaviour. Biomechanical Modelling and Mechanobiology 1:45-57.

Rayleigh, Lord (1879) On the capillary phenomena of jets. Proceedings of the Royal Society 29:71-97.

Rayleigh, Lord (1917) On the pressure developed in a liquid during the collapse of a spherical cavity. Philosophical Magazine 34:94-98.

Reissmann, H. & Pawlik, P. (1980) Elasticity Theory and Applications. New York: John Wiley.

Sassaroli, E. & Hynynen, K. (2004) Forced linear oscillations of microbubbles in blood capillaries. Journal of the Acoustical Society of America 114:2320.

Sato, K. Tomita, Y. & Shima, A. (1994) Numerical analysis of a gas bubble near a rigid boundary in and oscillatory pressure field. Journal of the Acoustical Society of America 95:2416-2424.

Sboros, V. Moran, C. Anderson, T. *et al* (2000) An *in vitro* comparison of ultrasonic contrast agents in solution with varying air levels. Ultrasound in Medicine and Biology 26:807:818.

Sboros, V. MacDonald, C. Pye, S. *et al* (2002) The dependence of ultrasound contrast agents backscatter on acoustic pressure: theory versus experiment. Ultrasonics 40:579-583.

Schrope, B. Newhouse, V.L. & Uhlendorf, V. (1992) Simulated capillary blood flow measurement using a nonlinear ultrasonic contrast agent. Ultrasonic Imaging 14:134-58.

Shi, W. & Forsberg, F. (2000) Ultrasonic characterization of the non-linear properties of contrast microbubbles - Stablization and simulations of cyclic changes of size and content. Ultrasound in Medicine & Biology 26:93-104.

Shi, W. Forsberg, F. Tornes, A. *et al* (2000) Destruction of contrast microbubbles and the association with inertial cavitation. Ultrasound in medicine & Biology 26: 1009-1019.

Snabre, P. & Mills, P. (1999) Rheology of concentrated suspensions of viscoelastic particles. Colloids & Surfaces A 152:79-88.

Soetanto, K. & Chan, M. (2000) Study on the lifetime and attenuation properties of microbubbles coated with carboxylic acid salts. Ultrasonics 38:969 – 977.

Sonin, A. Bonfillon, A. & Langevin, D. (1993) Role of surface elasticity in the drainage of soap films. Physical Review Letters 71:2342–2345.

Stokes, G. (1868) On the communication of vibration from a vibrating body to surrounding gas In: Mathematical and physical papers volume 4. London: Cambridge University Press.

Stride, E. & Saffari, N. (2003) On the destruction of microbubble ultrasound contrast agents. Ultrasound in Medicine & Biology 29:563-573.

Stride, E. & Saffari, N. (2004a) The potential for thermal damage posed by microbubble ultrasound contrast agents. Ultrasonics 42:907-913.

Stride, E. & Saffari, N. (2004b) The behaviour of microbubble ultrasound contrast agent particles in whole blood. Ultrasound in Medicine &Biology 30 144-158.

Stride, E. & Saffari, N. (2005) Investigating the significance of multiple scattering in ultrasound contrast agent particle populations. IEEE Transactions in Ultrasonics, Ferroelectrics & Frequency Control (in press).

Stride, E. (2005) Characterisation and Design of Microbubble-based Contrast Agents Suitable for Diagnostic Imaging. In: Contrast Media in Ultrasonography: Basic Principles and Clinical Applications. Ed. E. Quaia. Berlin: Springer-Verlag.

Stroud, K. (1997) Further Engineering Mathematics. Basingstoke, Macmillan Press Ltd.

Takeuchi, Y. (1997) Industrial use thermoplastic microballoon to mimic the contrast agents and its in-vitro behavior including released gas dynamics. Proceedings of the IEEE Ultrasonics Symposium 2:1579-1582.

Trilling, L. (1952) The collapse and rebound of a gas bubble. Journal of Applied Physics 23:14--17.

Uhlendorf, V. Scholle, F. & Reinhardt, M. (2000) Acoustic behaviour of current ultasound contrast agents. Ultrasonics 38:81-86.

Van Wijngaarden, L. (1968) On equations of motion for mixtures of liquids and gas bubbles. Journal of Fluid Mechanics 33:465-474.

Vogel, A. Lauterborn, W. & Timm, R. (1989) Optical and acoustic investigations of the dynamics of laser produced cavitation bubbles near a solid boundary. Journal of Fluid Mechanics 206:299-338.

Waterman, P. & Truell, R. (1961) Multiple scattering of waves. Journal of Mathematical Physics 2:512-537.

WFUMB Symposium on the safety of ultrasound in medicine (1998) Recommendations on the safe use of ultrasound. Ultrasound in Medicine & Biology 24 S1:xv-xvi.

Wu, J. (2002) Theoretical study on shear stress generated by microstreaming surrounding contrast agents attached to living cells. Ultrasound in Medicine & Biology 28:125-129.

Wyzalkowski, M. & Szeri, A. (2003) Optimization of acoustic scattering from dual frequency driven microbubbles at the difference frequency. Journal of the Acoustical Society of America 113:3073-3079.

Xu,W. & Kauffman, J. (1993) Diffraction correction methods for immersion ultrasound attenuation estimation. IEEE Transactions on biomedical engineering 40:563-570.

Ye, Z. (1996) On sound scattering and attenuation of Albunex bubbles Journal of the Acoustical Society of America 100:2011-2028.

Ye, Z. Hsu, H. & Hoskinson, E. (2000) Phase order and energy localization in acoustic propagation in random bubbly liquids. Physics Letters A 275:452-458.

Young, F. (1989) Cavitation. London: Imperial College Press.

Zabolotskaya & Khokhlov (1969) Soviet Physics. Acoustics 15:35.

Zhong, P. Zhou, Y. & Zhu, S. (2001) Dynamics of bubble oscillation in constrained media and mechanisms of vessel rupture in SWL. Ultrasound in Medicine & Biology 27:119-134.

A.i Propagation of the radiated field from non-spherical bubble oscillations

Lamb (1924) showed that the oscillations of a bubble of radius R_o containing gas of density ρ_G suspended in a liquid of density ρ_L may be described by

$$R(t) = R_o + A_n Y_n^o \cos(\omega_n t + \vartheta) \qquad \text{(Ai.1)}$$

Where is Y_n^o is the zonal spherical harmonic of order n, ω_n is the corresponding frequency and A_n the amplitude. ϑ is a phase angle.

The corresponding velocity potentials inside and outside the bubble are given by

$$\Phi_{in} = \frac{-\omega_n R_o}{n}\left(\frac{r}{R_o}\right)^n A_n Y_n^o \sin(\omega_n t + \vartheta) \qquad r \le Ro \qquad \text{(Ai.1)}$$

$$\Phi_{out} = \frac{\omega_n R_o}{n+1}\left(\frac{R_o}{r}\right)^{n+1} A_n Y_n^o \sin(\omega_n t + \vartheta) \qquad r \ge Ro \qquad \text{(Ai.2)}$$

From Kelvin's theorem in a conservative field for an incompressible, irrotational and inviscid fluid

$$p = -\rho\dot{\Phi} \qquad \text{(Ai.3)}$$

Thus the pressure radiated by the bubble may be found as

$$p_s = \frac{-\rho_L \omega_n^2 R_o}{n+1}\left(\frac{R_o}{r}\right)^{n+1} A_n Y_n^o \cos(\omega_n t + \vartheta) \qquad \text{(Ai.4)}$$

Hence it may be seen that the contribution to the overall radiated pressure from non-spherical oscillations ($n > 1$) would be expected to decay very rapidly with distance from the bubble. In addition, this analysis neglects the viscosity of the surrounding fluid so that even more rapid decay would be expected in practice as a result of absorption. Moreover, in the case of a CAP, the presence of the encapsulating shell would provide additional resistance to the initiation of non-spherical oscillations.

A.ii Modelling the pressure radiated by an oscillating CAP

Equation 2.15 for the pressure radiated by a bubble or CAP neglects the work done on the gas inside the bubble/CAP during compression and is therefore valid only for infinitesimally small amplitudes of oscillation. An improved estimate may be obtained by applying the analysis of Vokurka (Leighton 1994)

Assuming spherical symmetry, conservation of momentum yields

$$\rho\left(\frac{\partial u}{\partial t}+u\frac{\partial u}{\partial r}\right)+\frac{\partial p}{\partial r}=\frac{\partial T_{rr}}{\partial r}+\frac{2T_{rr}-T_{\theta\theta}-T_{\phi\phi}}{r}. \qquad (3.1)$$

Similarly, from conservation of mass

$$\frac{\partial \rho}{\partial t}+\rho\frac{\partial u}{\partial t}+u\frac{\partial \rho}{\partial r}+\frac{2\rho u}{r}=0. \qquad (3.2)$$

Integrating equation 3.1 in the surrounding liquid from R_2 to r gives

$$+\int_{R_2}^{r}\left[\rho_L\left(\frac{\partial u}{\partial t}+u\frac{\partial u}{\partial r}\right)+\frac{\partial p}{\partial r}=\frac{\partial T_{L,rr}}{\partial r}+\frac{2T_{L,rr}-T_{L,\theta\theta}-T_{L,\phi\phi}}{r}\right]dr=0 \qquad \text{(Aii.1)}$$

From the assumption of constant density in the surrounding fluid

$$u(r,t)r^2=const.=R_2^2(t)\dot{R}_2(t). \qquad (3.4)$$

From the assumption of spherical symmetry in a Newtonian fluid

$$T_{L,rr}=-(T_{L,\phi\phi}+T_{L,\theta\theta})=T_{L,rr}=2\mu_l\frac{\partial u}{\partial r} \qquad \text{(Aii.2)}$$

and

$$3\int_{R_2}^{\infty}\frac{T_{L,rr}}{r}dr=-4\mu_l\frac{R_1^2\dot{R}_1}{R_2^3}=T_{rr}(R_2,t) \qquad \text{(Aii.3)}$$

Thus substituting from equations 3.4, Aii.2 and Aii.3 into equation Aii.1 gives the pressure in the liquid at a distance r from the centre of the bubble/CAP

$$p_L(r)=\rho_L\left(\frac{R_2}{r}\left(R_2\ddot{R}_2+2\dot{R}_2^2\right)-\frac{\dot{R}_2^2R_2^4}{2r^4}\right)-\rho_L\left(R_2\ddot{R}_2+2\dot{R}_2^2\right)+p_L(R_2) \qquad \text{(Aii.4)}$$

Letting r tend to infinity gives

$$p_L(R_2) = \rho_L\left(R_2\ddot{R}_2 + 2\dot{R}_2^2\right) \tag{Aii.5}$$

Thus

$$p_L(r) = \rho_L\left(\frac{R_2}{r}\left(R_2\ddot{R}_2 + 2\dot{R}_2^2\right) - \frac{\dot{R}_2^2 R_2^4}{2r^4}\right) \tag{Aii.6}$$

and the pressure radiated by the CAP is then found by subtracting the incident field

$$p_s(r) = \rho_L\left(\frac{R_2}{r}\left(R_2\ddot{R}_2 + 2\dot{R}_2^2\right) - \frac{\dot{R}_2^2 R_2^4}{2r^4}\right) - p_\infty \tag{Aii.7}$$

It should be noted that this equation does not take into the effects of absorption or non-linear propagation in the surrounding fluid.

A.iii Calculation of the secondary radiation forces acting on a single CAP

According to the analysis by Coakley and Nyborg (1978), a particle of volume V_p and density ρ_p at a distance r from the centre of a pulsating bubble will experience a radiation force F given by[1]

$$F = \frac{3V_p(\rho_p - \rho_o)}{2\rho_p + \rho_o} \frac{\partial \langle \phi_K \rangle}{\partial r} \qquad \text{(Aiii.1)}$$

where $\frac{\partial \langle \phi_K \rangle}{\partial r} = \frac{-\rho_o \omega^2 |R|^2 R_o^4}{r^5}$ is the radial gradient of the time averaged kinetic energy density ϕ_K. ω and $|R|$ are the frequency and amplitude of bubble oscillation respectively, R_o is its initial radius and ρ_o the density of the surrounding fluid.

If the particle is approximated as a sphere of radius a, then the speed with which it will approach the bubble will be given by Stokes' law as

$$u_p = \frac{6a^2(\rho_p - \rho_o)}{9\mu_p(2\rho_p + \rho_o)} \frac{\partial \langle \phi_K \rangle}{\partial r}. \qquad \text{(Aiii.2)}$$

Thus the time taken for another bubble, initially at a distance $r > R_o$, to reach the wall of the first bubble, is given by

$$\int_r^{R_o} \frac{dr}{u} = \int_r^{R_o} \frac{-9\mu_p(2\rho_p + \rho_o) r^5}{6a^2(\rho_p - \rho_o)\rho_o \omega^2 |R|^2 R_o^4} dr = \frac{\mu_p(2\rho_p + \rho_o)(r^6 - R_o^6)}{4a^2(\rho_p - \rho_o)\rho_o \omega^2 |R|^2 R_o^4} \qquad \text{(Aiii.3)}$$

Since this equation requires only the initial radii of the two bubbles and the amplitude of oscillation to be known, there is no theoretical reason why it should not be applied to CAPs as well as to bubbles. Thus, first order estimates may be obtained for the time taken by one CAP to arrive at the wall of another. These are shown in table Aiii.1 for various starting locations of the two CAPs and various amplitudes of oscillation. For all these calculations the surrounding fluid was assumed to have the same properties as plasma.

[1] Please note that it has been necessary to reuse symbols in this appendix which have different meanings elsewhere in the thesis. Please refer to the definitions given in the text of the appendix rather than the list of symbols given on pages 11-14.

Amplitude of CAP oscillation	$\|R\|$	$(\%R_0)$	10	1	10	1
Initial distance from CAP centre	$r_{t=0}$	$(\times R_0)$	2	2	1.2	1.2
Initial speed of approach	$u(r_{t=0})$	(m/s)	0.07	0.0007	0.9	0.009
Time to reach CAP wall	T	(μs)	17.2	1720	0.54	54

Table Aiii.1: Initial speeds and approach times for a single CAP moving towards the wall of another under the influence of secondary radiation forces.

Hence it may be concluded that the time required for one CAP to reach the wall of its neighbour will generally be greater than the length of a typical imaging pulse (≈ 1 μs) unless: either the insonation pressure and hence the amplitude of CAP oscillation is high; or the CAPs are initially very close to one another.

At high pressures, corresponding to amplitudes of oscillation greater than 10% of the initial radius, CAP destruction would be expected which would invalidate the above analysis. At lower pressures, cluster formation might occur over a series of pulses, with each pulse bringing the CAPs closer together. For this to be the case however, it would be necessary for the motion of the CAPs between pulses to be small compared with their motion during insonation, i.e. the fluid would have to be relatively undisturbed and/or the pulse repetition frequency (PRF) quite high. Typically the PRFs used in medical imaging are between 5 and 30 kHz (Choice MS Inc. 2003). This corresponds to duty factors of between 1:20 and 1:100, which would allow adequate time for drift to occur between pulses. A detailed examination of the motion of CAPs *in vivo* has not been carried out however.

A.iv Examining the pressure dependence of attenuation in contrast agent suspensions.

It has been observed by a number of authors (e.g. Sboros *et al* 2002; Chen *et al* 2002) that the attenuation of ultrasound in contrast agent suspensions is sensitive to variations in the incident pressure. This has been found to be the case even under conditions for which CAP behaviour would be expected to be approximately linear. The reason for this is that, whilst the spectrum of the signal from the CAPs may indicate linear behaviour below a certain pressure threshold, the response of a CAP will become increasingly non-linear, with increasing amplitude of oscillation. This is due to the presence of non-linear terms in equation 3.14 such as R_1^2. As a result, the resonance frequency of the CAP falls continuously with increasing insonation pressure. Thus, if the insonation frequency is kept constant, the CAP is excited further and further from resonance as the pressure increase and hence the attenuation of the incident wave is reduced. The effects may be seen in figure Aiv.1 which shows the variation in attenuation coefficient with pressure at 3 MHz for Albunex® CAPs calculated from the numerical solution of 3.37 using equation 2.26.

$$s_{ext} = \frac{\langle P_{dis} \rangle_t}{I_i} \qquad (2.26)$$

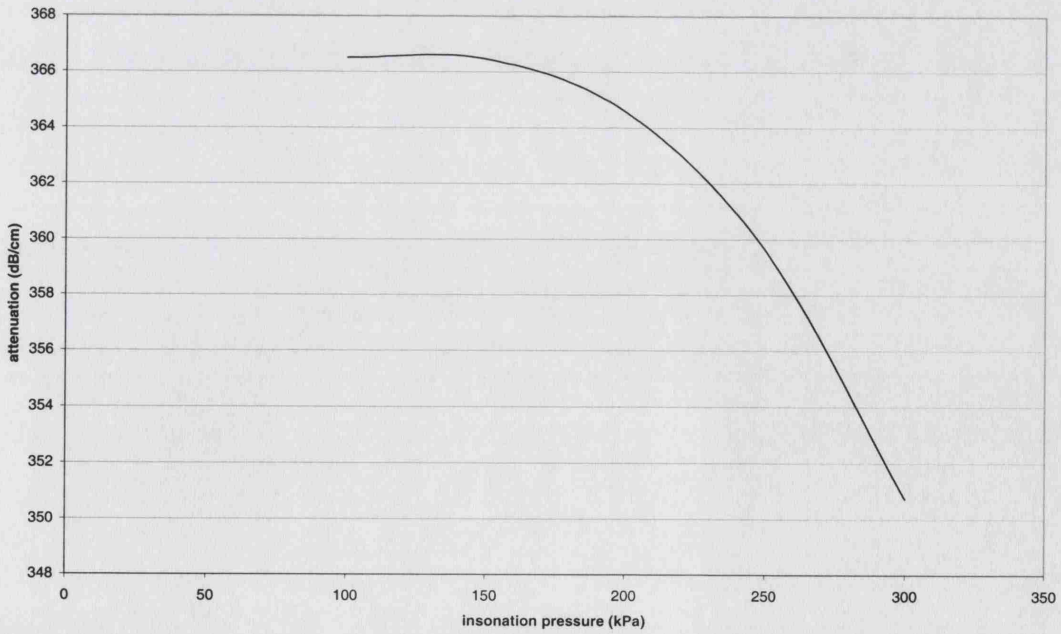

Figure Aiv.1: Variation in attenuation coefficient for Albunex® CAPs with insonation pressure at 3 MHz and 10^6 CAPs/ml (no multiple scattering effects were included).

B.i Investigating the influence of thermal damping upon CAP behaviour

Bi.1 Theory

The assumption of isothermal behaviour made in Chapter 3 implies that there will be no net thermal losses over the course of a complete CAP oscillation, and hence that the thermal damping factor may be neglected in equation 3.15. As described in Chapter 3, previous investigators have relaxed this condition and included approximate thermal damping correction factors whilst retaining the assumption of polytropic behaviour (e.g. de Jong *et al* 1992). For example

$$\frac{-4\mu_{th}\dot{R}_1}{R_1} \tag{Bi.1}$$

where μ_{th} is an "effective thermal viscosity."

Clearly, for conditions under which thermal damping is significant this treatment is unsatisfactory and a more rigorous model of the behaviour of the gas, such as that developed by Prosperetti (1988) for free bubbles, is appropriate. This is also required in order to determine the range of conditions for which it is valid to neglect thermal damping.

To determine accurately whether or not thermal damping is significant for CAPs, it is necessary to solve the equations for conservation of mass (3.24) and energy (3.25) inside the CAP, simultaneously with equation 3.15.

$$\frac{d\rho}{dt}+\rho\nabla\cdot u=0 \tag{3.24}$$

$$\nabla\cdot(K\nabla T)=\frac{\gamma}{(\gamma-1)}\frac{p}{T}\left(\frac{\partial T}{\partial t}+u\frac{\partial T}{\partial r}\right)-\frac{dp}{dt} \tag{3.25}$$

where ρ is density, r is the radial distance from the CAP centre, u is radial velocity, t is time, K is thermal conductivity , T is absolute temperature, γ is the ratio of specific heats and p is pressure[1].

[1] Please note that once again it has been necessary to repeat symbols with different meanings in this appendix and that the definitions given in the text should be referred to rather than the list of symbols.

As explained in Chapter 3 the surrounding fluid is assumed to be infinite, static and incompressible. The CAP is assumed to remain spherical and the filling gas to behave polytropically.

As shown previously, the contribution of the gas to bubble inertia is negligible and the internal pressure p may be treated as spatially uniform. Equations 3.24 and 3.25 may be combined and integrated with respect to r to give an equation for the pressure inside the CAP

$$\frac{dp}{dt} = \frac{3}{R}\left(-\gamma p\dot{R} + (\gamma - 1) K \left.\frac{\partial T}{\partial r}\right|_R \right) \qquad \text{(Bi.2)}$$

Similarly, since there must be continuity of temperature and heat flux at the inner shell surface, it may be deduced that

$$\frac{T_S - T_\infty}{T_c - T_S} = \frac{K_G C_{pG} \rho_G}{K_S C_{pS} \rho_S} \qquad \text{(Bi.3)}$$

where the heat flux from the gas to the interface is given by

$$K_g \left(\frac{T_c - T_{s1}}{\sqrt{\chi_g t_o}} \right) \qquad \text{(Bi.4)}$$

and the heat flux into the shell by

$$K_s \left(\frac{T_{g1} - T_s}{\sqrt{\chi_s t_o}} \right) \qquad \text{(Bi.5)}$$

Evaluating the right hand side of equation Bi.3 with properties for air and albumin (table Bi.1) yields a value of approximately 0.003. Thus, the variation in shell temperature due to heat conduction may be regarded as negligible compared with that of the gas. By the same token the temperature of the surrounding liquid may also be regarded as constant[2].

[2] This is without taking into account other heating effects

Again following Prosperetti *et al* (1988), new variables may be introduced

$$\tau = \int_{T_s}^{T} K(\theta) d\theta, \qquad y = \frac{r}{R(t)} \qquad \text{and} \qquad D = \frac{(\gamma - 1) KT}{\gamma p}$$

The equations for pressure and conservation of energy become respectively

$$\frac{dp}{dt} = \frac{3}{R}\left(-\gamma p \dot{R} + (\gamma - 1) \frac{D_o}{R} \frac{\partial \tau}{\partial y}\bigg|_{y=1} \right) \tag{Bi.6}$$

and

$$\frac{\partial \tau}{\partial t} = D\left(\frac{(\nabla^2 \tau)}{R_1^2} + \frac{dp}{dt} \right) + \left(\frac{\gamma - 1}{\gamma p R_1^2} \right) \left(\frac{\partial \tau}{\partial y} \right) \left[y \left(\frac{\partial \tau}{\partial y} \right)\bigg|_{y=1} - \left(\frac{\partial \tau}{\partial y} \right) \right] \tag{Bi.7}$$

The latter partial differential equation may be discretised over N+1 equispaced points to give N ordinary differential equations $\{\dot{\tau}_i\}$

$$\dot{\tau}_i = \frac{\partial \tau_i}{\partial t} = D_i \left(\frac{\chi}{R_1^2} (\nabla^2 \tau)_i + \frac{dp}{dt} \right) + \left(\frac{\gamma - 1}{\gamma} \right) \frac{\chi}{p R_1^2} \left[y_i \left(\frac{\partial \tau}{\partial y} \right)_N - \left(\frac{\partial \tau}{\partial y} \right)_i \right] \left(\frac{\partial \tau}{\partial y} \right)_i \tag{Bi.8}$$

evaluated at each point y_i where the spatial operators are approximated by

$$\left.\begin{aligned} (\nabla^2 \tau)_i &\cong \frac{1}{\Delta y^2} \left[\left(1 + \frac{\Delta y}{\partial y_i} \right) \tau_{i+1} - 2\tau_i + \left(1 - \frac{\Delta y}{\partial y_i} \right) \tau_{i-1} \right] \\ \left(\frac{\partial \tau}{\partial y} \right)_i &= \frac{\tau_{i+1} - \tau_{i-1}}{2\Delta y} \end{aligned}\right\} 0 < i < N \tag{Bi.9}$$

$$(\nabla^2 \tau)_0 = \frac{6(\tau_1 - \tau_0)}{\Delta y^2}, \quad \left(\frac{\partial \tau}{\partial y} \right)_0 = 0, \quad \left(\frac{\partial \tau}{\partial y} \right)_N = \frac{\tau_{N-2} - \tau_{N-1}}{2\Delta y},$$

$\Delta y = 1/N$ and $y_0 = 0$ $y_N = 1$

The relationship between temperature and conductivity is assumed to be linear

$$K = AT + B \tag{Bi.10}$$

where A and B are experimentally defined constants.

Bi.2 Solution

All equations were non-dimensionalised according to the following scheme

[Mass]	=	$[p_o R_o/\omega^2]$	[Length]	=	$[R_o]$
[time]	=	$[1/\omega]$	[Temperature] =		$[T_\infty]$

Since the focus of this investigation was the thermal behaviour of a CAP, the surrounding fluid and CAP shell were again modelled respectively as a Newtonian fluid and linear viscoelastic solid. Similarly, sinusoidal excitation was assumed. Thus

$$R_1\ddot{R}_1\left(1+\left(\frac{\rho_L-\rho_S}{\rho_S}\right)\frac{R_1}{R_2}\right)+\dot{R}_1^2\left(\frac{3}{2}+\left(\frac{\rho_L-\rho_S}{\rho_S}\right)\left(\frac{4R_2^3-R_1^3}{2R_2^3}\right)\frac{R_1}{R_2}\right)$$
$$=\frac{1}{\rho_S}\begin{pmatrix} p_G-p_o-p_A Sin(\omega t)-\dfrac{2\sigma_1}{R_1}-\dfrac{2\sigma_2}{R_2} \\ -\dfrac{4\mu_L R_1^2\dot{R}_1}{R_2^3}-\dfrac{4V_s G_s}{R_2^3}\left(1-\dfrac{R_{e1}}{R_1}\right)-\dfrac{4\mu_s V_s\dot{R}_1}{R_1R_2^3}\end{pmatrix} \qquad \text{(Bi.11)}$$

where p_G is determined from equation Bi.8 to which equation Bi.11 is coupled.

Equations Bi.8 and Bi.11 were solved simultaneously using purpose written code implementing a 4th Order Runge-Kutta procedure for a variety of insonation frequencies and pressures. The code is given in section Bi.4. The calculation error was monitored by repeating each test with a time step of half the length and ensuring that the differences were negligible. For comparison, results were also obtained using equation Bi.11 with p_G given by the polytropic approximation with and without the approximate correction factor given by equation Bi.1. The "effective thermal viscosity" was evaluated in terms of the undamped linear natural frequency ω_o (equation 2.17) as

$$\mu_{th}=\frac{p_o}{4\omega_o}\mathrm{Im}\,\Phi(\omega_o) \qquad \text{(Bi.12)}$$

where

$$\Phi=\frac{3\gamma}{1-ix(1-\gamma)\left(\sqrt{\frac{i}{x}}\coth\left(\sqrt{\frac{i}{x}}\right)-1\right)} \quad \text{and} \quad x=\frac{(\gamma-1)K_\infty T_\infty}{\gamma p_o\omega_o R_{o1}^2}$$

The polytropic constant κ was determined as Re(Φ)/3 but in terms of the driving frequency ω rather than the natural frequency.

Consistent with the other results presented in the thesis, properties for the contrast agent Albunex® and water were used in the simulations (table Bi.1).

	Parameter	Symbol	Value	Unit
Gas (air)	Polytropic constant	κ	Re(Φ)/3	
	Ambient pressure	P_o	0.1	MPa
	Surface tension	σ_1	0.04	Nm^{-1}
	Thermal conductivity	K_g	2.41	$Jm^{-1}s^{-1}K^{-1}$
	Specific heat capacity	C_{Pg}	1.01	$Jkg^{-1}K^{-1}$
Shell (Albunex®)	Shear modulus	G_s	88.8	MPa
	Density	ρ_s	1100	Kgm^{-3}
	Viscosity	μ_s	1.77	Pas
	Inner radius	R_1	3.635	μm
	Thickness	d_e	15	nm
	Thermal conductivity	K_s	0.2	$Jm^{-1}s^{-1}K^{-1}$
	Specific heat capacity	C_{Ps}	2100	$Jkg^{-1}K^{-1}$
Liquid (water)	Density	ρ_1	1000	Kgm^{-3}
	Viscosity	μ_1	0.001	Pas
	Surface tension	σ_2	0.005	Nm^{-1}
	Thermal conductivity	K_L	0.561	$Jm^{-1}s^{-1}K^{-1}$
	Specific heat capacity	C_{PL}	4190	$Jkg^{-1}K^{-1}$
	Thermal diffusivity	χ_L	1.4×10^{-7}	$s^{-1}m^2$
	Constant relating *K* & *T*	A	5.28×10^{-5}	$Jm^{-1}s^{-1}K^{-2}$
	Constant relating *K* & *T*	B	1165×10^{-5}	$Jm^{-1}s^{-1}K^{-1}$

Table Bi.1. Parameter values for an aqueous suspension of Albunex®. (Constants for air and water from Kaye & Laby (1995), properties for Albunex® from Church (1995) and Kaye and Laby (1995)).

The results are shown in figures Bi.1 and Bi.2.

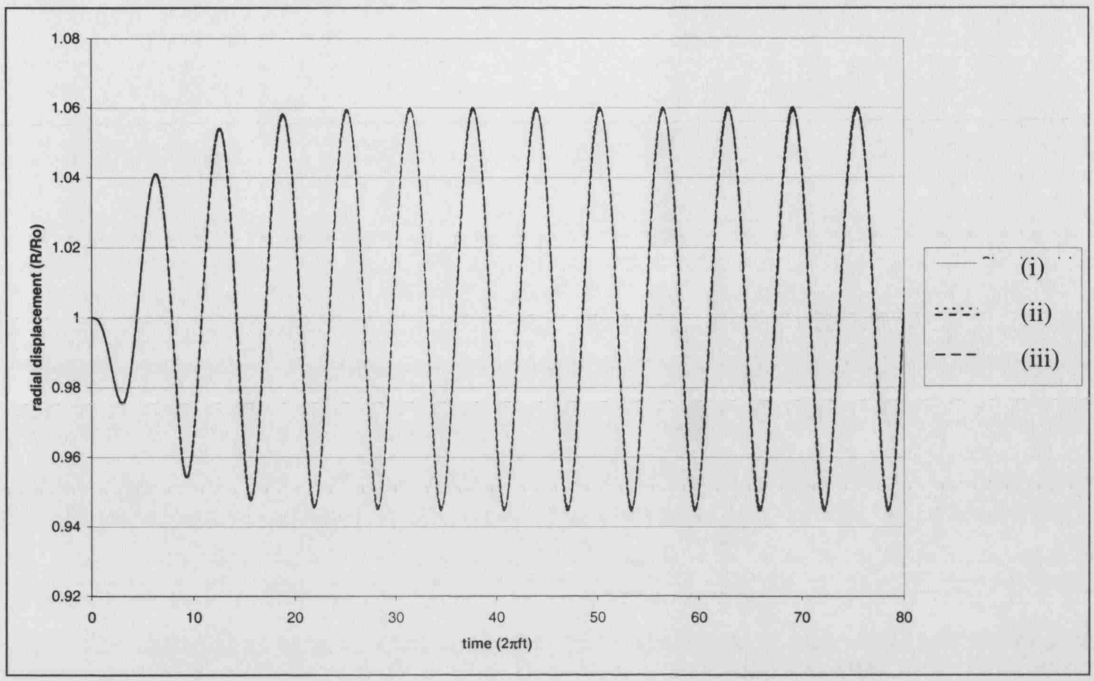

Figure Bi.1: Demonstrating the influence of thermal damping upon the amplitude of oscillation of a resonant Albunex®CAP insonified at 3 MHz and 0.1 MPa (i) with no correction for thermal damping (ii) including an approximate thermal damping factor (iii) full solution of equations Bi.8 and Bi.11.

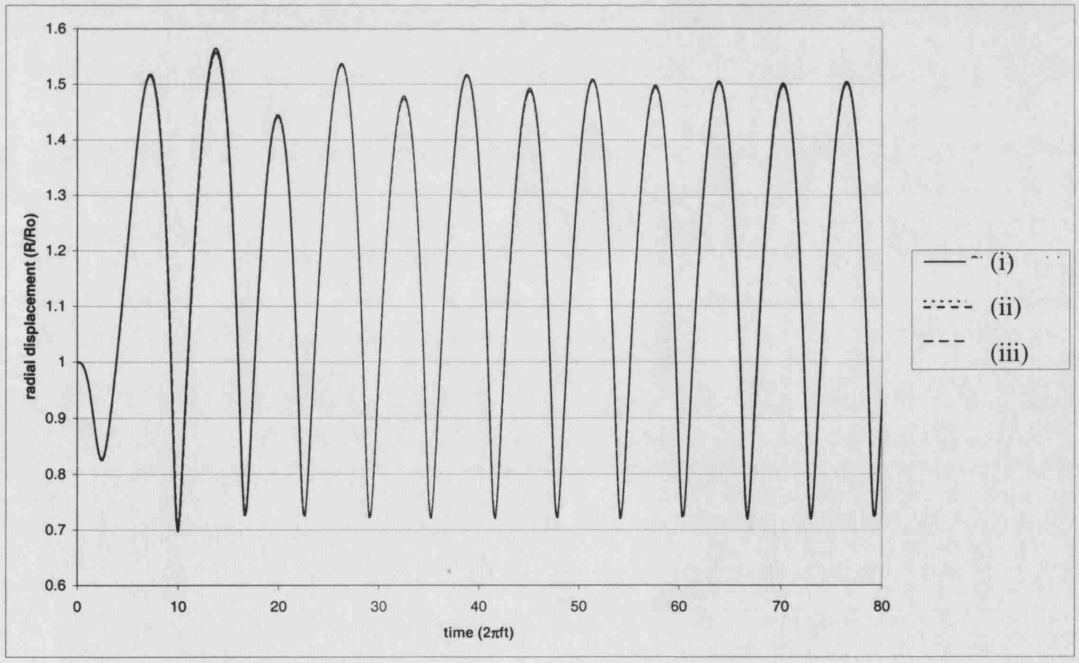

Figure Bi.2: Demonstrating the influence of thermal damping upon the amplitude of oscillation of a resonant Albunex®CAP insonified at 3 MHz and 1 MPa (i) with no correction for thermal damping (ii) including an approximate thermal damping factor (iii) full solution of equations Bi.8 and Bi.11.

Bi.3 Discussion

Figures Bi.1 and Bi.2 indicate that the effect of thermal damping upon CAP dynamics would be expected to be negligible under typical medical diagnostic conditions. Similar results were obtained over the whole range of pressures and frequencies tested. There would therefore appear to be no advantage to be gained by solving the full set of equations (Bi.8 and Bi.11) compared with using an approximate correction factor or neglecting thermal damping altogether. This finding is in agreement with the qualitative arguments put forward in Chapter 3. Its validity will be restricted to cases in which the viscosity of the shell is considerably greater than that of the surrounding liquid, however, and neglect of thermal damping should not be automatic, but based on a consideration of the shell characteristics of an individual CAP.

Bi.4 Program code

Listings for the following programs are included:

rk_thermal.c	C code implementing equations Bi.11 and Bi.8 for a single CAP
rknoth.c	C code implementing equations Bi.11 and Bi.1 for a single CAP

rk_thermal.c

```
/*4th order Runge Kutta numerical solution of model for a shelled CAP with thermal
damping*/

#include<stdio.h>
#include<stdlib.h>
#include<math.h>

/*defined constants*/

#define drhol   1000.0          /*surrounding fluid density (kg/m^3)*/
#define dmul    1.0e-3          /*surrounding fluid viscosity (Pas)*/
#define dcl             1481.0          /*surrounding fluid sound velocity (m/s)*/

#define drhos   1100.0          /*encapsulating shell density (kg/m^3)*/
#define dGs             88.8e6      /*encapsulating shell shear modulus (Pa)*/
#define dmus    1.77            /*encapsulating shell viscosity (Pas)*/
#define ddoq    15.0e-9         /*encapsulating shell thickness (m)*/
#define dRo1    3.635e-6        /*encapsulating shell initial diameter (m)*/

#define dsigma1 4.0e-2          /*gas/shell surface tension (N/m)*/
#define dsigma2 5.0e-3          /*liquid/shell surface tension (N/m)*/

#define dpo             1.0e5           /*ambient pressure (Pa)*/
#define k               1.4                     /*ratio of gas specific heats*/
                                                /*Kinf=A*Tinf + B      A= 5.28
erg/cm s K^2 B=1165 erg/cm s K */
#define dconstA 5.528e-5                /*constant relating temperature and conductivity
(N/sK^2)*/
#define dTinf   293.0           /*initial temperature (K)*/
#define dconstB 1165e-5         /*constant relating temperature and conductivity
(N/sK)*/

#define dff     1.0e5                   /*insonation frequency ratio*/
#define damp    1.0e5   /*insonation pressure amplitude (Pa)*/

#define dh              1.0e-10         /*time step (s)*/
```

```
#define N               50                      /*N+1 = number of grid elements (indices
run 0-N)*/
#define M               5000000                 /*M+1 = number of time steps (indices
run 0-M)*/
#define pi              3.141592654     /*pi*/


/*function declaration*/
void velocity(double *t,double *R,double *p,double *U,double *dpdt,double *dUdt);
void pressure(double *R,double *p,double *U,double Tau[N+1],double *dpdt);
void temperature(double Tau[N+1],double *R, double *p, double *U, double
dTaudt[N],double *dpdt);

void main (void){

/*declare variables*/
int     i,j,q;
double
dVs,dRo2,f,df,R,U,p,Tau[N+1],t,h,Rx,Ux,px,Taux[N+1],dUdt,dpdt,dTaudt[N],k1[N+4],k2[N+
4],k3[N+4],k4[N+4];

/*Initialise variables*/
for(q=0;q<=N;q++){
        Tau[q]=0.0;
        }
for(q=0;q<N;q++){
        dTaudt[q]=0.0;
        }
for(q=0;q<=N+3;q++){
        k1[q]=k2[q]=k3[q]=k4[q]=0.0;
        }
dpdt=dUdt=t=h=R=U=p=0.0;

/*constants*/
dRo2=dRo1+ddoq;
dVs=((pow(dRo2,3.0)-pow(dRo1,3.0)));
df=dff;/*sqrt((dpo*3.0*k-2.0*dsigma1/dRo1-
2.0*pow(dRo1,3.0)*dsigma2/pow(dRo2,4.0)+4*dGs*dVs*(1+2*pow(dRo2,3.0)*(dsigma1/dRo1+ds
igma2/dRo2)*(1+3*pow((dRo1/dRo2),3.0))/(4*dVs*dGs))/pow(dRo2,3.0))/(drhos*dRo1*dRo1*(
1+dRo1*(drho1/drhos-1.0)/dRo2)))/(2.0*pi);
/*printf("%f\n",df);   */

/*non-dimensionalise defined constants*/
h=dh*2*pi*df;

/*set initial conditions*/
R=1.0;
p=1.0;
U=0;
for(i=0;i<=N;i++){
        Tau[i]=0.0;
        }

/*start time loop for numerical solution*/
for (j=0;j<M;j++){

if(((float)j/10000)-j/10000==0.0)printf("%f\t%f\t%f\n",t,R,U);
                                /*

printf("%f\t%f\n",t,R);
/*step 1*/
pressure(&R,&p,&U,Tau,&dpdt);
velocity(&t,&R,&p,&U,&dpdt,&dUdt);
temperature(Tau,&R,&p,&U,dTaudt,&dpdt);
k1[0]=h*U;
k1[1]=h*dUdt;
k1[2]=h*dpdt;
for(i=3;i<=N+2;i++){
        k1[i]=h*dTaudt[i-3];
        }

/*intermediate parameter values*/
t+=h/2;
Rx=R+0.5*k1[0];
Ux=U+0.5*k1[1];
px=p+0.5*k1[2];
for(i=0;i<N;i++){
Taux[i]=Tau[i]+0.5*k1[i+3];
}               /*
printf("2\t%f\t%f\n",t,Ux);
```

```
                */
/*step 2*/
pressure(&Rx,&px,&Ux,Taux,&dpdt);
velocity(&t,&Rx,&px,&Ux,&dpdt,&dUdt);
temperature(Taux,&Rx,&px,&Ux,dTaudt,&dpdt);
k2[0]=h*Ux;
k2[1]=h*dUdt;
k2[2]=h*dpdt;
for(i=3;i<=N+2;i++){
        k2[i]=h*dTaudt[i-3];
        }


/*intermediate parameter values*/
Rx=R+0.5*k2[0];
Ux=U+0.5*k2[1];
px=p+0.5*k2[2];
for(i=0;i<N;i++){
Taux[i]=Tau[i]+0.5*k2[i+3];
}
                        /*
printf("3\t%f\t%f\n",t,Ux);
                          */
/*step 3*/
pressure(&Rx,&px,&Ux,Taux,&dpdt);
velocity(&t,&Rx,&px,&Ux,&dpdt,&dUdt);
temperature(Taux,&Rx,&px,&Ux,dTaudt,&dpdt);
k3[0]=h*Ux;
k3[1]=h*dUdt;
k3[2]=h*dpdt;
for(i=3;i<=N+2;i++){
        k3[i]=h*dTaudt[i-3];
        }

/*intermediate parameter values*/
t+=h/2;
Rx=R+k3[0];
Ux=U+k3[1];
px=p+k3[2];
for(i=0;i<N;i++){
Taux[i]=Tau[i]+k3[i+3];
}
                                /*
printf("4\t%f\t%f\n",t,Ux);*/
/*step 4*/
pressure(&Rx,&px,&Ux,Taux,&dpdt);
velocity(&t,&Rx,&px,&Ux,&dpdt,&dUdt);
temperature(Taux,&Rx,&px,&Ux,dTaudt,&dpdt);
k4[0]=h*Ux;
k4[1]=h*dUdt;
k4[2]=h*dpdt;
for(i=3;i<=N+2;i++){
        k4[i]=h*dTaudt[i-3];
        }

/*parameter values for next step*/
R=R+(k1[0]+2.0*k2[0]+2.0*k3[0]+k4[0])/6.0;
U=U+(k1[1]+2.0*k2[1]+2.0*k3[1]+k4[1])/6.0;
p=p+(k1[2]+2.0*k2[2]+2.0*k3[2]+k4[2])/6.0;
for(i=0;i<N;i++){
        Tau[i]=Tau[i]+(k1[i+3]+2.0*k2[i+3]+2.0*k3[i+3]+k4[i+3])/6.0;
               }
        }
}


/*function declarations*/

void pressure (double *R,double *p,double *U,double Tau[N+1],double *dpdt){
/*finds the time derivative of pressure*/

double dy,x,Do,dKinf,df,dRo2,dVs;
/*constants*/
dRo2=dRo1+ddoq;
dVs=((pow(dRo2,3.0)-pow(dRo1,3.0)));
df=dff;/*sqrt((dpo*3.0*k-2.0*dsigma1/dRo1-
2.0*pow(dRo1,3.0)*dsigma2/pow(dRo2,4.0)+4*dGs*dVs*(1+2*pow(dRo2,3.0)*(dsigma1/dRo1+ds
igma2/dRo2)*(1+3*pow((dRo1/dRo2),3.0))/(4*dVs*dGs))/pow(dRo2,3.0))/(drhos*dRo1*dRo1*(
1+dRo1*(drhol/drhos-1.0)/dRo2)))/(2.0*pi);
*/
```

```
dKinf=dconstA*dTinf+dconstB;
Do=(k-1)*dKinf*dTinf/(k*dpo);
x=Do/(2.0*pi*df*dRo1*dRo1);
dy=1.0/((double)N);
*dpdt=3.0*((k-1)*x*(Tau[N-2]-4.0*Tau[N-1])/(2.0*(*R)*dy)-k*(*p)*(*U))/(*R);
        }

void velocity(double *t,double *R,double *p,double *U,double *dpdt, double *dUdt){
/*finds the derivative of velocity*/

/*declare variables*/
double
df,rhol,mul,cl,Ro1,sigma1,rhos,mus,Gs,Ro2,sigma2,po,f,amp,req,Vs,R2,dRo2,dVs,doq;
/*constants*/
dRo2=dRo1+ddoq;
dVs=((pow(dRo2,3.0)-pow(dRo1,3.0)));
df=dff;/*sqrt((dpo*3.0*k-2.0*dsigma1/dRo1-
2.0*pow(dRo1,3.0)*dsigma2/pow(dRo2,4.0)+4*dGs*dVs*(1+2*pow(dRo2,3.0)*(dsigma1/dRo1+ds
igma2/dRo2)*(1+3*pow((dRo1/dRo2),3.0))/(4*dVs*dGs))/pow(dRo2,3.0))/(drhos*dRo1*dRo1*(
1+dRo1*(rhol/rhos-1.0)/dRo2)))/(2.0*pi);
                */
/*non-dimensionalise variables*/
rhol=drhol*dRo1*dRo1*4*pi*pi*df*df/dpo;
mul=dmul*df*2*pi/dpo;
cl=dcl/(2*pi*df*dRo1);
Ro1=dRo1/dRo1;
po=dpo/dpo;
f=df/(2*pi*df);
amp=damp/dpo;
rhos=drhos*dRo1*dRo1*4*pi*pi*df*df/dpo;
Gs=dGs/dpo;
mus=dmus*df*2*pi/dpo;
doq=ddoq/dRo1;
sigma1=dsigma1/(dpo*dRo1);
sigma2=dsigma2/(dpo*dRo1);

/*calculate constants*/
Ro2=Ro1+doq;
Vs=((pow(Ro2,3.0)-pow(Ro1,3.0)));
req=Ro1*(1+2*(sigma1/Ro1+sigma2/Ro2)*pow(Ro2,3.0)/(4.0*Vs*Gs));

/*calculate outer radius*/
R2=pow((pow((*R),3.0)+Vs),(1/3.0));

/*church equation*/
*dUdt=
(((*p)-po-amp*sin(2*pi*f*(*t))
        -2.0*sigma1/(*R)-2.0*sigma2/R2
        -4.0*(*U)*(Vs*mus+mul*pow((*R),3.0))/((*R)*pow(R2,3.0))
        -4.0*Gs*Vs*(1.0-req/(*R))/pow(R2,3.0))/rhos
        -pow((*U),2.0)*(3.0/2.0+(rhol-rhos)*((*R)/R2)*(4.0*pow(R2,3.0)-
pow((*R),3.0))/(2.0*rhos*pow(R2,3.0)))
        )/((*R)*(1.0+(rhol-rhos)*(*R)/(rhos*R2)));


}


void temperature (double Tau[N+1],double *R, double *p, double *U, double
dTaudt[N],double *dpdt){
/*declare variables*/
int i;
double
dRo2,dVs,df,G2Tau[N],dTaudy[N+1],dKinf,alpha,Tinf,Kinf,constA,dy,x,y[N+1],Do,D[N+1],T
[N+1],m,mmax,mmin;

/*calculate constants*/
dKinf=dconstA*dTinf+dconstB;
Do=(k-1)*dKinf*dTinf/(k*dpo);
dRo2=dRo1+ddoq;
dVs=((pow(dRo2,3.0)-pow(dRo1,3.0)));
df=dff;/*sqrt((dpo*3.0*k-2.0*dsigma1/dRo1-
2.0*pow(dRo1,3.0)*dsigma2/pow(dRo2,4.0)+4*dGs*dVs*(1+2*pow(dRo2,3.0)*(dsigma1/dRo1+ds
igma2/dRo2)*(1+3*pow((dRo1/dRo2),3.0))/(4*dVs*dGs))/pow(dRo2,3.0))/(drhos*dRo1*dRo1*(
1+dRo1*(drhol/drhos-1.0)/dRo2)))/(2.0*pi);
                */

/*non-dimensionalise variables*/
constA=dconstA*dTinf*dTinf/(dpo*dRo1*dRo1*2*pi*df);
Tinf=dTinf/dTinf;
```

```
Kinf=dKinf*dTinf/(dpo*dRo1*dRo1*2*pi*df);

/*calculate non-dimensional constants*/
alpha=dconstA*dTinf/dKinf;
x=Do/(2*pi*df*dRo1*dRo1);
dy=1/((double)N);

for(i=0;i<=N;i++){
        T[i]=(pow((1+2*alpha*Tau[i]*(k-1)/k),0.5)+alpha-1)/alpha;
        D[i]=(alpha*T[i]+1-alpha)*T[i]/(*p);
        }

for(i=0;i<=N;i++){
        y[i]=dy*(double)i;
        }

                G2Tau[0]=6*(Tau[1]-Tau[0])/(dy*dy);
                dTaudy[0]=0;
                dTaudy[N]=(Tau[N-2]-4*Tau[N-1])/(2*dy);

                for(i=1;i<N;i++){
                        G2Tau[i]=((1+dy/y[i])*Tau[i+1]-2*Tau[i]+(1-dy/y[i])*Tau[i-
1])/(dy*dy);
                        dTaudy[i]=(Tau[i+1]-Tau[i-1])/(2*dy);
                        }

        for(i=0;i<N;i++){
                dTaudt[i]=D[i]*(x*G2Tau[i]/((*R)*(*R))+(*dpdt))+(k-
1)*x*(dTaudy[N]*y[i]-dTaudy[i])*dTaudy[i]/(k*(*p)*(*R)*(*R));
                }

/*m=0.5*dy*(y[0]*y[0]/T[0]+y[N]*y[N]/T[N]);
for(i=1;i<N;i++) {
m+=y[i]*y[i]*dy/T[i];
}

m=3*(*p)*pow((*R),3.0)*m;
if(100*(m-1.0)>mmax)mmax=100*(m-1.0);
if(100*(m-1.0)<mmin)mmin=100*(m-1.0);

printf("%f\n",m);*/
}
```

rknoth.c

```
/*Runge Kutta numerical solution for model of a shelled CAP with no thermal damping*/

#include<stdio.h>
#include<stdlib.h>
#include<math.h>

/*defined constants*/

#define drhol   1000.0          /*surrounding fluid density (kg/m^3)*/
#define dmul    1.0e-3          /*surrounding fluid viscosity (Pas)*/
#define dcl             1481.0          /*surrounding fluid sound velocity (m/s)*/

#define drhos   1100.0          /*encapsulating shell density (kg/m^3)*/
#define dGs             88.8e6      /*encapsulating shell shear modulus (Pa)*/
#define dmus    1.77            /*encapsulating shell viscosity (Pas)*/
#define ddoq    15.0e-9         /*encapsulating shell thickness (m)*/
#define dRo1    3.635e-6        /*encapsulating shell initial diameter (m)*/

#define dsigma1 4.0e-2          /*gas/shell surface tension (N/m)*/
#define dsigma2 5.0e-3          /*liquid/shell surface tension (N/m)*/

#define dpo             1.0e5           /*ambient pressure (Pa)*/
#define k               1.4                     /*ratio of gas specific heats*/
                                                /*Kinf=A*Tinf + B      A= 5.28
erg/cm s K^2 B=1165 erg/cm s K */
#define df              3.0e6           /*insonation frequency (Hz)*/
#define damp    1.0e5           /*insonation pressure amplitude (Pa)*/
```

```
#define dh              1.0e-8          /*time step (s)*/
#define M               500             /*M+1 = number of time steps (indices run 0-M)*/
#define pi              3.141592654     /*pi*/
#define m       15
#define n       15
#define p1      1
#define p2      1


/*function declaration*/
void velocity (double *t,double *R,double *U,double *dUdt,double *p);

void main (void){

/*declare variables*/
int     i,j,q;
double
f,R,R2,U,t,h,p,Rx,Ux,dUdt,dpdt,k1[2],k2[2],k3[2],k4[2],Ro1,Ro2,Vs,mus,rhos,mul,rhol;
FILE *fp,*ft,*fr,*fv,*fps;

/*Initialise variables*/
for(q=0;q<=1;q++){
        k1[q]=k2[q]=k3[q]=k4[q]=0.0;
        }
R=U=dpdt=dUdt=t=h=0.0;

/*non-dimensionalise defined constants*/
h=dh*2*pi*df;
f=df/(2*pi*df);
rhol=drhol*dRo1*dRo1*4*pi*pi*df*df/dpo;
mul=dmul*df*2*pi/dpo;
rhos=drhos*dRo1*dRo1*4*pi*pi*df*df/dpo;
mus=dmus*df*2*pi/dpo;
Ro1=dRo1/dRo1;
Ro2=(dRo1+ddoq)/dRo1;
Vs=((pow(Ro2,3.0)-pow(Ro1,3.0)));

/*set initial conditions*/
R=1.0;
U=0.0;

/*open file*/
if((fp=fopen("data.m", "w"))==NULL){
printf("cannot open file.\n");
exit(1);}
/*print parameters*/
fprintf(fp,"drhol=%f;\n",drhol);
fprintf(fp,"dmul=%f;\n",dmul);
fprintf(fp,"dcl=%f;\n",dcl);
fprintf(fp,"dGs=%f;\n",dGs);
fprintf(fp,"drhos=%f;\n",drhos);
fprintf(fp,"dmus=%f;\n",dmus);
fprintf(fp,"dsigma1=%f;\n",dsigma1);
fprintf(fp,"dsigma2=%f;\n",dsigma2);
fprintf(fp,"dro1=%f;\n",dRo1*1e6);
fprintf(fp,"ddo=%f;\n",ddoq*1e6);
fprintf(fp,"dpo=%f;\n",dpo);
fprintf(fp,"df=%f;\n",df);
fprintf(fp,"damp=%f;\n",damp);
fprintf(fp,"N=%i;\n",M);
fprintf(fp,"dh=%f;\n",dh*1e6);
/*close file*/
fclose(fp);

/*open files*/
if((ft=fopen("time.m", "w"))==NULL){
printf("cannot open file.\n");
exit(1);}
fprintf(ft,"t=[");

if((fr=fopen("radius.m", "w"))==NULL){
printf("cannot open file.\n");
exit(1);}
fprintf(fr,"r=[");

if((fv=fopen("velocity.m", "w"))==NULL){
printf("cannot open file.\n");
exit(1);}
fprintf(fv,"u=[");
```

```
if((fps=fopen("pressure.m", "w"))==NULL){
printf("cannot open file.\n");
exit(1);}
fprintf(fps,"p=[");

/*start time loop for numerical solution*/
for (j=0;j<M;j++){
Rx=Ux=dUdt=0.0;

R2=pow((pow(R,3.0)+Vs),(1/3.0));

/*print parameters to file*/
fprintf(ft,"%f\n",t);
fprintf(fr,"%f\n",R);
fprintf(fv,"%f\n",U);
fprintf(fps,"%f\n",p);

/*printf("%f\t%f\n",t,pow((1.0/R),3*k));
printf("%f\t%f\t%f\n",t,R,U);*/

/*step 1*/
k1[0]=h*U;
velocity(&t,&R,&U,&dUdt,&p);
k1[1]=h*dUdt;

/*intermediate parameter values*/
t+=h/2;
Rx=R+0.5*k1[0];
Ux=U+0.5*k1[1];

/*step 2*/
k2[0]=h*Ux;
velocity(&t,&Rx,&Ux,&dUdt,&p);
k2[1]=h*dUdt;

/*intermediate parameter values*/
Rx=R+0.5*k2[0];
Ux=U+0.5*k2[1];

/*step 3*/
k3[0]=h*Ux;
velocity(&t,&Rx,&Ux,&dUdt,&p);
k3[1]=h*dUdt;

/*intermediate parameter values*/
t+=h/2;
Rx=R+k3[0];
Ux=U+k3[1];

/*step 4*/
k4[0]=h*Ux;
velocity(&t,&Rx,&Ux,&dUdt,&p);
k4[1]=h*dUdt;

/*parameter values for next step*/
R=R+(k1[0]+2*k2[0]+2*k3[0]+k4[0])/6.0;
U=U+(k1[1]+2*k2[1]+2*k3[1]+k4[1])/6.0;
       }

fprintf(ft,"];");
fprintf(fr,"];");
fprintf(fv,"];");
fprintf(fps,"];");

/*close files*/
fclose(ft);
fclose(fr);
fclose(fv);
fclose(fps);
}

/*function declarations*/
void velocity(double *t,double *R,double *U,double *dUdt,double *p){
/*finds the derivative of velocity*/

/*declare variables*/
double
z,w,rhol,mul,cl,rhos,Gs,mus,doq,Ro1,Ro2,R2,Vs,req,sigma1,sigma2,po,constA,Tinf,Kinf,f
,amp,dKinf,x,alpha,Do,dy,h;
```

```
/*pulsed insonation*/
z=m;
if(m>n)z=n;
w=0;
if((2*pi*f*(*t)/z)<2*pi)
{w=pow((1-cos(2*pi*f*(*t)/m)),p1)*pow((1-
sin(2*pi*f*(*t)/n)),p2)*cos(2*pi*f*(*t))*sin(2*pi*f*(*t));}
/*continuous wave insonation*/
/*w=sin(2*pi*f*(*t));*/

/*non-dimensionalise variables*/
rhol=drhol*dRo1*dRo1*4*pi*pi*df*df/dpo;
mul=dmul*df*2*pi/dpo;
cl=dcl/(2*pi*df*dRo1);
rhos=drhos*dRo1*dRo1*4*pi*pi*df*df/dpo;
Gs=dGs/dpo;
mus=dmus*df*2*pi/dpo;
doq=ddoq/dRo1;
Ro1=dRo1/dRo1;
sigma1=dsigma1/(dpo*dRo1);
sigma2=dsigma2/(dpo*dRo1);
po=dpo/dpo;
f=df/(2*pi*df);
amp=damp/dpo;

/*calculate constants*/
Ro2=Ro1+doq;
Vs=((pow(Ro2,3.0)-pow(Ro1,3.0)));
req=Ro1*(1+2*(sigma1/Ro1+sigma2/Ro2)*pow(Ro2,3.0)/(4.0*Vs*Gs));

/*calculate outer radius*/
R2=pow((pow((*R),3.0)+Vs),(1/3.0));

*dUdt=((
po*pow((Ro1/(*R)),3.0*k)
-po-amp*w
-2.0*sigma1/(*R)-2.0*sigma2/R2
-4*(*U)*(Vs*mus+mul*pow((*R),3.0))/((*R)*pow(R2,3.0))
-4.0*Gs*Vs*(1.0-req/(*R))/pow(R2,3.0))/rhos
-pow((*U),2.0)*(3.0/2.0+(rhol-rhos)*((*R)/R2)*(4*pow(R2,3.0)-
pow((*R),3.0))/(2*rhos*pow(R2,3.0))))
/((*R)*(1.0+(rhol-rhos)*(*R)/(rhos*R2)));

*p=
po*pow((Ro1/(*R)),k*3.0)
-po-amp*w
-2.0*sigma1/(*R)-2.0*sigma2/R2
-4.0*(*U)*pow((*R),2)*mul/pow(R2,3)
-4.0*(*U)*mus*pow((*R),2.0)*(1/pow((*R),3.0)-1/pow(R2,3.0))
-4.0*pow((*R),2)*Gs*((*R)-req)*(1/pow((*R),3.0)-1/pow(R2,3.0));
}
```

B.ii Demonstrating the equivalence of existing CAP models

It may be shown that the existing models for CAP behaviour are mathematically equivalent and, that in the absence of reliable experimental data, they are of equal value, despite the claims of various authors.

For example, equation 2.9 (Church 1995) for a CAP with a linear visco-elastic shell of finite thickness gives

$$R_1\ddot{R}_1\left(1+\left(\frac{\rho_L-\rho_S}{\rho_S}\right)\frac{R_1}{R_2}\right)+\dot{R}_1^2\left(\frac{3}{2}+\left(\frac{\rho_L-\rho_S}{\rho_S}\right)\left(\frac{4R_2^3-R_1^3}{2R_2^3}\right)\frac{R_1}{R_2}\right)$$
$$=\frac{1}{\rho_S}\left(p_o\left(\frac{R_{o1}}{R_1}\right)^{3\kappa}-p_\infty(t)-\frac{2\sigma_1}{R_1}-\frac{2\sigma_2}{R_2}-4\frac{\dot{R}_1}{R_1}\left(\frac{V_S\mu_S-R_1^3\mu_L}{R_2^3}\right)-\frac{4V_SG_S}{R_2^3}\left(1-\frac{R_{1e}}{R_1}\right)\right) \quad (2.9)$$

In the limit of an infinitesimally thin shell i.e. $R_2 \approx R_1 = R$ and $V_s = 3R^2d_S$ this may be expressed as

$$R\ddot{R}+\frac{3}{2}\dot{R}^2=\frac{1}{\rho_L}\left(p_o\left(\frac{R_o}{R}\right)^{3\kappa}-p_\infty(t)-\frac{2\sigma}{R}-\frac{4\mu_L\dot{R}}{R}-\frac{12\mu_SR_e^2d_S\dot{R}}{R^4}-\frac{12G_Sd_SR_e^2}{R^3}\left(1-\frac{R_e}{R}\right)\right) \quad (Bii.1)$$

Comparing with equation 2.8 (de Jong *et al* 1994)

$$R\ddot{R}+\frac{3}{2}\dot{R}^2=\frac{1}{\rho_L}\left(p_o\left(\frac{R_o}{R}\right)^{3\kappa}-p_\infty(t)-\frac{2\sigma}{R}-\frac{4\mu_L\dot{R}}{R}-\frac{S_f\dot{R}}{4\pi R^2}-2\frac{S_p}{R_o}\left(1-\frac{R_o}{R}\right)\right) \quad (Bii.2)$$

It may be seen that the two equations are equivalent if S_f and S_p are defined as

$$\frac{48\pi\mu_SR_e^2d_S}{R^2} \quad \text{and} \quad \frac{6G_Sd_SR_e^2}{R^2} \quad \text{respectively.}$$

Similarly, equation 2.7 (Glazman 1983) for a surfactant coated bubble gives

$$R\ddot{R}+\frac{3}{2}\dot{R}^2=\frac{1}{\rho_L}\left(p_o\left(\frac{R_o}{R}\right)^{3\kappa}-p_\infty(t)-\frac{2\sigma}{R}-\frac{4\mu_L\dot{R}}{R}-\frac{2}{R}\chi_S\left(\frac{R_o}{R}\right)^2\right) \quad (2.7)$$

This may also be shown to equivalent to Bii.1 and Bii.2 since χ_S is also an experimentally determined parameter. Thermal and acoustic damping factors have been neglected in the above but it may also be shown that the different forms included in equations 2.7-2.9 are equivalent.

B.iii Investigating the influence of pulsed insonation

The response of an Albunex® CAP insonified at 2.25 MHz and 0.1 MPa by (i) continuous wave and (ii) pulsed ultrasound is shown in figure Biii.1. The corresponding peak stresses and radial displacements are shown in table Biii.1. The pulse used was of the form given by Lord *et al* (1990)

$$P_\infty(t) = \begin{cases} P(1-\cos\left(\frac{\omega t}{m}\right))^a (1-\sin\left(\frac{\omega t}{n}\right))^b \sin(\omega t)\cos(\omega t), 0 \le \frac{\omega t}{\min(m,n)} \le 2\pi \\ 0, elsewhere \end{cases}$$

where $a = b = 5$ and $m=n=1$

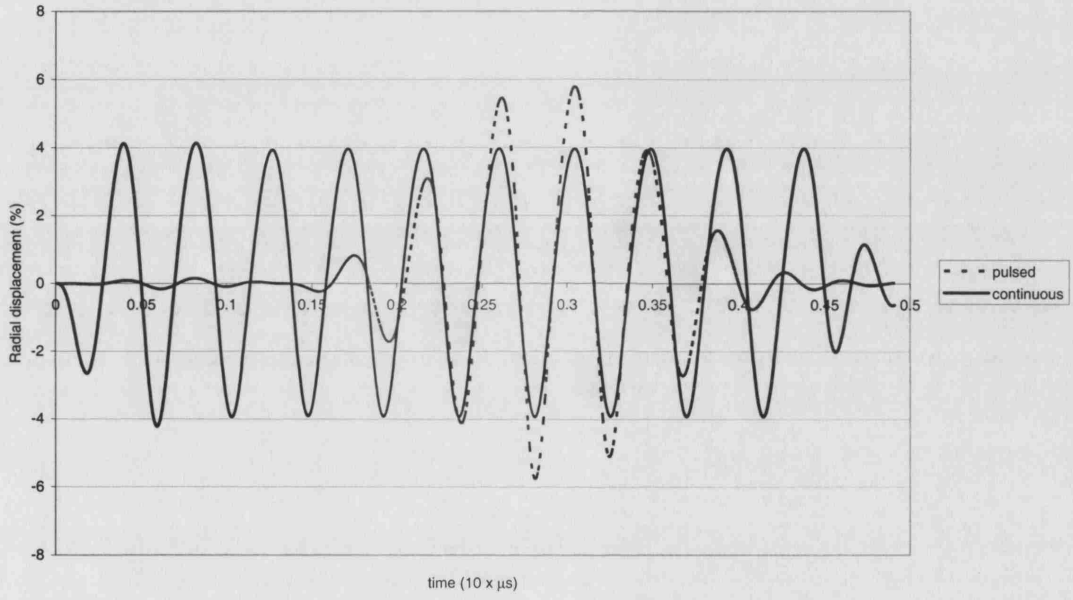

Figure Biii.1: Response of an Albunex® CAP to pulsed and continuous insonation at 2.25 MHz and 0.1MPa.

Insonation	Frequency	Pressure	R_{max}	R_{min}	$T_{eff\ comp.}$	$T_{eff\ tens.}$
	MHz	MPa	%	%	MPa	MPa
Continuous	2.25	0.1	4.1	-4.2	-21.9	24.8
Pulsed	2.25	0.1	5.8	-5.8	-30.0	34.4

Table Biii.1: Peak radial displacements and stresses for an Albunex® CAP.

It may be seen from the figure and table above that the type of insonation (pulsed or continuous wave) was not significant in terms of the results discussed in section 3.6. This may not be the case in general, however, and further discussion is therefore warranted. As shown in Chapter 5, the nature of the incident field may have a strong influence upon CAP behaviour. Whether or not this is the case depends upon the amplitude of the insonation pressure and the relationship between the insonation frequency(ies) and the CAP resonance frequency. Thus, a pulse containing a very wide range of frequencies may produce a very different response from continuous insonation at a single frequency.

There is also the possibility of exciting a significant transient response at the start of each pulse. This has been shown to be an important effect with free bubbles (Leighton *et al* 1989) producing an enhancement in the degree of inertial cavitation observed. An examination of the transients in CAP response was therefore made using equation 3.27. The results indicated, however, that the amplitude of transient oscillations is not significantly higher than in the steady state (figure Biii.2). Thus an analogy with free bubbles in this respect would seem to be inappropriate. It was also shown in Chapter 5 that at low to moderate insonation pressures it is the stiffness function (*SF*) that is dominant during CAP contraction, rather than the inertial or pressure function as is the case for free bubbles. In theoretical terms therefore CAP oscillation and cavitation (stable or inertial) should be regarded as different processes. Of course, if the influence of the shell were greatly diminished during the initial expansion/contraction, more "bubble-like" behaviour would be expected and the significance of transient oscillations might then be increased.

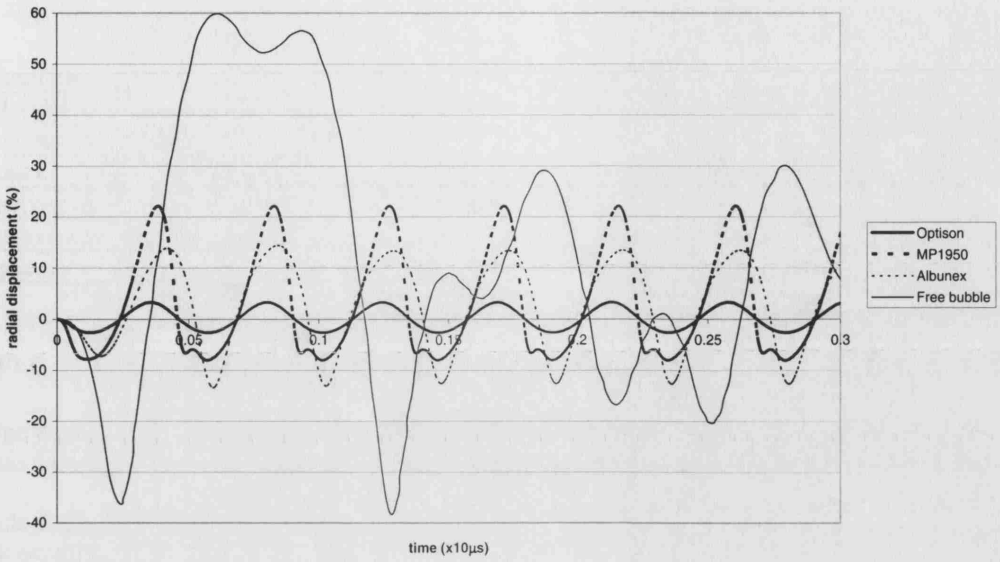

Figure Biii.2: Variation in radial displacement with time for CAPs insonated at 2.25 MHz and 0.3 MPa.

B.iv Program code

This appendix contains listings for the following programs

rknoth.c	implements a 4th order Runge-Kutta procedure for solving equation 3.15
blood.c	implements a 4th order Runge-Kutta procedure for solving equation 3.44
extinct.m	calculates the extinction cross section numerically for a single CAP
mss.c	implements a numerical solution of equation 3.66
henyey.m	determines the solution for equation 3.50
ksolve.m	determines the solution for equation 3.49
spec.m	determines the frequency spectra for the incident and radiated pulses

rknoth.c

```
/*Runge Kutta numerical solution of model for a shelled CAP with no correction for thermal or
acoustic damping*/

#include<stdio.h>
#include<stdlib.h>
#include<math.h>

/*defined constants*/

#define drhol  1000.0       /*surrounding fluid density (kg/m^3)*/
#define dmul   1.0e-3       /*surrounding fluid viscosity (Pas)*/
#define dcl    1481.0       /*surrounding fluid sound velocity (m/s)*/

#define drhos  1100.0 /*encapsulating shell density (kg/m^3)*/
#define dGs    88.8e6  /*encapsulating shell shear modulus (Pa)*/
#define dmus   1.77    /*encapsulating shell viscosity (Pas)*/
#define ddoq   15.0e-9  /*encapsulating shell initial thickness (m)*/
#define dRo1   3.0e-6   /*encapsulating shell initial inner radius(m)*/
#define dsigma1 4.0e-2    /*gas/shell surface tension (N/m)*/
#define dsigma2 5.0e-3   /*liquid/shell surface tension (N/m)*/

#define dpo    1.0e5        /*ambient pressure (Pa)*/
#define k      1.0          /*ratio of gas specific heats*/

/*for pulsed insonation, frequency entered here should be half desired frequency*/
#define df     1.5e6        /*insonation frequency (Hz)*/
#define damp   1.0e3        /*insonation pressure amplitude (Pa)*/
#define M      3000         /*M+1 = number of time steps (indices run 0-M)*/
#define pi     3.141592654   /*pi*/
#define m      5
#define n      5
#define p1     1
#define p2     1
#define dbw    0.45         /*bandwidth for Gaussian pulses*/
#define dtmax  9.4e-6       /*Gaussian pulse length*/
#define dr     1.e-6        /*distance from CAP outer wall*/

/*function declaration*/
void velocity (double *t,double *R,double *U,double *dUdt,double *p,double *ip);

void main (void){

/*declare variables*/
int   j,q;
double f,R,R2,U,t,h,p,ip,Rx,Ux,dUdt,dpdt,k1[2],k2[2],k3[2],k4[2],Ro1,Ro2,Vs,mus,rhos,mul,rhol,dh;
FILE *fp,*ft,*fr,*fv,*fps,*fips,*fa;
```

```
/*Initialise variables*/
for(q=0;q<=1;q++){
      k1[q]=k2[q]=k3[q]=k4[q]=0.0;
      }
R=U=dpdt=dUdt=t=h=0.0;

/*set time step*/
dh=1.0/20.0/2.0/df/((float)M/3000);
/*dh=1.0/20.0/2.0/df;*/

/*non-dimensionalise defined constants*/
h=dh*2*pi*df;
f=df/(2*pi*df);
rhol=drhol*dRo1*dRo1*4*pi*pi*df*df/dpo;
mul=dmul*df*2*pi/dpo;
rhos=drhos*dRo1*dRo1*4*pi*pi*df*df/dpo;
mus=dmus*df*2*pi/dpo;
Ro1=dRo1/dRo1;
Ro2=(dRo1+ddoq)/dRo1;
Vs=((pow(Ro2,3.0)-pow(Ro1,3.0)));

/*set initial conditions*/
R=1.0;
U=0.0;

/*open file*/
if((fp=fopen("data.m", "w"))==NULL){
printf("cannot open file.\n");
exit(1);}
/*print parameters*/
fprintf(fp,"drhol=%f;\n",drhol);
fprintf(fp,"dmul=%f;\n",dmul);
fprintf(fp,"dcl=%f;\n",dcl);
fprintf(fp,"dGs=%f;\n",dGs);
fprintf(fp,"drhos=%f;\n",drhos);
fprintf(fp,"dmus=%f;\n",dmus);
fprintf(fp,"dsigma1=%f;\n",dsigma1);
fprintf(fp,"dsigma2=%f;\n",dsigma2);
fprintf(fp,"dro1=%f*1e-6;\n",dRo1*1e6);
fprintf(fp,"ddo=%f*1e-6;\n",ddoq*1e6);
fprintf(fp,"dpo=%f;\n",dpo);
fprintf(fp,"df=%f;\n",df);
fprintf(fp,"damp=%f;\n",damp);
fprintf(fp,"N=%i;\n",M);
fprintf(fp,"dh=%f*1e-6;\n",dh*1e6);
fprintf(fp,"m=%i;\n",m);
fprintf(fp,"k=%f;\n",k);
/*close file*/
fclose(fp);

/*open files*/
if((ft=fopen("time.m", "w"))==NULL){
printf("cannot open file.\n");
exit(1);}
fprintf(ft,"t=[");

if((fr=fopen("radius.m", "w"))==NULL){
printf("cannot open file.\n");
exit(1);}
fprintf(fr,"r=[");

if((fv=fopen("velocity.m", "w"))==NULL){
printf("cannot open file.\n");
```

```
exit(1);}
fprintf(fv,"u=[");

if((fps=fopen("pressure.m", "w"))==NULL){
printf("cannot open file.\n");
exit(1);}
fprintf(fps,"p=[");

if((fips=fopen("ipressure.m", "w"))==NULL){
printf("cannot open file.\n");
exit(1);}
fprintf(fips,"ip=[");

if((fa=fopen("acceleration.m", "w"))==NULL){
printf("cannot open file.\n");
exit(1);}
fprintf(fa,"a=[");

/*start time loop for numerical solution*/
for (j=0;j<M;j++){

Rx=Ux=dUdt=0.0;

R2=pow((pow(R,3.0)+Vs),(1/3.0));

/*print parameters to file*/
fprintf(ft,"%f\n",t);
fprintf(fr,"%f\n",R);
fprintf(fv,"%f\n",U);
fprintf(fps,"%f\n",p);
fprintf(fips,"%f\n",ip);

/*step 1*/
k1[0]=h*U;
velocity(&t,&R,&U,&dUdt,&p,&ip);
k1[1]=h*dUdt;

/*intermediate parameter values*/
t+=h/2;
Rx=R+0.5*k1[0];
Ux=U+0.5*k1[1];

/*step 2*/
k2[0]=h*Ux;
velocity(&t,&Rx,&Ux,&dUdt,&p,&ip);
k2[1]=h*dUdt;

/*intermediate parameter values*/
Rx=R+0.5*k2[0];
Ux=U+0.5*k2[1];

/*step 3*/
k3[0]=h*Ux;
velocity(&t,&Rx,&Ux,&dUdt,&p,&ip);
k3[1]=h*dUdt;

/*intermediate parameter values*/
t+=h/2;
Rx=R+k3[0];
Ux=U+k3[1];

/*step 4*/
k4[0]=h*Ux;
```

```
velocity(&t,&Rx,&Ux,&dUdt,&p,&ip);
k4[1]=h*dUdt;

/*parameter values for next step*/
R=R+(k1[0]+2*k2[0]+2*k3[0]+k4[0])/6.0;
U=U+(k1[1]+2*k2[1]+2*k3[1]+k4[1])/6.0;

fprintf(fa,"%f\n",dUdt);

    }

fprintf(ft,"];");
fprintf(fr,"];");
fprintf(fv,"];");
fprintf(fps,"];");
fprintf(fips,"];");
fprintf(fa,"];");

/*close files*/
fclose(ft);
fclose(fr);
fclose(fv);
fclose(fps);
fclose(fips);
fclose(fa);
}

/*function declarations*/
void velocity(double *t,double *R,double *U,double *dUdt,double *p,double *ip){
/*finds the derivative of velocity*/

/*declare variables*/
double z,w,rhol,mul,cl,rhos,Gs,mus,doq,Ro1,Ro2,R2,Vs,req,sigma1,sigma2,po,f,amp,r,tmax,bw;

/*non-dimensionalise variables*/
rhol=drhol*dRo1*dRo1*4*pi*pi*df*df/dpo;
mul=dmul*df*2*pi/dpo;
cl=dcl/(2*pi*df*dRo1);
rhos=drhos*dRo1*dRo1*4*pi*pi*df*df/dpo;
Gs=dGs/dpo;
mus=dmus*df*2*pi/dpo;
doq=ddoq/dRo1;
Ro1=dRo1/dRo1;
sigma1=dsigma1/(dpo*dRo1);
sigma2=dsigma2/(dpo*dRo1);
po=dpo/dpo;
f=df/(2*pi*df);
amp=damp/dpo;
r=dr/dRo1;
tmax=dtmax*2*pi*df;
bw=dbw;

/*pulsed insonation*/
z=m;
if(m>n)z=n;
w=0;
if((2*pi*f*(*t)/z)<2*pi)
{w=pow((1-cos(2*pi*f*(*t)/m)),p1)*pow((1-
sin(2*pi*f*(*t)/n)),p2)*cos(2*pi*f*(*t))*sin(2*pi*f*(*t));}

/*Gaussian pulse with quadratic chirp*/
/*w=0;
```

```
if((*t)<tmax){w=sin(2*pi*(*t)*f*(1-dbw/2+dbw*pow((*t)/tmax,2)))/exp(2*(*t-tmax/2)*(*t-
tmax/2)/tmax/tmax);}
*/

/*continuous wave insonation (with cut off)*/
/*w=sin(2*pi*f*(*t));
*//*w=0.0;
if((2*pi*f*(*t)/m)<2*pi){
   w=sin(2*pi*f*(*t));}
*/

/*continuous wave insonation with additional harmonics*/
/*w=0.8*sin(2*pi*f*(*t))+0.15*sin(4*pi*f*(*t))+0.035*sin(6*pi*f*(*t))+0.0015*sin(8*pi*f*(*t));
*/
/*w=0.0;
if((2*pi*f*(*t)/m)<2*pi){
w=0.75*sin(2*pi*f*(*t))+0.15*sin(4*pi*f*(*t))+0.075*sin(6*pi*f*(*t))+0.025*sin(8*pi*f*(*t));
}*/

/*calculate constants*/
Ro2=Ro1;
Vs=0.0;
req=Ro1;
if(ddoq>0.0){
Ro2=Ro1+doq;
Vs=((pow(Ro2,3.0)-pow(Ro1,3.0)));
req=Ro1*(1+2*(sigma1/Ro1+sigma2/Ro2)*pow(Ro2,3.0)/(4.0*Vs*Gs));
}

/*calculate outer radius*/
R2=pow((pow((*R),3.0)+Vs),(1/3.0));

*dUdt=((
po*pow((Ro1/(*R)),3.0*k)
-po-amp*w
-2.0*sigma1/(*R)-2.0*sigma2/R2
-4*(*U)*(Vs*mus+mul*pow((*R),3.0))/((*R)*pow(R2,3.0))
-4.0*Gs*Vs*(1.0-req/(*R))/pow(R2,3.0)
/*-rhos*pow((Ro1*2*pi*f),2.0)*Ro2*(*U)/(cl*(*R)*(1+pow((2*pi*f*Ro2/cl),2.0)))*/
)/rhos
-pow((*U),2.0)*(3.0/2.0+(rhol-rhos)*((*R)/R2)*(4*pow(R2,3.0)-
pow((*R),3.0))/(2*rhos*pow(R2,3.0))))
/((*R)*(1.0+(rhol-rhos)*(*R)/(rhos*R2)));

*ip=amp*w;

/*scattered pressure at CAP outer wall*/
*p=
po*pow((Ro1/(*R)),k*3.0)
-po-amp*w
-2.0*sigma1/(*R)-2.0*sigma2/R2
-4.0*(*U)*pow((*R),2)*mul/pow(R2,3)
-4.0*(*U)*mus*pow((*R),2.0)*(1/pow((*R),3.0)-1/pow(R2,3.0))
-4.0*pow((*R),2)*Gs*((*R)-req)*(1/pow((*R),3.0)-1/pow(R2,3.0))
-rhos*pow((Ro1*2*pi*f),2.0)*Ro2*(*U)/(cl*(*R)*(1+pow((2*pi*f*Ro2/cl),2.0)));

/*scattered pressure at distance r from CAP outer wall (Vokurka type equation)*/
/**p=rhol*(*R)*(pow((*U),2.0)*(pow(((*R)/r),3.0)/2.0-2.0)-(*dUdt)*(*R))/r;*/

/*radiated pressure at distance r treating CAP as rigid sphere*/
/**ip=2*pi*f*rhol*pow((Ro2*(*R)/R2),2.0)*(*U)*cos(2*pi*f/r/cl)/r;*/

}
```

Blood.c

```
/*simple Runge Kutta solution of Church's equation for a CAP with an outer layer representing the
effects of blood*/

#include<stdio.h>
#include<stdlib.h>
#include<math.h>

/*Define dimensional constants*/

/*Surrounding fluid: plasma*/
#define drhol   1030.0  /*check*/
#define dmul    1.5e-3

/*Encapsulating shell material*/
#define drhos   1100.0
#define dGs     88.8e6
#define dmus    1.77
#define ddos    15.0e-9

/*Blood layer parameters*/
#define drhob   1050.0
#define dGb     5.0e2
#define dmub    6.0e-3
#define ddob    8.0e-6

/*Interfacial tensions*/
#define dsigma1 40.0e-3
#define dsigma2 5.0e-3   /*check*/
#define dsigma3 1.0e-4   /*check*/

/*intial CAP inner radius*/
#define dRo1    3.635e-6

/*filling gas parameters*/
#define k       1.0
#define dpo     1.0e5

/*Sound field parameters*/
#define df          0.5e6   /*insonation frequency or half pulse centre frequency*/
#define damp          1.0e5
#define m           5
#define n           5
#define p1          1
#define p2          1

/*Numerical solution parameters*/
#define dh      1e-8                    /*timestep*/
#define N       500                     /*no. steps*/
#define pi      3.141592654                 /*pi*/

/*function prototypes*/
void    full_bubble(double *a,double *t,double *R,double *u);

/*main function*/
void main (void){

/*variable declarations*/
int i;
double K1,K2,K3,K4,Q1,Q2,a,tempt,tempr,tempu,t,r,u,h;
FILE *fp,*ft,*fr,*fv;
```

```
/*Initialise variables*/
K1=K2=K3=K4=Q1=Q2=a=h=0;
for(i=0;i<N;i++){
t=0;
r=0;
u=0;
}

/*non-dimensionalise*/
h=dh*2*pi*df;
/*set initial conditions*/
r=1.0;

/*open file*/
if((fp=fopen("data.m", "w"))==NULL){
printf("cannot open file.\n");
exit(1);}
/*print parameters*/
fprintf(fp,"drhol=%f;\n",drhol);
fprintf(fp,"dmul=%f;\n",dmul);
fprintf(fp,"dGs=%f;\n",dGs);
fprintf(fp,"drhos=%f;\n",drhos);
fprintf(fp,"dmus=%f;\n",dmus);
fprintf(fp,"dGb=%f;\n",dGb);
fprintf(fp,"drhob=%f;\n",drhob);
fprintf(fp,"dmub=%f;\n",dmub);
fprintf(fp,"dsigma1=%f;\n",dsigma1);
fprintf(fp,"dsigma2=%f;\n",dsigma2);
fprintf(fp,"dsigma3=%f;\n",dsigma3);
fprintf(fp,"dro1=%f;\n",dRo1*1e6);
fprintf(fp,"ddos=%f;\n",ddos*1e6);
fprintf(fp,"ddob=%f;\n",ddob*1e6);
fprintf(fp,"dpo=%f;\n",dpo);
fprintf(fp,"df=%f;\n",df);
fprintf(fp,"damp=%f;\n",damp);
fprintf(fp,"N=%i;\n",N);
fprintf(fp,"dh=%f;\n",dh*1e6);
fprintf(fp,"m=%i;\n",m);
/*close file*/
fclose(fp);

/*open files*/
if((ft=fopen("time.m", "w"))==NULL){
printf("cannot open file.\n");
exit(1);}
fprintf(ft,"t=[");

if((fr=fopen("radius.m", "w"))==NULL){
printf("cannot open file.\n");
exit(1);}
fprintf(fr,"r=[");

if((fv=fopen("velocity.m", "w"))==NULL){
printf("cannot open file.\n");
exit(1);}
fprintf(fv,"u=[");

/*time loop implementing Runge Kutta procedure*/

for(i=0;i<N;i++){

/*print parameters to file*/
fprintf(ft,"%f\n",t);
```

```
fprintf(fr,"%f\n",r);
fprintf(fv,"%f\n",u);

tempt=tempr=tempu=0;
full_bubble(&a,&t,&r,&u);
K1=0.5*h*h*a;

tempt=t+0.5*h;
tempr=r+0.5*h*u+K1/4;
tempu=u+K1/h;
full_bubble(&a,&tempt,&tempr,&tempu);
K2=0.5*h*h*a;

tempt=t+0.5*h;
tempr=r+0.5*h*u+K1/4;
tempu=u+K2/h;
full_bubble(&a,&tempt,&tempr,&tempu);
K3=0.5*h*h*a;

tempt=t+h;
tempr=r+h*u+K3;
tempu=u+2*K1/h;
full_bubble(&a,&tempt,&tempr,&tempu);
K4=0.5*h*h*a;

Q1=(K1+K2+K3)/3;
Q2=(K1+2*K2+2*K3+K4)/3;

if(i<N-1){
r=r+h*u+Q1;
u=u+Q2/h;
t=t+h;}
      }
/*end of loop*/

fprintf(ft,"];");
fprintf(fr,"];");
fprintf(fv,"];");

/*close files*/
fclose(ft);
fclose(fr);
fclose(fv);
}

/*end of main*/

/*functions*/

/*implements the equation of motion for an encapsulated CAP with an outer layer representing the
effects of blood*/

void   full_bubble(double *a,double *t,double *R,double *u){

/*declare variables*/
double
rhol,mul,Gs,mus,dos,rhos,Gb,mub,dob,rhob,Ro1,Ro2,Ro3,R2,R3,Vb,Vs,req1,sigma1,sigma2,sigma3,
po,f,amp,z,w,alpha,beta,gamma;

/*non-dimensionalise variables*/
rhol=drhol*dRo1*dRo1*4*pi*pi*df*df/dpo;
mul=dmul*df*2*pi/dpo;
rhos=drhos*dRo1*dRo1*4*pi*pi*df*df/dpo;
```

```
Gs=dGs/dpo;
mus=dmus*df*2*pi/dpo;
dos=ddos/dRo1;
rhob=drhob*dRo1*dRo1*4*pi*pi*df*df/dpo;
Gb=dGb/dpo;
mub=dmub*df*2*pi/dpo;
dob=ddob/dRo1;
Ro1=dRo1/dRo1;
sigma1=dsigma1/(dpo*dRo1);
sigma2=dsigma2/(dpo*dRo1);
sigma3=dsigma3/(dpo*dRo1);
po=dpo/dpo;
f=df/(2*pi*df);
amp=damp/dpo;

w=0;
/*calculate constants*/
Ro2=Ro1+dos;
Ro3=Ro2+dob;
Vs=((pow(Ro2,3.0)-pow(Ro1,3.0)));
Vb=((pow(Ro3,3.0)-pow(Ro2,3.0)));
req1=Ro1*(1+(sigma1/Ro1+sigma2/Ro2+sigma3/Ro3)*pow(Ro2*Ro3,3.0)/(2.0*(Vs*Gs*pow(Ro3,3.
0)+Vb*Gb*pow(Ro1,3.0))));

/*calculate outer radii*/
R2=pow((pow((*R),3.0)+Vs),(1/3.0));
R3=pow((pow((R2),3.0)+Vb),(1/3.0));

/*pulsed insonation*/
z=m;
if(m>n)z=n;
if((2*pi*f*(*t)/z)<2*pi)
{w=pow((1-cos(2*pi*f*(*t)/m)),p1)*pow((1-
sin(2*pi*f*(*t)/n)),p2)*cos(2*pi*f*(*t))*sin(2*pi*f*(*t));}

/*continuous wave insonation*/
/*w=sin(2*pi*f*(*t));*/

if((*R)<0)printf("negative radius");

/*acceleration*/
alpha=
po*pow((Ro1/(*R)),k*3.0)
-po
-amp*w
-2.0*sigma1/(*R)
-2.0*sigma2/R2
-2.0*sigma3/R3
-
4.0*pow((*R),2.0)*(*u)*(mul/pow(R3,3.0)+mus*Vs/(pow((*R),3.0)*pow(R2,3.0))+mub*Vb/(pow((
R3),3.0)*pow(R2,3.0)))
-4.0*pow((*R),2.0)*((*R)-req1)*(Gs*Vs/pow((*R),3.0)+Gb*Vb/pow(R3,3.0))/pow(R2,3.0);

beta=pow((*u),2.0)*(
(3.0/2.0)*rhos
+(rhol-rhob)*((*R)/R3)*(2.0-0.5*pow(((*R)/R3),3.0))
+(rhob-rhos)*((*R)/R2)*(2.0-0.5*pow(((*R)/R2),3.0))
);

gamma=(*R)*(rhos+(rhol-rhob)*(*R)/R3+(rhob-rhos)*(*R)/R2);

*a=(alpha-beta)/gamma;
}
```

extinct.m

```
%calculates the extinction cross section numerically for a single CAP
%initialise variables
t=0;
p=0;
r=0;
u=0;
ip=0;

%read in data
data
time
velocity
radius
pressure
ipressure

%non dimensionalise variables
dro2=dro1+ddo;
w=2.0*pi*df;
h=dh*w;
cl=dcl/(w*dro1);
rhol=drhol*dro1^2.0*w^2.0/dpo;
mul=dmul*w/dpo;
mus=dmus*w/dpo;
s1=dsigma1/(dpo*dro1);
s2=dsigma2/(dpo*dro1);
pa=damp/dpo;
ro1=dro1/dro1;
do=ddo/dro1;
ro2=ro1+do;

%find pulse length Tp
for i=1:length(t)
    tstart=t(i);
    if abs(ip(i))>0.05,
        break
   end
end

for i=0:length(t)-1
   tend=t(length(t)-i);
  if abs(ip(length(t)-i))>0.05,
   break
 end
end

Tp=pi*ceil((tend-tstart)/pi);

%redimensionalise
dTp=Tp/w;


%find average intensity over pulse
Ip=trapz(t,(ip.*ip))/(2*rhol*cl*Tp);
%redimensionalise
dIp=Ip*dpo*dro1*w;

%find average dissipated power over pulse
Vs=(ro2^3-ro1^3);
dVs=Vs*dro1^3;
for i=1:length(t)
```

```
r2(i)=(Vs+r(i)^3.0)^(1.0/3.0);
de(i)=16.0*pi*u(i)^2.0*r(i)*(mul*r(i)^3.0+mus*Vs)/r2(i)^3.0;
end
Wa=trapz(t,de)/Tp;
%redimensionalise
dWa=Wa*dpo*dro1^3*w;

%find average scattered power over pulse
Ws=4*pi*ro2^2*trapz(t,p.*p)/(2*cl*rhol*Tp);
%redimensionalise
dWs=Ws*dpo*dro1^3*w;

%calculate absorption cross-section
sa=dWa/dIp;
%calculate scattering cross-section
ss=dWs/dIp;
%calculate extinction cross-section
se=sa+ss;

%calculate the attenuation coefficient for a monodisperse suspension
conc=[1.0e5;1e6;1e7;1e8;1e9]*1.0e6;                %CAPs per m^3
for i=1:length(conc)
   alpha(i)=10.0*log10(exp(1))*conc(i)*se;

%Church's estimates for comparison
w=2*w;
a=1.0+(drhol-drhos)*dro1/dro2/drhos;
beta(i)=conc(i)*4.0*pi*dro1^3/3.0;
dd=4.0*(dVs*dmus+dro1^3*dmul)/(drhos*dro1^2*dro2^3*a);
alphac(i)=20.0*log10(exp(1))*beta(i)*dcl*dd*(w)^2*dro1^2*drhol^2/6.0/a/dpo^2;

Z=(2*dsigma1/dro1+2*dsigma2/dro2)*dro2^3/(4*dVs*dGs);
wo=sqrt((3*k*dpo-2*dsigma1/dro1-
2*dsigma2*dro1^3/dro2^4+4*dVs*dGs*(1+Z*(1+3*(dro1/dro2)^3))/dro2^3)/(drhos*dro1^2*a));
d=dd/wo;
O=w/wo;
x1=1/sqrt((1-O^2)^2+O^2*d^2);
ssc=4*pi*dro1^2*O^4*x1^2*drhol^2/a^2/drhos^2;
end

%db/cm
al=alpha/100
%ac=alphac/100
```

mss.c

```
/*4th order Runge-Kutta numerical solution of model for one dimensional multiple scattering in a
suspension of albumin shelled CAPs with no thermal or acoustic damping*/

#include<stdio.h>
#include<stdlib.h>
#include<math.h>

/*defined constants*/

#define drhol  1000.0      /*surrounding fluid density (kg/m^3)*/
#define dmul   1.0e-3      /*surrounding fluid viscosity (Pas)*/
#define dcl    1481.0      /*surrounding fluid sound velocity (m/s)*/

#define drhos  1100.0      /*encapsulating shell density (kg/m^3)*/
#define dGs    88.8e6      /*encapsulating shell shear modulus (Pa)*/
#define dmus   1.77        /*encapsulating shell viscosity (Pas)*/
#define ddos   15.0e-9     /*encapsulating shell thickness (m)*/
#define dRo1   4.0e-6              /*encapsulating shell initial diameter (m)*/

#define dsigma1 4.0e-2     /*gas/shell surface tension (N/m)*/
#define dsigma2 5.0e-3     /*liquid/shell surface tension (N/m)*/

#define dpo    1.0e5       /*ambient pressure (Pa)*/
#define k      1.0         /*ratio of gas specific heats*/

#define ddf    0.0e6       /*insonation frequency (need to use half required value for pulsed field)*/
#define damp   1.0e3       /*insonation pressure amplitude (Pa)*/
#define conc   1.0e5       /*CAP concentration (CAPs/ml)*/
#define X      2.5e-3      /*propagation distance (m)*/
#define xfl    50          /*space step fraction of wavelength*/
#define C      30          /*time step fraction of space step*/
#define N      299         /*N+1 = number of grid elements>xfl(cyc+1) (indices run 0-N)*/
#define M      8999        /*M+1 = number of time steps>C(cyc+1)xfl (indices run 0-M)*/
#define pi     3.141592654 /*pi*/
#define cyc    5                   /*pulse parameter*/
#define z                  55

/*global variables*/
double df,R[N+1], U[N+1], dUdt[N+1];

/*function declaration*/
void cap(int *i, double *pa, double *pb, double *f,double *l);
void rp(double *R, double *U, double *a, double *p);

/*main function*/

void main (void){

/*declare variables*/
int    i,j,fi;
double t,l,dl,h,dh,m,rhol,c,n,f,amp,po,pnow[N+1],pold[N+1],polder[N+1],F[N+1];
FILE *fp,*fF,*fip,*fd;

/*open files*/

if((fd=fopen("data.m", "w"))==NULL){
printf("cannot open file.\n");
exit(1);
}
if((fip=fopen("ipressure.m", "w"))==NULL){
printf("cannot open file.\n");
```

```
exit(1);
}
if((fp=fopen("pressure.m", "w"))==NULL){
printf("cannot open file.\n");
exit(1);
}
if((fF=fopen("caps.m", "w"))==NULL){
printf("cannot open file.\n");
exit(1);
}

fprintf(fp,"p=[");
fprintf(fip,"ip=[");
fprintf(fF,"F=[");

df=ddf;


/*write data to files*/

fprintf(fd,"dcl=%f;\n",dcl);
fprintf(fd,"M=%i;\n",M);
fprintf(fd,"z=%i;\n",z);
fprintf(fd,"xfl=%i;\n",xfl);

/*frequency loop*/
for (fi=1;fi<=10;fi++){
/*Initialise variables*/
df+=0.5e6;

/*set grid size*/
dh=dcl/xfl/df;

/*set timestep*/
dl=dh/C/dcl;

/*non-dimensionalise defined constants*/
l=dl*2*pi*df;
h=dh/dRo1;
c=dcl/(2*pi*df*dRo1);
m=c*c*l*l/h/h;
rhol=drhol*dRo1*dRo1*4*pi*pi*df*df/dpo;
n=1.0e6*conc*dRo1*dRo1*dRo1;
po=dpo/dpo;
amp=damp/dpo;
f=df/2.0/pi/df;

/*set initial conditions*/
for(i=0;i<=N;i++){
pnow[i]=po;
pold[i]=po;
polder[i]=po;
R[i]=1.0;
U[i]=0.0;
dUdt[i]=0.0;
F[i]=0.0;
}

/*first timestep*/
t=l;
/*pold[0]=po+amp*sin(2*pi*f*t);*/

if((2*pi*f*t/cyc)<2*pi)
```

```
{pold[0]=po+amp*((1-cos(2*pi*f*t/cyc)))*((1-sin(2*pi*f*t/cyc)))*cos(2*pi*f*t)*sin(2*pi*f*t);}

t+=l;

/*fprintf(fip,"ip=[");*/
fprintf(fip,"%f\n",pnow[0]);

/*fprintf(fp,"p%i=[",fi);*/
fprintf(fp,"%f\n",pnow[z]);

/*fprintf(fF,"F%i=[",fi);*/
fprintf(fF,"%f\n",F[z]);


/*start time loop for numerical solution*/
for (j=2;j<=M;j++){

/*printf("%f\n",F[z]);*/
/*pnow[0]=po+amp*sin(2*pi*f*t);*/
if((2*pi*f*t/cyc)<2*pi)
{pnow[0]=po+amp*((1-cos(2*pi*f*t/cyc)))*((1-sin(2*pi*f*t/cyc)))*cos(2*pi*f*t)*sin(2*pi*f*t);}

for(i=1;i<N;i++){

/*find pressure*/
pnow[i]=m*(pold[i+1]+pold[i-1])-2*(m-1)*pold[i]-polder[i]+l*l*4*c*c*rhol*n*pi*F[i];

/*evaluate CAP function*/
cap(&i,&pold[i],&pnow[i],&F[i],&l);
}

/*print parameters to file*/
fprintf(fip,"%f\n",pnow[0]);
fprintf(fp,"%f\n",pnow[z]);
fprintf(fF,"%f\n",F[z]);

/*update variables for next timestep*/
for(i=0;i<=N;i++){
polder[i]=pold[i];
pold[i]=pnow[i];
}

t+=l;

/*end of time loop*/
}

/*end of frequency loop*/
}

fprintf(fip,"];");
fprintf(fp,"];");
fprintf(fF,"];");

/*close files*/
fclose(fip);
fclose(fp);
fclose(fd);
fclose(fF);

/*end of program*/
}
/*function declaration*/
```

```
void cap(int *i, double *pa, double *pb, double *f, double *l){

double k1[2],k2[2],k3[2],k4[2],Rx,Ux,p1,p2,px;
p1=(*pa);
p2=(*pb);


/*step 1*/
rp(&R[*i],&U[*i],&dUdt[*i],&p1);
k1[0]=*l*U[*i];
k1[1]=*l*dUdt[*i];

/*intermediate parameter values*/
Rx=R[*i]+0.5*k1[0];
Ux=U[*i]+0.5*k1[1];
px=0.5*(p2+p1);
/*step 2*/

rp(&Rx,&Ux,&dUdt[*i],&px);
k2[0]=*l*Ux;
k2[1]=*l*dUdt[*i];

/*intermediate parameter values*/
Rx=R[*i]+0.5*k2[0];
Ux=U[*i]+0.5*k2[1];


/*step 3*/
rp(&Rx,&Ux,&dUdt[*i],&px);
k3[0]=*l*Ux;
k3[1]=*l*dUdt[*i];


/*intermediate parameter values*/
Rx=R[*i]+k3[0];
Ux=U[*i]+k3[1];


/*step 4*/
rp(&Rx,&Ux,&dUdt[*i],&p2);
k4[0]=*l*Ux;
k4[1]=*l*dUdt[*i];


/*parameter values for next time step*/
R[*i]=R[*i]+(k1[0]+2.0*k2[0]+2.0*k3[0]+k4[0])/6.0;
U[*i]=U[*i]+(k1[1]+2.0*k2[1]+2.0*k3[1]+k4[1])/6.0;

(*f)=R[*i]*R[*i]*dUdt[*i]+2*R[*i]*U[*i]*U[*i];

if(conc==0)(*f)=0.0;

}


void   rp(double *R, double *U, double *a, double *p){

/*declare variables*/
double rhol,mul,Gs,mus,dos,rhos,Ro1,Ro2,R2,Vs,req1,sigma1,sigma2,po,alpha,beta,gamma;


/*non-dimensionalise variables*/
```

```
rhol=drhol*dRo1*dRo1*4*pi*pi*df*df/dpo;
mul=dmul*df*2*pi/dpo;
rhos=drhos*dRo1*dRo1*4*pi*pi*df*df/dpo;
Gs=dGs/dpo;
mus=dmus*df*2*pi/dpo;
dos=ddos/dRo1;
Ro1=dRo1/dRo1;
sigma1=dsigma1/(dpo*dRo1);
sigma2=dsigma2/(dpo*dRo1);
po=dpo/dpo;

/*calculate constants*/
Ro2=Ro1+dos;
Vs=((pow(Ro2,3.0)-pow(Ro1,3.0)));
req1=Ro1*(1+2*(sigma1/Ro1+sigma2/Ro2)*pow(Ro2,3.0)/(4.0*Vs*Gs));

/*calculate outer radius*/
R2=pow((pow((*R),3.0)+Vs),(1/3.0));


/*acceleration*/
alpha=
po*pow((Ro1/(*R)),k*3.0)
-(*p)
-2.0*sigma1/(*R)
-2.0*sigma2/R2
-4.0*pow((*R),2.0)*(*U)*mul/pow(R2,3.0)
-4.0*mus*Vs*(*U)/((*R)*pow(R2,3.0))
-4.0*pow((*R),2.0)*(1-req1/(*R))*Gs*Vs/pow(R2,3.0);


beta=pow((*U),2.0)*((3.0/2.0)+(rhol/rhos-1)*(*R)*(4.0*pow(R2,3.0)-
pow((*R),3.0))/pow(R2,4.0)/2.0);

gamma=rhos*(*R)*(1+(*R)*(rhol-rhos)/R2/rhos);

*a=(alpha-beta)/gamma;

}
```

henyey.m

```
%define constants
damp=   1.00E+04;
drhol=1000;
dmul=   0.001;
dc=     1481;
drhos=1100;
dmus=   1.77;
dGs=    8.88E+07;
ds1=    0.04;
ds2=    0.005;
dpo=    1.00E+05;
dde=    1.50E-08;

j=1;

fid = fopen('hen.txt','wb');

for(j1=4:6)
        dn=10^j1;

    for(j2=2:4)
      dRo1=j2*1e-6;

                for(j3=1:10)
                df=j3*1e6;

dw=2*pi*df;

%non-dimensionalise
amp=    damp/dpo;
rhol=   drhol*dRo1^2*dw^2/dpo;
mul=    dmul*dw/dpo;
c=              dc/dRo1/dw;
rhos=   drhos*dRo1^2*dw^2/dpo;;
mus=    dmus*dw/dpo;
Gs=     dGs/dpo;
s1=     ds1/dpo/dRo1;
s2=     ds2/dpo/dRo1;
kap=    1;
po=     dpo/dpo;
de=     dde/dRo1;
Ro1=    dRo1/dRo1;
n=              dn*dRo1^3;

N=n*1e6;
w=dw/dw;
k=w/c;
Ro2=Ro1+de;
Vs=Ro2^3-Ro1^3;
Z=(2*s1/Ro1+2*s2/Ro2)*Ro2^3/Vs/4/Gs;
alpha=1+Ro1*(rhol/rhos-1)/Ro2;
wo=sqrt((3*kap*po-2*s1/Ro1-
2*s2*Ro1^3/Ro2^4+4*Vs*Gs(1+Z*(1+3*Ro1^3/Ro2^3))/Ro2^3)/(rhos*Ro1^2*alpha));
dvis=4*(Vs*mus+Ro1^3*mul)/Ro1^2/Ro2^3/alpha/rhos;
drad=w^2*Ro1*rhol/c/rhos/alpha;
d=dvis+drad;
denom=((wo^2-w^2)^2+d^2*w^2);

a=(-1)*rhol*Ro1*w^2*(wo^2-w^2)/rhos/alpha/denom;
b=rhol*Ro1*w^2*d*w/rhos/alpha/denom;
```

```
ff1=a+b*(0+i);
ff2=a*(0+i)+b;

%eq=[ff2 (-k*ff2-1) -k^2*ff2 (k^3*ff2+4*pi*N*ff1+k^2)];

eq=[1 (-k-1/ff2) -k^2 (k^3+4*pi*N*ff1/ff2+k^2/ff2)];

%eq=[1 (-k-1/ff2) -k^2 (k^3-4*pi*N*(0+i)+k^2/ff2)];

K=roots(eq);

KK(j,1)=real(K(1));
KK(j,2)=imag(K(1));
%fprintf(fid,'%f\t%f\n',KK(j,1)*1e6,KK(j,2)*1e6);

KK(j+1,1)=real(K(2));
KK(j+1,2)=imag(K(2));
%fprintf(fid,'%f\t%f\n',KK(j+1,1)*1e6,KK(j+1,2)*1e6);

KK(j+2,1)=real(K(3));
KK(j+2,2)=imag(K(3));
%fprintf(fid,'%f\t%f\n',KK(j+2,1)*1e6,KK(j+2,2)*1e6);

if (KK(j,1)>KK(j+1,1))
if(KK(j+1,1)>0)
fprintf(fid,'%f\t%f\n',KK(j+1,1)*1e6,KK(j+1,2)*1e6);
else
fprintf(fid,'%f\t%f\n',KK(j+2,1)*1e6,KK(j+2,2)*1e6);
end
end


j=j+3;

end
end
end

fclose(fid);
%w=dw;
%Ro1=dRo1;
%n=dn;
%amp= damp;%/dpo;
%rhol= drhol;%*dRo1^2*dw^2/dpo;
%mul= dmul;%*dw/dpo;
%c=          dc;%/dRo1/dpo;
%rhos= drhos;%*dRo1^2*dw^2/dpo;;
%mus= dmus;%*dw/dpo;
%Gs= dGs;%/dpo;
%s1= ds1;%/dpo/dRo1;
%s2= ds2;%/dpo/dRo1;
%kap= 1;
%po= dpo;%/dpo;
%de= dde;%/dRo1;
%Ro1= dRo1;%/dRo1;
%f=          df;%/dw;
%n=          dn;%*dRo1^3;
```

ksolve.m

```
function waveno = ksolve(K)
dRo1=3.0e-6;
df=3.0e6;
N=10^11;

dde=15e-9;
drhol=1000;
dcl=1481;
dmul=.001;
drhos=1100;
dGs=88.8e6;
dmus=1.77;
ds1=.04;
ds2=.005;
dpo=1e5;

dw=2*pi*df;
k=dw/dcl;
dRo2=dRo1+dde;
dVs=dRo2^3-dRo1^3;
alpha=1+dRo1*(drhol-drhos)/drhos/dRo2;
dvis=4*(dVs*dmus+dRo1^3*dmul)/(dRo2^3*dRo1^2*alpha*drhos);
drad=0;%dw^2*dRo1*drhol/dcl/drhos/alpha;
dd=dvis+drad;
Z=(2*ds1/dRo1+2*ds2/dRo2)*dRo2^3/(4*dGs*dVs);
wo=sqrt((3*dpo-2*ds1/dRo1-
2*ds2*dRo1^3/dRo2^4+4*dVs*dGs*(1+Z*(1+3*dRo1^3/dRo2^3))/dRo2^3)/(drhos*dRo1^2*alpha))
;

%a=-drhol*dRo1*(wo^2/dw^2-1)/((wo^2/dw^2-1)^2+(dd/dw)^2)/drhos/alpha;
%b=drhol*dRo1*(dd/dw)/((wo^2/dw^2-1)^2+(dd/dw)^2)/drhos/alpha;
%m=a^2+b^2;

%waveno=[K(1)^2-K(2)^2-k^2-(4*pi*N*m/((a+m*K(2))^2+(b+m*(K(1)-k))^2))*(a+m*K(2));
%  2*K(1)*K(2)-(4*pi*N*m/((a+m*K(2))^2+(b+m*(K(1)-k))^2))*(b+m*(K(1)-k))];

p=drhos*alpha*(wo^2/dw^2-1)/drhol/dRo1;
q=drhos*alpha*dd/dw/drhol/dRo1;

waveno=[(p+K(2))*(K(1)^2-K(2)^2-k^2)-2*q*K(1)*K(2)-4*pi*N+(K(1)-k)*2*K(1)*K(2);
(q-K(1)+k)*(K(1)^2-K(2)^2-k^2)-2*p*K(1)*K(2)+2*K(1)*K(2)^2];

end

%Ko=[1,1];
%K=fsolve(@ksolve,Ko)

%f=drhol*dRo1/(wo^2/dw^2-1+i*dd/dw)/drhos/alpha;
%waveno=K^2-k^2-4*pi*N/(1/f-i*(K-k));
%K=fzero(@ksolve,Ko)

%waveno=[4*pi*N*m*(K(1)^2-K(2)^2-k^2)-(a+K(2)*m)*((K(1)^2-K(2)^2-
k^2)^2+4*K(1)^2*K(2)^2);
%8*pi*N*m*K(1)*K(2)-(b+(K(1)-k)*m)*((K(1)^2-K(2)^2-k^2)^2+4*K(1)^2*K(2)^2)];
```

spec.m

```
% finds the frequency spectra for the incident and radiated pulses generated by program mss.c

%initialise variables
t=0;
p=0;
ip=0;
a=0;

%constants
data

for g=1:10
%read in data
pressure
ipressure
px=p(M*g-M+1:M*g);
ipx=ip(M*g-M+1:M*g);
df=g*0.5e6;
dh=dcl/xfl/df;
dt=1/1000/df;
q=(length(px));
t=(1:q)*dt;
w=2.0*pi*df;

%obtain incident pulse frequency spectrum
ipr=ipx-mean(ipx);
ipr(length(ipr):length(ipr)*5)=0;
iP = fft(ipr,length(ipr));
iPpp = iP.* conj(iP)/length(ipr);
fi = (1.0/dt)*(0:(0.5*length(ipr)))/length(ipr)/1e6;
%figure
%plot(fi,iPpp(1:(0.5*length(ipr)+1)))

%obtain radiated pulse frequency spectrum
pr=px-mean(px);
pr(length(pr):length(pr)*5)=0;
P = fft(pr,length(pr));
Ppp = P.* conj(P)/length(pr);
f = (1.0/dt)*(0:(0.5*length(pr)))/length(pr)/1e6;
%plot spectra
%figure
%plot(fi,iPpp(1:(0.5*length(ipr)+1)),f,Ppp(1:(0.5*length(pr)+1)))
%axis([0,4*df/1e6,0,max(iPpp)*1.05])

%plot spectra normalised with respect to maxima
%figure
%plot(fi,iPpp(1:(0.5*length(ipr)+1))/max(iPpp),f,Ppp(1:(0.5*length(pr)+1))/max(Ppp))
%axis([0,4e5,0,1])

%calculate attenuation coefficient (dB/cm)
a(g)=10*log10(exp(1))*log(max(iPpp)/max(Ppp))/z/dh/100;
end

figure
plot(1:10,a)
```

B.v Estimating the phase velocity in CAP suspensions

An estimate for the acoustic velocity in a CAP suspension may be obtained from equation 2.27.

$$K_{eff}^2 = k_L^2 + 4\pi\eta f \qquad (2.27)$$

Assuming linear propagation, the wave number for a given medium is, by definition, complex: $K_{eff} = \mathrm{Re}(K_{eff}) + i\mathrm{Im}(K_{eff})$, and the attenuation coefficient may be found from the imaginary component as

$$a = 20\log_{10}(e)\ \mathrm{Im}(K_{eff}) \qquad (3.48)$$

Similarly, the phase velocity for the effective medium may be found from the real component as

$$c_L = \frac{2\pi}{\mathrm{Re}(K_{eff})} \qquad (Bv.1)$$

The corresponding values for the conditions considered in section 3.9.3 are shown in figure Bv.1. It should be noted that these values are only estimates, however, and unlikely to be accurate at the higher concentrations, owing to the fact that equation 2.27 was developed on the assumption of a non-dispersive medium.

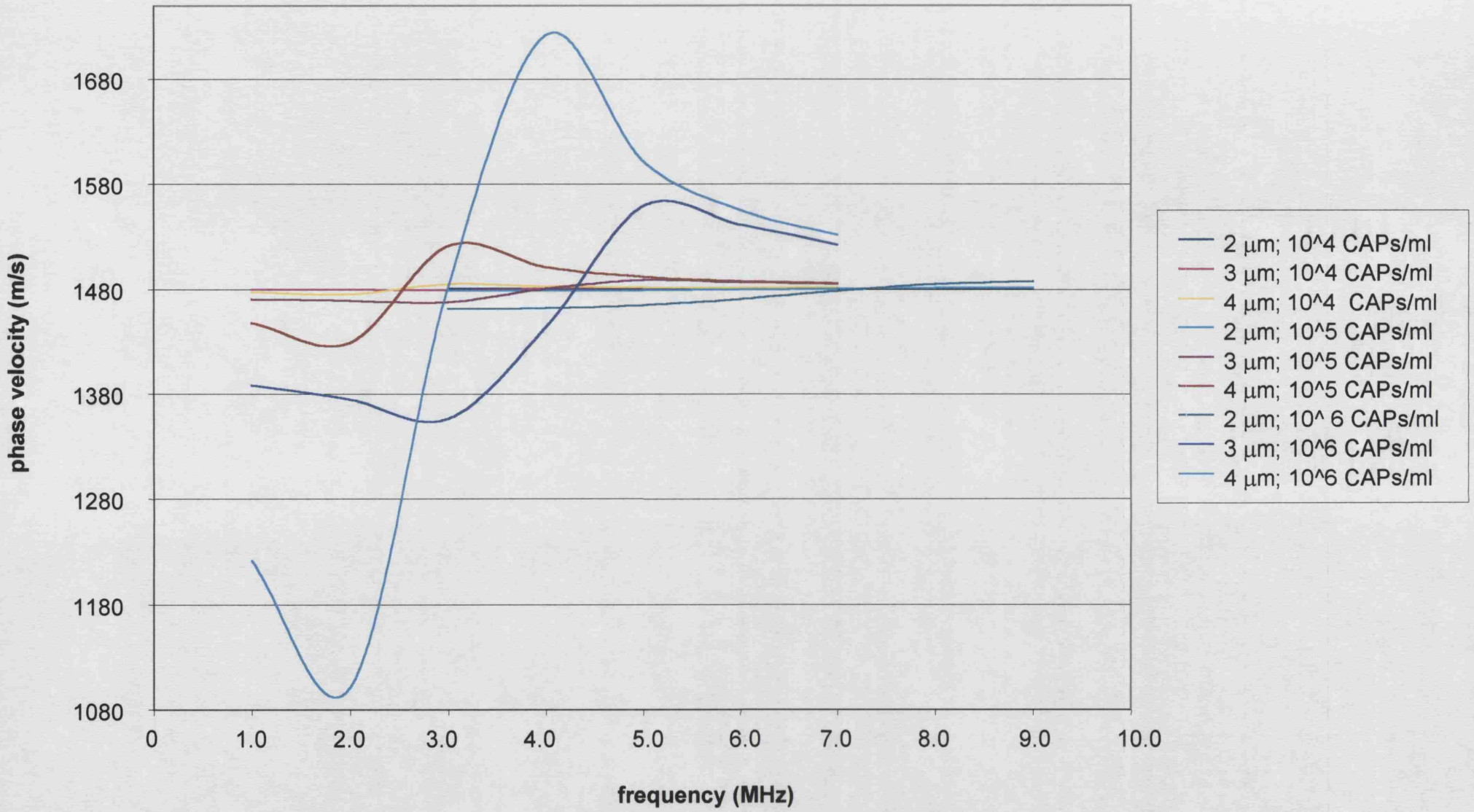

Figure Bv.1: Demonstrating the variation in phase velocity in CAP suspensions with frequency for different CAP sizes and concentrations.

C.i Diffraction compensation

The following is a description of the diffraction compensation methods used in the analysis of the experimental results presented in Chapter 4. Considering the experimental system as a whole, the initial electrical input signal to the transducer $A_v(f)$ will be modified by:

(i) the transducer (transmission and reception)
(ii) transmission through the medium
(iii) reflection by the base plate
(iv) diffraction

Following Xu & Kauffman (1993) and representing these effects as transfer functions, $A_T(f)$, $A_m(f)$, R, and $A_d(f)$, the first echoes received from a plate positioned at distances d_1 and d_2 from the transducer face (figure Ci.1) are given respectively by[1]

$$A_1(f) = A_v(f).A_T^{\,2}(f).R.A_{m1}(f).A_{d1}(f,z) \qquad \text{(Ci.1)}$$

$$A_2(f) = A_v(f).A_T^{\,2}(f).R.A_{m2}(f).A_{d2}(f,z) \qquad \text{(Ci.2)}$$

Thus

$$\frac{A_2(f)}{A_1(f)} = \frac{A_{d2}(f,z)}{A_{d1}(f,z)} e^{2\alpha(d_1-d_2)} \qquad \text{(Ci.3)}$$

Where α is the attenuation coefficient and f is the insonation frequency component.

A_d is found by applying the Fresnel approximation for the near field

$$A_d(f,z) = \left| 2e^{-jkz} \int_0^\infty \frac{J_1^2(Y)}{Y} e^{-jY^2\frac{S}{4\pi}} dY \right| \qquad \text{(Ci.4)}$$

where z is axial distance from the transducer face J_1 is the first order Bessel function $S = \frac{z\lambda}{a^2}$ is the Fresnel parameter, $\lambda = \frac{c}{f}$ is the acoustic wavelength and a is the transducer radius.

[1] Please note that once again it has been necessary to repeat symbols with different meanings in this appendix and that the definitions given in the text should be referred to rather than the list of symbols.

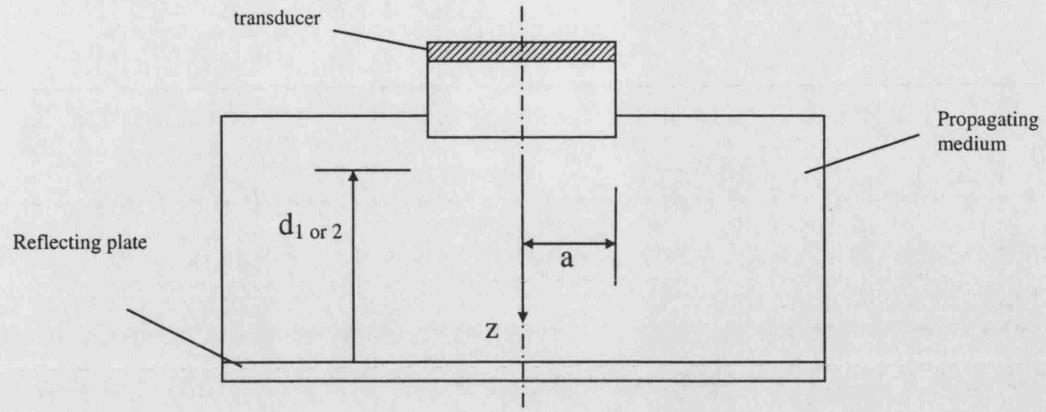

Figure Ci.1: Geometry of the experimental system.

A_1, A_2, c, d_1 and d_2 were measured for particular values of f. Equation Ci.4 was then integrated numerically to yield A_{d1} and A_{d2}. The code used for the latter is shown in Appendix C.iii and was validated using results published by Xu and Kaufman (1993). The presence of the CAPs may lead to variation in the value of c with frequency. In order to determine suitable values of c to be used in equation Ci.4, time of flight measurements were made using transducers of different centre frequencies. As described in Chapter 4 it was found that the variations were not significant.

C.ii Transducer characterisation

Cii.1 Bandwidth measurement

The apparatus was set up as described in section 4.2 but with the test chamber filled with water which had been left standing overnight to reduce its gas content. The echo from the stainless steel reflecting plate at the base of the chamber was captured for 3 different transmission distances and the corresponding frequency spectra obtained via Fourier transform, again as described earlier. The results are shown in figure Cii.1.

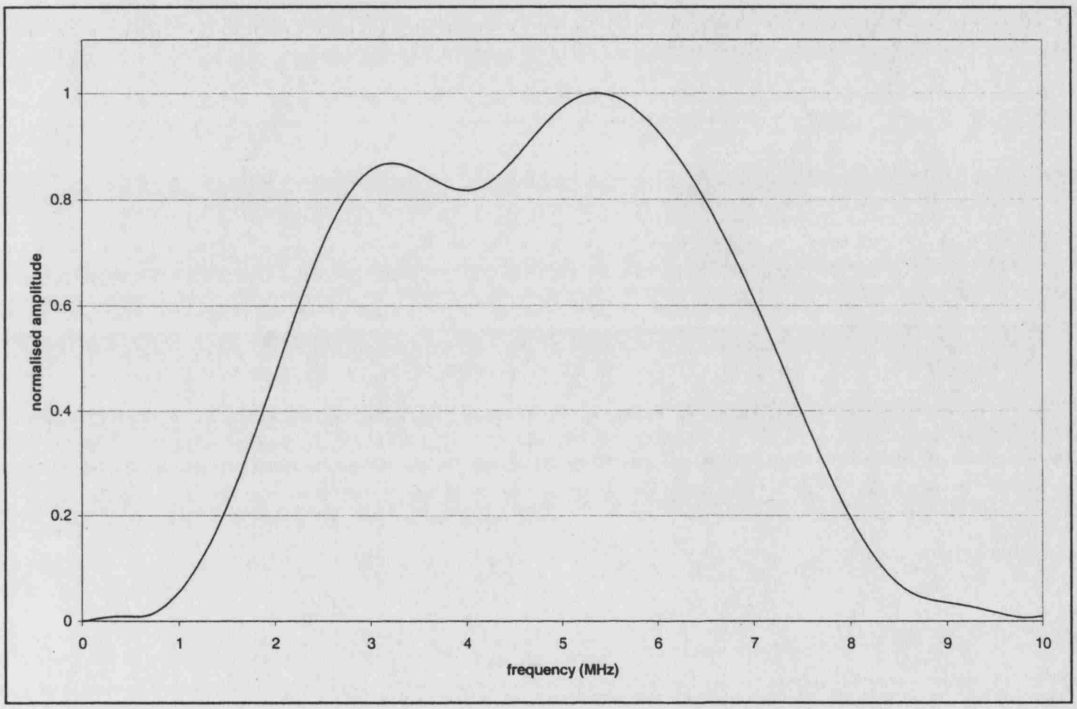

Figure Cii.1: Average frequency spectra for transmission through water.

The bandwidth was found conventionally from the amplitude spectrum, as the difference between the 3dB points on either side of the maximum (5.35 MHz).

Bandwidth 5.2 MHz	Standard deviation 0.06 MHz (1.1%)

This width was only an approximate value, however, since the spectrum was not found to be symmetrical. This was thought to have been due to interference between the main beam and the waves emanating from the edge of the transducer. The same asymmetry was observed in the spectra obtained for plasma and blood, but to a lesser degree, owing to the increased attenuation. Without modelling the effect of cells

upon ultrasound attenuation it was not possible to conclude whether the differences between the shapes of the spectra in water, plasma and blood were as expected or not. The presence of cells and/or CAPs would modify the attenuation in different ways so the shape of the spectrum for each of the fluids in the experiment would be expected to be different. The fact that the shapes were reproducible in separate tests on different days indicates that the differences were probably due to differences in the fluid properties rather than the experimental set up. The possibility of a systematic error cannot be ruled out without repeating the tests using different apparatus, however.

Making the bandwidth measurements in water rather than in one of the test fluids was thought to have been acceptable for the purposes of this experiment, since the contrast agent concentrations used were relatively low. This was confirmed by the fact that the bandwidth of the spectra obtained from the plasma/blood samples was of a similar magnitude. At higher CAP concentrations, however, the CAPs nearest to the transducer could significantly modify the sound field incident upon the remainder of the CAP population, in which case water measurements would not be representative. The same restriction applies to the pressure measurements made in water using the needle hydrophone described subsequently.

Cii.2 Hydrophone measurements in water

The output pressure from the transducer was determined using a needle hydrophone (Precision Acoustics, UK) with a 0.2 mm tip which was scanned across the transducer face at different planes to capture the beam profile (figure Cii.2). A C scan was performed in water at a depth of 2 cm. The apparatus was set up as described in section 4.3 but the transducer was moved along the horizontal axes of the rig rather than the vertical. The hydrophone was coupled to a 28V DC power supply and to the digital oscilloscope from where its output was captured and downloaded to the PC. Again signal capture and rig positioning was controlled using purpose written software and signal processing was performed in Matlab® (Appendix Ciii).

The corresponding insonation pressures were calculated using the calibration chart provided with the hydrophone (figure Cii.3). It was found that the peak negative pressure over the range 3-5 MHz varied between 0.0188 to 0.0192 MPa which corresponded to approximately 50 kPa. The uncertainty for this frequency range was given by the manufacturers as 1.9% and the average deviation over the insonified area was 0.4 kPa (2%). Thus it was confirmed that a sufficient fraction of the fluid samples would have been excited at a uniform pressure to obtain a representative response and that the CAPs should not have been excited sufficiently to induce significant non-linear behaviour or destruction.

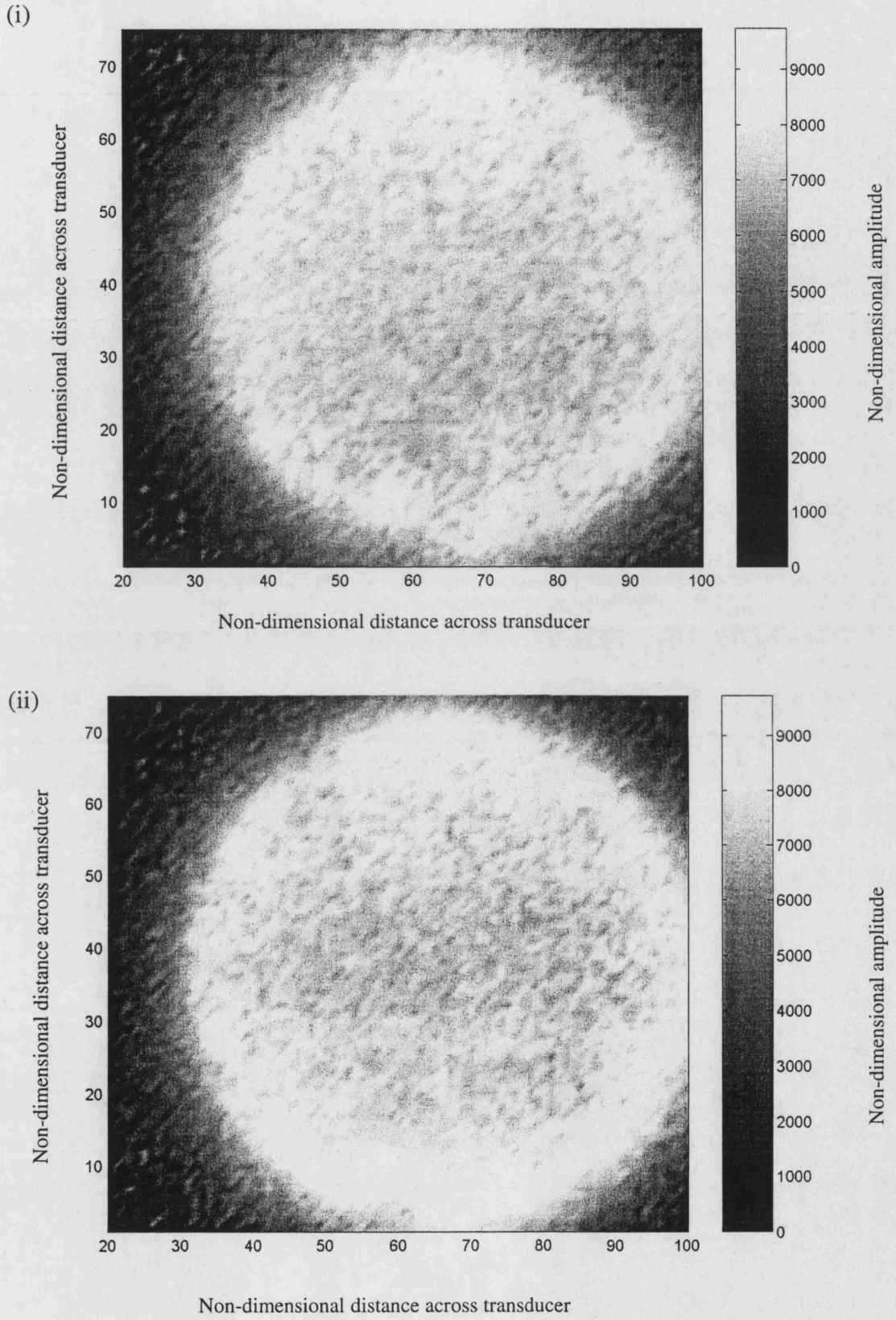

Figure Cii.2: Transducer beam profile in water at (i) 2 cm and (ii) 3 cm from the transducer face.

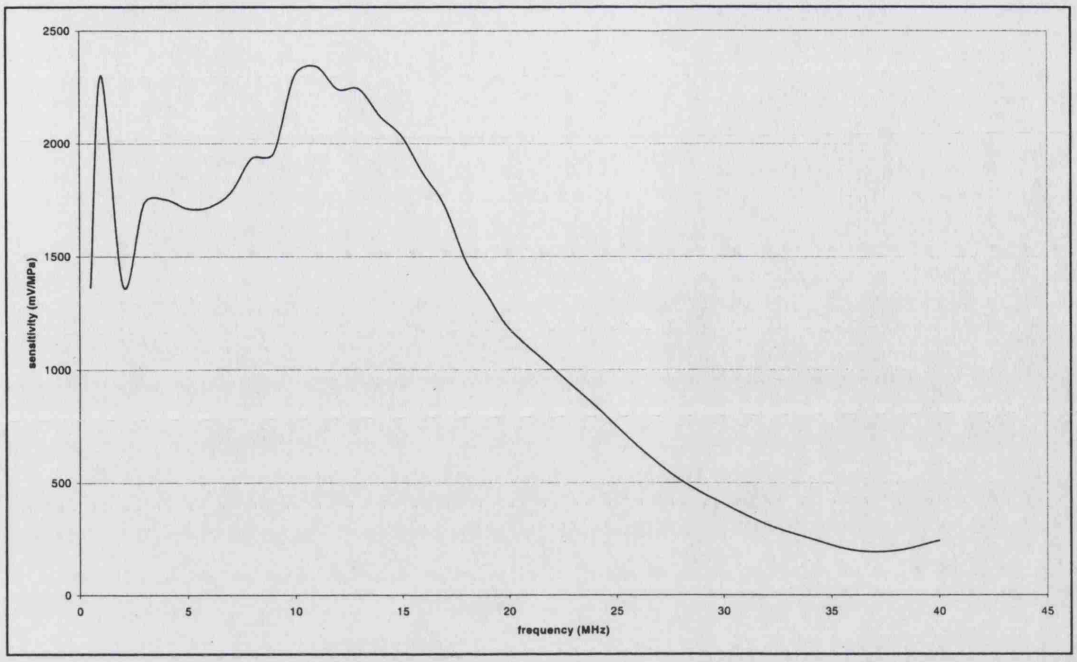

Figure Cii.3: Variation in hydrophone sensitivity with frequency.

The addition of gas-filled particles to a liquid would be expected to result in a change in velocity, owing to the change in effective density, but the CAP concentration used was too low for a significant change to be observed. Consequently, the dispersive nature of the fluid samples was not investigated. If dispersion had been significant, a change in the shape of the pulse and frequency spectrum would have been observed between the first and second echoes, due to the differing velocities of individual frequency components. As shown in figure Cii.4 this was not seen.

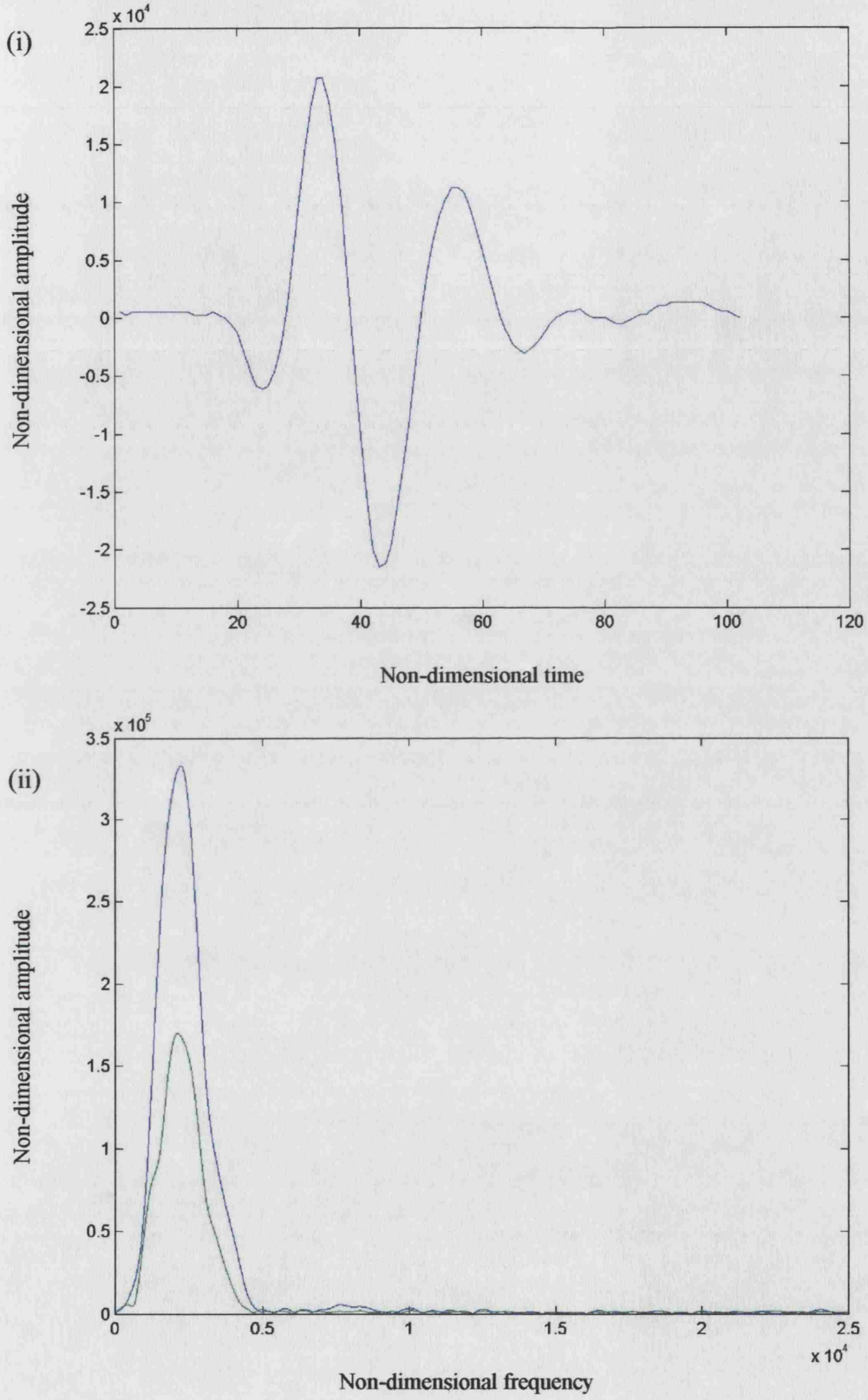

Figure Cii.4: Insonating pulse in (i) Time domain and (ii) Frequency domain for different transmission distances (blue = 2cm from transducer face; green = 3cm).

C.iii Program code

This appendix contains listings for the following programs

diffract.m	calculates the diffraction correction factor for transmission through a medium
val_diffract.m	produces results to compare with published values (Xu and Kaufman 1993) in order to validate the code for diffract.m

Diffract.m

```
%This program calculates the diffraction correction factor for transmission through a medium

%user defined parameters
c=1544.94;      %medium sound velocity
f=6.0e6;      %insonating frequency
d=0.05058;       %transmission distance
R=0.01;       %transducer radius

%
%don't forget to alter the red text according to these parameters too!!
%

%calculated variables
l=c/f;        %acoustic wavelength
k=2*pi/l;      %acoustic wave number
s=d*l/R^2;     %Fresnel parameter

%quadratic numerical integration
Z=
quad('besselj(1,Y).*besselj(1,Y).*exp(i*0.05058*1544.94*Y.*Y/4/pi/0.01^2/5.0e6)./Y',0.00000001,1
000);
A=2*exp(-i*k*d)*Z;
abs(A)

Z=
quadl('besselj(1,Y).*besselj(1,Y).*exp(i*0.05058*1544.94*Y.*Y/4/pi/0.01^2/5.0e6)./Y',0.00000001,1
000);
B=2*exp(-i*k*d)*Z;
abs(B)

%trapezoidal numerical integration
y=1e-8:1e-3:1000;    %frequency parameter of integration
b=besselj(1,y);
F=b.*b.*exp(i*s*y.*y/4/pi)./y;
z=trapz(F,y);

a=2*exp(-i*k*d)*z;
abs(a)
```

Val_diffract.m

```
%This program calculates the diffraction correction factor for transmission through water with and
without a sample present

%It produces results to compare with published values (Xu and Kaufman 1993) in order to validate
the code

R=0.0095;        %transducer radius (m)
f=1.0e6;         %insonating frequency  (Hz)
d=0.2;           %transducer separation (m)

%water only path
cw=1492;                  %medium sound velocity
lw=cw/f;                  %acoustic wavelength
kw=2*pi/lw;               %acoustic wave number
sw=d*lw/R^2;              %Fresnel parameter

%Z=
quad('besselj(1,Y).*besselj(1,Y).*exp(i*0.2*1492.0*Y.*Y/4/pi/0.0095^2/1.0e6)./Y',0.00000001,1000)
;
%A=2*exp(-i*kw*d)*Z;

%water-sample-water path
cs=2710;                  %medium sound velocity
ds=0.024;                 %sample transmission distancce
ls=cs/f;                  %acoustic wavelength
ks=2*pi*d/(ls*ds+(d-ds)*lw);      %composite acoustic wave number
ss=(lw*(d-ds)+ls*ds)/R^2;         %composite Fresnel parameter

%Z=
quad('besselj(1,Y).*besselj(1,Y).*exp(i*0.2*1492.0*Y.*Y/4/pi/0.0095^2/1.0e6)./Y',0.00000001,1000)
;
%B=2*exp(-i*ks*d)*Z;

abs(A/B)


y=1e-8:1e-3:1000;         %frequency parameter of integration
b=besselj(1,y);
Fw=b.*b.*exp(i*sw*y.*y/4/pi)./y;
zw=trapz(Fw,y);
aw=2*exp(-i*kw*d)*zw;
Fs=b.*b.*exp(i*ss*y.*y/4/pi)./y;
zs=trapz(Fs,y);
as=2*exp(-i*ks*ds)*zs;
abs(as)
abs(aw)
abs(as)/abs(aw)
```

D.i Program code

This appendix contains listings for the following programs

factors.m	determines the acceleration factors for a CAP from a solution of equation 3.15
spec.m	determines the frequency spectra for the incident and radiated pulses

factors.m

```
%This file calculates the acceleration factors for a CAP
data;
time;
radius;
velocity;
acceleration;
ipressure;

dro2=dro1+ddo;
Vs=(dro2)^3-dro1^3;
re1=dro1*(1+2*(dsigma1/dro1+dsigma2/dro2)*(dro2^3.0)/(4.0*Vs*dGs));

for i=1:length(r)

r1=r(i)*dro1;
r2=(Vs+r1^3)^(1/3);
u1=u(i)*2*pi*df*dro1;
dt=t(i)/2/pi/df;
%a=a(i)*dro1*(2*pi*df)^2;

%A=drhos*r1*(1+(drhol/drhos-1)*r1/r2);

PF(i)=dpo*(dro1^3/r1^3)-dpo;
IF(i)=-drhos*(u1^2)*(1.5+(drhol/drhos-1)*0.5*(4*r2^3-r1^3)*r1/r2^3);
AF(i)=ip(i)*dpo;%-damp*sin(2*pi*df*dt);
%TF(i)=-2*(dsigma1/r1+dsigma2/r2);
LvF(i)=-4*u1*r1^2*dmul/(r2^3);
SvF(i)=-4*u1*Vs*dmus/(r1*r2^3);
SsF(i)=-4*Vs*dGs*(1-re1/r1)/(r2^3)-2*(dsigma1/r1+dsigma2/r2);

end
x=1;
y=250;
plot(t(x:y),PF(x:y),t(x:y),IF(x:y),t(x:y),AF(x:y),t(x:y),LvF(x:y),t(x:y),SvF(x:y),t(x:y),SsF(x:y))
legend('PF','IF','AF','LvF','SvF','SsF')

%free plot
%plot(t(x:y),PF(x:y),t(x:y),IF(x:y),t(x:y),AF(x:y),t(x:y),LvF(x:y))
%legend('PF','IF','AF','LvF')
```

Spec.m

```
%initialise variables
t=0;
p1=0;
p2=0;
ip=0;
a1=0;
a2=0;

%constants
data1
data2

for g=1:10
%read in data
pressure1
pressure2
ipressure
px1=p1(M*g-M+1:M*g);
px2=p2(M*g-M+1:M*g);
ipx=ip(M*g-M+1:M*g);
df=g*dfinc;
dh=dcl/xfl/df;
dt=1/xfl/C/df;
q=(length(px1));
t=(1:q)*dt;
w=2.0*pi*df;

%obtain incident pulse frequency spectrum
ipr=ipx-mean(ipx);
ipr(length(ipr):800000)=0;
iP = fft(ipr,length(ipr));
iPpp = iP.* conj(iP)/length(ipr);
fi = (1.0/dt)*(0:(0.5*length(ipr)))/length(ipr)/1e6;
%figure
%plot(fi,iPpp(1:(0.5*length(ipr)+1)))

%obtain radiated pulse frequency spectrum
pr1=px1-mean(px1);
pr1(length(pr1):800000)=0;
P1 = fft(pr1,length(pr1));
Ppp1 = P1.* conj(P1)/length(pr1);
f = (1.0/dt)*(0:(0.5*length(pr1)))/length(pr1)/1e6;
pr2=px2-mean(px2);
pr2(length(pr2):800000)=0;
P2 = fft(pr2,length(pr2));
Ppp2 = P2.* conj(P2)/length(pr2);

%plot spectra
if g==3
  figure
plot(fi,iPpp(1:(0.5*length(ipr)+1)),f,Ppp1(1:(0.5*length(pr1)+1)))
axis([0,4*df/1e6,0,max(iPpp)*1.05])
end
```

```
%plot spectra normalised with respect to maxima
%figure
%plot(fi,iPpp(1:(0.5*length(ipr)+1))/max(iPpp),f,Ppp(1:(0.5*length(pr)+1))/max(Ppp))
%axis([0,4e5,0,1])

%calculate attenuation coefficient (dB/cm)
%a(g)=10*log10(exp(1))*log(max(iPpp)/max(Ppp))/z/dh/100;

for u=1:length(f)
   if f(u)<=df/.5e6;
   b=u;
   end
   end
b
f(b)
a1(g)=10*log10(exp(1))*log(iPpp(b)/Ppp1(b))/z1/dh/100;
a2(g)=10*log10(exp(1))*log(iPpp(b)/Ppp2(b))/z2/dh/100;

%a1(g)=10*log10(exp(1))*log(max(iPpp)/max(Ppp1))/z1/dh/100;
%a2(g)=10*log10(exp(1))*log(max(iPpp)/max(Ppp2))/z2/dh/100;
end

%figure
%plot(1:10,a1,1:10,a2)
%figure
%plot(a1-a2)

transpose(a1)
transpose(a2)
```

D.ii Investigating the influence of an additional drug containing layer upon CAP behaviour

The presence of an additional viscous layer may be modelled using the equations developed for modelling the behaviour of a CAP surrounded by a cluster of blood cells. In this case the outer layer is modelled as having the properties of the encapsulating shell and the inner layer that of the drug containing fluid.

$$\rho_S\left[R_1\ddot{R}_1\left(1-\frac{R_1}{R_2}\right)+\dot{R}_1^2\left(\frac{3}{2}+\frac{R_1^4}{2R_2^3}-\frac{2R_1}{R_2}\right)\right]+\rho_L\left[R_1\ddot{R}_1\frac{R_1}{R_3}+\dot{R}_1^2\left(\frac{2R_1}{R_3}-\frac{R_1^4}{2R_3^3}\right)\right]$$
$$+\rho_B\left[R_1\ddot{R}_1\left(\frac{R_1}{R_2}-\frac{R_1}{R_3}\right)+\dot{R}_1^2\left(\frac{R_1^4}{2R_3^4}-\frac{2R_1}{R_3}+\frac{2R_1}{R_2}-\frac{R_1^4}{2R_2^4}\right)\right] \qquad (3.44)$$
$$=p_o\left(\frac{R_{o1}}{R_1}\right)^3-\frac{2\sigma_1}{R_1}-\frac{2\sigma_2}{R_2}-\frac{2\sigma_3}{R_3}-p_\infty(t)-\frac{4\mu_L R_1^2\dot{R}_1}{R_3^3}$$

$$-4R_1^2\left(\frac{V_D}{R_2^3R_1^3}\right)\left(G_D(R_1-R_{1e})+\mu_D\dot{R}_1\right)-4R_1^2\left(\frac{V_S}{R_2^3R_3^3}\right)\left(G_S(R_1-R_{1e})+\mu_S\dot{R}_1\right)$$

Parameters for Albunex® were used for the encapsulating shell, the surrounding fluid was taken to be plasma and the drug containing layer was treated as a Newtonian viscous fluid having properties similar to those of light oil (table Dii.1).

	Parameter	Symbol	Value	Unit
Drug layer	Density	ρ_D	1050	kgm^{-3}
	Viscosity	μ_D	0.1	Pas
	Thickness	d_D	50	nm
Liquid (plasma)	Density	ρ_L	1030	kgm^{-3}
	Viscosity	μ_L	0.0015	Pas
	Surface tension	σ_1	0.04	Nm^{-1}
Shell	Shear modulus	G_S	88.8	MPa
	Density	ρ_S	1100	kgm-3
	Viscosity	μ_S	1.77	Pas
	Thickness	d_S	15	nm

Table Dii.1: Parameter values used in the simulations.

The results are shown in figure Dii.1.

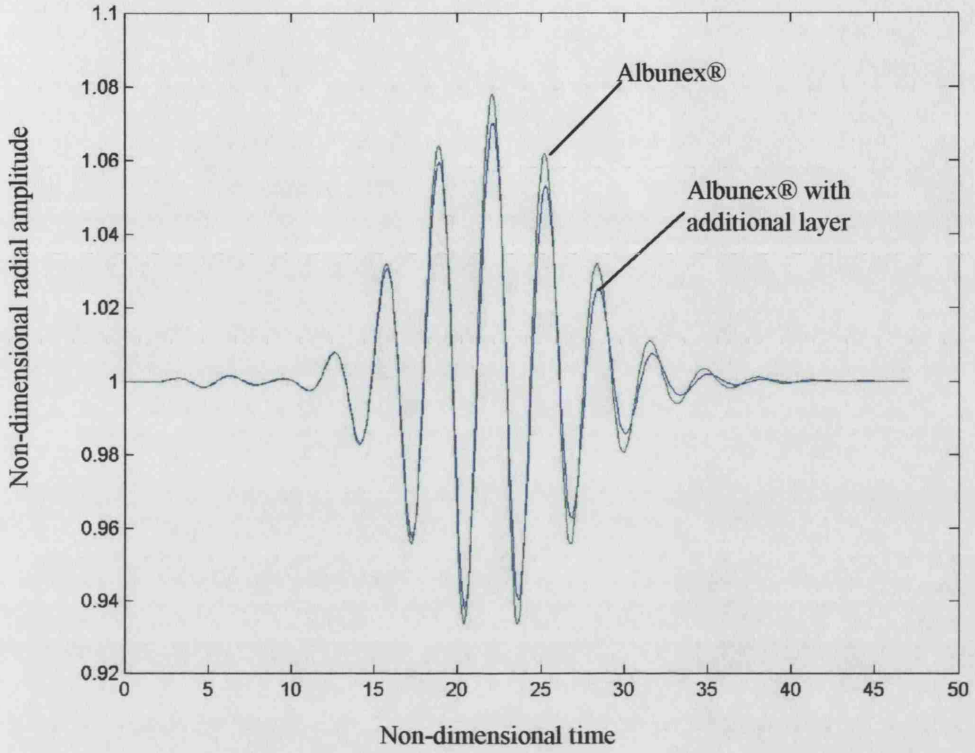

Figure Dii.1: Radial amplitude of oscillation for an Albunex® CAP with and without an inner viscous layer.

The results demonstrate, as might be expected, that CAP oscillations experience increased damping compared with normal Albunex® CAPs and hence have smaller amplitudes for a given insonation pressure. This would also give rise to increased heating due to viscous dissipation as discussed in Appendix D.iii.

D.iii Contrast enhanced heating

Diii.1 Overview

In Chapter 5, the possibility of designing contrast agents to enhance their acoustic response for diagnostic applications was examined. It was noted, however, that, in addition to improving CAP performance, it is important to consider their potential for causing harmful bio-effects. The main focus of previous investigations of CAP safety has been their ability to initiate inertial cavitation (c.f. e.g. Nyborg 2001), but there are a number of other mechanisms by which CAPs may cause damage. These include cell rupture, due to the shear stresses produced by micro-streaming currents around oscillating CAPs, and enhanced heating of the surroundings. The aim of this appendix is to investigate the significance of the latter theoretically, and to discuss the implications for the validity of existing safety guidelines and potential therapeutic applications.

Diii.2 Theory

Diii.2.1 Background

One of the concerns regarding the use of ultrasound contrast agents is the fact that they may produce a temperature rise in their surroundings (Mornstein 1997). There are three mechanisms responsible for this rise: (i) conduction of heat from the filling gas during CAP compression, (ii) absorption of the ultrasound field radiated by the bubbles and (iii) viscous dissipation in the shell and the surrounding fluid. On account of their greater potential for undergoing inertial cavitation, previous assessments of contrast agent safety have concentrated on the behaviour of free, unencapsulated bubbles (e.g. Hilgenfeldt *et al* 2000). These analyses have concluded that the primary mechanism for heating is radiation absorption and that the resulting temperature rise would be significant only at very high insonation pressures, outside the typical diagnostic range.

However, whilst the heating effect due to conduction has been shown to be small (Appendix B.i), the results of the sensitivity study described in Chapter 5 indicate that viscous dissipation is much more significant for a CAP compared with a free bubble. This is due to the fact that the viscosity of the shell may be much greater than that of the surrounding fluid. The validity of using a free bubble model to assess

heating risk must therefore be questioned and the aim of this section is to estimate the temperature rise produced in the fluid surrounding a CAP under typical diagnostic conditions.

Diii.2.2 Analysis

In the absence of accurate values for the shell parameters, it was only possible to make an approximate comparison between the heating effects produced by a CAP and a free bubble. The form of equation 3.15 used for the sensitivity analysis was therefore considered to be adequate to obtain the response of the CAP.

$$R_1\ddot{R}_1\left(1+\left(\frac{\rho_L-\rho_S}{\rho_S}\right)\frac{R_1}{R_2}\right)+\dot{R}_1^2\left(\frac{3}{2}+\left(\frac{\rho_L-\rho_S}{\rho_S}\right)\left(\frac{4R_2^3-R_1^3}{2R_2^3}\right)\frac{R_1}{R_2}\right)$$
$$=\frac{1}{\rho_S}\left(\begin{array}{l} p_o\left(\frac{R_1}{R_2}\right)^3-p_o-p_A Sin(\omega t)-\frac{2\sigma_1}{R_1}-\frac{2\sigma_2}{R_2} \\ -\frac{4\mu_L R_1^2\dot{R}_1}{R_2^3}-\frac{4V_S G_S}{R_2^3}\left(1-\frac{R_{1e}}{R_1}\right)-\frac{4\mu_S V_S\dot{R}_1}{R_1R_2^3}\end{array}\right) \qquad (5.6)$$

The heating effect was then estimated as follows: For a Newtonian fluid of viscosity μ_L, the instantaneous power dissipated as a result of viscosity is given by

$$P_{vis}=-2\mu_L\frac{\partial u}{\partial r}\times 4\pi r^2\times u=\frac{-4\mu_L\dot{R}_1R_1^2}{r^3}\times 4\pi r^2\times\frac{\dot{R}_1R_1^2}{r^2}. \qquad \text{(Diii.1)}$$

The derivative with respect to the radial direction r is

$$\frac{\partial P_{vis}}{\partial r}=\frac{-48\pi\mu_L\dot{R}_1^2R_1^4}{r^4}. \qquad \text{(Diii.2)}$$

Thus the power dissipated in the shell of the CAP is given by

$$P_{S,vis}=\int_{R_1}^{R_2}\frac{-48\pi\mu_S\dot{R}_1^2R_1^4}{r^4}dr=\frac{16\pi\mu_S V_S\dot{R}_1^2R_1}{R_2^3}dr \qquad \text{(Diii.3)}$$

and in the surrounding liquid by

$$P_{L,vis}=\int_{R_2}^{\infty}\frac{-48\pi\mu_L\dot{R}_1^2R_1^4}{r^4}dr=\frac{16\pi\mu_L\dot{R}_1^2R_1^4}{R_2^3}dr \qquad \text{(Diii.4)}$$

Over the course of a pulse of length t_p the total energy dissipated is given by

$$E_{vis} = \int_0^{t_p} \left(P_{S,vis} + P_{L,vis}\right) dt = 16\pi \int_0^{t_p} \frac{\dot{R}_1^2 R_1}{R_2^3} \left(\mu_S V_S + \mu_L R_1^3\right) dt \qquad \text{(Diii.5)}$$

The resulting temperature rise (ΔT) at time t and radius r in the liquid may be estimated by considering the heat to be concentrated close to the shell and released only after oscillation has ceased, i.e. treating the CAP as a heat source. This is justifiable since the distance travelled by the temperature pulse in the surrounding fluid over a typical pulse length would be small compared with the CAP radius (≈ 0.3 μm for thermal diffusivity in plasma η_L = 1.4 x 10^{-7} m^2s^{-1}). On the other hand this distance is large compared with the shell thickness (≈15 nm). Thus it is practical, if mathematically somewhat inelegant, to assume that the temperature change in the shell would be negligible.

Under these conditions, solving the equation for heat conduction (Stroud 1996) in spherical polar coordinates

$$\frac{\partial T(r,t)}{\partial r} = \sqrt{\eta} \nabla^2 T(r,t) \qquad \text{(Diii.6)}$$

gives in the liquid

$$\Delta T(r,t) = \frac{E_{vis\,or\,scat}}{8\pi^{1.5} b_{pL} \rho_L R_{o1} \sqrt{\eta_L t}} \frac{1}{r} \left[\exp\left(-\frac{(r - R_{o1})^2}{4\eta_L t} \right) - \exp\left(-\frac{(r + R_{o1})^2}{4\eta_L t} \right) \right] \qquad \text{(Diii.7)}$$

The temperature rise due to absorption of the outgoing wave will also primarily affect the surrounding fluid, rather than the shell, because the shell thickness is too small for it to absorb a significant amount of energy. Also, if the CAP is considered to behave as a source of sound, the wave should not in fact travel through the shell at all. Hilgenfeldt *et al*'s analysis for free bubbles may therefore be applied to give an estimate of the maximum heating effect due to linear propagation of the radiated sound from a CAP, as follows:

The time for the wave to propagate outwards to radius r is $r/c_l \approx 1$ ns for a distance of 1 μm in water. During this time a temperature profile will be set up in the fluid given by

$$\Delta T(r,0) = \frac{E}{r^2 b_{pL} \rho_L c_L} \int_{-\infty}^{+\infty} a(\omega) |p_s(\omega)|^2 e^{-a(\omega)r} d\omega \qquad \text{(Diii.8)}$$

Due to its dependency upon r^2, the temperature rise will only be significant close to the CAP. Moreover, the diffusion time will be much greater than either the wave propagation time or the time over which the CAP oscillates ($r^2/D_L = 10$ μs compared with $r/c_l = 1$ ns or $2\pi/\omega = 0.1$ μs). All of the heat generated during oscillation may therefore be considered as spreading out from the CAP wall, after oscillation has ceased. The resulting temperature rise may then be found using equation Diii.7 as before where

$$E_{scat}(r) = \int_{R_2}^{r} dr \int_{-\infty}^{+\infty} \frac{4\pi a(\omega) |p_s(\omega)|^2 e^{-a(\omega)r}}{\rho_L c_L} d\omega \qquad \text{(Diii.9)}$$

Additional heating might be expected to occur due to non-linear propagation of the radiated field and subsequent absorption. However, this was neglected since relatively low insonation pressures were being considered. Hence, as explained in Chapters 2 and 3 the harmonic content of the signal would not become significant until the wave had propagated several centimetres from the CAP wall, whereas it was the temperature changes in the immediate vicinity of the CAP which were of interest in this investigation.

Diii.2.3. Calculations

Once again, equation 5.6 was non-dimensionalised and solved, as described in Chapter 3, using the properties for Albunex®, Optison® and plasma. When calculating the results for a free bubble, the shell parameters G_S and μ_S were set to zero, $\rho_L = \rho_S$ and $R_1 = R_2$ to obtain the RPNNP equation (equation 2.2). The results from these simulations were used to estimate the changes in temperature in the surrounding fluid using equations Diii.5 and Diii.7. These were also implemented numerically using purpose written code (Appendix D.iv) in Matlab® (The Mathworks, Natick, MA) to enable contour plots to be produced.

The form of the incident field was again based on equation 3.45. Results were obtained for pulse repetition frequencies between 4 and 30 kHz, insonation pressures between 30 and 200 kPa and pulse centre frequencies between 1 and 10 MHz to cover a range of diagnostic conditions.

$$p_{inc}(t) = p_A\left(1-\cos\left(\frac{\omega t}{m}\right)\right)\left(1-\sin\left(\frac{\omega t}{m}\right)\right)\cos(\omega t)\sin(\omega t) \qquad (3.45)$$

In calculating the temperature rise, both single CAPs and CAP populations were considered. In the latter, a CAP distribution based on a concentration of 10^8 CAPs/ml and a blood vessel diameter of 50 μm was considered (figure Diii.1). This was only intended to provide a first order estimate of heating in a CAP population, however. Blood vessel diameters may vary from 10 μm to 50 mm (Guyton & Hall 2000) and whilst the initial injected CAP concentrations are 10^8 – 10^9 CAPs/ml, (Becher & Burns 2002) the mechanisms for contrast agent dilution in the body are not clear at present.

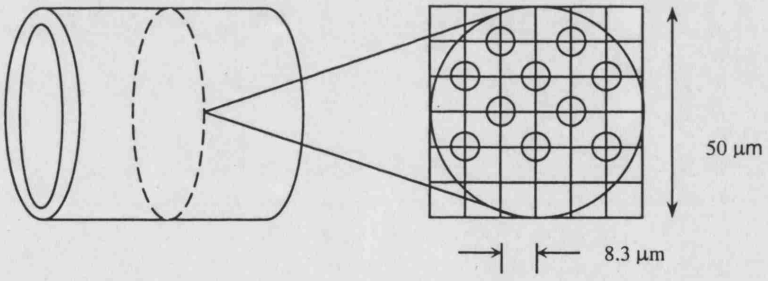

Figure Diii.1: Model used to calculate temperature rise generated within a CAP population.

When calculating the heating effect due to multiple pulses, it was necessary to take in to account the motion of the CAP along the blood vessel[1]. In order to do this, it was assumed that the CAP would travel in a straight line, parallel to the axis of the vessel with a velocity equal to that of the surrounding blood. The latter was obtained from blood flow data (Guyton & Hall 1990) for vessels of the diameters considered above (approx. 5 x 10^{-4} ms^{-1}). The variation in temperature over a plane through the blood vessel (figure Diii.2) was then found at 2 μm intervals for various times during

[1] Since relatively large vessels were being considered it was invalid to consider the potentially worse case of a trapped CAP.

insonation. In accordance with the assumptions made above regarding the heating of the surrounding fluid, it was assumed that the CAP could be regarded as stationary at the point at which the energy was released after each pulse.

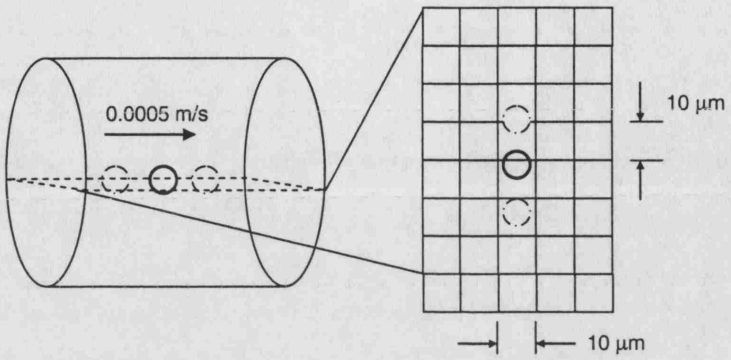

Figure Diii.2: Model used to calculate temperature rise generated by CAP oscillation over a series of pulses.

Diii.2.4. Results

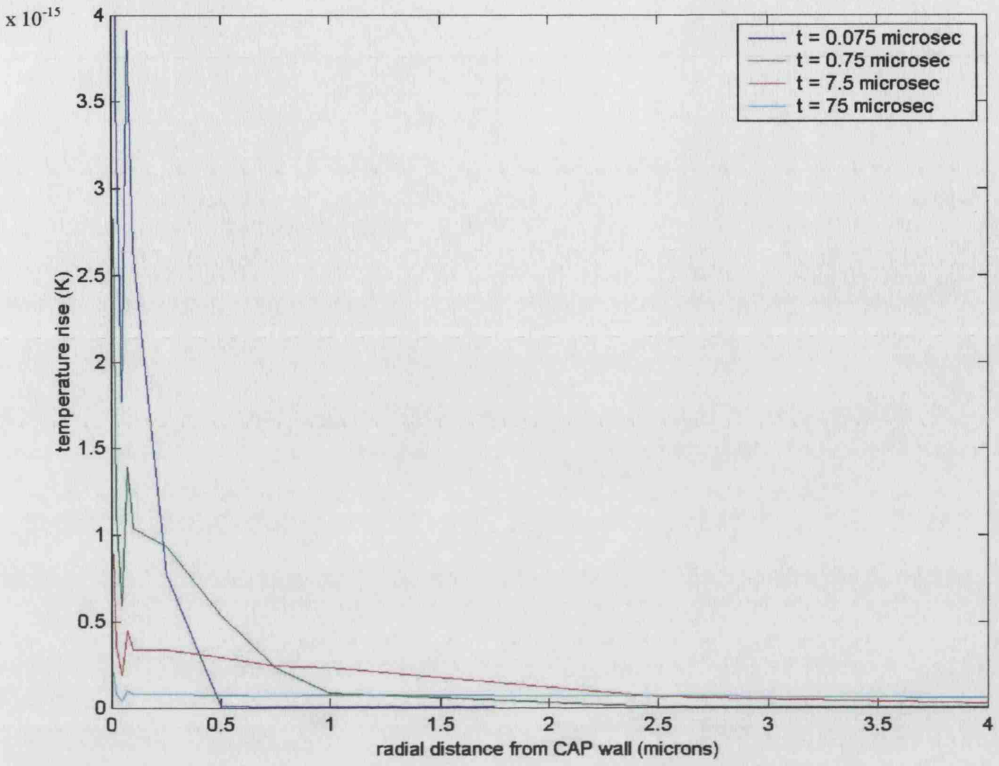

Figure Diii.3: Change in temperature in the water surrounding a CAP insonified by a single pulse of 3 MHz, 0.1 MPa due to acoustic radiation at different times, t, after the end of the pulse.

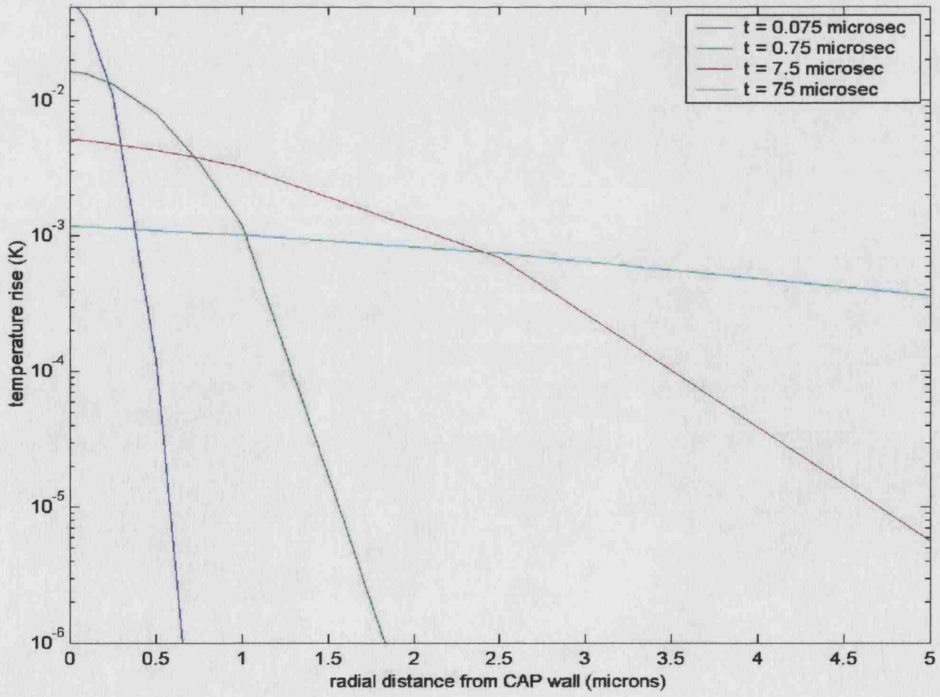

Figure Diii.4: Change in temperature in the water surrounding a CAP insonified by a single pulse of 3 MHz, 0.1 MPa due to viscous dissipation at different times, t, after the end of the pulse.

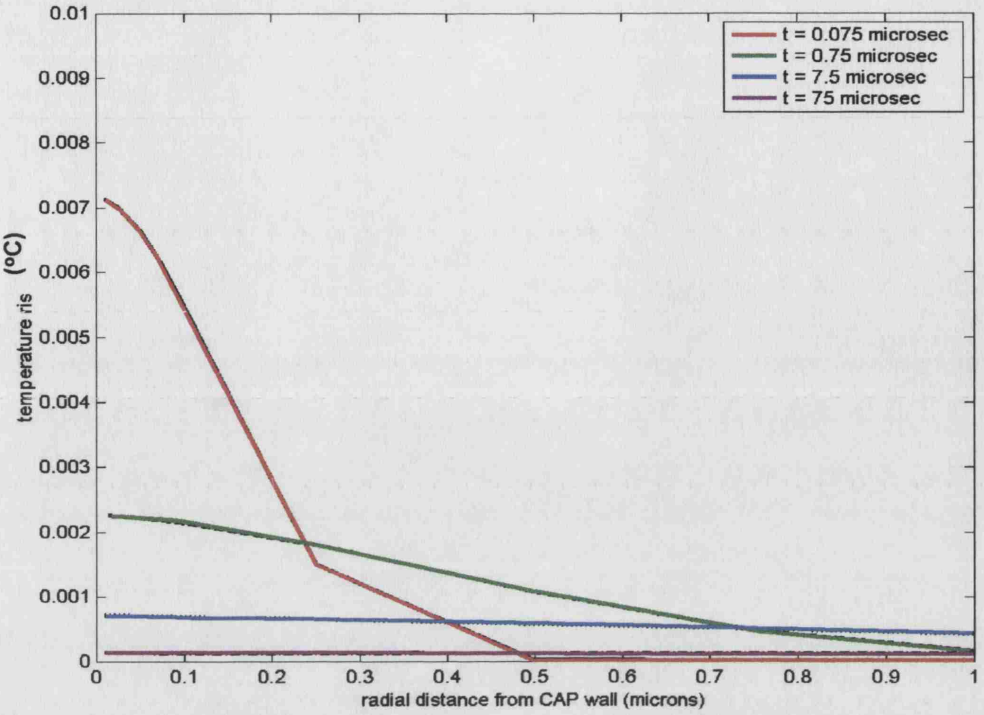

Figure Diii.5: Change in temperature in the water surrounding a free bubble insonified by a single pulse of 3 MHz, 0.2 MPa due to viscous dissipation at different times, t, after the end of the pulse.

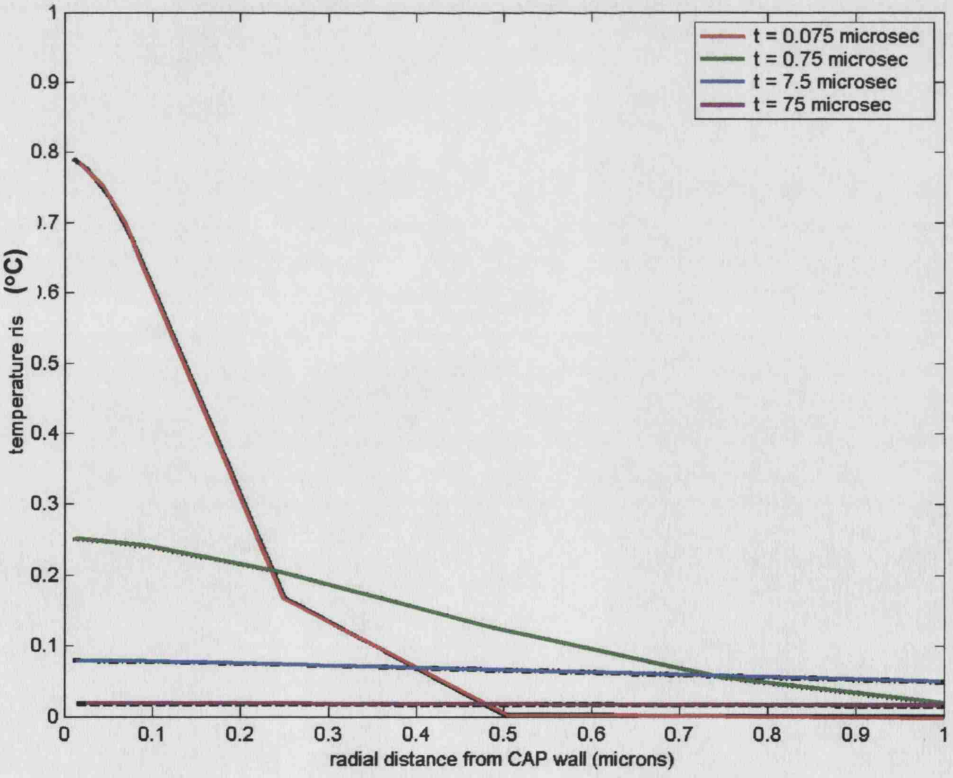

Figure Diii.6: Change in temperature in the water surrounding a CAP insonified by a single pulse of 3 MHz, 0.2 MPa due to viscous dissipation at different times, t, after the end of the pulse.

Figure Diii.7a: Temperature rise in water surrounding an Albunex® CAP insonified by 5 pulses of 3 MHz, 0.1 MPa at a pulse repetition frequency of 30 kHz.

ai) after 0.075 ms

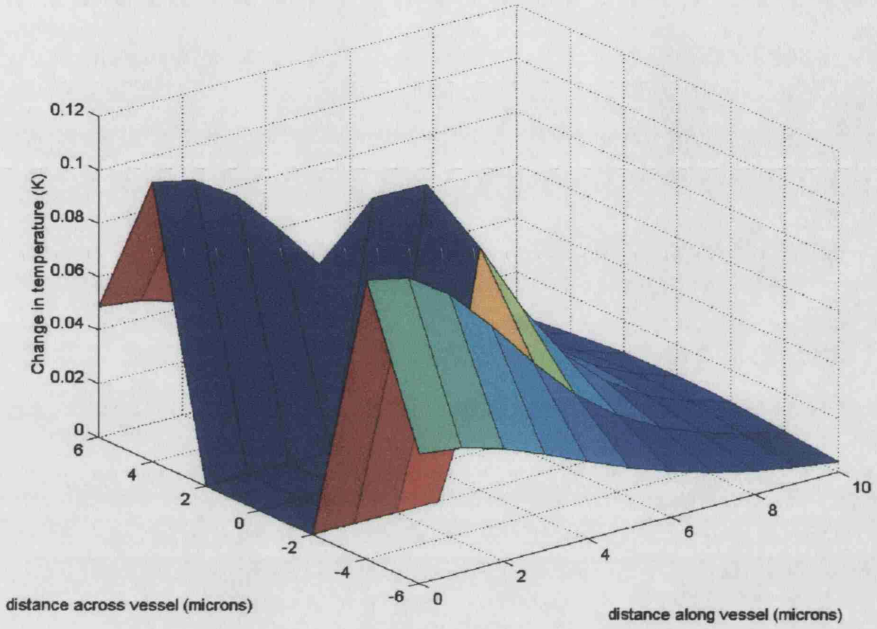

aii) after 0. 75 ms

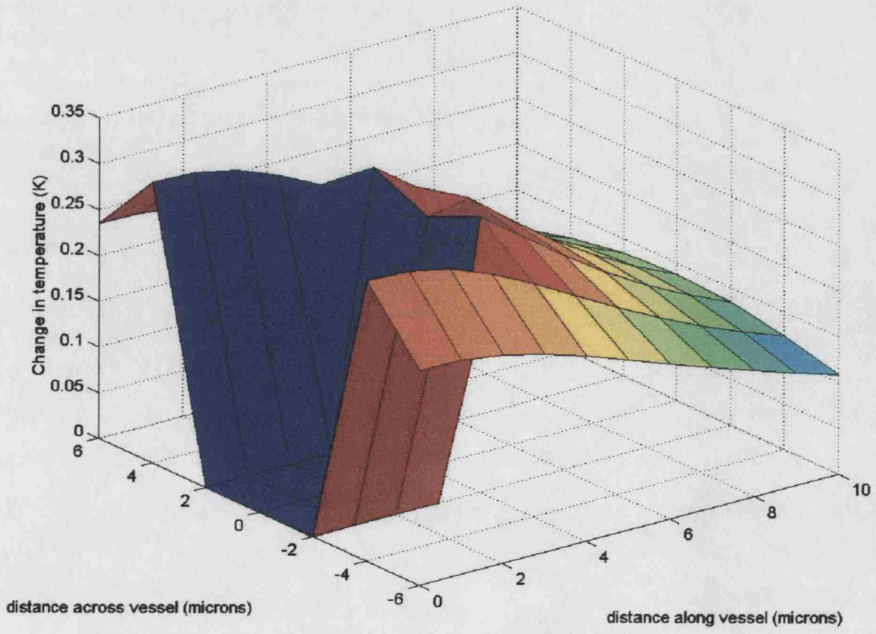

aiii) after 7.5 ms

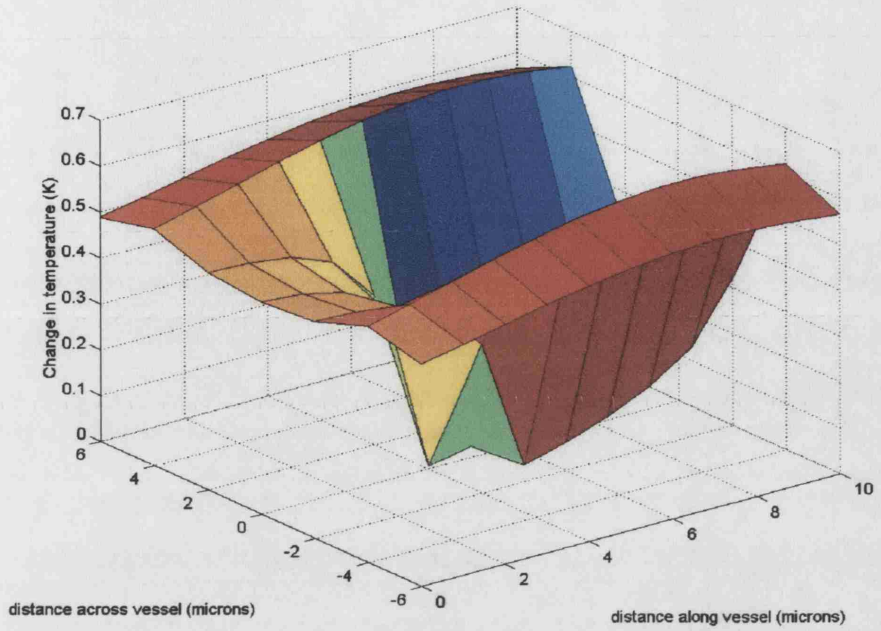

aiv) after 11.25 ms

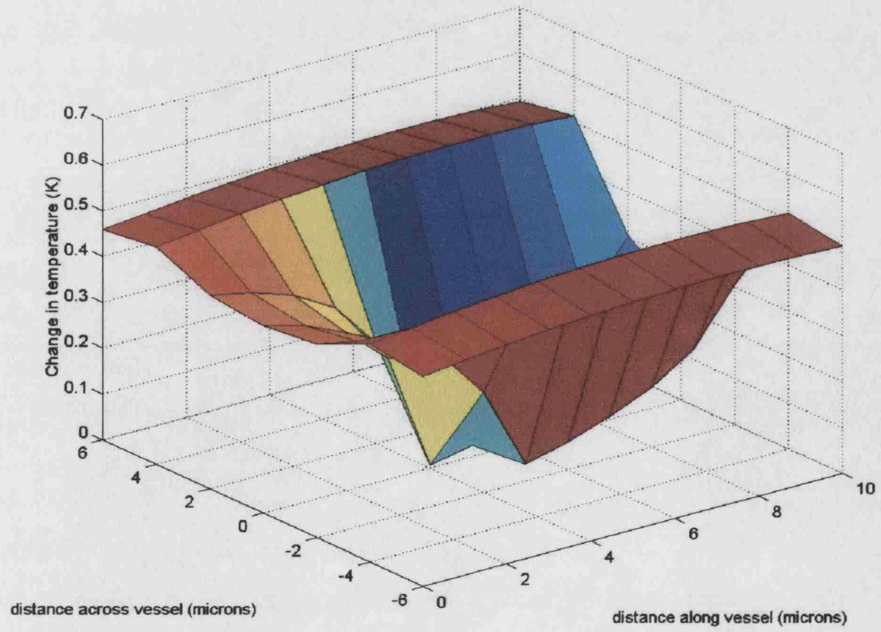

av) after 15 ms

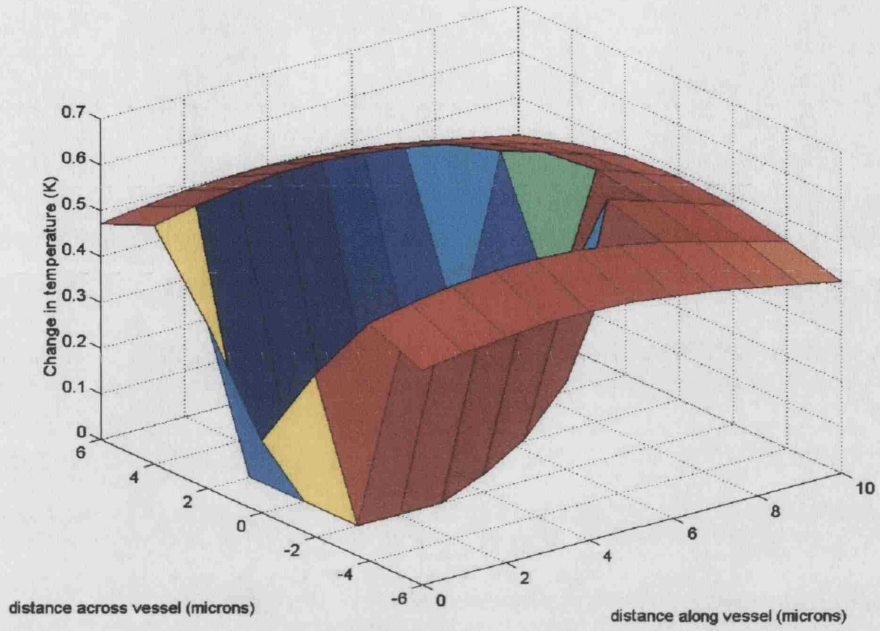

avi) after 15.1 ms

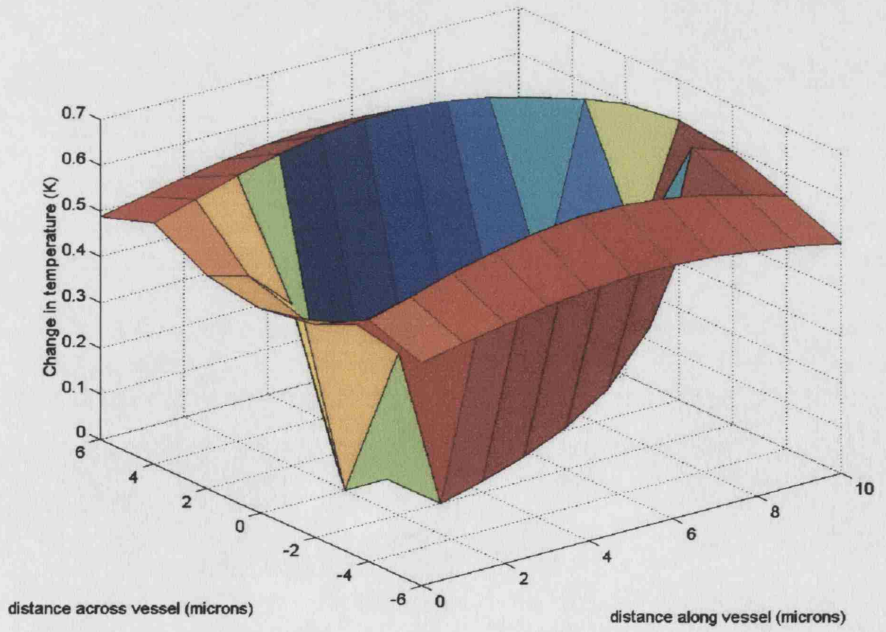

Figure Diii.7b: Temperature rise in water surrounding an Optison® CAP insonified by 5 pulses of 3 MHz, 0.1 MPa at a pulse repetition frequency of 10 kHz.

ai) after 0.075 ms

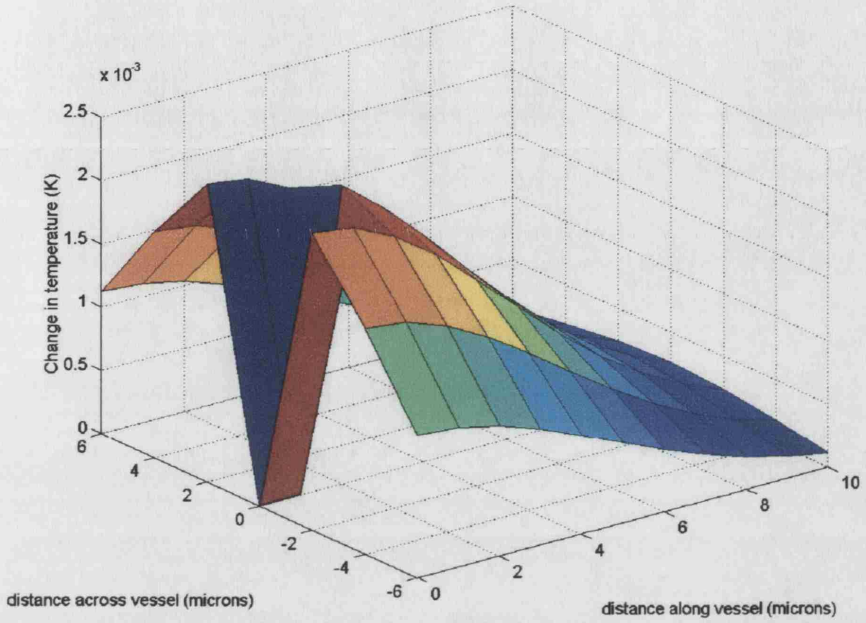

aii) after 0. 75 ms

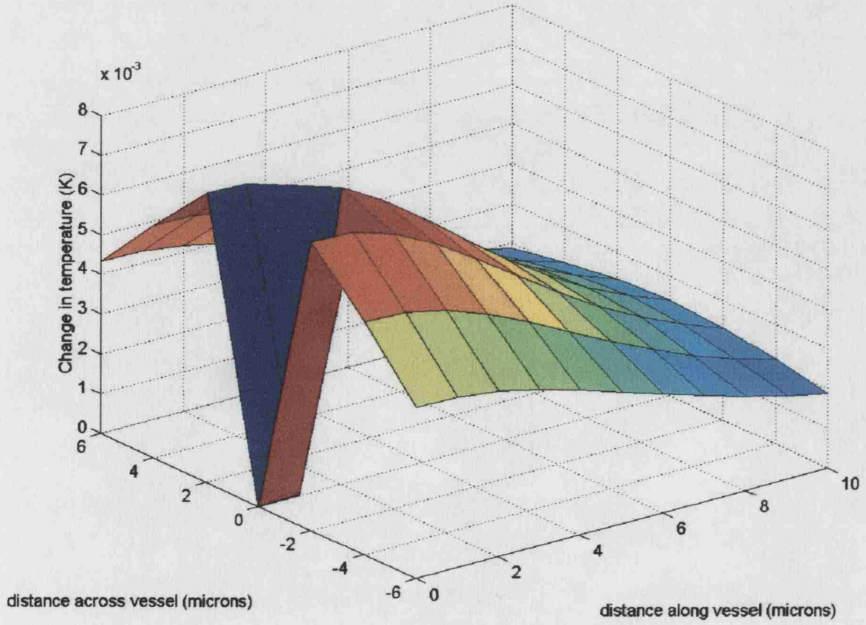

aiii) after 7.5 ms

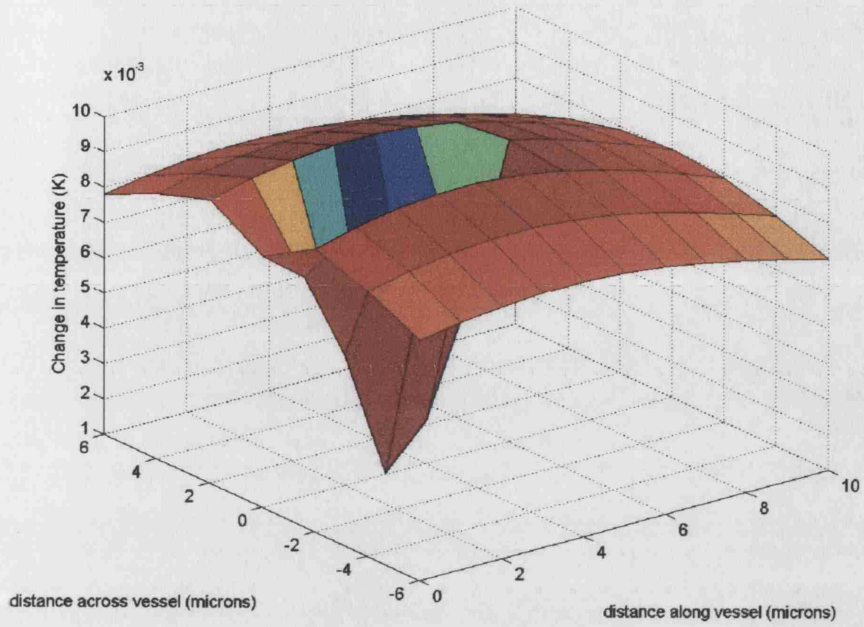

aiv) after 11.25 ms

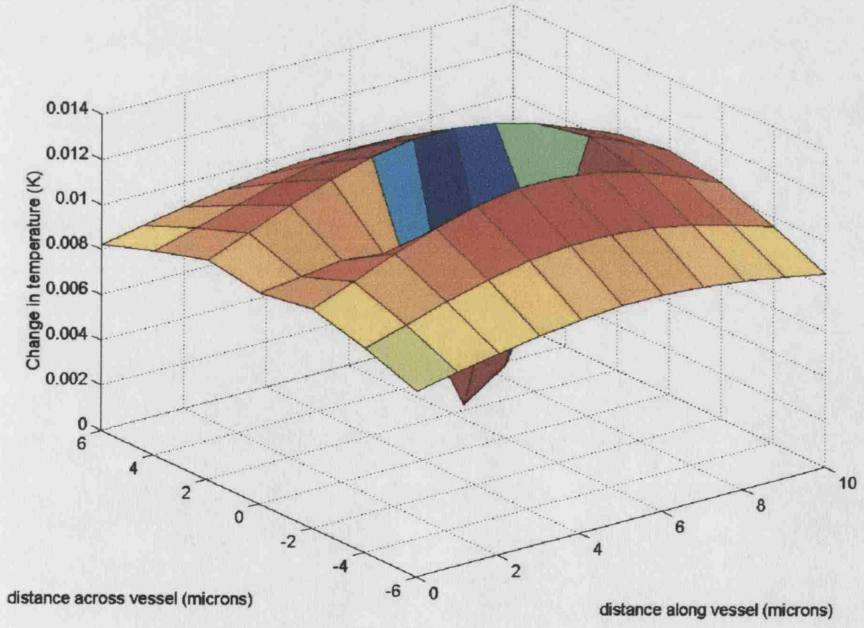

av) after 15 ms

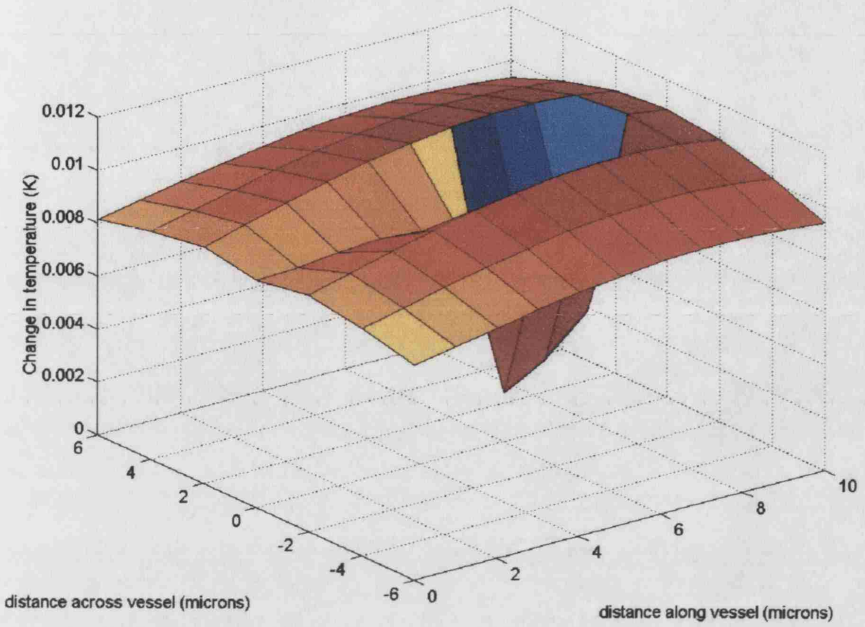

avi) after 15.1 ms

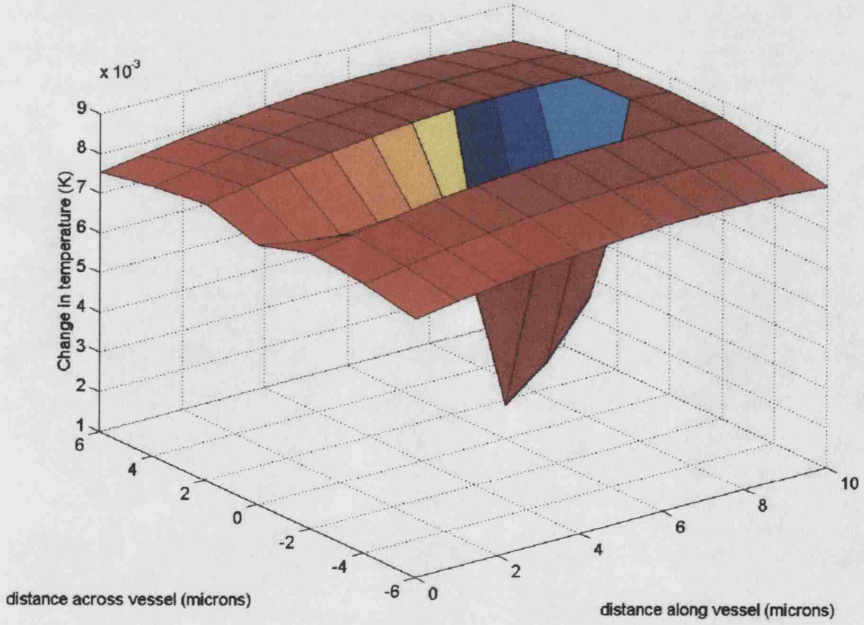

Figure Diii.8: Temperature rise in fluid surrounding a population of 10 Albunex® CAPs insonified by a single pulse of 3 MHz, 0.1 MPa.

i) after 0.1 μs

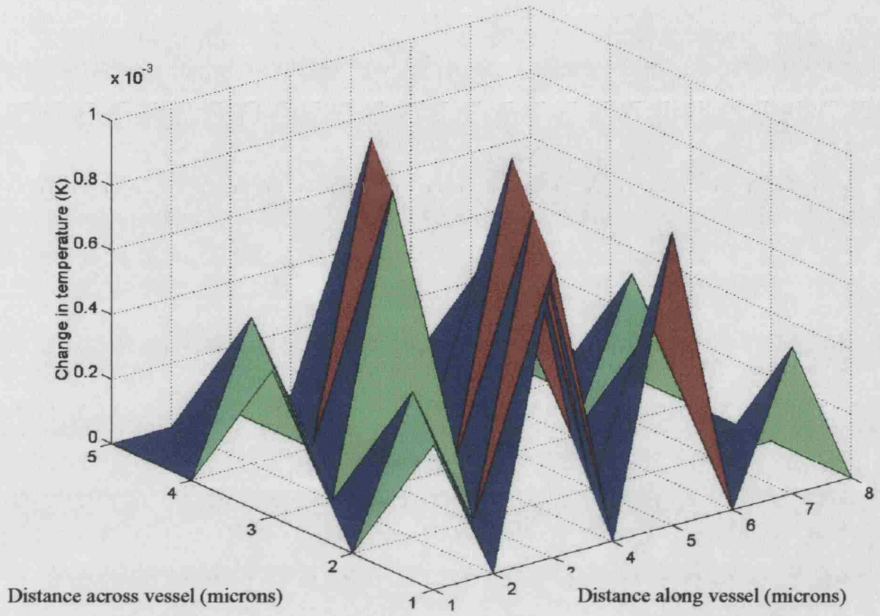

ii) after 1 μs

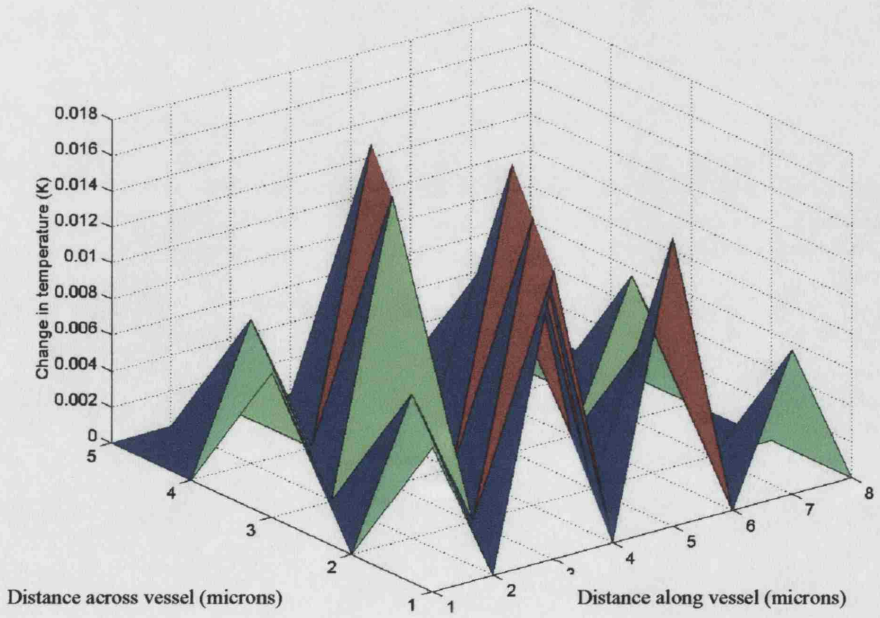

iii) after 10 μs

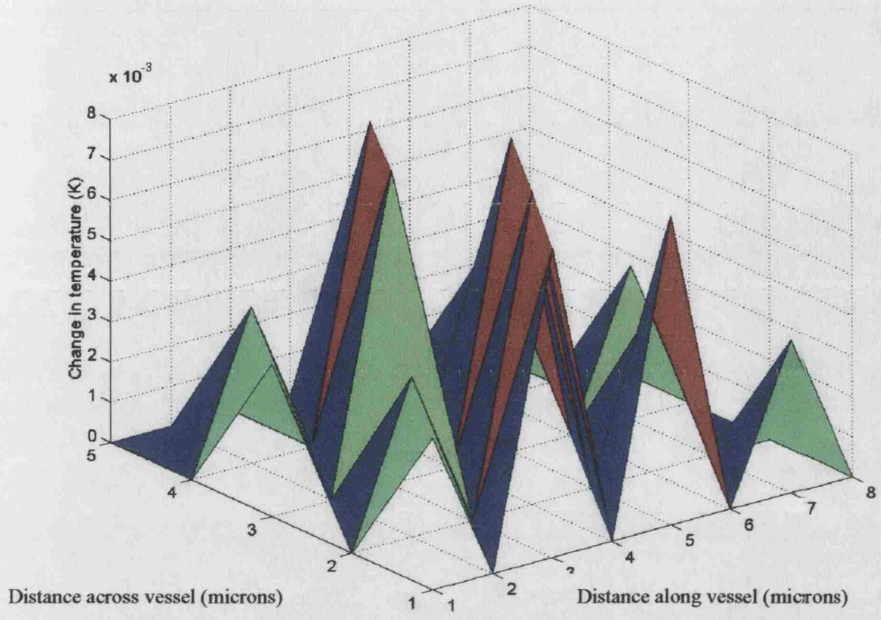

iv) after 100 μs

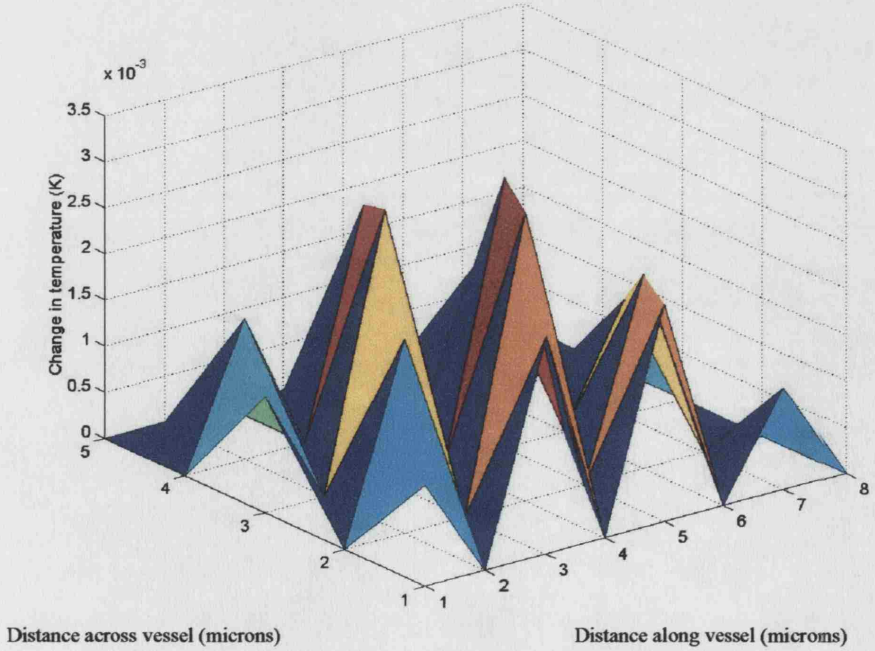

Diii.2.5 Discussion

The conclusion that there should be negligible heating of the surrounding fluid as a result of conduction has already been explained in Chapter 3. It has likewise been argued that the temperature of the shell should remain constant throughout CAP oscillation. Figure Diii.3 indicates that there would be some heating of the surrounding fluid due to absorption of the radiated ultrasound but that this would be very small compared with the heating due to viscous dissipation shown in figure Diii.4. This concurs with the fact that viscosity is the dominant damping mechanism. Qualitatively, the results discussed so far may be summarised as shown in table Diii.1.

		Effect upon		
Effect of		CAP Dynamics	Shell heating	Fluid heating
Conduction		*Negligible*	*Negligible*	*Negligible*
Viscous dissipation		*Significant*	*Negligible*	*Moderate*
Acoustic radiation		*Negligible*	*Negligible*	*Negligible*

Table Diii.1: Summary of the relative significance of the different CAP damping mechanisms.

Figures Diii.4 and Diii.5 clearly demonstrate that there is a significant difference in the temperature rise predicted for the CAP and the free bubble for identical insonation conditions. Even allowing for the fact that the CAP is oscillating close to its resonance frequency, whilst the free bubble of the same diameter is outside its resonant range, the difference is still considerable[2].

Notwithstanding the relative size of the temperature rises, in absolute terms the temperature rise produced by insonation of a CAP with a single pulse is still fairly small (< 1°C) and decays very rapidly, in both space and time. When the more realistic situation of a train of pulses is considered, however, a larger, more persistent heating effect is observed, as shown in figure Diii.7. This is due to the relatively low speed of CAP travel compared with typical pulse repetition frequencies (PRFs) and the consequent compounding of the temperature fields produced by each pulse. The results shown in figure Diii.7 (b) are for a PRF which is fairly high compared with those used for typical imaging procedures, but by no means unrealistic.

[2] It is in fact more appropriate to compare the CAP and bubble in this way rather than at their individual resonance frequencies, since it is the response under diagnostic conditions which is of interest and one of the aims of the work is to examine the validity of using free bubble models for assessment of CAP safety.

Similarly, increasing the CAP concentration was seen to increase the uniformity of the temperature rise across the region considered and to lead to further compounding of the fields of individual CAPs. However, even at the maximum recommended concentrations, the average CAP spacing (10-25 μm for 10^8-10^9 CAPs/ml) would be too large for this to be significant compared with the effect of increasing the pulse repetition frequency. This is demonstrated in figure Diii.8. Moreover, as shown in Chapters 3 and 4, at these concentrations multiple scattering effects would be expected. This could result in certain parts of the population being shielded from insonation and thus in localisation of the heating effect. It might have been possible to use the new model derived in Chapter 3 (equation 3.66) to investigate this. However, the modifications suggested in Chapter 3 would have had to have been implemented to enable the high concentrations to be modelled and, in addition, the acoustic velocity, c_L, would have become a function of direction which would have further complicated the analysis.

As would be expected, the temperature rise due to viscous dissipation was found to be largest when the insonation frequency was close to that of CAP resonance (figure Diii.3), i.e. when radial amplitude and velocity were maximised. Increasing the pulse peak pressure was also found to increase the amplitude and velocity of CAP oscillations and hence the amount of energy dissipated (figure Diii.6). As discussed in Chapter 3, shell disruption would be expected to occur above a certain pressure, at which point it would no longer be valid to predict viscous heating using the model presented above. The insonation pressures used in this study, however, were limited to those within the range identified in Chapter 3 as non-destructive.

The heating effect is potentially important for two reasons. Firstly, heating of the surrounding fluid may alter the fluid properties and hence the behaviour of the CAP. Secondly, the temperature rise might damage the surrounding tissue. This could be desirable or undesirable according to the application but in either case the effect should be accurately characterised. Simulations indicate that the heating of the fluid would have a relatively small effect upon CAP dynamics. For example, figure Diii.9 shows the changes in CAP response corresponding to a rise in fluid temperature of 100 K and the corresponding changes in viscosity and density.

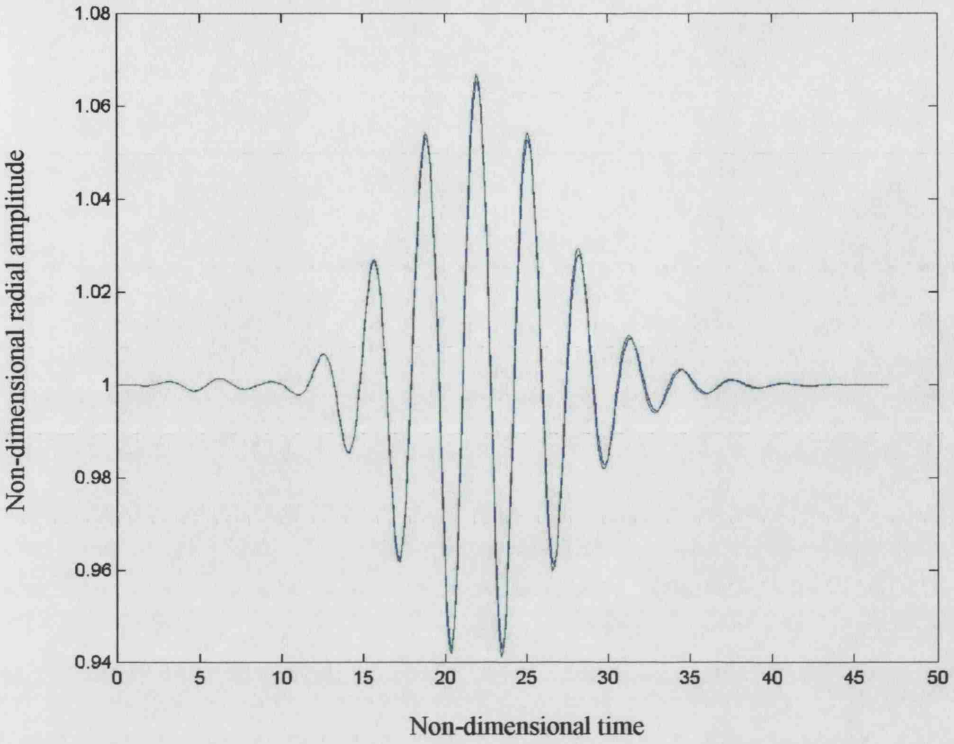

Figure Diii.9: Variation in radial displacement of a CAP insonified by a single pulse of 3 MHz, 0.1 MPa at 293 K (dashed) and 373 K (solid).

As shown in figures Diii.4-Diii.6, the actual temperature rise would decay rapidly with both time and distance from the CAP, so that the change in CAP response would be even smaller.

In terms of the risk posed to patients, the significance of underestimating the temperature rise produced by a CAP by using an inappropriate model is difficult to assess. According to radiological guidelines, (e.g. WFUMB 1998), a rise of 4 °C sustained for more than 30 seconds is considered to be potentially damaging. The temperature rises predicted here are of this order of magnitude and may, in theory, persist sufficiently between pulses to produce a sustained heating effect. However, some clarification regarding the mechanisms of thermal damage is needed before any useful conclusions may be drawn. For example, it is unclear whether it is the rate or the total amount of energy absorbed which is more significant. Moreover, as suggested by Hilgenfeldt *et al* (2000) in their work on free bubbles, there may be some additional factors such as convective cooling which might alleviate conditions inside the body.

If further study does indicate that CAPs produce significant temperature rises under diagnostic conditions which are currently considered "safe," then it may be necessary to review existing radiological guidelines. The heating effect may also need to be taken into account in selecting appropriate materials for CAP shells, both to avoid excessive temperature rises and to increase the efficiency of the CAPs. The larger the ratio of reradiated to dissipated energy, the more efficient the CAP. Alternatively, it may be appropriate to select shells having very large viscosities, if the heating effect is, in fact, desirable. For example, it might be possible to use CAPs in therapeutic applications such as HIFU (high intensity focused ultrasound) to enhance the localised heating of e.g. cancerous tissue.

D.iv Investigating the influence of thermal damping upon CAP behaviour

This appendix contains listings for the following programs

eac.m	Matlab® code implementing equations 6.7 and 6.9 for a single CAP
evis.m	Matlab® code implementing equations 6.5 and 6.7 for a single CAP
mevis.m	Matlab® code implementing equations 6.5 and 6.7 for multiple CAPs
pevis.m	Matlab® code implementing equations 6.5 and 6.7 for multiple pulses

eac.m

```
%get data
data
time
pressure

dTinf=293;              %ambient temperature
dDl=1.4e-7;             %liquid thermal diffusivity
dCpl=4190;              %liquid specific heat
da=[1e-8;2.5e-8;5e-8;7.5e-8;1e-7;2.5e-7;5e-7;7.5e-7;1e-6;2.5e-6;5e-6;7.5e-6;1e-
5;2.5e-5;5e-5;7.5e-5]; %radial interval
dtt=[1e-8;2.5e-8;5e-8;7.5e-8;1e-7;2.5e-7;5e-7;7.5e-7;1e-6;2.5e-6;5e-6;7.5e-6;1e-
5;2.5e-5;5e-5;7.5e-5];                %radial interval
dao=3.8;
bo=1.5;

%non dimensionalise
drol=drol*1e-6;
w=2.0*pi*df;
h=1e-6*dh*w;
cl=dcl/(w*drol);
rhol=drhol*drol^2.0*w^2.0/dpo;
mul=dmul*w/dpo;
s1=dsigma1/(dpo*drol);
s2=dsigma2/(dpo*drol);
pa=damp/dpo;
rol=drol/drol;
a=da/drol;
tt=dtt*w;
Cpl=dCpl*dTinf/(w*drol)^2.0;
Dl=dDl/(w*drol^2.0);
ao=dao*drol;

pr=p-mean(p);
P = fft(pr,length(pr));
Ppp = P.* conj(P) /length(pr);
f = (1.0/h)*(0:(0.5*length(pr)))/length(pr);
%figure
%plot(f,Ppp(1:(0.5*length(pr)+1)))

ps=abs(P);
ps2=ps.*ps;

for z=1:length(tt)
    for j=1:length(a)
        for i=1:length(f)
        x(i)=(1.0/exp(rol*ao*(1e-6*f(i))^bo)-1.0/exp((a(j)+rol)*ao*(1e-
6*f(i))^bo))*ps2(i);
        end
    ea=4*pi*trapz(f,x)/(rhol*cl);
    dT(j,z)=ea*(exp((-1.0)*a(j)^2.0/(4.0*Dl*tt(z)))-exp((-
1.0)*(a(j)+2*rol)^2.0/(4.0*Dl*tt(z))))/(8.0*pi^(3.0/2.0)*Cpl*rhol*sqrt(Dl*tt(z))*rol*
a(j));
    end
end

figure
plot(a*drol*1e6,dT(4,:)*dTinf,a*drol*1e6,dT(8,:)*dTinf,a*drol*1e6,dT(12,:)*dTinf,a*dr
ol*1e6,dT(16,:)*dTinf)
title('Temporal variation in surrounding fluid temperature for a CAP insonated with
one pulse of 3 MHz 0.1 MPa');
legend('a = 0.075 microns','a = 0.75 microns','a = 7.5 microns','a = 75 microns');
xlabel('time (microsecs)');
ylabel('temperature rise (K)');
```

```
%axis([0,15,0,.5]);
figure
plot(tt*1e6/w,dT(:,4)*dTinf,tt*1e6/w,dT(:,8)*dTinf,tt*1e6/w,dT(:,12)*dTinf,tt*1e6/w,d
T(:,16)*dTinf)
%axis([0,3,0,.5])
title('Radial variation in surrounding fluid temperature for a CAP insonated with one
pulse of 3 MHz 0.1 MPa')
legend('t = 0.075 microsec','t = 0.75 microsec','t = 7.5 microsec','t = 75 microsec')
xlabel('radial distance from CAP wall (microns)')
ylabel('temperature rise (K)');
```

evis.m

```
%get data
%cd d:\eleanor\bubbles_work
data
time
radius
velocity
pressure
ipressure

dTinf=293;              %ambient temperature
dao=3.8;                %attenuation coefficient
dDl=1.4e-7;             %liquid thermal diffusivity
dCpl=4190;              %liquid specific heat
da=[1e-8;2.5e-8;5e-8;7.5e-8;1e-7;2.5e-7;5e-7;7.5e-7;1e-6;2.5e-6;5e-6;7.5e-6;1e-
5;2.5e-5;5e-5;7.5e-5];                %radial interval
dtt=[1e-8;2.5e-8;5e-8;7.5e-8;1e-7;2.5e-7;5e-7;7.5e-7;1e-6;2.5e-6;5e-6;7.5e-6;1e-
5;2.5e-5;5e-5;7.5e-5];                %radial interval

%non dimensionalise
dro1=dro1*1e-6;
w=2.0*pi*df;
h=1e-6*dh*w;
ro1=dro1/dro1;
c1=dc1/(w*dro1);
rhol=drhol*dro1^2.0*w^2.0/dpo;
mul=dmul*w/dpo;
s2=dsigma2/(dpo*dro1);
s1=dsigma1/(dpo*dro1);
rhos=drhos*dro1^2.0*w^2.0/dpo;
Gs=dGs/dpo;
mus=dmus*w/dpo;
pa=damp/dpo;
d=1e-6*ddo/dro1;
a=da/dro1;
tt=dtt*w;
Cpl=dCpl*dTinf/(w*dro1)^2.0;
Dl=dDl/(w*dro1^2.0);

%calculate other constants (non dimensional)
ro2=ro1+d;
                                        %intial outer radius
Vs=ro2^3.0-ro1^3.0;
                            %volume constant
re1=ro1*(1.0+(2.0*s1/ro1+2.0*s2/ro2)*ro2^3.0/(4.0*Gs*Vs));  %unstrained inner radius

%figure
%plot(t*1e6/w,r)
%title('Variation in radial amplitude of a CAP insonated with one pulse of 3 MHz 0.1
MPa');
%xlabel('time (microsecs)');
%ylabel('radial amplitude (R1/Ro1)');
%figure
%plot(t*1e6/w,p)
%title('Variation in radiated pressure of a CAP insonated with one pulse of 3 MHz 0.1
MPa');
%xlabel('time (microsecs)');
%ylabel('radiated pressure (p/po)');

for i=1:N
r2(i)=(Vs+r(i)^3.0)^(1.0/3.0);
de(i)=16.0*pi*u(i)^2.0*r(i)*(mul*r(i)^3.0+mus*Vs)/r2(i)^3.0;
end
%plot(t,de)
ev=trapz(t,de)

dT=zeros(length(a),length(tt));
```

```
for j=1:length(a)
    for i=1:length(tt)
        dT(j,i)=ev*(exp((-1.0)*(a(j))^2.0/(4.0*Dl*tt(i)))-exp((-
1.0)*(a(j)+2.0*ro1)^2.0/(4.0*Dl*tt(i))))/(8.0*pi^(3.0/2.0)*Cpl*rhol*sqrt(Dl*tt(i))*ro
1*(ro1+a(j)));
    end
end
figure
plot(a*dro1*1e6,dT(4,:)*dTinf,a*dro1*1e6,dT(8,:)*dTinf,a*dro1*1e6,dT(12,:)*dTinf,a*dr
o1*1e6,dT(16,:)*dTinf)
title('Temporal variation in surrounding fluid temperature for a CAP insonated with
one pulse of 3 MHz 0.2 MPa');
legend('a = 0.075 microns','a = 0.75 microns','a = 7.5 microns','a = 75 microns');
xlabel('time (microsecs)');
ylabel('temperature rise (K)');
%axis([0,15,0,.5]);
figure
plot(tt*1e6/w,dT(:,4)*dTinf,tt*1e6/w,dT(:,8)*dTinf,tt*1e6/w,dT(:,12)*dTinf,tt*1e6/w,d
T(:,16)*dTinf)
%axis([0,3,0,.5])
title('Radial variation in surrounding fluid temperature for a CAP insonated with one
pulse of 3 MHz 0.2 MPa')
legend('t = 0.075 microsec','t = 0.75 microsec','t = 7.5 microsec','t = 75 microsec')
xlabel('radial distance from CAP wall (microns)')
ylabel('temperature rise (K)')
```

mevis.m

```
% calculates the temperature variation in the fluid surrounding a distribution of
CAPs
%get data
data
time
radius
velocity
pressure

%variables
dTinf=293;              %ambient temperature
dao=3.8;                %attenuation coefficient
dDl=1.4e-7;             %liquid thermal diffusivity
dCpl=4190;              %liquid specific heat
dro1=dro1*1e-6;
w=2.0*pi*df;
dsp=1e-6;
n=10;
%CAP location coordinates
dxc=[dsp+dro1,2*dsp+3*dro1,3*dsp+5*dro1,1.5*dsp+2*dro1,2.5*dsp+4*dro1,dsp+dro1,2*dsp+
3*dro1,3*dsp+5*dro1,1.5*dsp+2*dro1,2.5*dsp+4*dro1];
dyc=[dsp+dro1,dsp+dro1,dsp+dro1,1.5*dsp+3*dro1,1.5*dsp+3*dro1,2*dsp+5*dro1,2*dsp+5*dr
o1,2*dsp+5*dro1,2.5*dsp+7*dro1,2.5*dsp+7*dro1];
%grid coordinates
dxa=[0.5*dsp,2*dro1+1.5*dsp,4*dro1+2.5*dsp,6*dro1+3.5*dsp,dsp+dro1,2*dsp+3*dro1,3*dsp
+5*dro1,0.5*dsp,2*dro1+1.5*dsp,4*dro1+2.5*dsp,6*dro1+3.5*dsp,dsp+dro1,2*dsp+3*dro1,3*
dsp+5*dro1];
dya=[dsp+dro1,dsp+dro1,dsp+dro1,dsp+dro1,1.5*dsp+3*dro1,1.5*dsp+3*dro1,1.5*dsp+3*dro1
,2*dsp+5*dro1,2*dsp+5*dro1,2*dsp+5*dro1,2*dsp+5*dro1,2.5*dsp+7*dro1,2.5*dsp+7*dro1,2.
5*dsp+7*dro1];
%time array
dtt=[1e-7,1e-6,1e-5,1e-4,1e-3];
%dtt=1e-6;

%non dimensionalise
h=1e-6*dh*w;
ro1=dro1/dro1;
cl=dcl/(w*dro1);
rhol=drhol*dro1^2.0*w^2.0/dpo;
mul=dmul*w/dpo;
s2=dsigma2/(dpo*dro1);
s1=dsigma1/(dpo*dro1);
rhos=drhos*dro1^2.0*w^2.0/dpo;
Gs=dGs/dpo;
mus=dmus*w/dpo;
pa=damp/dpo;
d=1e-6*ddo/dro1;
tt=dtt*w;
Cpl=dCpl*dTinf/(w*dro1)^2.0;
Dl=dDl/(w*dro1^2.0);
```

```
xc=dxc/dro1;
yc=dyc/dro1;
xa=dxa/dro1;
ya=dya/dro1;

%calculate other constants (non dimensional)
ro2=ro1+d;
                                        %intial outer radius
Vs=ro2^3.0-ro1^3.0;
                                %volume constant
re1=ro1*(1.0+(2.0*s1/ro1+2.0*s2/ro2)*ro2^3.0/(4.0*Gs*Vs));              %unstrained
inner radius

%calculate energy dissipation for one CAP
for i=1:N
r2(i)=(Vs+r(i)^3.0)^(1.0/3.0);
de(i)=16.0*pi*u(i)^2.0*r(i)*(mul*r(i)^3.0+mus*Vs)/r2(i)^3.0;
end
ev=trapz(t,de)


%intitialise temperature array
for i=1:length(tt)
    for j=1:length(xa)
dT(i,j)=0;
        end
    end
r(1:length(xc))=0;
%calculate temperature change over grid
for i=1:length(tt)
    for j=1:length(xa)
        for k=1:length(xc)
        r(k)=sqrt((xa(j)-xc(k))^2+(ya(j)-yc(k))^2);
        dT(i,j)=dT(i,j)+ev*(exp((-1.0)*(r(k)-ro1)^2.0/(4.0*Dl*tt(i)))-exp((-
1.0)*(r(k)+ro1)^2.0/(4.0*Dl*tt(i))))/(8.0*pi^(3.0/2.0)*Cpl*rhol*sqrt(Dl*tt(i))*ro1*r(
k));
        end
    end
figure
T=293*[dT(i,1),0,dT(i,2),0,dT(i,3),0,dT(i,4),0;0,dT(i,5),0,dT(i,6),0,dT(i,7),0,0;dT(i
,8),0,dT(i,9),0,dT(i,10),0,dT(i,11),0;0,dT(i,12),0,dT(i,13),0,dT(i,14),0,0;0,0,0,0,0,
0,0,0];
surf(T);

zlabel('Change in temperature (K)');
title(['Temperature gradient in surrounding fluid            after end of pulse, 3
MHz 0.1 MPa']);
end

%plot(a*dro1*1e6,dT(4,:)*dTinf,a*dro1*1e6,dT(8,:)*dTinf,a*dro1*1e6,dT(12,:)*dTinf,a*d
ro1*1e6,dT(16,:)*dTinf)
%title('Temporal variation in surrounding fluid temperature for a CAP insonated with
one pulse of 3 MHz 0.1 MPa');
%legend('a = 0.075 microns','a = 0.75 microns','a = 7.5 microns','a = 75 microns');
%xlabel('time (microsecs)');
%ylabel('temperature rise (K)');
%axis([0,15,0,20]);
```

pevis.m

```
% calculates the temperature variation in the fluid surrounding a CAP over the course
of several pulses
%get data
data
time
radius
velocity
pressure
ipressure

%variables
dTinf=293;              %ambient temperature
dao=3.8;                %attenuation coefficient
dDl=1.4e-7;             %liquid thermal diffusivity
dCpl=4190;              %liquid specific heat (J/kgK)
dro1=dro1*1e-6;     %initial CAP outer radius
w=2.0*pi*df;        %angular frequency
dvb=5e-4;           %blood flow velocity (m/s)
PRF=30e3;            %pulse repetition frequency
```

```
dtis=.015;            %insonation time
NP=dtis*PRF;        %no. pulses
dtp=m/2/df;      %pulse length (s)
dtx=dtis/NP-dtp;    %time between pulses (s)
dtot=[dtis*5e-3,dtis*5e-2,dtis*0.5,dtis*0.75,dtis*1.0,dtis*1.01];           %time at
which temperature is to be evaluated (s)
dxco=0;             %intial CAP position x coordinate
dyco=0;             %initial CAP position y coordinate
dxa=[0,0,0,0,0,0,0,1e-6,1e-6,1e-6,1e-6,1e-6,1e-6,1e-6,2e-6,2e-6,2e-6,2e-6,2e-6,2e-
6,2e-6,3e-6,3e-6,3e-6,3e-6,3e-6,3e-6,3e-6,4e-6,4e-6,4e-6,4e-6,4e-6,4e-6,4e-6,5e-6,5e-
6,5e-6,5e-6,5e-6,5e-6,5e-6,6e-6,6e-6,6e-6,6e-6,6e-6,6e-6,6e-6,7e-6,7e-6,7e-6,7e-6,7e-
6,7e-6,7e-6,8e-6,8e-6,8e-6,8e-6,8e-6,8e-6,8e-6,9e-6,9e-6,9e-6,9e-6,9e-6,9e-6,9e-
6,10e-6,10e-6,10e-6,10e-6,10e-6,10e-6,10e-6,10e-6];
dya=[-6e-6,-4e-6,-2e-6,0,2e-6,4e-6,6e-6,-6e-6,-4e-6,-2e-6,0,2e-6,4e-6,6e-6,-6e-6,-4e-
6,-2e-6,0,2e-6,4e-6,6e-6,-6e-6,-4e-6,-2e-6,0,2e-6,4e-6,6e-6,-6e-6,-4e-6,-2e-6,0,2e-
6,4e-6,6e-6,-6e-6,-4e-6,-2e-6,0,2e-6,4e-6,6e-6,-6e-6,-4e-6,-2e-6,0,2e-6,4e-6,6e-6,-
6e-6,-4e-6,-2e-6,0,2e-6,4e-6,6e-6,-6e-6,-4e-6,-2e-6,0,2e-6,4e-6,6e-6,-6e-6,-4e-6,-2e-
6,0,2e-6,4e-6,6e-6,-6e-6,-4e-6,-2e-6,0,2e-6,4e-6,6e-6];

%non dimensionalise
h=1e-6*dh*w;
cl=dcl/(w*dro1);
rhol=drhol*dro1^2.0*w^2.0/dpo;
mul=dmul*w/dpo;
s2=dsigma2/(dpo*dro1);
s1=dsigma1/(dpo*dro1);
rhos=drhos*dro1^2.0*w^2.0/dpo;
Gs=dGs/dpo;
mus=dmus*w/dpo;
pa=damp/dpo;
d=1e-6*ddo/dro1;
Dl=dDl/(w*dro1^2.0);
Cpl=dCpl*dTinf/(w*dro1)^2.0;
ro1=dro1/dro1;
vb=dvb/(w*dro1);
tp=dtp*w;
tx=dtx*w;
tot=dtot*w;
xco=dxco/dro1;
yco=dyco/dro1;
xa=dxa/dro1;
ya=dya/dro1;

%calculate other constants (non dimensional)
ro2=ro1+d;
                                                %intial outer radius
Vs=ro2^3.0-ro1^3.0;
                                    %volume constant

%calculate energy dissipation for one CAP
for i=1:N
r2(i)=(Vs+r(i)^3.0)^(1.0/3.0);
de(i)=16.0*pi*u(i)^2.0*r(i)*(mul*r(i)^3.0+mus*Vs)/r2(i)^3.0;
end
ev=trapz(t,de)

%intitialise temperature array
for j=1:length(tot)
    for k=1:length(xa)
        dT(j,k)=0;
        end
    end

    %calculate temperature in the plane of the initial CAP position after nop pulses
for j=1:length(tot)
          nop=1.0+floor(tot(j)/(tp+tx));
    if nop>NP;
        nop=NP;
         end

for k=1:length(xa)
    for i=1:nop
  tt=tot(j)-(i-1)*(tx+tp);
  if tt==0;
      break;
  end
            xc=xco+(i-1)*vb*(tx+tp);
            yc=yco;
            r=sqrt((xa(k)-xc)^2+(ya(k)-yc)^2);
                if r>ro1
```

```
                    dT(j,k)=dT(j,k)+ev*(exp((-1.0)*(r-ro1)^2.0/(4.0*Dl*tt))-exp((-
1.0)*(r+ro1)^2.0/(4.0*Dl*tt)))/(8.0*pi^(3.0/2.0)*Cpl*rhol*ro1*r*sqrt(Dl));
            end
        end
    end
end


y=[dya(1);dya(2);dya(3);dya(4);dya(5);dya(6);dya(7)];
x=[dxa(1),dxa(8),dxa(15),dxa(22),dxa(29),dxa(36),dxa(43),dxa(50),dxa(57),dxa(64),dxa(
71)];
for i=1:length(tot)
Txy=reshape(dT(i,:),7,11);
figure;
surf(x*1e6,y*1e6,Txy*dTinf);
xlabel('distance along vessel (microns)');
ylabel('distance across vessel (microns)');
zlabel('Change in temperature (K)');
title(['Temperature gradient in surrounding fluid after       of pulsed insonation at
3 MHz 0.1 MPa']);
%axis([0,10e-6,-6e-6,6e-6,0,150]);
end
```

subharmonic emission, may be established to enable reliable and convenient monitoring.

9 **Allen, J. S.** and **Roy, R. A.** Dynamics of gas bubbles in viscoelastic fluids. II: non-linear viscoelasticity. *J. Acoust. Soc. Am.*, 2000, **108**(4), 1640–1651.

10 **Medwin, H.** Counting bubbles acoustically: a review